Ion Channel Crystallisation for Structural Studies

Anling Kuo

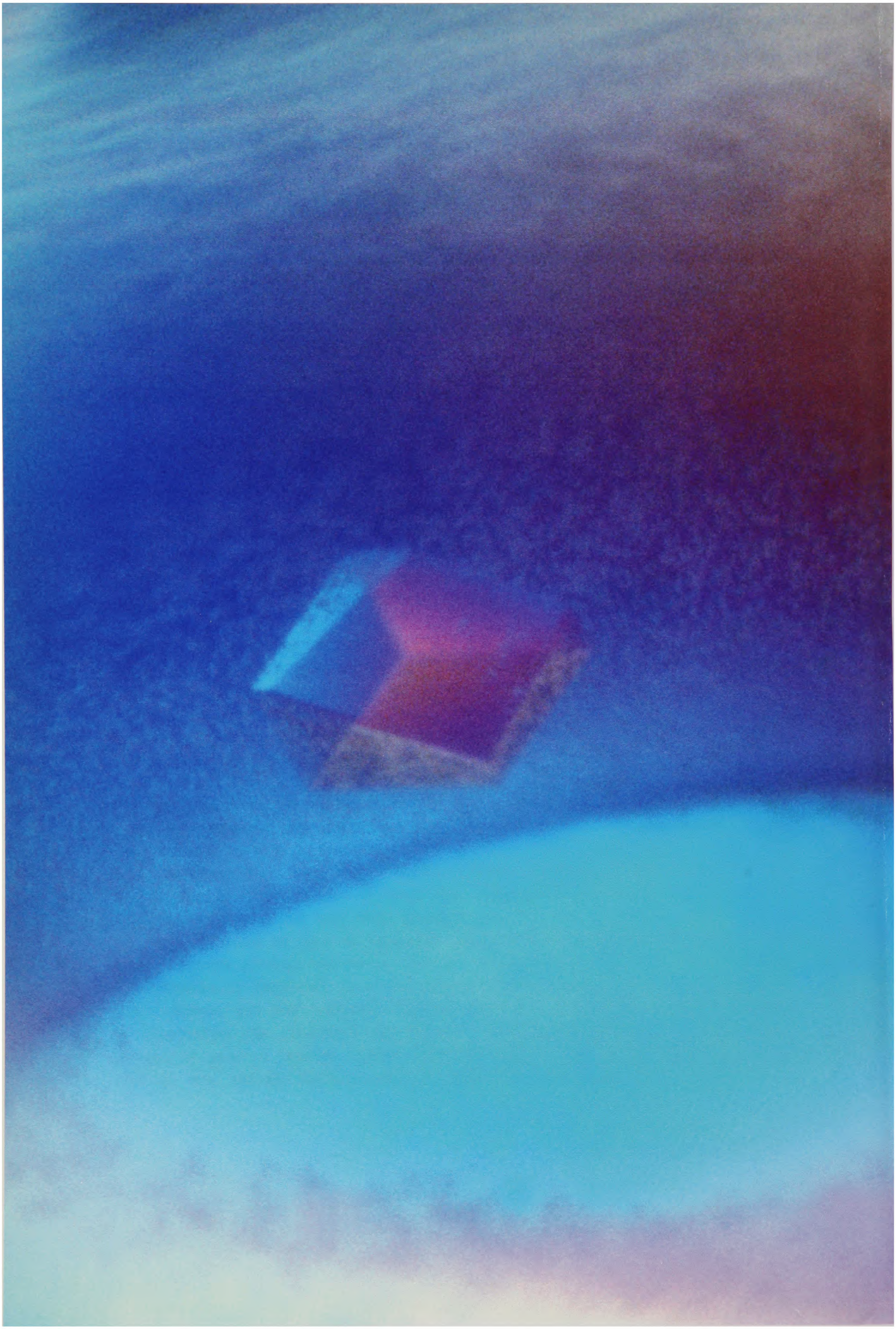
Laboratory of Molecular Biophysics,
Department of Biochemistry, University of Oxford

Linacre College, University of Oxford

A thesis submitted in partial fulfilment of the requirements for the degree of Doctor of Philosophy at University of Oxford

Hilary Term 2004

HAUGHTON SCIENCE LIBRARY OXFORD
18 JUN 2004



Abstract

Ion channels control the movement of ions allowing specific ions to pass across biological membranes. This apparently simple process is used to control many essential physiological processes including the generation and propagation of neuronal excitation, regulation of insulin secretion, heartbeat and cell volume. Ion channels are able to do this by having multiple means of controlling the opening and closing of the ion conduction pathway. Several recent ion channel structures have shed light on the important process of ion selectivity as well as providing clues on channel gating. However, it is not yet completely clear how ion channels control the passage of ions across the membrane. My work is centred on understanding the gating process through structural analysis mostly using X-ray crystallography. In order to get to this point, crystals of the target ion channels need to be grown. This thesis presents four projects that were aimed at developing the techniques for over-expression, purification and crystallisation of ion channels or transporters making them amenable for structural studies.

One of the difficult steps in the structure determination pathway is obtaining well-ordered crystals of the target membrane protein. Crystals of the EcCLC channel (now found to be a transporter) from *E. coli* were initially unacceptable for structure determination. It was shown that the process of dehydration improved the quality and diffraction limit of the EcCLC crystals. This simple method provides a possible procedure for improving the resolution limit of soluble and membrane protein crystals.

Inward rectifier potassium channels (Kir channels) are a distinct subfamily that preferentially allows K^+ ions to move into the cell. Two bacterial homologues of Kir channels, KirBac1.1 and KirBac3.1, were crystallised in 3-D and 2-D forms, respectively. As the crystal structure revealed the full-length model provided an excellent starting point for understanding the gating process in these channels.

The 3-D structure of KirBac1.1 was captured in the closed state. This K^+ channel prevents ion movement by using hydrophobic residues to occlude the ion conduction pathway, altering the conformation of selectivity filter, misaligning the pore helices and decreasing the volume of the cavity.

The 2-D projection maps of KirBac3.1 were obtained in both closed and a potentially open conformations. These two maps provided evidence as to how the structural elements of the inner, outer, slide helices and the C-terminal domains change relative to one another as the channel moves between these two gating states. These motions were modelled as rigid body movements. They included bending of the inner helices, a rotation of the outer helices as they straighten in the membrane, translocation of the slide helices and C-terminal domain rotations.

It is hoped that the information gained from these projects, the plasmids construction, the expression systems and the protocols that were established for crystallisation of the ion channels and transporter will provide guidelines for future structural studies of membrane proteins.

Acknowledgments

This thesis would never have reached the final stage without my supervisor Dr. Declan Doyle's help including all the proofreading and manuscript corrections. I would like to thank him for giving me the opportunity to work in his laboratory during my time in Oxford. Over this time, I have gained tremendous in self-confidence through daily interactions with him. His enthusiasm for the ion channel research field and encouragement during difficult stages was an inspiration. I will certainly miss his scientific arguments which lead both of us to achieve success even with this tough project.

I must also thank Dr. C. Venien-Bryan who has helped me considerably with the 2-dimensional crystallisation of KirBac3.1. All projection map pictures in this thesis were kindly supplied by Catherine.

I would like to thank all members of the KirBac1.1 project who worked together intensively over a short period of time in order to finish this difficult project. This includes Dr. Jacqueline M. Gulbis, Jennifer F. Antcliff, Dr. Tahmina Rahman, Dr. Edward D. Lowe, Jochen Zimmer and Jonathan Cuthbertson.

The DD group in G3 (or G4) is now part of my memoirs, reflected good times in Oxford. I am grateful to all the members in this group and my thanks go out to Tahmina, Jenny, Matthew, Thomas, Jochen and Jonathan.

I am very grateful to Professor Dame Louise Johnson FRS for helpful support and advice during my time in Oxford. I extend my thanks to all the members of LMB at the University of Oxford.

Linacre College is a friendly and supportive home. Without its generous support my research work would have been more difficult. Providing accommodation close to the laboratory allowed me to be safe particularly returning late at night. My deepest thanks to all the college members and staffs.

My last thank to my family and friends for whom my words cannot express how grateful I am for everything that they do for me.

Table of contents

1 Chapter 1 - Introduction **1**

1.1 Biological membrane 1
1.2 Membrane proteins 1
1.3 Target membrane proteins for structural studies 2
1.4 Potassium channels 4
1.5 Chloride channels 8
1.6 Magnesium transport protein 9
1.7 The layout of this thesis 12

2 Chapter 2 - A chloride ion channel from *Escherichia coli* **13**

2.1 Introduction 13
2.2 The voltage-gated CLC family 13
2.3 General features of the CLC family 15
2.3.1 Topology 15
2.3.2 Dimers 17
2.3.3 Filter region 17
2.3.4 Gating 18
2.4 Same *E.coli* chloride channel different crystal forms 20
2.5 Methods 21
2.5.1 Outline of methods 21
2.5.2 Plasmid transformation 22
2.5.3 Protein expression 22
2.5.4 Protein purification 22
2.5.5 Protein crystallisation 24
2.5.6 Data collection 25
2.5.7 Rehydration experiment 25
2.5.8 Dehydration experiment 26
2.6 Results and Discussion 28
2.6.1 Protein expression and purification - results and discussion 28
2.6.2 Protein crystallisation and data collection - results and discussion 31
2.6.3 Rehydration experiment – results and discussion 33
2.6.4 Dehydration experiment – results and discussion 34

3 Chapter 3 - A magnesium transport domain from *E.coli* **38**

3.1 Introduction 38
3.2 Outlines of methods 41
3.2.1 Cloning of the *CorA* domain 42
3.2.1.1 Design of primers to produce *CorA* truncation domain 42

3.2.1.2 Amplification of *CorA* domain by PCR 42
3.2.1.3 Enzyme digestion to generate overhang 43
3.2.1.4 Ligation and transformation 44
3.2.1.5 Screening for positive clones 45
3.2.2 Test expression 46
3.2.3 Protein expression 47
3.2.4 Thirty sparse matrix buffer trials 47
3.2.5 Optimisation of buffers 49
3.2.6 Purification of CorA domain using the optimised buffers 49
3.2.7 Purification of CorA domain using IMAC 50
3.2.8 Gel filtration 51
3.2.9 Crystallisation trial one 51
3.2.10 Crystallisation trial two 51
3.3 Results and Discussion 52
3.3.1 Cloning – results and discussion 52
3.3.2 Protein expression – results and discussion 53
3.3.3 Thirty matrix extraction buffer – results and discussion 54
3.3.4 Gel filtration – results and discussion 56
3.3.5 Crystallisation trial one and trial two - results and discussion 59

4 Chapter 4 - An inward rectifier K^+ channel from *Burkholderia pseudomallei* 60

4.1 Introduction 60
4.1.1 Voltage-gated potassium channels (K_v channels) 60
4.1.2 Ca^{2+} activated K^+ channels 62
4.1.3 Inwardly rectifying K^+ channels (K_{ir} channels) 63
4.1.4 Tandem pore potassium channels (K_{2P} channels) 64
4.1.5 Bacterial Kir channels 65
4.2 Materials and Methods 67
4.2.1 Materials 67
4.2.2 Methods 67
4.2.3 Cloning of *KirBac1.1* 69
4.2.3.1 Assigning the starting codon for *KirBac1.1* 69
4.2.3.2 *KirBac1.1Δ12* 69
4.2.4 Bacteria growth and expression 70
4.2.5 Affinity purification 70
4.2.5.1 Cell harvesting 70
4.2.5.2 Cell disruption 71
4.2.5.3 Membrane protein purification and solubilisation 71
4.2.5.4 IMAC purification 71
4.2.6 Cleavage of the his-tag 72
4.2.7 Gel filtration 72
4.2.8 Ion exchange chromatography 73
4.2.9 N-terminal sequencing and mass spectrometry 74

4.2.10 Crystallisation of KirBac1.1 74
4.2.10.1 Determine protein concentration 74
4.2.10.2 Initial screening 74
4.2.10.3 Sitting drop vapour diffusion crystallisation 76
4.2.11 Improve crystal qualities 76
4.2.11.1 Optimisation of screen solutions 76
4.2.11.2 Choices of detergents and optimisation of detergent exchange 77
4.2.11.3 Using detergents as additives 78
4.2.11.4 Optimise additive detergents 78
4.2.11.5 Other optimisations 78
4.2.12 Heavy metal derivatisation 79
4.2.12.1 Generation of cysteine residues for heavy metal soaking 79
4.2.12.2 Heavy metal soaking 80
4.2.12.3 Heavy metal co-crystal 80
4.2.12.4 Seleno-methionine labelling 81
4.2.13 Structure determination 82
4.2.13.1 Cryoprotection 83
4.2.13.2 Data collection 83
4.2.14 Data processing 86
4.2.14.1 Autoindexing 86
4.2.14.2 Refine cell 88
4.2.14.3 Intergration 88
4.2.14.4 Scaling and merging data 88
4.2.15 Phases 89
4.3 Results and Discussion 90
4.3.1 KirBac1.1 expression – results and discussion 90
4.3.2 Protein purification – results and discussion 91
4.3.2.1 Choice of detergents and optimisation of detergent exchange 94
4.3.3 His-tag – results and discussion 95
4.3.4 Gel filtration – results and discussion 95
4.3.5 Ion-exchange chromatography – results and discussion 99
4.3.6 N-terminal sequencing and mass spectrometry - results and discussion 99
4.4 Crystallisation – results and discussion 102
4.4.1 KirBac1.1 crystallised in DDM 102
4.4.2 Improvement of KirBac1.1 crystal packing 105
4.4.2.1 Reducing KCl concentration and changing detergent 105
4.4.2.2 Detergents as additives 106
4.4.2.3 Optimisation of precipitants 108
4.4.2.4 Dehydration of the crystals 108
4.4.2.5 Other optimisation trials 112
4.5 Heavy metal derivatisation – results and discussion 114
4.5.1 Heavy metal soaking and co-crystallisation with heavy atoms 114
4.5.2 Rb^+ and Cs^+ ions replacement of K^+ ions 115

4.5.3 Seleno-methionine labelled KirBac1.1Δ12 115
4.6 Data processing and structure determination - results 117
4.7 Structure description and functional implications 118
4.7.1 Overview of KirBac1.1 122
4.7.2 Structural evidence for KirBac1.1 in the closed state 122
4.7.2.1 Phe146 blocks ion conduction pathway 122
4.7.2.2 An altered selectivity filter 125
4.7.2.3 Misaligned pore helices 129
4.7.2.4 A decrease in cavity volume 131
4.7.3 The key residues of inward rectification 133
4.7.4 Gating hypothesis 136

5 Chapter 5 - A Kir channel from *Magnetospirillum magnetotacticum* 140

5.1 Introduction 140
5.2 Outline of the methods employed in the KirBac3.1 143
5.2.1 Growing the *Magnetospirillum* strain 144
5.2.2 Purification of genomic DNA from *Magnetospirillum magnetotacticum* 144
5.2.3 Cloning 144
5.2.3.1 pET-30a vector 145
5.2.3.2 PCR 147
5.2.3.3 Endonuclease digestion 148
5.2.3.4 Ligation and transformation 148
5.2.3.5 Confirmation of the *KirBac3.1* clones 149
5.2.4 Expression 150
5.2.4.1 Test expression 150
5.2.4.2 Optimisation of expression 150
5.2.5 Purification 151
5.2.5.1 IMAC 151
5.2.5.2 Gel filtration 152
5.2.5.3 N-terminal sequencing and mass spectrometry 153
5.2.6 2-D Crystallisation 153
5.2.6.1 Reconstitution 153
5.3 Results and Discussion 155
5.3.1 Purification of genomic DNA from *Magnetospirillum magnetotacticum* – results and discussion 155
5.3.2 Cloning of KirBac3.1 – results and discussion 155
5.3.3 Protein expression and purification - results and discussion 157
5.3.4 N-terminal sequencing and mass spectroscopic analysis - results and discussion 162
5.3.5 2-D crystal formation – results and discussion 163
5.3.6 Implication of EM projection map of KirBac3.1 165
5.3.6.1 Closed conformation of KirBac3.1 165
5.3.6.2 Potential open conformation of KirBac3.1 167

6	**Chapter 6 - Conclusions**	**169**
6.1	Cell culture manipulation	170
6.2	Important role of detergent	170
6.3	Anisotropically diffracting crystals	172
6.4	Future direction for the chloride ion channel EcCLC project	172
6.5	CorA domain future direction	173
6.6	Future direction of inwardly rectifier potassium channel KirBac1.1	173
6.7	Future study of KirBac3.1	173
6.8	Concluding remarks	174
Appendix A	**pET Vector Map**	**175**
Appendix B	**Procedure for Production of Chemical Competent Cells**	**176**
Appendix C	**Protein Analysis**	**178**
	1. Protein Concentration Determination	178
	2. Silver Staining	178
Appendix D	**Seleno-methionine Label Medium**	**179**
Appendix E	**Home Salt/PEG Crystal Screen Solution**	**180**
References		**181**
Publication		**191**

Abbreviations:

Å	Angstrom
A_{260}	Absorbance at 260 nm
A_{280}	Absorbance at 280 nm
A_{600}	Absorbance at 600 nm
ATP	Adenosine triphosphate
Bis/Tris	Bis(2-hydroxyethyl)iminotris(hydroxymethl)methane; 2-bis(2-hydroxyethyl)amino-2-(hydroxymethyl)-1,3-propanediol
bp	Base pairs
CCP4	Collaborative Computational Project Number 4
CLC	Member of the voltage dependent CLC family of chloride channel
CMC	Critical Micelle Concentration of a detergent
C-teminal	Carboxy terminal end of a protein
CYMAL-4	Cyclohexyl-butyl-β-D-maltoside
Da	Dalton
$_dH_2O$	Distilled water
DM	n-Decyl-β-D-maltoside
DDM	n-Dodecyl-ß-D-maltoside
DHPC	1,2-diheptanoyl-sn-phosphocholine
DOPC	1,2-dioleoyl-sn-phosphocholine
DNA	Deoxyribose nucleic acid
dNTP	Deoxyribose nucleoside triphosphate
DTT	Dithiothreitol
EcCLC	An *E.coli* CLC type channel, the product of *YadQ*
E.coli	*Escherichia coli*
EDTA	Ethylenediaminetetraacetic acid
ESRF	European Synchrotron Radiation Facility
FPLC	Past protein liquid chromatography
HEPES	N-(2-hydroxyethyl)piperazine-N'-(2-ethanesulphonic acid)
HEGA-10	Decanoyl-N-hydroxyethylglucamide
His-tag	Hexa-histidine tag

hrs	Hours
IMAC	Immobilized metal affinity chromatography
IPTG	Isopropyl β-D-thiogalactopyranoside
kDa	kiloDalton
Kir	Inwardly rectifying K^+ channel
LB	Luria-Bertini broth
LDAO	Lauryl diethylamine N-oxide
MALDI-MS	Matrix assisted laser desorption ionization mass spectrometry
MCS	Multiple cloning site (of an expression plasmid)
MEGA-10	Decanoyl-N-methylglucamide
MES	2-(N-morpholino) ethane sulphonic acid
N-terminal	Amino terminal of a protein
NEB	New England BioLabs
ODxxx	Optical density at xxx nm
PCR	Polymerase chain reaction
PEG	Polyethylene glycol
PMSF	Phenylmethylsulphonyl fluoride
SDS	Sodium dodecylsulphate
SDS-PAGE	Sodium dodecylsulphate polyacrylamide gel electrophoresis
SEC	Size exclusion chromatography
TB	Terrific Broth
TEA	Tetraethylammonium
TEMED	N,N,N',N'-tetramethylethylenediamine
TM	Transmembrane
triDM	n-Tridecyl-β-D-maltoside
Tris	Tris(hydroxymethyl)aminomethane
UV	Ultra-violet light
V	Volts
v/v	Percentage volume per volume
w/v	Percentage weight per volume
Z_{3-12}	Zwittergent 3-12

Chapter 1 - Introduction

1.1 Biological membrane

The biological membrane forms a boundary between the living cell and its extra-cellular compartments. The membrane is planar and mainly formed by phospholipids which serve as an effective barrier against the movement of charged particles in and out of cells.

1.2 Membrane proteins

In addition to the phospholipids bilayer the biological membrane also contains membrane proteins: integral proteins and peripheral proteins. Integral membrane proteins are the doorways through which charged particles such as ions are able to move across a bilayer. Channels control the movement of ions and allow specific ions to pass through them. As an example, potassium channels preferentially choose potassium over the smaller monovalent cation sodium by approximately $1x10^3$ or $1x10^4$ to 1. Another example is the chloride channel which preferentially allows chloride ions to cross the membrane.

Transporters use a solute gradient to drive the translocation of substances in and out of cells. The transporter proteins transport sugars, neurotransmitters, nucleosides, peptides, amino acids, drugs and other hydrophilic solutes across the phospholipid bilayer. Both channels and transporters function in diverse physiological processes such as control of heartbeat, insulin secretion, neuronal excitation and regulation of cell volume.

1.3 Target membrane proteins for structural studies

Ion channels and transporters maintain the right balance of ions and solutes in cells. These proteins reside within the cell membrane and are vital for transmitting signals in all tissues.

Much of what we knew about ion channels and transporters has come from physiological studies. Physiologists traditionally separated channels and transporters into two classes: carrier proteins and pore proteins based largely on the rate of solute transport. A classical transport protein such as valinomycin was considered as a cargo or boat responsible for importing and exporting solutes across the biological membrane. Ion channels are generally viewed as narrow water-filled tunnels containing a region that forms a selectivity filter (Hille, 2001).

In the last three decades the knowledge of ion channels and transporters has advanced remarkably with the development of patch-clamp (Neher and Sakmann, 1976) and molecular biology techniques (Alberts, 2002). From the initial experiments that described channels in terms of selective currents we now know the atomic structures of several ion channels. A number of these will be described in greater detail later in the thesis.

Many results showed that defects in ion channels and transporters are linked to a wide range of diseases (Ashcroft, 2000). In a renal tubule, defects in potassium channels do not allow proper salt uptake, resulting in the malfunction of K^+ recycling in the loop of Henle causing Bartter's syndrome (Derst *et al.*, 1997). Genetic mutations in human skeletal muscle Cl^- channels cause myotonia, a disease characterized by muscle stiffness (Koch *et al.*, 1992). Another well-characterized channel disease is congenital long QT syndrome. In the heart, defects in voltage-dependent potassium channels do not allow proper transmission of electrical impulses.

resulting in sudden cardiac death in healthy young individuals (Wang *et al.*, 1995; Wang *et al.*, 1996).

Recognition of the medical importance of ion channels and transporters has increased over the years since their first identification. In 1996 a survey reported that 5 % of the genes present in the human genome were ion channels. However, the Human Genome project revealed that approximately 25% of all the membrane proteins were ion channels. All these channels are potential targets for new drugs (Terstappen and Reggiani, 2001). Atomic models of the channels will be necessary to reveal the precise relationships between structure and function. Unfortunately, most X-ray structure models available to date are of soluble proteins. Membrane proteins such as transporters and ion channels present many biochemical and biophysical difficulties making them difficult for structural studies. My work focuses mainly on the biochemical methods used in membrane protein structural projects. One of my main goals was to improve these methods making structural studies of membrane proteins more amenable.

One of the crucial steps in obtaining a membrane protein crystal structure is producing large amounts of the target protein in a highly purified, homogeneous state. Milligram levels of the target membrane protein are required during crystallisation screens. Eukaryotic expression systems generally can only produce small quantities of membrane proteins leaving only the possibility of functional studies. This leaves only the *E. coli* expression system as the present method of choice for over-expression of membrane protein in a structural project thus potentially limiting the target proteins to those of the prokaryotic world.

Recently, many complete prokaryotic genomes have been sequenced. Fortunately, homologues of many ion channels and transporters exist in the

membranes of prokaryotic cells. This opens up the potential of structural studies of key eukaryotic membrane proteins through the bacterial homologue. This approach has been successfully used for many of the recent membrane protein structures (Doyle *et al.*, 1998; Dutzler *et al.*, 2001; Jiang *et al.*, 2002; Huang *et al.*, 2003). These structures are being used as the basis for analysis of the structure and function of their eukaryotic homologues.

The remaining steps in the crystallisation of membrane proteins also remain challenging. Many membrane proteins lack large extra-membranous domains. Normally these parts of the protein form the main protein-protein contacts in a crystal. An essential component used in all parts of a membrane protein structural project is the use of detergents. These types of proteins mixed with detergents typically produce anisotropic diffraction patterns adding to the difficulty in structure determination. Although membrane protein structure determination has advanced recently, detailed procedures for protein expression and crystallisation are sparse.

Recently our laboratory successfully solved the three-dimensional crystal structure of a bacterial inwardly rectifying (Kir) potassium channel (KirBac1.1), a homologue of the eukaryotic Kir channel family. The strategy used for protein expression, the condition for crystal nucleation, screening and optimisation of crystal quality are included in the following thesis beginning with a quick overview of the different membrane protein targets.

1.4 Potassium channels

Structural studies of potassium ion channels started more than five years ago when the first K^+ channel structure (KcsA) was published (Doyle *et al.*, 1998). This was the first direct view of a member of the Na^+, Ca^{2+} and K^+ super family of channels.

KcsA is a two transmembrane K^+ selective ion channel containing 160 amino acids from the gram-positive bacterium *Streptomyces lividans* (Schrempf *et al.*, 1995). The KcsA structure revealed that the ion conduction pathway is formed at the interface between the four subunits. At the extracellular side of the membrane the ion conduction pathway narrows to form the selectivity filter. This section is created from the highly conserved Val-Gly-Tyr-Gly linear sequence, found in all potassium channels. Figure 1-1 shows a general overview of the KcsA structure. Other important structural features revealed in KcsA included the centrally filled water cavity, pore helix dipoles, and the potential gate located on the intracellular side of the membrane. In terms of function these features combine to stabilize an ion in the centre of the membrane and control the movement of the ions across the membrane (Figure 1-1).

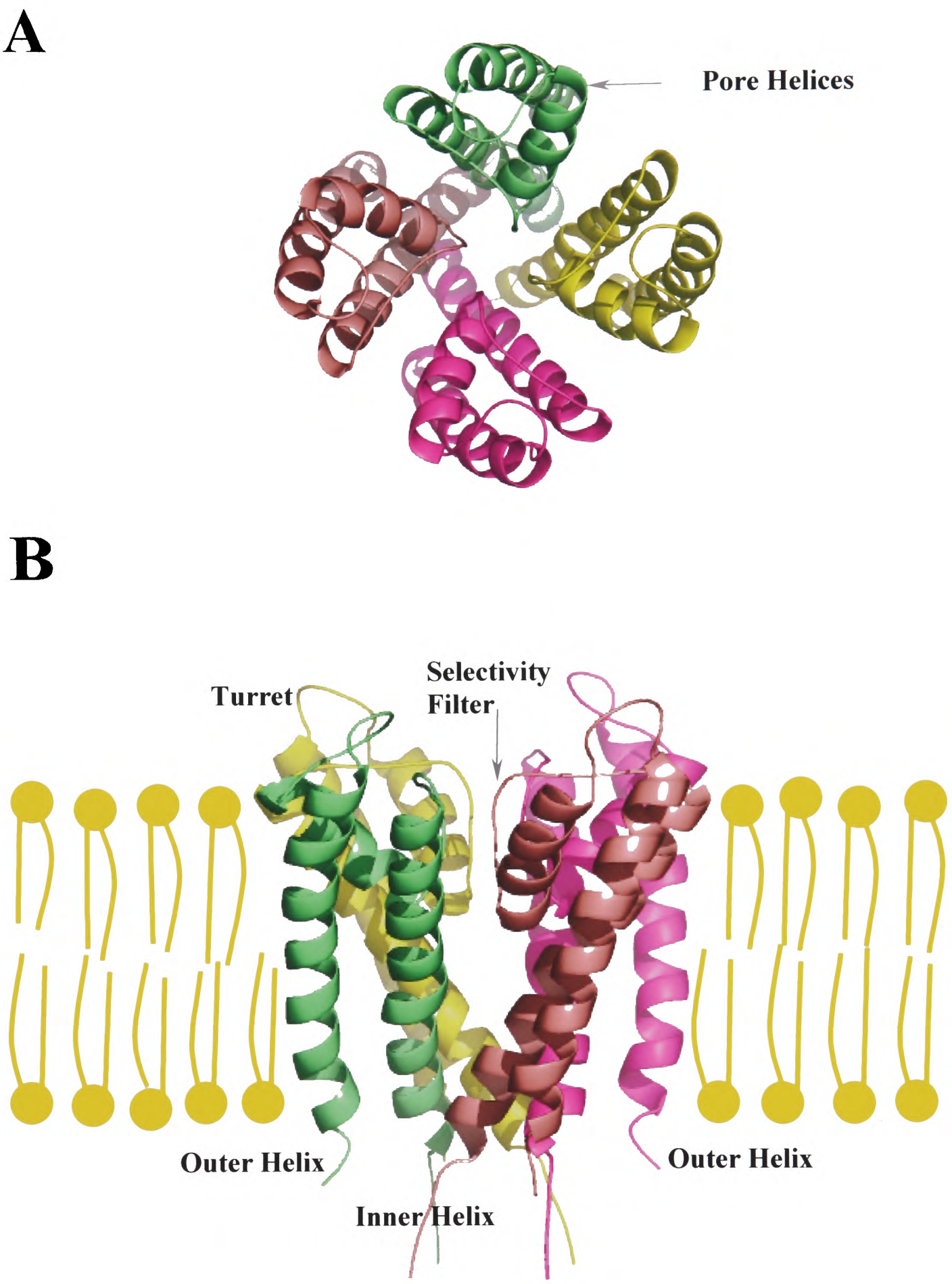


Figure 1-1. An overview of the structure of KcsA.
A. An extra-cellular side view of the structure of KcsA. The four subunits are distinguished by green, yellow, magenta and salmon respectively.
B. Another view of the structure perpendiclular to A.
All the structure models are prepared with PyMOL and cartoon lipids are generated with Microsoft word drawing tools. The KcsA PDB code is 1BL8.

The pore region is similar to the eukaryotic Shaker potassium channel (Figure 1-2).

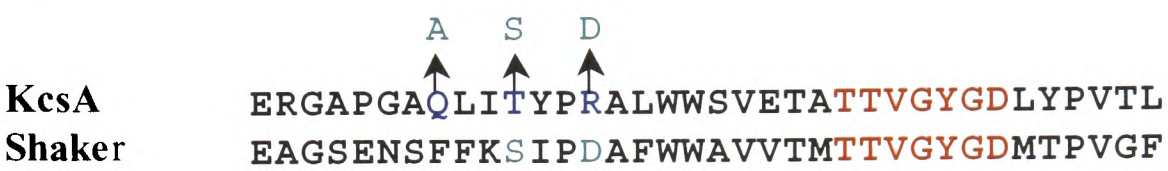


Figure 1-2. Sequence alignment of the KcsA and the Shaker K^+ channel pore regions.
The arrows indicated that when the three KcsA amino acids were mutated to those of the residues KcsA was then able to bind the Shaker blocker toxin agitoxin2 (MacKinnon *et al.*, 1998).

The extracellular entryway to the Shaker K^+ channel, formed from the turrets binds agitoxin2, a scorpion toxin (Figure1-1). By mutating residues in KcsA's turret to resemble Shaker's (Figure 1-2) and studying binding of radioactive agitoxin2 it was shown that the prokaryotic KcsA resembled that of eukaryotic K^+ channels (MacKinnon *et al.*, 1998). As for many eukaryotic K^+ channels, KcsA shows TEA (tetraethylammonium) and Ba^{2+} block. KcsA has also been shown to be K^+ selective (Heginbotham *et al.*, 1999).

This bacterial KcsA K^+ channel is an excellent model for eukaryotic K^+ channels. The structure confirmed many of the functional studies going back at least 30 years. Based on the structure of KcsA, the selectivity of K^+ ions in the filter region results from the formation of a complex with the backbone carbonyl oxygen atoms. This ion - carbonyl oxygen atom complex is believed to be optimised for K^+ ions over the other monovalent cations. Even though many of the properties of the channel are better resolved the gating process of potassium channels was still unclear. In order to uncover the exact molecular mechanism of potassium channel gating, new potassium channel structures caught in different gating states need to be determined. Therefore

the continuing progress in determining different structures of the ion channels is one of the main objectives of my research.

Each step on the road to structure determination of a membrane protein is time consuming. Added to this the lack of time to study the problems in detail due to the worldwide competition makes it more difficult still. This thesis presents a successful example of a membrane protein structural project that was completed in a short period of time.

1.5 Chloride channels

Almost 20 years ago, an anion chloride channel was discovered from the electric organ of the *Torpedo* ray using biophysical techniques (Miller and White, 1984). It took ten years to uncover the important physiological role for this family of channels through studies of ion channel diseases (channelopathies). Chapter 2 focuses on a bacterial chloride channel (yadQ) from *Escherichia coli*. The aim of this project was to determine the structure of the channel and suggest a mechanism of the ion conduction pathway.

This protein is a homologue of a large family of anion channels. The chloride ion channels are important for regulation of excitability in nerves and muscles, controlling cell volume and maintaining pH in organelles. Genetic defects of the CLC-1 protein results in a disease called myotonia (Koch *et al.*, 1992). Obviously the structure of the chloride ion channel is important for its potential medical application. While we were trying to improve the quality of our crystals both from 2-D and 3-D crystallography, the 3-D crystal structures of two bacterial chloride ion channels were determined (Dutzler *et al.*, 2001). At this point we were at a "cross road" in the project and needed to decide which direction we should go next. Should we carry on with some aspects of protein structural/functional experiments or put the project on

hold and focus on another target? We decided to take the chance and completely switch to a new project that targeted the bacterial inwardly rectifying potassium channel KirBac1.1. Even though we did not solve the structure of the chloride channel, the experience gained working on this channel provided the foundations for the KirBac1.1 project.

In order to finish the chloride channel project, experiments on crystal dehydration were performed. In the experimental section details describing the results on dehydration of these crystals which increased the diffraction limit and internal order are described. The information is useful to the structural area of membrane proteins since dehydration may be used to improve the resolution of existing membrane protein crystals (Kuo *et al.*, 2003).

1.6 Magnesium transport protein

A soluble domain from a magnesium transporter was chosen as my second project. This choice was based on two considerations:

1. Mg^{2+} ions play a central role in many biological processes, for example enzyme catalysis.

2. Since the complete transporter protein in BL21(DE3) cells was toxic after induction in expression trials the non-transmembrane domain was considered a viable option.

3. Mg^{2+} ions are known to play an important physiological role in Kir channels. Study of the magnesium transporter may shed light on the activity of these channels.

A magnesium ion possesses a number of unique properties. It has a small ionic radius about 0.65 Å with a +2 charge. This means that generally water molecules are tightly associated with the ion in solution. In protein crystal structures magnesium ion tends to bind to the carboxylate oxygen atoms of aspartate and

glutamate side chains (Katz and Glusker, 1998). The amino acid sequences of the *E.coli* magnesium transporter show a total of fifty-three aspartate and glutamate residues all of which are in the non-transmembrane domain (Figure 1-3). Our aim was to first solve the domain structure, to explore the specific ion binding sites, and later to find a way to express the whole transporter protein.

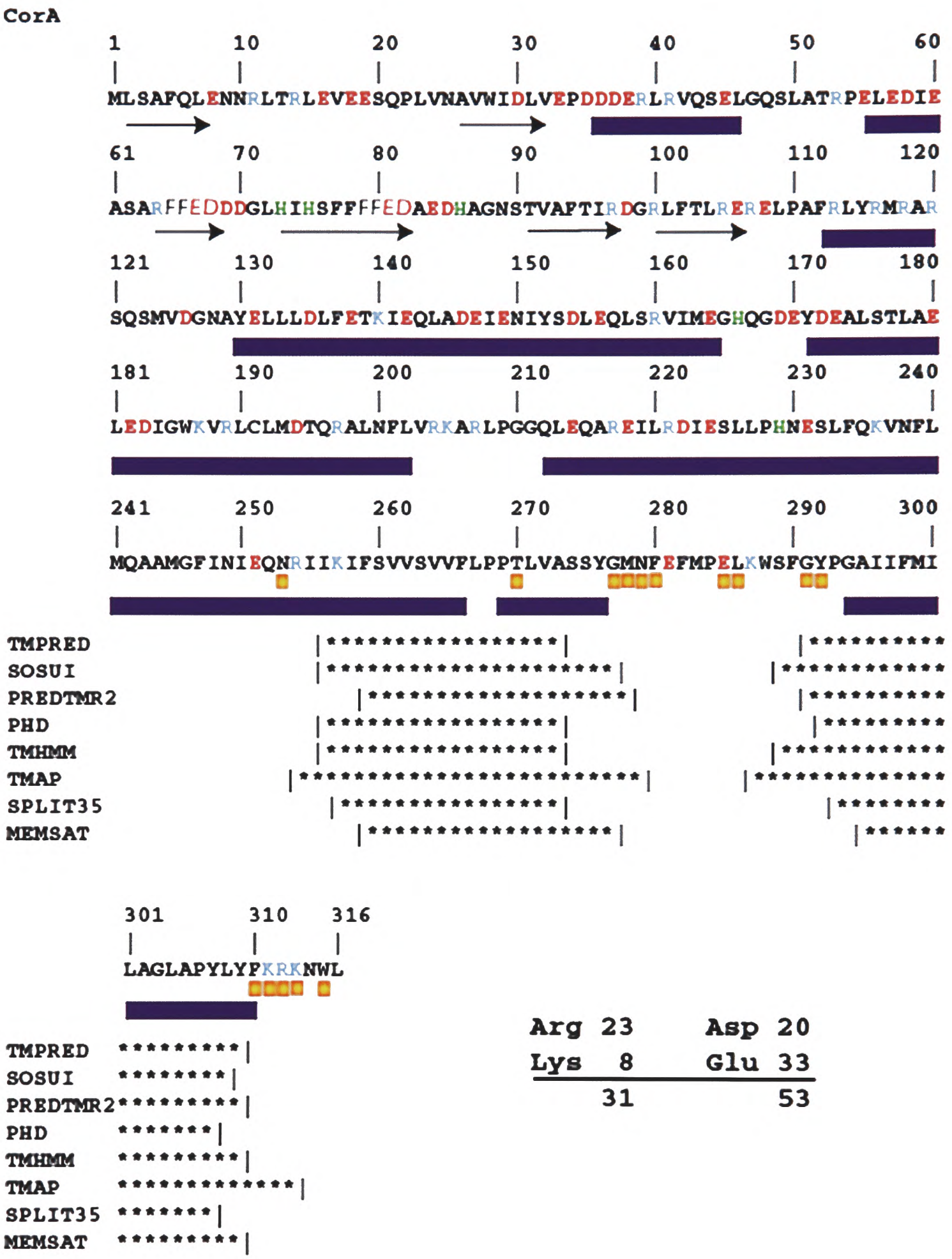


Figure 1-3. Secondary sequence predictions of the *E.coli* magnesium transporter. Bars represent helixes and arrows represent β-sheets predicted using the program PSIPRED. Stars represent the transmembrane prediction from 7 different programs as indicated. Red colour highlights Asp and Glu residues and blue colour represents Lys and Arg residues.

1.7 The layout of this thesis

The thesis is divided into six chapters. **Chapter 1** introduces the projects covered in this thesis. **Chapter 2** describes how we crystallised a chloride ion channel from *E .coli.* **Chapter 3** covers cloning of the magnesium transporter domain and expression of the protein. **Chapter 4** will review the whole family of inwardly rectifying potassium channels and describe the biochemistry and crystallisation procedures used during the structural analysis of the bacterial Kir channel KirBac1.1.

In order to understand the gating process of Kir channels another bacterial Kir channel (KirBac3.1) was selected as the target protein. The idea behind this comes from the fact that each new K^+ channel structure has revealed new details of all processes from selectivity to gating. We believe that a new Kir channel will add new information that will be applicable to K^+ channel activity. **Chapter 5** describes the cloning, expression, purification, and 2-D crystallisation of the KirBac3.1 channel from *Magnetospirillum magnetotacticum.* These crystals added to our knowledge of gating movements in Kir channels as will be described in this chapter. The thesis concludes in **Chapter 6** with discussions on the future directions for each project.

Chapter 2 – A chloride ion channel from *Escherichia coli*

2.1 Introduction

Chloride is the most abundant physiological anion in all cells. The cytoplasmic Cl^- concentration is always lower than that from outside cells, therefore, Cl^- channels are expected to help repolarize a depolarized cell by allowing the passive diffusion of negatively charged ions along their electrochemical gradient into the cells.

Unlike K^+ channels that mainly select potassium ions, chloride channels may conduct other anions such as Br^-, I^-, NO_3^-, HCO_3^- or SCN^-. They even pass many small organic acids hence are also called anion channels (Hille, 2001).

The chloride channels can be located in the plasma membrane or in membranes of intracellular organelles. These channels are important in the regulation of excitability in nerves and muscles, controlling cell volume and maintaining pH in organelles (Hille, 2001; Jentsch *et al.*, 2002).

Many kinds of chloride ion channels exist but not all of them have been studied or characterized at the molecular level. Today three major Cl^- channel families have been cloned and extensively studied in mammals: voltage-dependent CLC family, cystic fibrosis transmembrane conductance regulator (CFTR) and a family of ligand GABA and glycine gated Cl^- channels (Jentsch *et al.*, 2002; Ashcroft, 2000). This chapter will only focus on the voltage-gated Cl^- channels.

2.2 The voltage-gated CLC family

Approximately 20 years ago an anion channel from an electric organ of the *Torpedo* ray was discovered using biophysical techniques (Miller and White, 1984). Six years later the report of the first CLC Cl^- channel gene was published. This

voltage-gated Cl^- channel was named CLC-0 (Jentsch *et al.*, 1990). The cloning of CLC-0 led to the discovery of a large gene family of CLC chloride channels. Now we know that CLC chloride channel family is found both in prokaryotes and eukaryotes. Nine different CLC members were defined by sequence homology in mammals. They are named *CLCN1, CLCN2, CLCNka, CLCNkb, CLCN3, CLCN4, CLCN5, CLCN6* and *CLCN7* (Jentsch *et al.*, 2002).

To fully understand the functioning of any protein requires its structure to be determined. This is particularly true for an integral membrane protein like a CLC channel as structural prediction of membrane proteins greatly lags behind that for soluble proteins. The best approach at present is to start with a prokaryotic member of the integral membrane protein family. This provides the opportunity for high-level protein expression in the *E. coli* system. Fortunately for the CLC channel research field, *E. coli* has a number of CLC genes as part of its genome. This opens up the possibility of structural studies using the *E. coli* CLC genes.

Successful over-expression of the bacterial chloride channel in *E. coli* produced sufficient quantities of channel protein required for 3-D crystallisation trials. As a consequence, two bacterial chloride channel structures emerged two years ago (Durzler *et al.*, 2002). Although both bacterial channels lack the C terminal CBS domains found in mammalian CLC channels, the structures revealed the architecture of this important family of channels. The structure showed that a chloride channel has a total of 18 α-helices.

2.3 General features of the CLC family

2.3.1 Topology

The 3-D structure of the bacterial CLC protein showed that these channels have an unusual topology (Durzler *et al.*, 2002). The membrane-associated part of the CLC channel is composed of 17 α-helices with one helix located in the cytoplasm. To everyone's surprise most of the helices vary in length and are not perpendicular to the membrane surface. Many of the helices are tilted, with some up to 30-45°. Also, not all of the helices span the width of the bilayer (Figure 2-1-A).

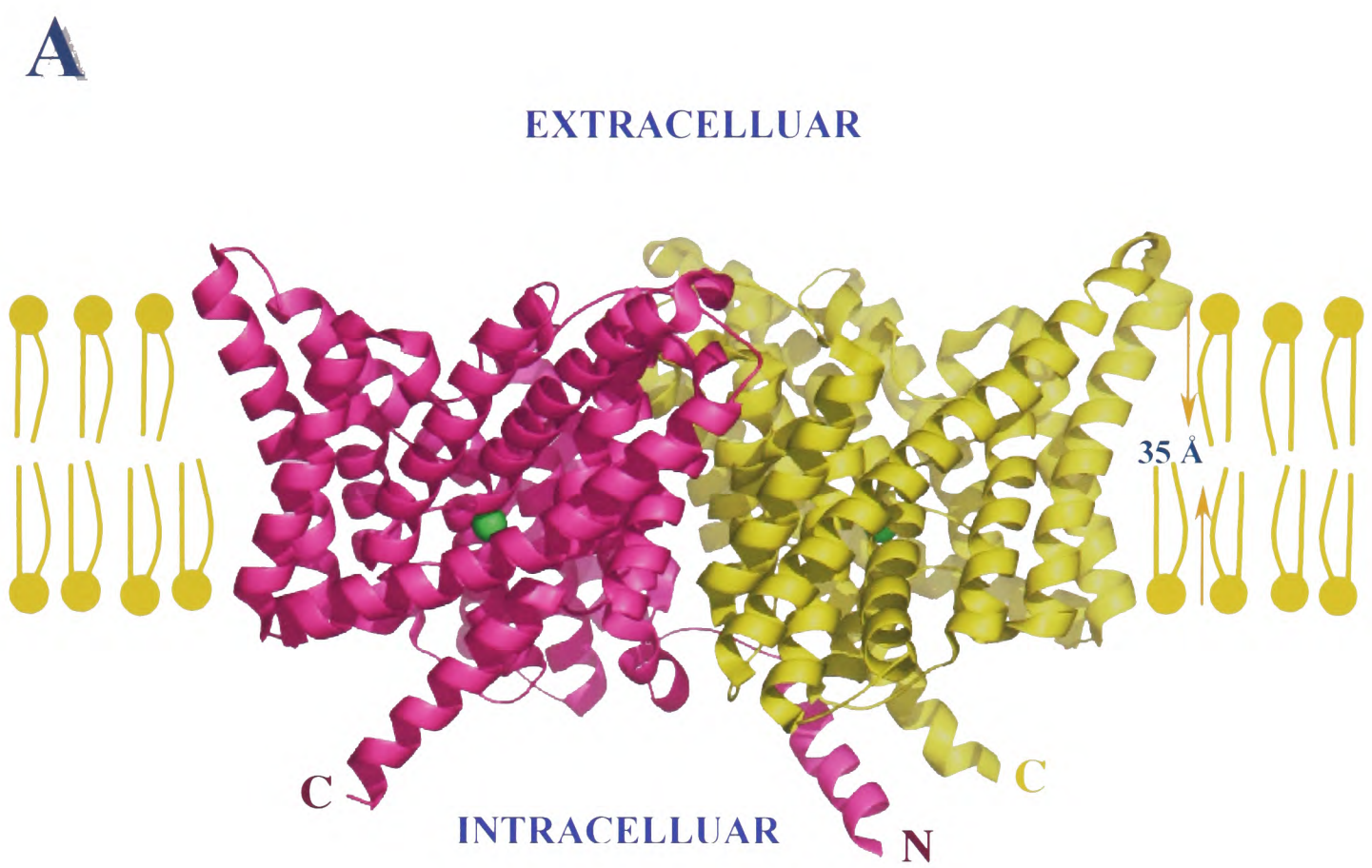


Figure 2-1. Structural overview of the bacterial CLC channel from *Salmonella typhimurium* (StCLC) (Dutzlet *et al.*, (2002).
A. The side view of a CLC channel in the membrane. The magenta and yellow colours represent two subunits of the StCLC channel. The N terminus of the yellow subunit was not ordered and excluded in the PDB file.
B. An extra-cellular view of a channel showing two identical subunits identified by magenta and yellow colour.
The models are generated using PyMOL program. The StCLC PDB code is 1KPL.

2.3.2 Dimers

All CLC channels are believed to be dimers and behaved as 'double-barreled' channels. This means that the active channel has two independent ion conduction pathways like a double-barreled shotgun. The conclusion was based on:

1. The single channel recording of the *Torpedo* channel CLC-0 showed two open conductance levels of equal amplitude (Middleton *et al.*, 1996).

2. The co-expression of both mutant and wild-type subunits of CLC-0 showed two conductance levels in single-channel recordings (Ludewig *et al.*, 1996).

3. Extended studies of co-expression of a concatameric construct of CLC-0 with CLC-1 or CLC-0 with CLC-2 displayed two different conductances. In a single channel recording one pore displayed CLC-0 properties while the other pore displayed either CLC-1 or CLC-2 properties depending on the tested construct. This further indicated that each monomer of a chloride channel formed a self-contained pore (Weinreich and Jentsch, 2001) (Figure 2-1-B).

4. The 3-D structures of two bacteria chloride channels confirmed that a functional channel was formed by dimers (Figure 2-1-A).

2.3.3 Filter region

The filter region in a chloride channel is made up with the helices of αN, αF and αD (Figure 2-2).

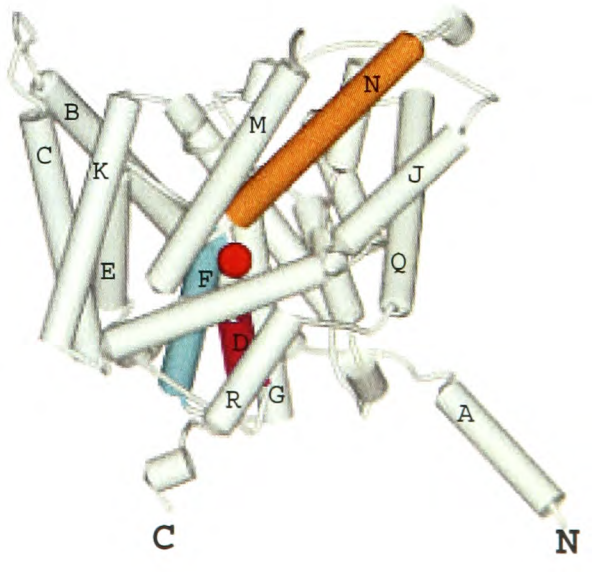


Figure 2-2. One subunit of the StCLC.
The α helices are drawn as cylinders. The helix αN is colored orange, αF is colored light turquoise and αD is colored magenta with a Cl⁻ ion in red. The model is generated using WebLab ViewerPro5.0.
The StCLC PDB ID is 1KPL.

Their amino termini are directed toward the center of the selectivity filter with each positive end of the dipole being oriented toward the pore. This creates a partial positive charge that forms part of the ion binding site. The helices form a funnel structure directing the Cl^- ions into the filter. Once the Cl^- ion enters the filter region the binding site is dominated by backbone amide nitrogen atoms of Ile^{356} and Phe^{357} and interactions with the side-chain oxygen atoms of Ser^{107} and Tyr^{445} (Figure 2-3).

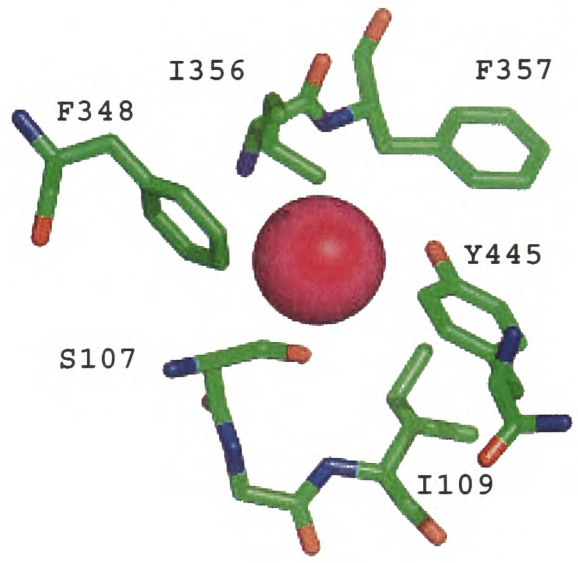


Figure 2-3. The Cl^- ion binding site.
In the structure the magenta sphere represents one Cl^- ion and the atoms are colored according to their type with carbon in green, oxygen in red and nitrogen in blue.
The structure is drawn with PyMOL and PDB ID is 1KPL.

2.3.4 Gating

Extracellular anions and pH play an important role in modulating gating (Pusch *et al.*, 1995; Chen and Miller, 1996). Statistical analysis proved that CLC-0 channels conduct ions in such a way that one pore opens and closes independently of the other pore. This phenomenon of opening and closing is called **fast gating**. The outside chloride concentration modulates the channel opening in which the binding of the chloride within the pore promotes the opening of the channel (Pusch, *et al.*, 1995; Chen and Miller 1996). Another unusual event is dependent on both subunits of the CLC-0 dimer closing simultaneously. This process is called **slow gating**. The slow gate is a function of both subunits (Ludewig *et al.*, 1996). Further studies are necessary in order to reveal whether slow gating is a common feature in the CLC family.

The recent 3-D structure of the bacterial chloride channel identified the fast gating element as glutamate residue 148 in helix F. This Glu^{148} is a conserved residue among the chloride channels. Its side chain projects into the center of the filter region and acts as a blocking residue suggesting a closed conformation of the channel (Figure 2-4 and Figure 2-5).

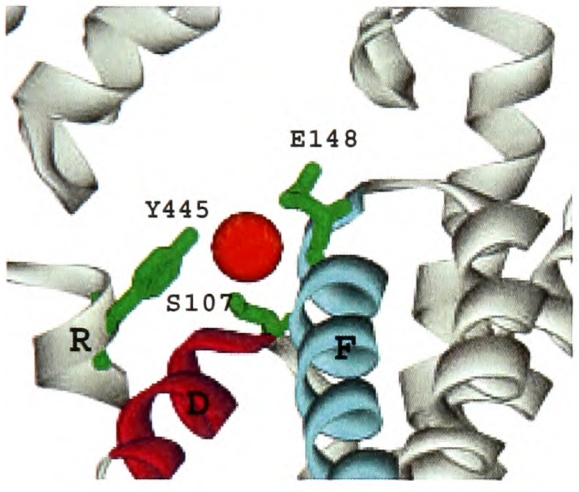


Figure 2-4. A cut-away view of the Glu^{148} blocking region.
αF is colored light turquoise and αD is colored magenta with a sphere Cl^- ion in red. Side chain atoms are in green. The model is generated using WebLab ViewerPro5.0.
The StCLC PDB ID is 1KPL.

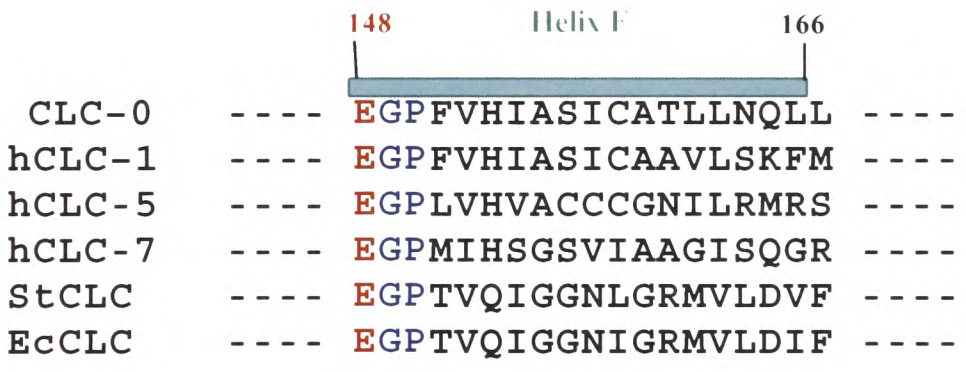


Figure 2-5. Sequence alignment of the helix F of CLC channels.
The colored letters indicate the conserved residues in helix F among CLC channels.

In order to let the Cl^- ion through the filter region, the glutamate side chain must move away from its position in the crystal structure. The recent new structures of the EcCLC mutants E148A and E148Q show a potential open channel conformation (Dutzler *et al.*, 2003). This result supports the glutamate residue 148 as

a control residue in the filter region. It is likely that the glutamate side chain controls ion movement by blocking and unblocking the ion conduction pathway.

2.4 Same *E. coli* chloride channel different crystal forms

Although our group worked on the same *E. coli* chloride channel as Dutzler, our crystal forms were significantly different. The crystal form that we produced was difficult to work with due to the ever-changing unit cell dimensions. As a result the structural determination process was greatly delayed. This gave the advantage to our competitors, allowing them to solve the structure first.

All was not lost for we learnt a great deal about working with integral membrane proteins on this difficult project. This information we were able to apply to a later project which proved to be successful.

One of the major difficulties in structure determination of membrane proteins is finding relatively good quality crystals. Often detergents in the crystallisation set up prevent the formation of good diffracting crystals. The cause of the change in unit cell dimensions in our CLC channel crystals was a result of dehydration. It eventually transpired that as the crystals lost water this improved the limits of diffraction. This provided a simple method for improving the diffraction limit of a membrane protein crystal. Chapter 2 reports the scientific evidence for this result.

2.5 Methods

2.5.1 Outline of methods

The procedure for CLC experiments is highlighted in Figure 2-6.

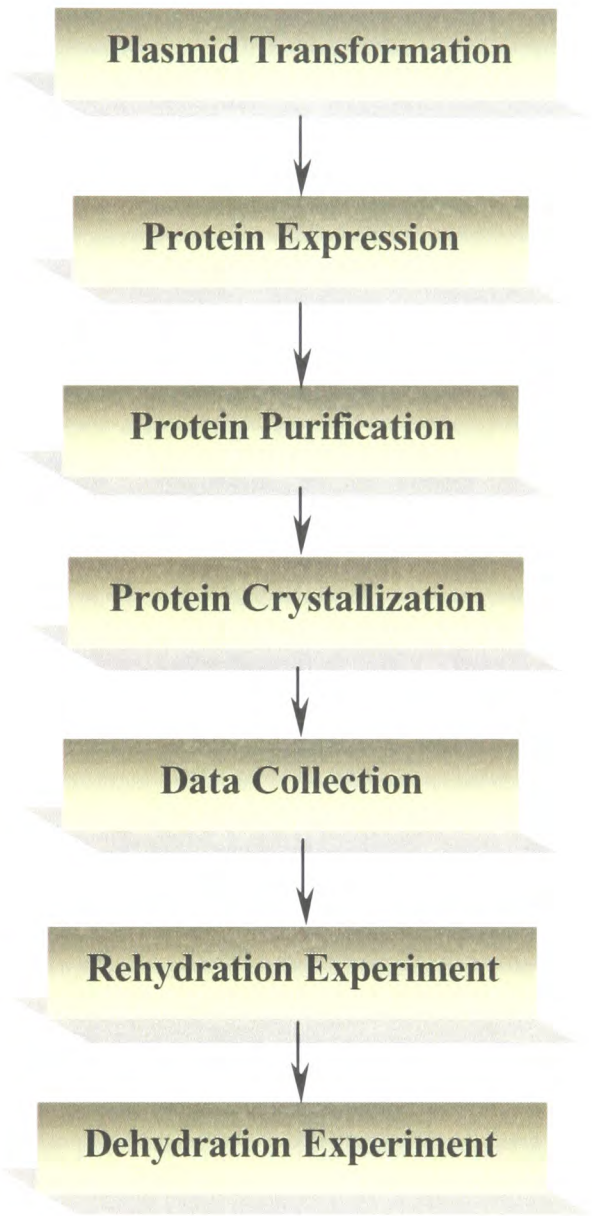


Figure 2-6.

Flowchart indicating procedures employed in the chloride ion channel project in the chapter 2.

2.5.2 Plasmid transformation

The *E. coli* chloride channel (EcCLC) was cloned into the pET-30a vector (Bowler, 2001). The construct was named pCl2B3. Each preparation always started with freshly transformed BL21(DE3) cells one day before the protein expression. The plate was monitored properly in order to prevent the colonies from overgrowing. If the colonies were grown too large on the plate this generally had a detrimental effect on the protein yield.

2.5.3 Protein expression

Transformed cells were grown in TB media at 37°C until they reached an OD_{600} value of approximately 1.3. A total of 6 litres of TB were used for each preparation. The protein expression was induced with 0.25 mM isopropyl-ß-D-tiogalactopyranoside (IPTG) in a shaker-incubator at 36°C for 6 hours.

2.5.4 Protein purification

The cells were then harvested by centrifugation in a Beckman Avanti™ J-20 at 4,200 g for 20 minutes. The pelleted cells were suspended in suspension buffer (50 mM Tris-HCl pH 8.0, 200 mM NaBr and 0.4 M glucose). Protease inhibitor cocktail (5 µM leupeptin, 5 µM pepstatin A, 1 mM benzamidine and 1 mM PMSF) was added.

Cells were lysed using a high-pressure homogenizer at 6°C. The lysed cells were brought to a final volume of 180 ml. All membrane proteins were extracted using 40 mM $Zwittergent_{3\text{-}12}$ (Fluka) on ice for 2 hour 30 minutes. Extract was centrifuged at 18.5 K rpm for 40 minutes in a Beckman J-20 centrifuge.

The supernatant was collected and TALON cobalt resin (Clontech, U.K.) was added to it. The solubilized Cl^- channel bound to the cobalt resin using the his-tag at the C-terminal end of the protein. The batch binding was performed on ice for 1 hour.

The resin was subsequently transferred to an Econo-column (Bio-Rad) and washed with both Buffer I and Buffer II (Table 2-1).

The Cl⁻ channel was eluted in Elution Buffer (Table 2-1). The detergent lauryl dimethylamine N-oxide (LDAO) was used in the crystallisation setup. To ensure complete detergent exchange, LDAO was solely used during the wash and elution steps.

Table 2-1. Wash, elution and dialysis buffers used in the purification of EcCLC

Components	*Buffer I*	*Buffer II*	*Elution*	*Dialysis I*	*Dialysis II*
Tris-HCl pH8.0	50 mM	50 mM	50 mM	50 mM (pH 7.5)	50 mM
NaBr	1.0 M	200 mM	200 mM	200 mM	200 mM
LDAO	10 mM	10 mM	10 mM	5.0 mM	1.5 mM
Imidazole	0 mM	10 mM	400 mM	0 mM	0 mM

The peak fractions were combined together and dialysed overnight in 200 ml of dialysis buffer I to reduce the imidazole and detergent concentrations. All the purification steps were carried out at room temperature.

The Cl⁻ channel protein was removed from the dialysis tubing and concentrated to approximately 7 mg/ml in a Centriprep 50 (Millipore). A Bio-Sil SEC250 silica based column (Bio-Rad) or Superdex 200 (Pharmacia) was used during size exclusion chromatography.

The column was equilibrated with 30 ml of dialysis buffer I (Table 2-1). A total of 1.5 mg of protein was injected onto the column at a flow rate of 0.5 ml/minute with dialysis buffer I. The elution profile was monitored at 280 nm.

After gel filtration the protein was concentrated in a Centricon 50 (Millipore). Two ranges of concentration were chosen, a high concentration of Cl channel protein between 19 and 20 mg/ml and a low concentration of protein between 7 and 10 mg/ml. The concentration was measured by absorbance at 280 nm. The protein was dialyzed in a Spectra/Por 50,000 Da molecular weight cut off membrane bag in 100 ml of Dialysis buffer II (Table 2-1) overnight at room temperature. Three concentrations of LDAO were tested in the final dialysis buffer: 1.5 mM, 2 mM and 3.0 mM LDAO.

2.5.5 Protein crystallisation

Commercial screen kits Cryo I and II, Wizard I and II from Emerold BioStructures (USA) and crystal screen kits MDL I and II from Molecular Dimensions Laboratory (UK) were used. A twenty-four sitting drop well tray (Cryschem MVD/24) was purchased from Charles Supper Co. (USA).

After the initial crystallisation conditions were identified, they were optimised to 22-28% Jeffamine ED2001 and 0.1 M Bis/Tris-HCl pH 6.2 – pH 6.8. All crystals were grown using the sitting drop vapor diffusion method. Each reservoir contained 300 µl of the appropriate buffer. Equal volumes of protein and reservoir solution (2 µl by 2 µl) were added without mixing in the well. Then the top of the tray was sealed with Crystal Clear tape. In the adding cobalt experiment 1 mM cobalt was added to the protein prior to setting up the trays with the rest of the steps kept the same as the normal procedures.

The trays were incubated at 20°C for 3 to 4 weeks before crystals appeared. Crystals steadily grew over a period of 7 to 8 weeks.

2.5.6 Data collection

The quality of the crystals was tested in-house first. Crystals were removed from the well using a nylon cryoloop attached to a nickel base and directly frozen in the cryostream, 100 K nitrogen gas stream. Each crystal was exposed for 40 minutes with an oscillation angle of 1°. Some crystals diffracted to approximately 8 Å resolution limit indicating that the quality of the crystals had improved as the initial crystals diffracted to approximately 20 Å resolution in-house.

Most datasets were collected from crystals that were frozen directly in the nitrogen gas stream (100 K) at a Synchrotron X-ray source (Daresbury, beamline 14.2, ESRF/Grenoble, beamline 14.2 and 14.4, and Hamburg/Germany, beamline X11). For those crystals with high mosaicity 1° angle oscillation was used.

2.5.7 Rehydration experiment

To establish that the change in unit cell lengths was a result of an alteration of the water content in the crystal, a large 3 months old crystal, 0.2 mm x 0.2 mm x 0.5 mm, was chosen so that crystal-to-crystal variation could be avoided. The crystal was fragmented into three pieces, X, Y, and Z using a fine needle. The three fragments were placed into three separate crystallisation conditions that varied in the length of time they were set up. It was believed that slow loss of water occurred through the crystallisation trays over time. Table 2-2 listed all the components in this experiment. After the crystal fragments were transferred into the soaking solution all fragment morphologies were monitored under a dissecting microscope.

Table 2-2. Rehydration of an EcCLC protein crystal

Name of the Crystal Fragment	Reservoir Condition	Soaking Length
X	36% JeffamineED2001, 0.1M Bis/Tris, pH 6.6 (90 days)	Without soaking as a control.
Y	36% Jeffamine ED2001, 0.1M Bis/Tris, pH 6.6 (12 days)	Soaking 4 hrs before data collection.
Z	36% Jeffamine ED2001, 0.1M Bis/Tris, pH 6.6 (9 days)	Soaking 4 hrs before data collection.

Note:

1). The well contained a 1:1 ratio of protein buffer (50 mM Tris, pH 8.0, 200 mM NaBr and 2 mM LDAO) and reservoir solution.

2). The sizes of the fragments were not the same as each other since the fragments were taken based on the natural cracks in the crystal.

In order to determine the unit cell lengths four images were collected for each crystal fragment at 0^{o}, 30^{o}, 60^{o} and 90^{o}. The method of data collection used here is the oscillation method which rotates the crystal around a single axis to the X-ray beam (Dauter, 1999). The rotation angle is 1^{o} and all the crystals were exposed between 10 and 60 seconds depending on the X-ray sources. MOSFLM was used to auto-index the images (Leslie, 1992). CCP4 programs were used for data reduction (Collaborative Computing Project No.4, 1994).

2.5.8 Dehydration experiment

Several methods were used for removing water from EcCLC protein crystals.

Method 1: After crystals formed the Jeffamine concentration of the reservoir solution was slowly increased from 26 % to 46 % by increments of 4 % a time every week. The whole procedure lasted 5 weeks.

Method 2: After crystals formed, several small holes were punched in the seal above the crystallisation setup using a fine needle. The trays were also in the incubator for a total of 5 weeks.

Method 3: After crystals formed, the crystal trays were left for more than 90 days in the incubator. This acted as a control.

Method 4: After crystals formed, the tape was peeled off for 1 or 2 minutes before closing again. This was repeated once a week for a total of 5 weeks.

2.6 Results and Discussion

2.6.1 Protein expression and purification - results and discussion

Each **protein expression** always used fresh transformed cells because expression levels can vary substantially among colonies. The whole plate was used to inoculate the medium.

The culture medium, cell density and post-induction length are important factors in the EcCLC protein expression. TB medium is a very rich medium that typically leads to higher cell density with more protein expressed. For best expression levels, the induction time was found to be 6 hours.

During **protein purification** all the wash and elution steps were monitored using an Econo UV monitor (Bio-Rad) attached to a chart recorder. The presence of protein was determined by following the change in absorbance at 280 nm (Figure 2-7). We lost a significant amount of Cl⁻ channel protein during the Buffer II wash step. The low concentration of imidazole in the wash buffer II was used to remove non-specific binding proteins. The wash buffers are essential for removing many contaminants. One of the contaminating proteins was just a little larger than the channel protein and this contaminant was washed away only when the wash buffer containing 10 mM imidazole.

The SDS-PAGE gel showed a high molecular weight contaminant band just above the Cl⁻ channel protein that was removed at the Buffer II wash step (Figure 2-8). Even though 30 % of the Cl⁻ channel protein was removed during this step, we still managed to obtain 3 - 5 mg/litre of protein after the Co^{2+} affinity purification step.

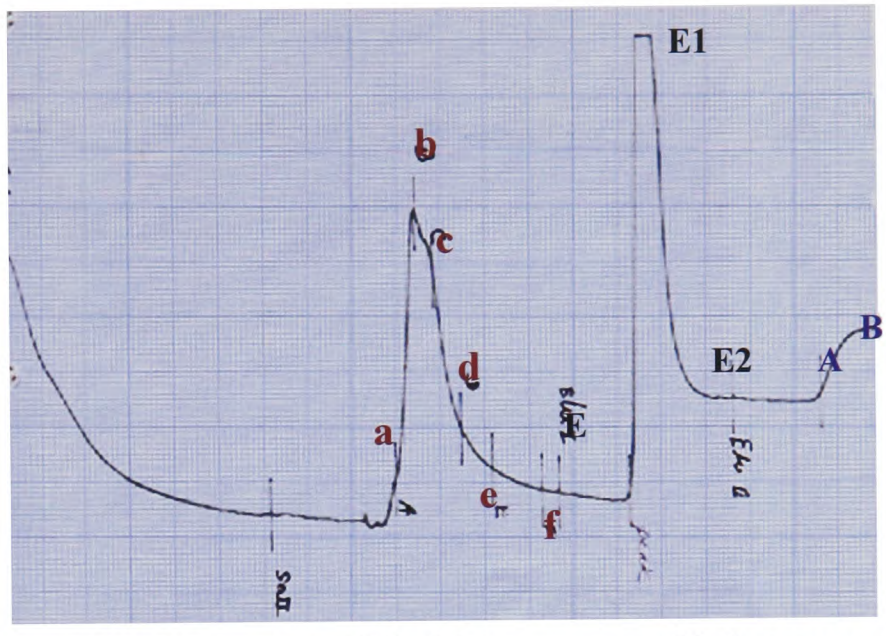


Figure 2-7. Chromatogram showing Cl^- channel eluted from a Co^{2+} affinity resin.
All proteins were monitored at A280. Fractions **a** through **f** were eluted with a low concentration of imidazole wash. **E1** was the main peak after the application of the elution buffer. Peak **A** and **B** were the peaks after using 500 mM imidazole buffer after the elution.

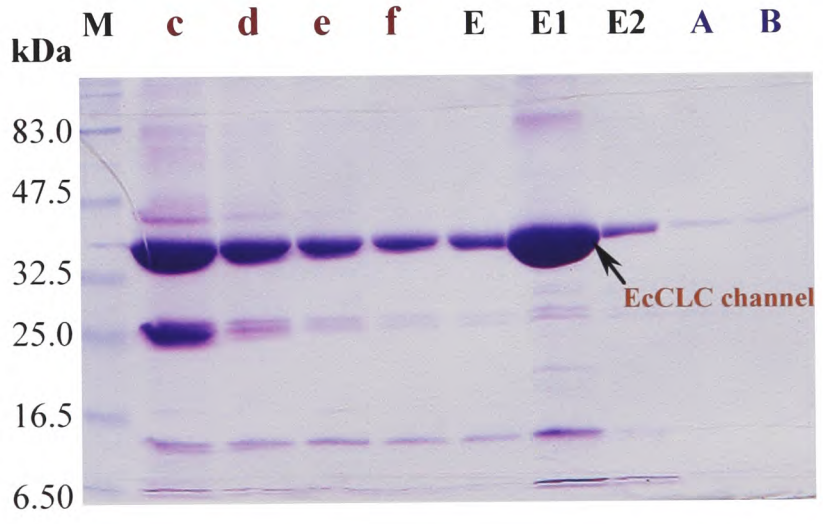


Figure 2-8. 12% SDS-PAGE gel of EcCLC Cl^- channel fractions during IMAC purification.
A volume of 12 μl from each fraction was loaded into each well.

During purification the EcCLC protein was stable as a dimer in the detergent Zwittergent$_{3\text{-}12}$. Further purification was carried out by analytical size exclusion chromatography and yielded a protein purity of higher than 95 %. After the protein was concentrated a Coomassie Blue-stained SDS-PAGE gel of the purified sample showed a 36 kDa monomer. The size of the monomer was smaller than the expected 50.35 kDa as calculated from the protein sequences (University of Geneva; http://www.expasy.ch). This phenomenon is often observed with membrane proteins since the SDS detergent is a native like environment for membrane proteins (Wang, 2003). Interestingly there was a weak dimer band above the monomer in the SDS-PAGE gel (Figure 2-9 A, Figure 2-9 B).

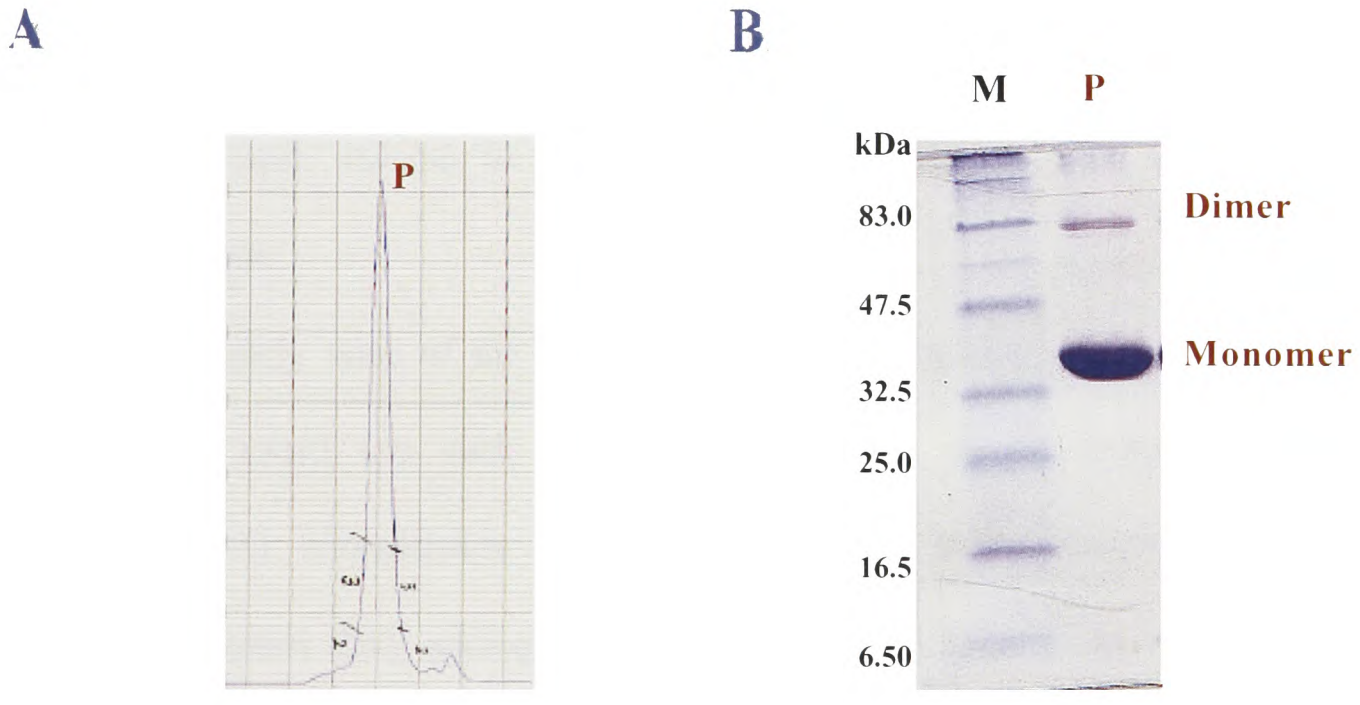


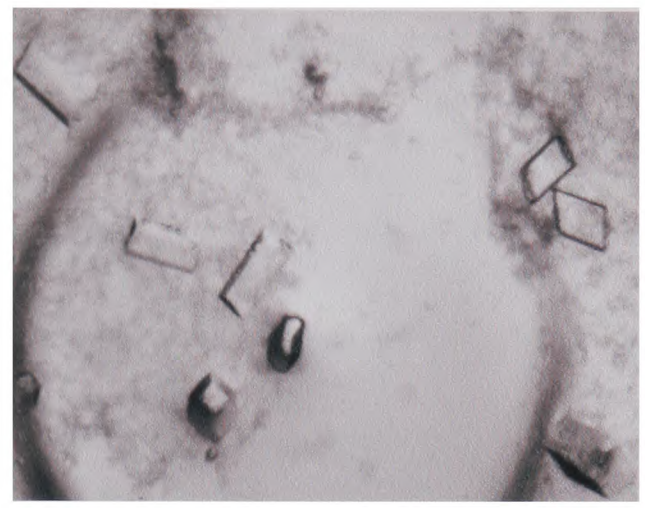
Figure 2-9-A. Size exclusion chromatogram.
Figure 2-9-B. The corresponding 12% SDS-PAGE showing the Cl^- channel.
The **P** represented a peak fraction that was concentrated to 10 mg/ml. A total of 10 μg of protein was loaded on the gel.

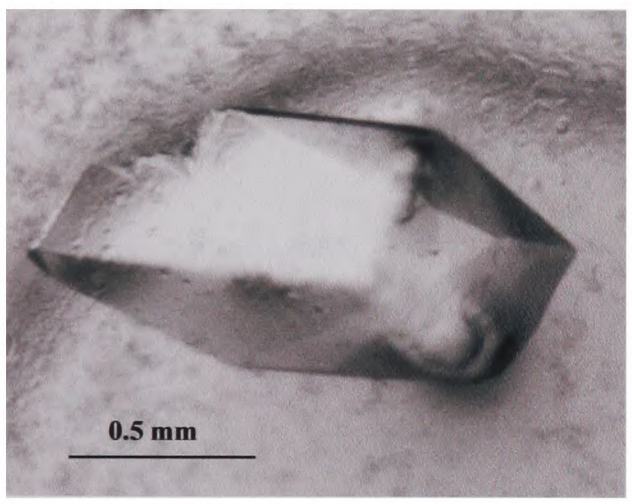
2.6.2 Protein crystallisation and data collection - results and discussion

The concentration of detergent is critical to the formation of crystals. If the concentration of the detergent is too high the protein may not form good crystals. After the gel filtration step the protein was concentrated resulting in the concentration of the detergent too. To overcome this problem the concentrated protein always was dialysed in a Spectra/Por 50 K Da molecular weight cut off membrane bag in 100 ml of Dialysis II buffer for at least 12 hours before setting up crystal trays.

Initially after the refined crystal screen condition was used all of the crystals diffracted poorly, approximately 6 - 7 Å resolution limit even though some crystals were large, approximately 0.2 mm x 0.2 mm x 0.5 mm. In an attempt to improve the quality of the crystals repeated channel preparations were performed in different ways such as using a new LDAO batch, finding another supplier of LDAO, increasing the wash volume to remove binding of non-specific protein from the cobalt resin and decreasing the wash volume to include the contaminants in case one contaminant aided crystallisation.

Unfortunately none of the methods improved the quality of the crystals. Other methods were tested too such as changing to DM as an extracting detergent, decreasing LDAO concentration from 2 mM to 1.5 mM, changing gel filtration column to Superdex 200, adding 1 mM cobalt to the protein (in case of leaching cobalt from the resin supported crystallisation) and changing crystallisation temperature to 15°C or 25°C. The crystals still diffracted poorly (Figure 2-10). Table 2-3 indicates the unit cell dimensions from a number of these crystals.





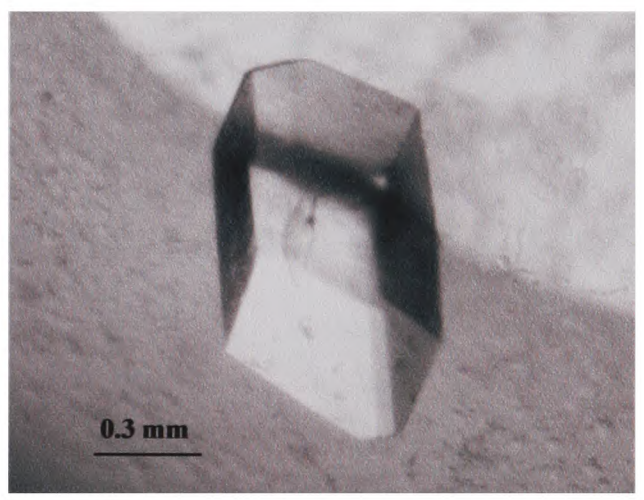


Figure 2-10. Cl^- channel crystals grown using Jeffamine ED2001 as a precipitant. The pictures show the Cl^- channel crystals grown in 26% Jeffamine ED 2001, 0.1 M Bis-Tris-HCl pH 6.6 after 8 to 10 weeks.

Table 2-3. Unit cell dimensions of the *E. coli* Cl^- channel crystals

Crystals Orthorhombic P222	*a*	*b*	*c*	Resolution Å
1	95.87	102.12	120.92	8.0
2	103.20	108.20	139.74	7.5
3	102.96	108.04	141.60	7.0
4	99.10	104.84	122.78	4.5

It was noticed that after each synchrotron trip the unit cell dimensions of the crystals were different (Table 2-3). This was most apparent for the *c* axis. In a number of cases several crystallisation setup trays were brought to two or three consecutive synchrotron trips. It was observed that the solution around the crystals became more viscous as compared with the previous time the crystallisation well was opened. A data set was collected from a crystal taken from a well that was previously used for data collection. To our surprise the resolution increased and the estimated mosaicity decreased. This was the initial indication that the change in cell dimensions occurred because of a dehydration process.

2.6.3 Rehydration experiment - results and discussion

To confirm the change in unit cell lengths was a result of an alteration of the water content of the crystal a large 3 months old crystal was tested in Daresbury. Table 2-4 listed the rehydration result after fragments Y and Z were soaked in a stabilized solution for 4 hours.

Table 2-4. Unit cell lengths and mosaicity values from three fragments of the same crystals

Fragment	Unit cell length (Å) (*a* *b* *c*)	Resolution (Å)	Esimated mosaicity(°)	Space Group *Othorhombic*
X	93.86 100.98 117.68	4.9 – 5.0	1.8	P222
Y	94.11 104.02 124.02	5.0	6.0	P222
Z	94.18 103.14 131.08	5.0	4.0	P222

After soaking for four hours there were no observable morphological changes in fragment Y or Z as observed under a microscope. After data collection images were processed using MOSFLM. It was found that the unit cell's ***c*** axis increased dramatically up to 13.4 Å in fragment Z. Both Y and Z fragments were accompanied by a large increase in the mosaicity (Table 2-4). It was noticed that the unit cell's ***c*** axis in fragment Y increased less than the fragment Z. The well for fragment Y was equilibrated 12 days earlier resulting in a greater loss of water from this well than from the well for fragment Z. This produced a lesser degree of expansion for fragment Y than for Z.

2.6.4 Dehydration experiment - results and discussion

The rehydration experiment indicated that water content is important in crystal order. When we reduce the water in the EcCLC crystals, the mosaicity reduced and the resolution increased. Several crude experiments were tried without much success to remove water. The following table (Table 2-5) summarized the results of four methods that were carried out.

Table 2-5. Dehydration of EcCLC channel crystals

Name	Experiment	Diffraction Resolution	Mosaicity(°)	Space Group *Othorhombic*
Method 1	Change concentration of Jeffamine from 26%-46%	6 to 7 Å	2.0-3.0	P222
Method 2	Punching small holes on the top seal.	very poor 8 to 9 Å	around 2.0-4.0	P222
Method 3	Without any treatment for more than 90 days.	around 4.5 Å	2.0	P222
Method 4	Peel off the top seal for 1 to 2 minutes every week.	5 to 6 Å	2.0-3.0	P222

Note: Several crystals were tested for each method.

All attempts to remove water quickly from the crystals resulted in poorly diffracting crystals except the control method which left the tray at 20°C untouched over the experimental period. After processing the data set the unit cell lengths were 96.00 x 103.64 x 122.40 Å.

About one month later the same crystal tray was brought to the synchrotron source and a data set collected from another crystal in the well that was used previously. The mother liquor in the well was very viscous making it difficult to mount the crystal. This time the unit cell dimensions were 93.69 x 100.96 x 117.60 Å. The crystal diffracted to 4 Å and the mosaicity was around 1.0° to 1.5°. It was noted that all of the crystals in the tray were cracked (Figure 2-11).

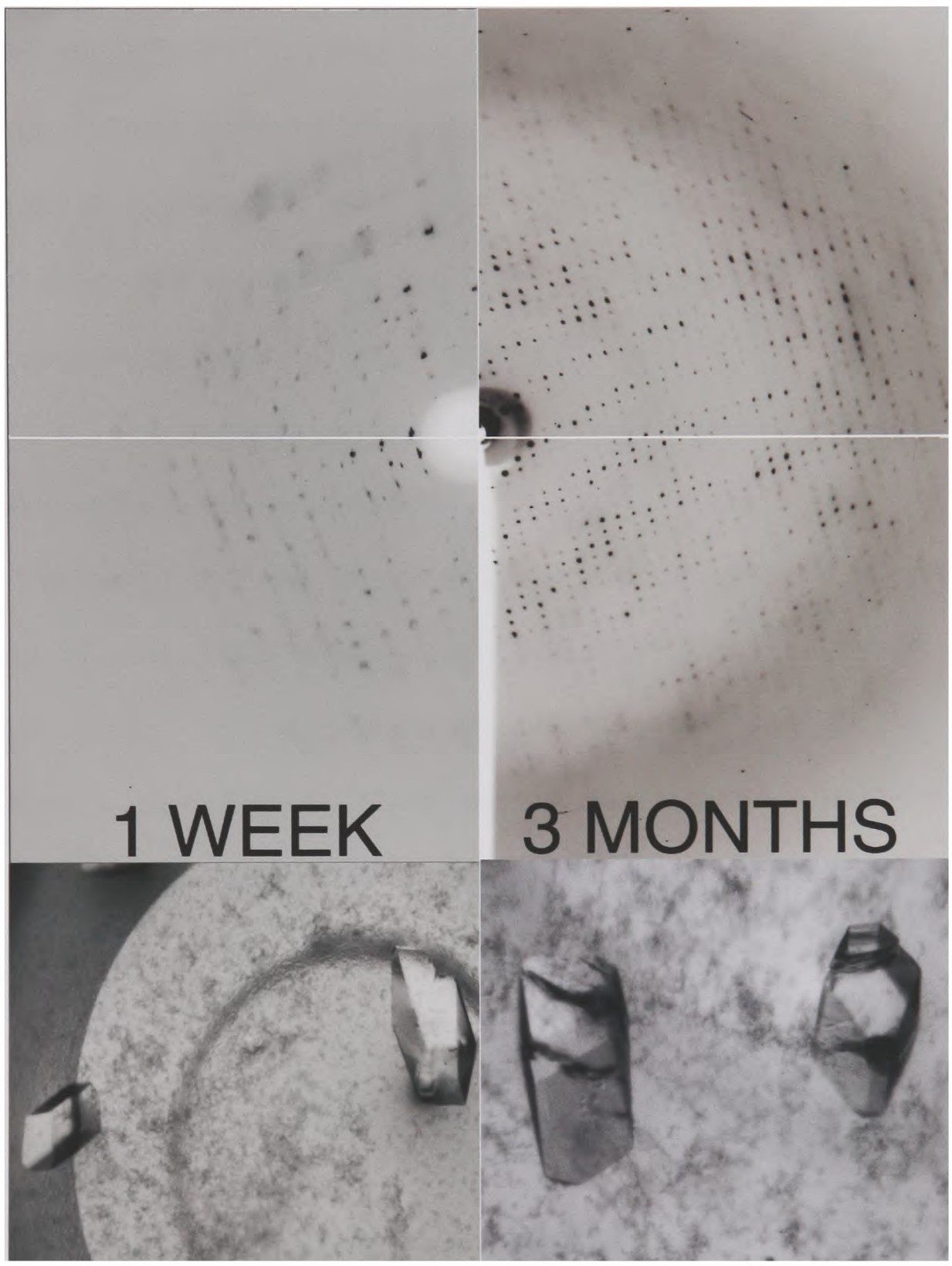


Figure 2-11. Diffraction images and crystal appearances before (left) and after (right) dehydration.
The pictures show the Cl^- channel crystals grown in 25% Jeffamine ED2001, 0.1 M Bis-Tris-HCl pH 6.6 over a period of 3 months. The dehydrated crystal was broken into pieces using a needle and the partial crystal mounted directly in the cryostream before data collection.

Data sets were only collected from crystal fragments by breaking the crystals along their natural fracture lines using a fine needle. Many data sets were collected to characterize the change in unit cell dimensions.

One of the drawbacks of membrane protein crystallisation is the anisotropic nature of the crystals as a result of the possible lack of protein-protein contact. The dehydration changed the EcCLC crystal anisotropic nature from 8.0 x 7.5 x 7.5 Å to 4.5 x 4.0 x 3.5 Å as estimated visually from different images. However, complete dehydration resulted in total loss of diffraction.

The most difficult step in structure determination of membrane proteins is the production of good quality crystals which should be good enough to diffract to 3Å resolution or better. However, most that we have observed diffract to 4 - 5 Å. Further improvement is quite difficult. Several methods have been used to overcome the problem. The recent successful use of antibody fragments is one example (Hunte *et al.*, 2000; Zhou *et al.*, 2001; Dutzler *et al.*, 2003). This method forms a large protein-protein contact region within the crystal and decreased the detergent-detergent or protein-detergent contacts. The big drawback is that it is very expensive and time consuming project.

The dehydration method that we report here has been incorporated into the KirBac1.1 project and did improve the resolution in KirBac 1.1 crystals, indicating that it should be one of the first methods used during crystal optimisation.

Chapter 3 – A magnesium transport domain from *E. coli*

3.1 Introduction

The *E. coli* metal ion transporter *CorA* gained its name as a result of an increased cellular sensitivity to Co^{2+} ions after deletion of the gene (Silver, 1969; Nelson and Kennedy, 1971). Later the *CorA* gene was cloned from *E. coli* and *Salmonella typhimurium.* The main physiological function of CorA is to mediate Mg^{2+} transport across the cell membrane (Hmiel *et al.*, 1986; 1989). The deduced amino acid sequences of these proteins are both 316 amino acids in length and are 98% homologous (Smith *et al.*, 1993). Using southern blot hybridization and PCR techniques another eighteen gram-negative bacterial species were screened for the presence of *CorA*. It turned out that all strains were positive for the presence of *CorA* and it is therefore likely to be a major Mg^{2+} influx system in bacteria (Smith and Maguire, 1995).

Further knowledge of the molecular structure of CorA will be crucial in understanding the function of the protein. The transmembrane analysis predicts CorA to have two transmembrane helices at the C-terminal region (Figure 3-1).

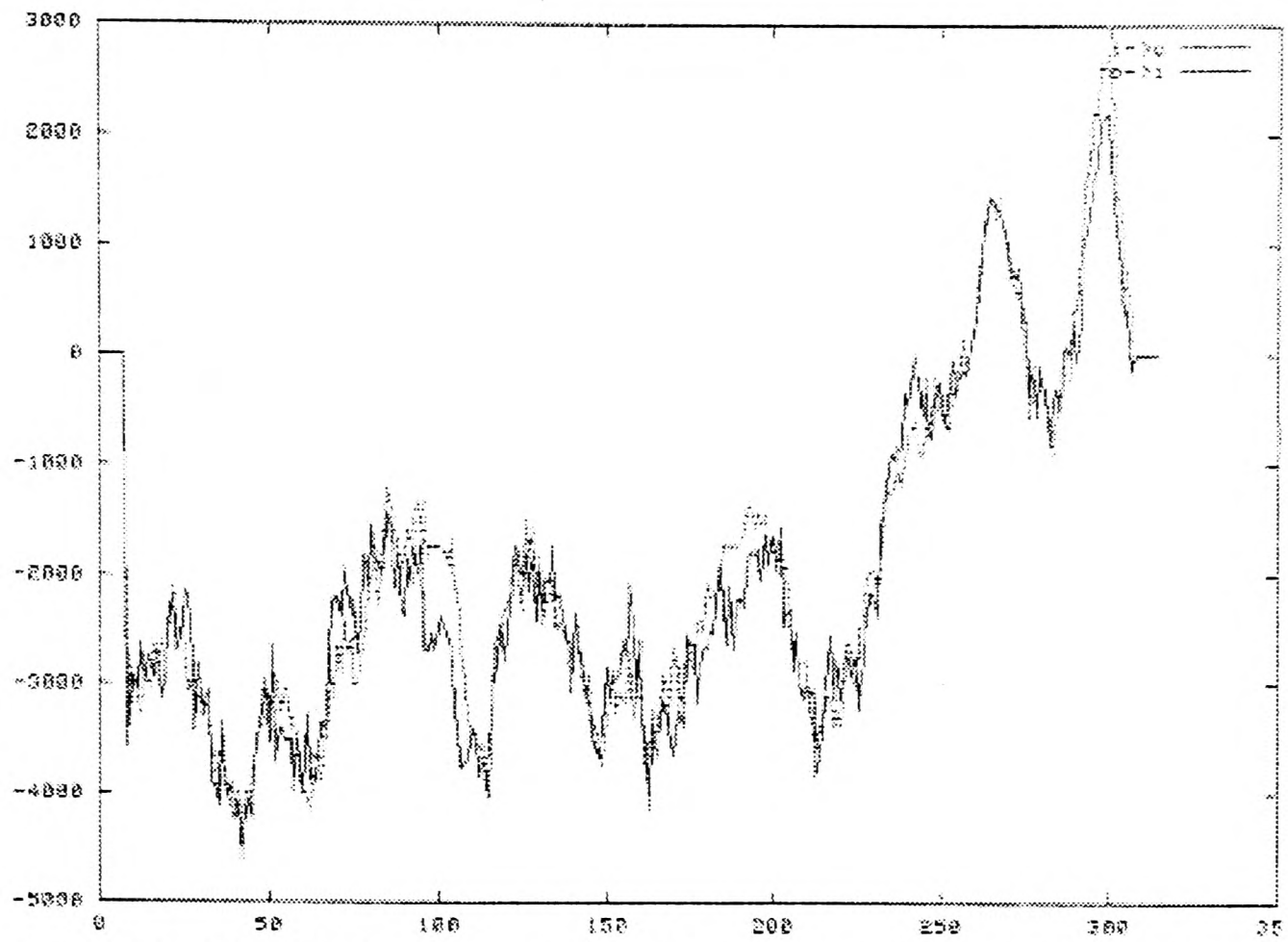


Figure 3-1. Graphical representative of the transmembrane prediction using the TMpred prediction program (Hofmann and Stoffel, 1993). The x axis shows the amino acid number, N to C-terminal. The y axis indicates the scoring numbers. In CorA the putative transmembrane segments are shown by the trace above 0.

There is the possibility that CorA has three trans-membrane helices. This is based on an enzyme tag assay (Smith *et al.*, 1993). A problem with this method is that of making the assumption that truncation of a membrane protein does not affect its native topology. It is known that some proteins do not handle a single amino acid change in a transmembrane helix and fold properly (Deber and Therien, 2002). It is possible that the chosen truncations affect the fold and orientation of the protein. Also the research did not show sufficient LacZ data to support the hypothesis. Therefore the transmembrane topology and orientation is still unclear. Based on the transmembrane helix predictions, two constructs were designed. The first one is at residue Arg^{254} and the second one is at residue Glu^{231}. The first construct includes the potential third transmembrane helix. After cloning and small scale expression of the

1-231E construct, it was noted that all of the expressed protein formed inclusion bodies. The first construct produced soluble protein, therefore, we focused on this construct.

3.2 Outlines of methods

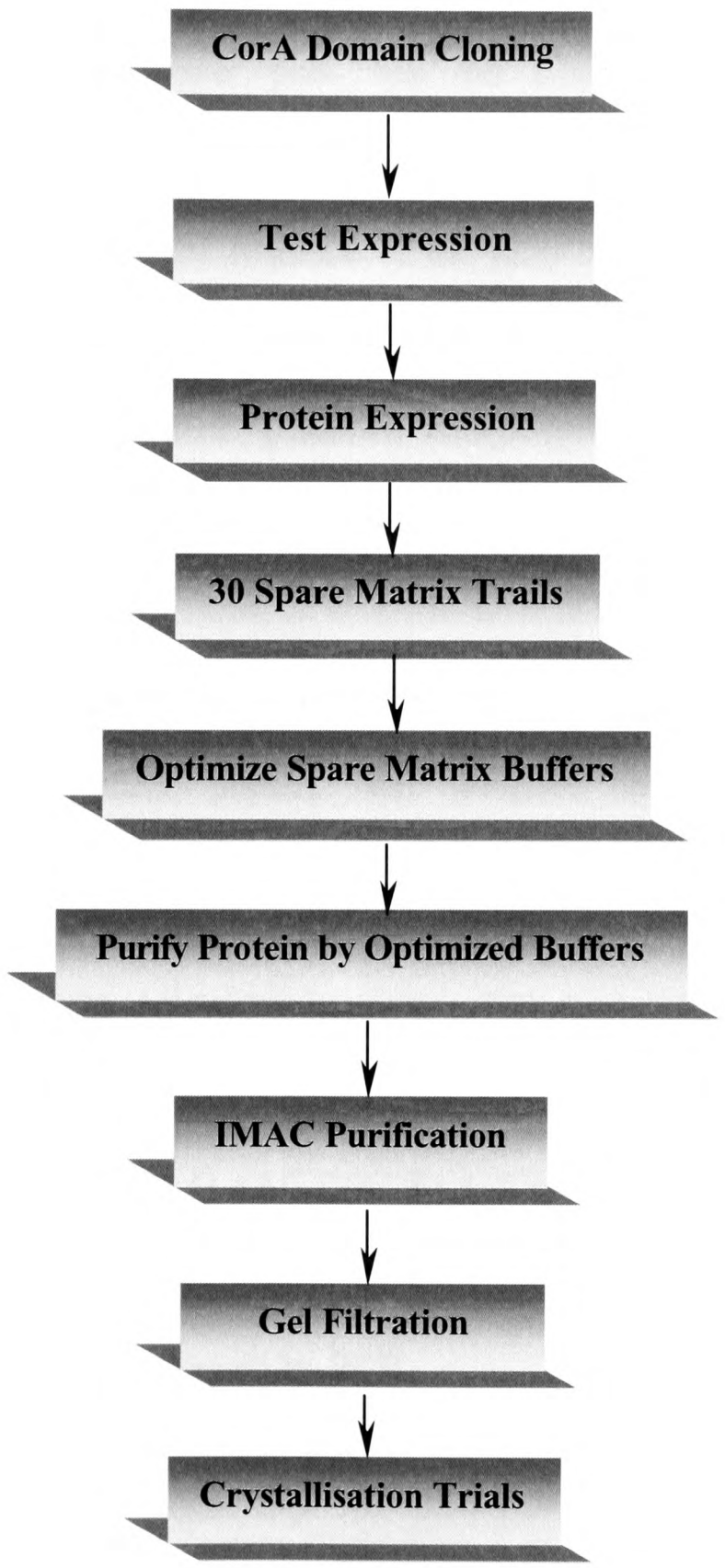


Figure 3-2.

Flowchart indicating procedures employed in the CorA domain project.

3.2.1 Cloning of the *CorA* domain

The DNA sequence of a CorA magnesium transporter gene was obtained from PubMed BLAST (Basic Local Alignment Search Tool, Altschul *et al.*, 1997). The sequence of the CorA transporter gene was run through the program TACG2 (www.cmbi.kun.nl/bioinf/tools/tacg/tacg2.form.html) to predict which restriction enzymes will not digest within the sequence of the gene. Based on the program two suitable enzymes, *Nhe*I and *Eco*RI, were chosen for cloning into the pET-28a vector (Novagen, Inc). These digestions generated complementary overhand ends in the *CorA* domain and the pET-28a vector. The pET-28a vector was selected for the expression vector as it produces a construct with a N-terminal hexahistidine tag.

3.2.1.1 Design of primers to produce *CorA* truncation domain

The following synthetic primers were designed and then synthesized by Sigma-Genosys.

Forward Primer

5'—CAT CTA *GCT AGC* CTG AGC GCA TTT CAA CTG ---3'
*Nhe*I

Reverse Primer

5'---AAC ATC GAG CAG AAC CGC **TAA** *GAA TCC* CGG---3'
Stop *Eco*RI

3.2.1.2 Amplification of *CorA* domain by PCR

Genomic *E.coli* K-12 DNA was used as the DNA template. All PCR reactions were run in a Gene Amp 2400 System (PerkinElmer) in 200 µl thin-wall tubes with a final volume of 50 µl. A Pwo DNA polymerase was used (Thermo Hybaid, U.K.). This polymerase from *Pyrococcus woesei* has a proof reading capability which introduces fewer mutations into the PCR products. Table 3-1 indicates the PCR reaction for cloning of the *CorA* domain.

Table 3-1. PCR components and reaction volumes

Components	Volumes
Pwo PCR Buffer (10x)	5.0 µl
dNTP (10 mM)	1.0 µl
Forward primer (20 pmole/µl)	2.5 µl
Reverse primer (20 pmole/µl)	2.5 µl
K-12 DNA	5.0 µl
DMSO	2.5 µl
Pwo DNA polymerase	0.3 µl
$_dH_2O$	31.2 µl
Total	**50.0 µl**

The PCR reactions were run under the following conditions.

1. 94°C for 5:00 minutes----- denaturing
2. 95°C for 0:45 seconds----- denaturing
3. 51°C for 1:00 minute ----- annealing
4. 72°C for 1:30 minutes----- extension (step 2 to 4 was repeated 20 times)
5. 4°C for 10 minutes or more

After the reaction finished the product was either stored at 4°C or run on a 1% agarose gel.

3.2.1.3 Enzyme digestion to generate overhang

The PCR product was purified using QIAGEN PCR kit. This purification step was necessary to remove excess primers and enzymes. After purification the PCR product and the pET-28a vector were digested with *Nhe*I and *Eco*RI resulting in both 5' and 3'sticky ends. Table 3-2 showed the components and digestion conditions for these reactions.

Table 3-2. Enzymatic digestion components and volumes used during *CorA* domain cloning

Components	CorA Domain DNA	pET-28a
H_2O	Final volume to 60 µl	Final volume to 60 µl
DNA	50 µl	4.0 µg
NEB BUFFER 10X	6.0 µl	6.0 µl
*Nhe*I	20 units	20 units
*Eco*RI	20 units	20 units
CIP	0	10 units

The enzyme *Nhe*I was used first to cut the DNA at 37°C for 1 hour 30 minutes then *Eco*RI was added to the reaction tubes for a further 1 hour 30 minutes at 37°C. In order to prevent "empty vector" religation Calf Intestinal Alkaline Phosphatase (CIP) was added to pET-28a for another hour at 37°C. CIP catalyzes the hydrolysis of the vector DNA 5'-terminal phosphate groups. The enzyme CIP was deactivated by adding EDTA to a final concentration of 1 mM followed by heating to 75°C for 10 minutes. All samples were run on a 1% agarose gel in order to separate the correct DNA band contaminants. The QIAquick gel purification kit was used to purify the DNA from the gel slot.

3.2.1.4 Ligation and transformation

In order for ligation to work the DNA concentration needed to be known. The DNA concentration was assessed by comparing the relative intensities of the sample to the DNA ladder which is a known. Hence an approximate concentration was obtained for the enzymatic digested pET-28a and PCR *CorA* domain DNA. The insert concentration was obtained using the following calculation:

pET-28a(80ng) x 0.783kbps(insert)/5.3kbps(vector) x 2 or 3(ratio)
=24 ng (insert, ratio of 2) or 36 ng (insert, ratio of 3)

In the ligation reaction the following components were used:

80 ng of vector + 36 ng of insert + 2 µl of DNA dilution buffer (5x) + H_2O to a final volume 10 µl.

Then 10 µl of T7 ligase buffer (2x) was added to the sample and mixed well by pipeting the sample up and down. Finally 1 µl of T7 ligase was added and gently mixed. The reaction was left at room temperature for 15 – 20 minutes. After ligation, transformation was carried out in order to select for plasmids with inserts.

The host stain for transformation was *E.coli* DH5α made competent using the Hanahan Method (Hanahan *et al*, 1991). Three microlitres of ligation reactions was used in the transformation. The cells were placed on ice for 30 minutes then heated at 42°C for 45 seconds. After heat shock the cells were returned to the ice for 5 minutes. One millilitre of the pre-warmed LB was added to the cells before shaking at 37°C for 1 hour. Then the cells were plated out on kanamycin LB agar plates and incubated at 37°C overnight.

3.2.1.5 Screening for positive clones

After overnight incubation at 37°C, four colonies from each plate were picked. Each colony was inoculated into 10 ml of LB broth containing 50 µg/ml of kanamycin to propagate the plasmids overnight at 37°C. To ascertain whether the colony contains an insert, a sample of 100 µl of overnight culture from each colony was taken out. The samples were spun at maximum speed in a microcentrifuge for 10 minutes and 20 µl of disruption buffer (100 mM Tris-HCl pH7.5, 1% SDS and 100 mM NaCl) was added to each pellet and mixed well. The mixtures were heated to 100°C for 15 minutes, mixed before cooling for 1 minute on ice. Next the samples were centrifuged for 10 minutes at

maximum speed to precipitate cell debris, genomic DNA and denatured protein. All centrifugations were carried out in a bench top microcentrifuge. The supernatant contained plasmid DNA that served as a DNA template in the PCR reaction to select for positive clones. The forward and reverse primers complementary to the pET-28a vector were used to avoid a false positive result from *E. coli* genomic DNA.

After PCR screening, the positive clones were identified and plasmids were purified using QIAGEN spin columns (QIAGEN protocol). The correct insert was confirmed by sequencing.

3.2.2 Test expression

Two *E. coli* cell lines were used for expression of *CorA* domain: BL21(DE3) and HMS174(DE3). BL21 cell line has the advantage of being deficient in both *lon* and *ompT* (outer membrane protease) protease genes which can degrade proteins during purification steps. However, some target genes are more stable in HMS174 (DE3). Both cell lines were tested at the same time. The pre-culture from a single colony was used to inoculate 500 ml of LB broth containing kanamycin antibiotic (50 µg/ml). The culture was grown to an OD_{600} of 0.8 at 30°C then the CorA domain protein was induced for 4 hours by adding IPTG to a final concentration of 0.1 mM. The cells were harvested by centrifugation in a Solval centrifuge at 5,000 g for 15 minutes. The supernatant was removed and each cell pellet was resuspended in 40 ml of buffer (20 mM Tris-pH 7.5, 150 mM NaCl, 10 mM $MgCl_2$, 250 mM glucose and protease inhibitors). The solution was kept on ice while the cells were disrupted by running the cells through a high-pressure homogeniser three or four times (Glen Creston) at 6°C. After the cells were broken, the cell debris was removed by centrifugation in a Beckman Ultracentrifuge at 30,000 rpm for one hour at 4°C. A

small amount of supernatant and a small amount of pellet from each cell lines were taken out for SDS-PAGE gel analysis.

3.2.3 Protein expression

In order to keep more of the CorA domain refolded correctly and in solution during protein synthesis, a modified expression protocol was employed. Induced cells were grown in the presence of 0.1 mM IPTG for 4 hours. After that the cells were spun down in a centrifuge at 4,000 g for 10 minutes. The supernatant was removed and fresh LB media plus 50 μg/ml kanamycin without IPTG was added to the cells. The cells were grown at 25°C for another 8 hours to allow protein recovery under arresting condition (Carrio and Villaverde, 2001). The cells were harvested by centrifugation. The rest of the purification steps were the same as 3.2.2.

3.2.4 Thirty sparse matrix buffer trials

When *E. coli* is used to express recombinant proteins it is hard to predict which extraction buffer will be the best at keeping a protein in the correct folded state especially for protein domains. Therefore it is necessary to test different extraction buffers before pursuing the purification of the CorA domain. Lindwall *et al.* (2000) developed an initial spare matrix screen to extract over expressed proteins. The principle of the thirty buffers is to test buffers that contain (1) different types of salts, (2) additives to modify the structure of water bound to proteins, (3) small organic molecules at low concentration to break up nonspecific aggregation, (4) glycerol or sugars believed to stabilize folding and (5) detergents to overcome aggregation by binding to hydrophobic surface patches on the protein. Table 3-3 lists all components in the thirty buffers.

Table 3-3. The 30 buffers tested during the extraction of the over expressed CorA domain

1. 100 mM Tris, 10% glycerol, pH 7.6
2. 100 mM Tris, 50 mM LiCl, pH 7.6
3. 100 mM HEPES, 100 mM KCl, pH 7.0
4. 100 mM Tris, 50 mM NaCl, 10% isopropanol, pH 8.2
5. 100 mM sodium acetate, 100 mM KCl, 0.1% n-octyl-ß-D-glucoside, pH 5.5
6. 100 mM HEPES, 1 M $MgSO_4$, pH 7.0
7. 100 mM sodiumacetate, 1 M $MgSO_4$, pH 5.5
8. 100 mM Tris, 2 M NaCl, 0.1% n-octyl-ß-D-glucoside, pH 7.6
9. 100 mM Tris, 100 mM KCl, 0.1% deoxycholate, 25% glycerol, pH 7.6
10. 100 mM HEPES, 50 mM $(NH_4)_2SO_4$, 10% Glycerol, pH 7.0
11. 100 mM K_2HPO_4/KH_2PO_4, 50 mM $(NH_4)_2SO_4$, 1% TritonX-100, pH 6.0
12. 100 mM triethanolamine, 100 mM KCl, 10 mM DTT, pH 8.5
13. 100 mM Tris, 100 mM sodium glutamate, 10 mM DTT, pH 8.2
14. 200mM KH_2PO_4/K_2HPO_4, 0.1% CHAPS, pH 6.0
15. 100 mM triethanolamine, 50 mM LiCl, 5 mM EDTA, pH 8.5
16. 100 mM HEPES, 50 mM LiCl, 0.1% CHAPS, pH 7.0
17. 100 mM KH_2PO_4/K_2HPO_4, 2.5 mM $ZnCl_2$, pH 4.7
18. 100 mM Tris, 50 mM NaCl, 5 mM calcium acetate, pH 7.6
19. 100 mM triethanolamine, 50 mM $(NH_4)_2SO_4$, 10 mM $MgSO_4$, pH 8.5
20. 100 mM Tris, 100 mM KCl, 2 mM EDTA, 1% TritonX-100, pH 8.2
21. 100 mM Tris, 1 M $(NH_4)_2SO_4$, 10 mM DTT, pH 8.2
22. 100 mM sodium acetate, 50 mM LiCl, 5 mM calcium acetate, pH 5.5
23. 100 mM HEPES, 100 mM sodium glutamate, 5 mM DTT, pH 7.0
24. 100 mM triethanolamine, 100 mM sodium glutamate, 0.02% n-octyl-ß-D-glucoside, 10% glycerol, pH 8.5
25. 100 mM Tris, 50 mM NaCl, 100 mM urea, pH 8.2
26. 100 mM HEPES, 50 mM LiCl, 0.1% deoxycholate, pH 7.0
27. 100 mM potassium acetate, 50 mM NaCl, 0.05% dextran sulfate, 0.1% CHAPS, pH 5.5
28. 100 mM sodium acetate, 100 mM glutamine, 10 mM DTT, pH 5.5
29. 100 mM triethanolamine, 100 mM KCl, 0.05% dextran sulfate, pH 8.5
30. 100 mM KH_2PO_4/K_2HPO_4, 50 mM $(NH_4)_2SO_4$, 0.05% dextran sulfate, pH 6.0

In order to assess whether the total amount of over expressed protein was fully extracted, a control buffer containing 2 M urea, 1% SDS, 1.25% 2-mercaptoethanol, 2.5% glycerol and 15 mM Tris, pH 6.8 was added to one sample resulting in complete protein solubilization.

The total 250 ml of expressed HMS174(DE3) cells were collected by centrifugation and the pellet resuspended in 15 ml of buffer (10 mM Tris pH 8.5, 100 mM NaCl and 1 mM EDTA). The suspended cells were divided into 31 samples, 500 µl portions in 1.5 ml micro-centrifuge tubes. The cells again were pelleted by centrifugation in the micro-centrifuge at maximum speed. This step serves to wash

the cells, removing any excess LB that would otherwise make the results less reproducible (Lindwall *et al*, 2000). The 31 pellets were suspended in 500 µl of one of the buffers from Table 3-3 and then the cells were disrupted by sonication (3 x 10 second pulse). The samples were mixed gently for about 15 minutes at 4°C. The extracts were centrifuged at 16,000 g for 15 minutes to obtain a soluble fraction. The thirty cell extracts should contain the same amount of over expressed CorA domain. An equal volume of 12 µl for each sample was run on a SDS-PAGE gel.

3.2.5 Optimisation of buffers

From a careful observation of the SDS-PAGE gels, the effect of the various buffer components was assessed. The components that seem to promote solubilization were chosen to design a new set of buffers (Table 3-4).

Table 3-4. Optimised reagents for solubilization of over expressed CorA domain

1. 40 mM Tris, 10% glycerol, 50 mM NaCl, 50 mM KCl, 10 mM $MgCl_2$, pH 7.5
2. 40 mM Tris, 100 mM KCl, 100 mM triethanolamine, 10% glycerol, 10 mM $MgCl_2$, pH 7.9
3. 20 mM Tris, 25 mM KCl, 25 mM LiCl, 5 mM $MgCl_2$, 10% glycerol, 0.3 M sucrose, 3 mM n-octyl-ß-D-glucoside, pH 8.0

These buffers were tested separately in the following experiments.

3.2.6 Purification of CorA domain using the optimised buffers

These expression trials were essentially the same as previously described. A total volume of 500 ml of LB culture was used. The pellet was resuspended in 100 ml of buffer containing 50 mM Tris-HCl pH 8.0, 100 mM NaCl, 10 mM $MgCl_2$ and 10% glycerol. The suspended cells were divided into 2 x 50 ml portions and pelleted by centrifugation. One sample was used to purify the protein and another one was stored at -80°C.

3.2.7 Purification of CorA domain using IMAC

The optimised extraction buffer 2 (Table 3-4) was tested in a large scale purification procedure. A pellet from 250 ml of culture medium was re-suspended in 40 ml of the extraction buffer. Before homogenizing the cells the protease inhibitors pepstatin A, leupeptin, benzamidine and PMSF were added. Cells were disrupted using a high-pressure homogenizer at 6°C. The supernatant was obtained by centrifugation in a Beckman Ultracentrifuge at 30,000 rpm for 1 hour at 4°C. Cobalt affinity resin (home made, 2 cm bed volume) was equilibrated with buffer 2 (Table 3-4). Equilibrated resin was added to the supernatant and mixed gently for one hour at 4°C to bind the hexahis tagged CorA domain. The total slurry was poured into a 2.5 cm diameter 13 cm long low-pressure chromatography Econo-column (Bio-Rad, Ltd). The resin was left in the column and the run through samples collected for SDS-PAGE analysis. The resin was washed with 20 ml of buffer 2. At this stage a peristaltic pump (Anachem, Ltd) was connected to the column. An Econo UV monitor (Bio-Rad, Ltd) was linked to the bottom of the column to monitor the elution by following the change in OD_{280}. Finally a chart recorder was used to record the elution profile. The wash was continued until the base line was stable and flat before changing to the next buffer.

Impurities were removed using a high salt wash (1.0 M) and a low concentration imidazole wash (10 mM). The CorA domain was eluted by applying 250 mM imidazole. Eluted fractions were dialysed overnight in a 12,000 Da molecular weight cut off dialysis tubing in buffer without imidazole at room temperature.

3.2.8 Gel filtration

Final purification was achieved by applying the protein to a size exclusion column to yield milligram quantities of highly purified CorA domain. Gel filtration was performed using a Phamacia Superdex 200 column running on a Phamacia FPLC (Amersham Pharmacia Biotech). The column was equilibrated with two column volumes of buffer 2, 40 mM Tris, 100 mM KCl, 100 mM triethanolamine, 10% glycerol and 10 mM $MgCl_2$, pH 7.9 (Table 3-4). After the gel filtration the purified protein was concentrated to 10 mg/ml using a 50 kDa molecular weight cut-off concentrator.

3.2.9 Crystallisation trial one

All commercial screen kits were used in the crystallisation trial. The sitting drop vapour diffusion method was used. The crystal growth tray was a 24 well setup from Charles Supper Company (USA). The reservoir volume used was 300 µl of the screen solution. In the well 2 µl of the protein was pipetted then 2 µl of reservoir solution was added to the drop. The crystal tray was sealed with Clear Sealing tape (Charles Supper Company) and incubated at 20°C.

3.2.10 Crystallisation trial two

This trial tried to reduce the ionic strength in the reservoir solution. The first trial did not produce any crystals instead 90% of the wells showed heavy brown precipitation. In the second trial 150 µl of commercial screen solution was added to the reservoir well and 150 µl of water was added to dilute the well solution. The rest of the steps were the same as 3.2.9.

3.3 Results and Discussion

3.3.1 Cloning – results and discussion

Both truncated and full length *CorA* genes were successfully amplified by Pwo DNA polymerase. The products of the PCR reaction were run on a 1% agarose gel. Figure 3-3 shows the product running to the expected size of 783 DNA base pairs. As a comparison the full length *CorA* gene PCR product is also shown.

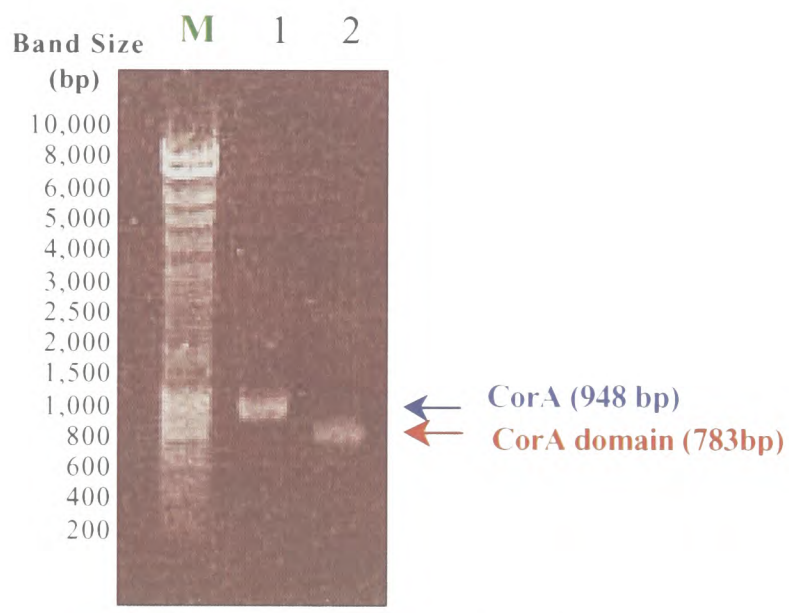


Figure 3-3. 1% agarose gel analysis of the *CorA* PCR products.
M -1kb DNA ladder, Lane 1 - Full length *CorA* 948 bp,
Lane 2 - *CorA* domain 783 bp.

No other products were generated.

The amplified *CorA* domain was successfully digested with endonuclease *Nhe*I and *Eco*RI to generate overhand DNA. The purified insert was successfully ligated into the pET-28a vector. The ligation rate was quite high. All the colonies contained the correct size of insert. An important feature of the ligation method was that both the vector and the insert needed to be freshly digested before the ligation reaction. Freezing and thawing the samples reduced the success rate of ligation tremendously.

The following DNA gel analysis shows that all plasmids contained *CorA* DNA insert (Figure 3-4).

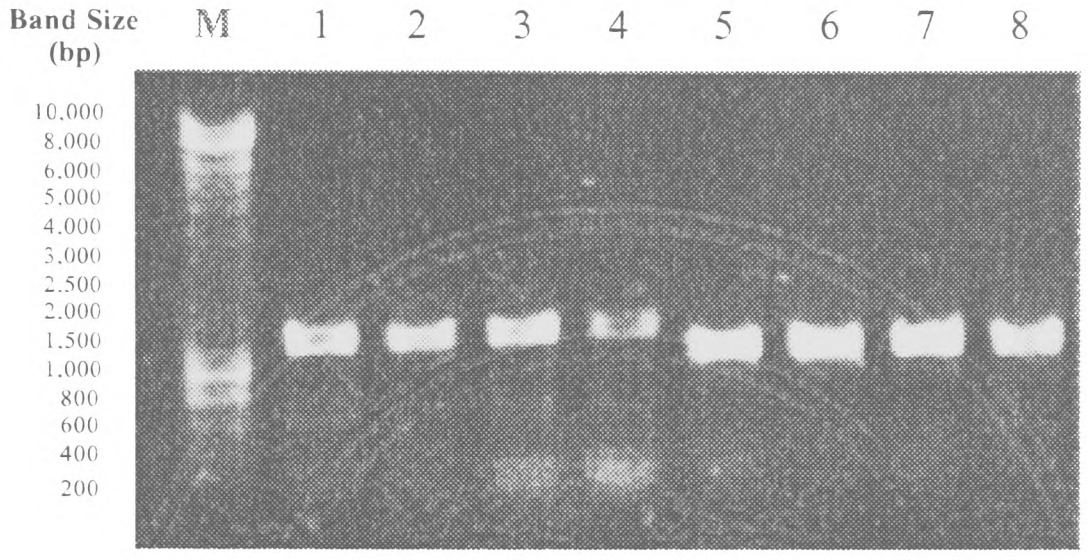


Figure 3-4. 1% agarose gel analysis of PCR products using pET-28a vector primers.
M - 1 kb ladder, lane1 to lane 4 full length *CorA*, lanes 5 to lane 8 *CorA* domain. All the conditions of the PCR reaction are the same as previously described.

Primers complementary to pET-28a were used for screening the correct clones to avoid products from *E. coli* genomic DNA being considered as false positive results. The primers are 150 bps and 130 bps away from the *CorA* gene which makes the PCR product size larger than the gene itself (Figure 3-4). The advantage of this method is speed and is also a relatively cheap experiment to perform. Only those plasmids containing the *CorA* gene were purified and the empty plasmid samples discarded.

3.3.2 Protein expression – results and discussion

Two cell lines were tested in the test expression trials. HMS174(DE3) produced more soluble protein, herefore, it was chosen as the expression host cells. The results are shown in (Figure 3-5).

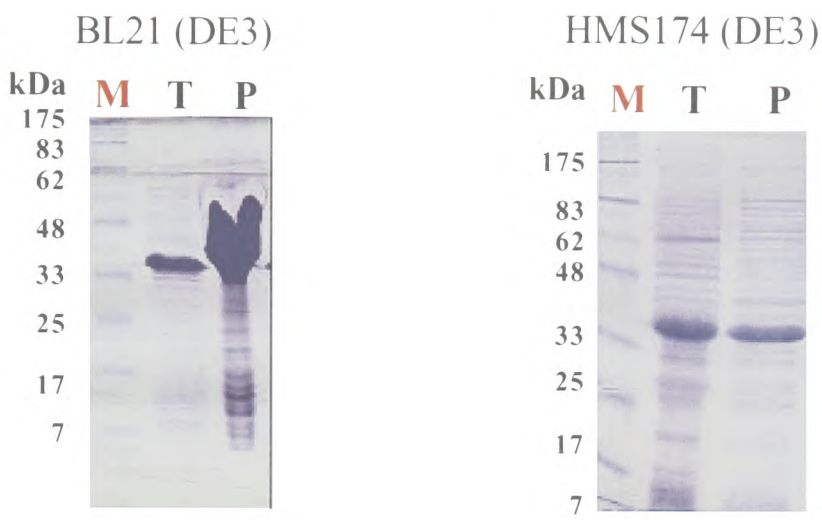


Figure 3-5. 12% SDS-PAGE gel of CorA domain from BL21 (DE3) and HSM174 (DE3) cells.
M - molecular marker, **T** - total supernatant, **P** - pellet.

From the results BL21(DE3) cells produced more CorA domain protein but a lot of the protein was still insoluble and in the pellet. The protein yield was quite high. One litre of culture can produce 50 - 60 mg of protein.

3.3.3 Thirty matrix extraction buffer - results and discussion

The samples were compared to determine the amount of protein extracted (Figure 3-6). The extraction volume from each sample was the same and the loading volume was the same ensuring that the differences in quantity between extraction buffers were caused by differences in the solubility of the domain in each buffer.

After staining with Coomassie Blue solution, the 30 extraction buffer samples were compared by visual inspection to the fully solubilized sample (U: the sample buffer containing 2 M urea). A list of those buffers that were successful in extracting the domain was made based on empirical observations (Table 3-5). Using the condition of the buffer components optimised buffers were designed (Table 3-4). After Co^{2+} affinity purification the protein was further purified using S-200 column in a FPLC.

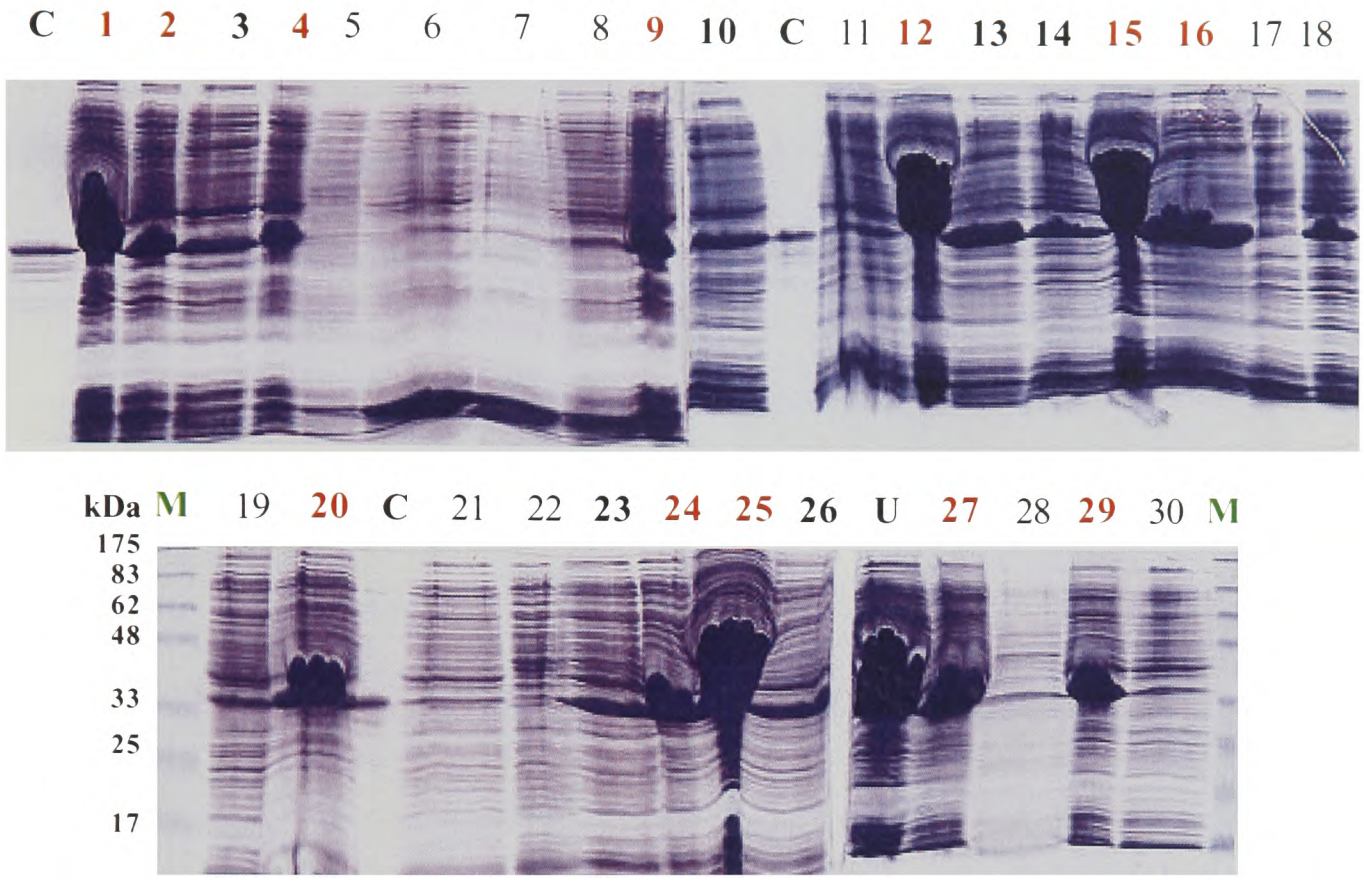


Figure 3-6. 12% SDS-PAGE showing the results from the extraction of the over expressed CorA domain using 30 different extraction buffers.

M - Broad range MW standard, **C** - Purified CorA domain as a marker, **U** - Urea denatured CorA domain which serves as a positive control. Red numbering highlights good extraction buffers.

Table 3-5. List of successful buffers that were able to maintain the over-expressed CorA domain in solution

1. 100 mM Tris pH 7.6, 10% glycerol
2. 100 mM Tris, 50 mM LiCl, pH 7.6
4. 100 mM Tris, 50 mM NaCl, 10% isopropanol, pH 8.2
9. 100 mM Tris, pH 7.6, 100 mM KCl, 0.1% deoxycholate, 25% glycerol
12. 100 mM triethanolamine pH 8.5, 100 mM KCl, 10 mM DTT
15. 100 mM triethanolamine pH 8.5, 50 mM LiCl, 5 mM EDTA
16. 100 mM HEPES, 50 mM LiCl, 0.1% CHAPS, pH 7.0
20. 100 mM Tris pH 8.2, 100 mM KCl, 2 mM EDTA, 1% TritonX-100
24. 100 mM triethanolamine, 100 mM sodium glutamate, 0.02% n-octyl-ß-D-glucoside, 10% glycerol, pH 8.5
25. 100 mM Tris pH 8.2, 50 mM NaCl, 100 mM urea
27. 100 mM potassium acetate pH 5.5, 50 mM NaCl, 0.05% dextran sulphate
29. 100 mM triethanolamine pH 8.5, 100 mM KCl, 0.05% dextran sulphat

3.3.4 Gel filtration – results and discussion

CorA domain eluted as a single symmetrical peak. The result from a run using the extraction buffer 2 is shown in Figure 3-7.

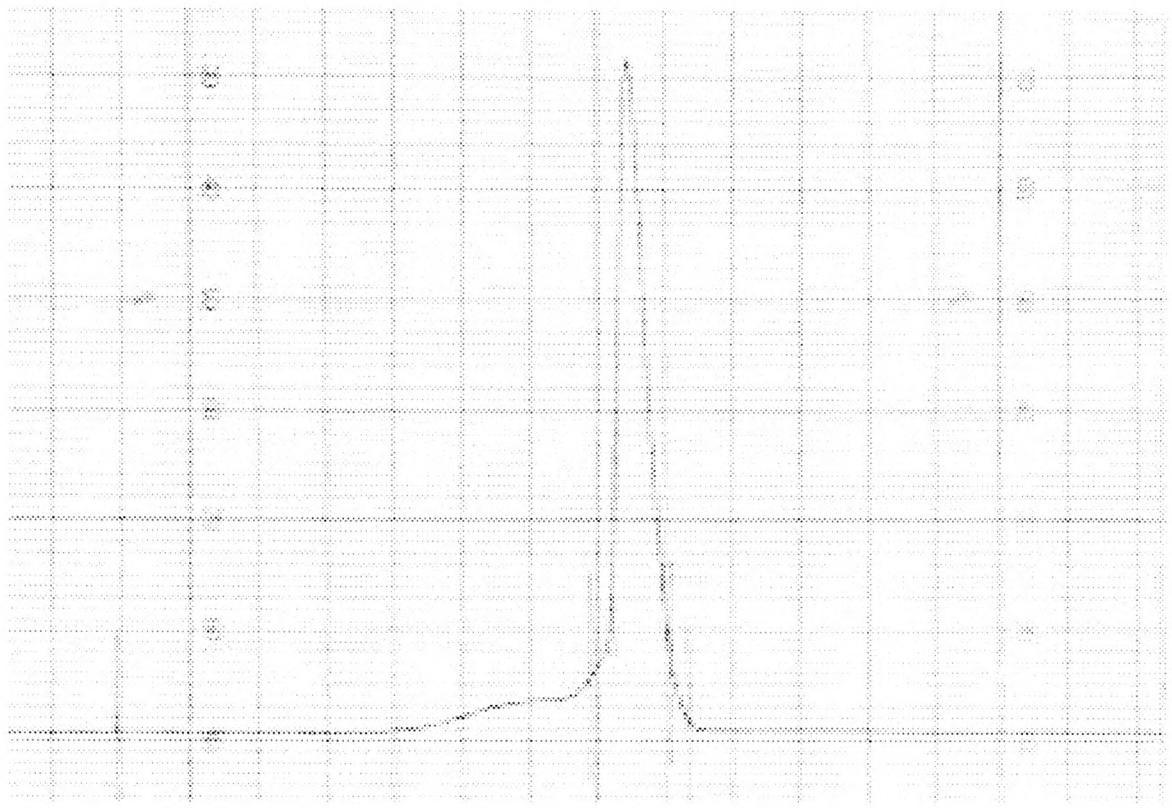


Figure 3-7. Example gel filtration chromatogram using extraction buffer 2 (Table 3-4).
The buffer contains 40 mM Tris-pH 7.9, 100 mM KCl, 10 mM $MgCl_2$, 100 mM triethanolamine and 10% glycerol.

A molecular mass standard was also run using the same buffer. Using a plot of elution volume versus the logarithm of molecular mass for a variety of protein mass standards, a rough molecular mass for the CorA domain was estimated at approximately 32 kDa. As the CorA domain construct should be 32 kDa, the domain appears to run as a monomer. The sample was concentrated to approximately 10 mg/ml and dialysed in the same buffer overnight before being used in crystallisation screens. A total of 480 conditions were screened, however, more than 95% of all conditions showed heavy, brownish precipitation. As a result we decided to investigate whether or not the protein had changed its conformation before or after the

screen. The protein was expressed and purified as mentioned before. After the gel filtration step the protein was dialysed overnight, concentrated to 10 mg/ml and re-injected onto the gel filtration column. This time the elution profile showed the protein was beginning to aggregate (Figure 3-8).

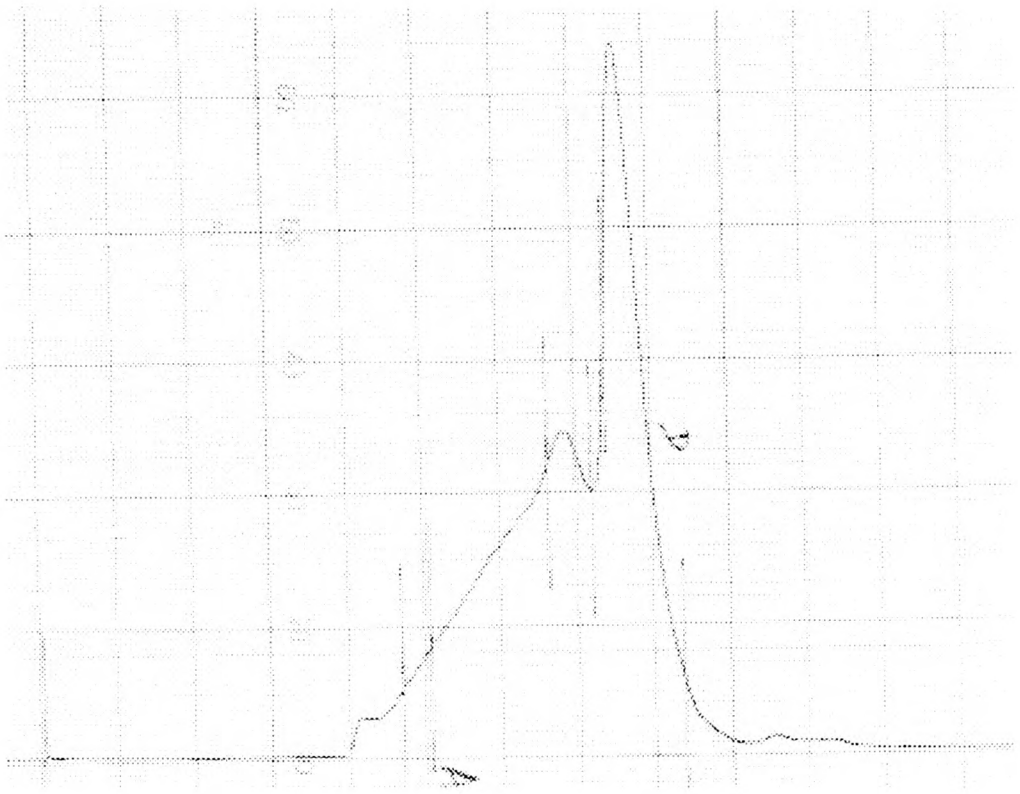


Figure 3-8. Gel filtration chromatogram of the CorA domain after re-loading. The buffer contains 40 mM Tris-pH 7.9, 100 mM KCl, 10 mM $MgCl_2$, 100 mM triethanolamine and 10% glycerol.

In another experiment the protein was dialysed in the same buffer 2 (Table 3-4) for 48 hours after the protein was eluted from the Co^{2+} affinity column. Using gel filtration chromatography it was apparent that the aggregation state of the CorA domain increased over time (Figure 3-9).

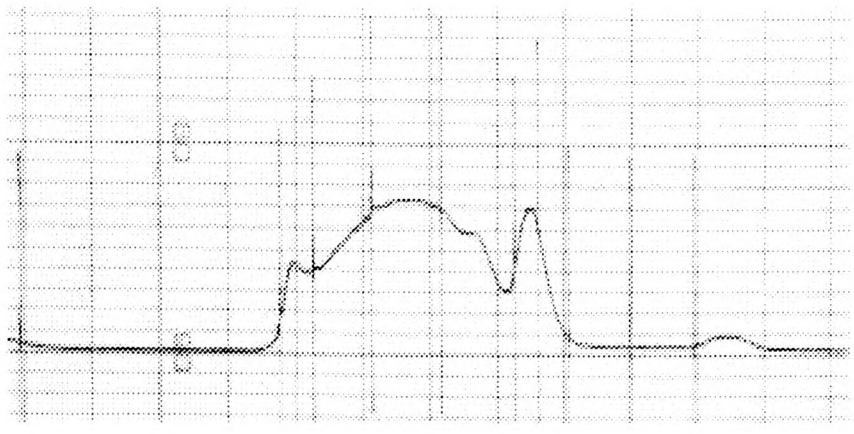


Figure 3-9. Gel filtration elution profile 48 hours after the first purification step. The buffer contains 40 mM Tris-pH 7.9, 100 mM KCl, 10 mM $MgCl_2$, 100 mM triethanolamine and 10% glycerol.

Aggregation as a result of a conformation change is the most likely reason why the protein precipitated out during the crystallisation attempts.

A new CorA domain construct was designed based on the secondary structure prediction program PSIPRED with glutamine 212 chosen as the end of the construct (Figure 1-3 and Figure 3-1). The same cloning sites were used in the PCR reaction. The clone was confirmed by DNA sequencing. All over-expression and purification procedures were followed as previously written. The result was poor with a large amount of the expressed protein in the pellet (Figure 3-9). Different constructs aggregated to different levels indicating that the domains needed some region of the protein to prevent aggregation. A recent paper published by Dr. Wang's group from NYU (USA) used chaperones to help CorA protein fold properly (Chen *et al.*, 2003). With the help of the chaperones the CorA protein formed fewer inclusion bodies after induction.

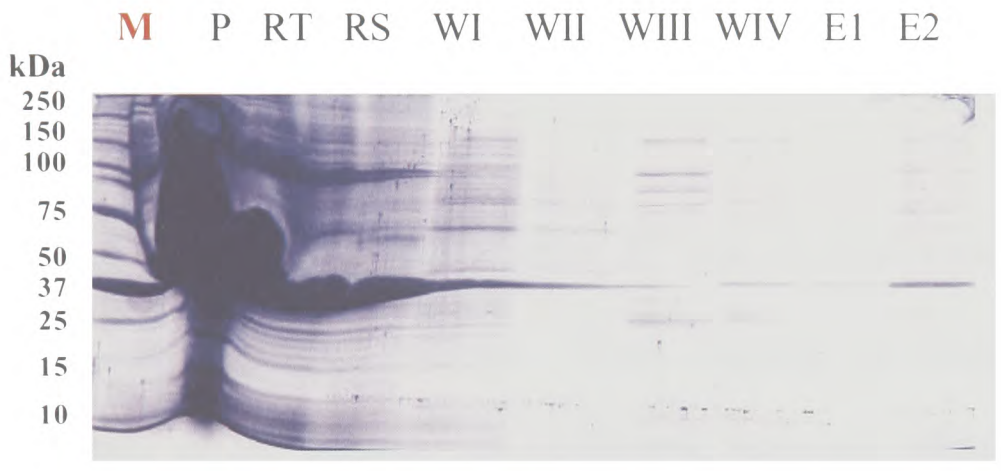


Figure 3-10. 12% SDS-PAGE showing the results from the expression trial of the small CorA domain.
M - Broad range MW standard from BioRad, P - pellet, RT - run through, WI - wash I which is 500 mM NaCl, WII - wash II which is 150 mM NaCl, WIII - wash III which applied 10 mM imidazole, WIV - wash IV which was 20 mM imidazole, E1 - elution 1 and E2 - elution 2 use 200 mM imidazole to knock off the protein.

3.3.5 Crystallisation trial one and trial two - results and discussion

All the trays were monitored daily under a microscope. Brown precipitation appeared immediately after setting up the trays for most of the trials. This is a good indication that the protein was misfolded. The crystallisation trial two used low ionic precipitant strength to induce crystal formation but unfortunately no crystals formed. The few crystals that did grow proved later to be salt crystals.

Chapter 4 – An inward rectifier K^+ channel from *Burkholderia pseudomallei*

4.1 Introduction

Potassium channels preferentially allow K^+ ions to cross a membrane which is almost impermeable to charged particles. These channels are known to play major roles in the control of cell volume, cell excitability, hormonal release, and K^+ uptake in the kidneys. K^+ channels have been identified in both prokaryotic and eukaryotic genomes. In the human body every cell expresses several different potassium channel genes.

Most potassium channels are tetrameric membrane-spanning proteins, comprising four identical subunits containing either two or six transmembrane segments (Hille, 2001). All K^+ channels contain the following properties: (1) they allow K^+ ions to lose their hydration shell as the ion moves through the selectivity filter, (2) each subunit possesses the signature sequence GYG or GFG which forms the selectivity filter (Heginbotham *et al.*, 1992; 1994; Doyle *et al.*, 1998) and (3) they possess a means to control the movement of ions by opening and closing the ion conduction pathway, the process called gating (Hille, 2001).

According to their different electrophysiological and biophysical properties, potassium channels can be divided into voltage-gated K^+ channels (Kv channels), Ca^{2+}-activated K^+ channels (K_{Ca} channels), inwardly rectifying K^+ channels (Kir channels) and tandem pore K^+ channels (Hille, 2001).

4.1.1 Voltage-gated potassium channels (K_v channels)

K_v channels represent a large diverse family of the potassium channels whose permeability to ions is extremely sensitive to the membrane potential differences. The

importance of K_v channels to living cells is illustrated in the following example. In human nerve cells when a signal molecule, such as glutamate, binds to its receptors, it causes the receptor channel to open. The resulting rapid change in membrane voltage triggers Na^+ channels to open and allow Na^+ ions to enter into the cells. The rush of Na^+ ions into the negatively charged intracellular space depolarises the membrane's potential. The inside of the cell becomes more positive. This triggers the K_v channels to open, allowing K^+ ions to move out of the cell thus returning the membrane potential back to the resting state (Hille, 2001).

A functional voltage-gated K^+ channel generally contains four identical subunits. Each subunit contains six transmembrane segments and one signature sequence loop (Figure 4-1).

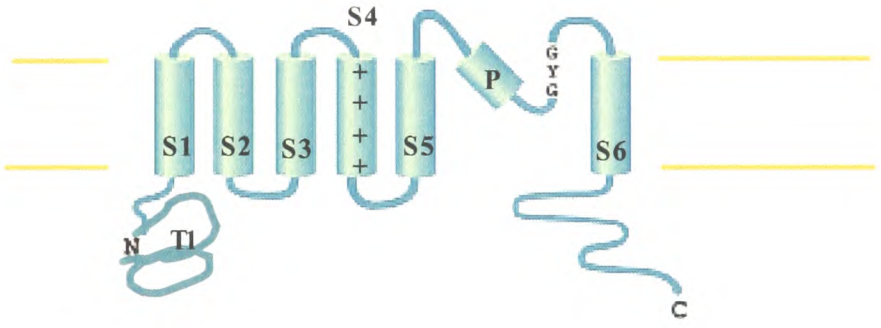


Figure 4-1. Membrane topologies and features of K_v channels. Schematic representation of one subunit of the tetrameric structure is shown.

The transmembrane segment S4 has four to seven positively charged amino acid residues, either arginines or lysines, depending on the channel type (Figure 4-2). This is believed to be the voltage sensor.

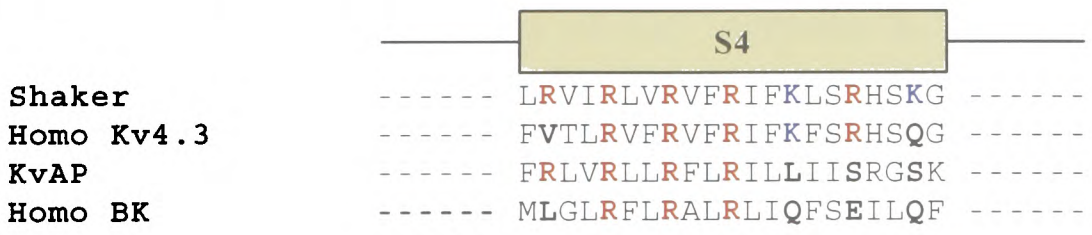


Figure 4-2. S4 segments of some voltage dependent K^+ channels. The amino acid Args are conserved from prokaryotic to eukaryotic organisms. The positive charged arginies (red) and lysines (blue) are highlighted.

Mutations of these residues alter voltage gating (Papazian *et al.*, 1991; Larrson *et al.*, 1996; Seoh *et al.*, 1996; Aggarwal *et al.*, 1996). This unique architecture contributes to the flexible region known as the voltage sensor (Noda *et al.*, 1984). The recent X-ray structure of a bacterial K_vAP channel provides an initial picture of this type of K^+ channel (Jiang *et al.* 2003). More work will be required to see if this crystal form truly is the structure of the K^+ channel as it exists in the membrane.

A typical example of a voltage activated K^+ channel is the Shaker K^+ channel from the fruit fly *Drosophila*. Another well-studied example is the voltage-dependent KCNQ channel. Human cardiac cells use KCNQ channels as delayed rectifiers in order to help repolarise the action potential. Many mutations in the subunits of the KCNQ gene give rise to excessively long cardiac action potentials (Wang *et al.*, 1996). This condition is called the long QT syndrome and can result in cardiac arrhythmias leading to sudden death.

4.1.2 Ca^{2+} activated K^+ channels

Another diverse family of K^+ channels is the Ca^{2+}-activated potassium channels. These channels open in response to an increase in intracellular Ca^{2+} ion concentration. Physiologically they regulate cell excitability and control the action potential waveform.

There are three major types of Ca^{2+} activated K^+ channels: maxi K_{Ca} (BK) channels, intermediate K_{Ca} (IK) and small K_{Ca} (SK) channels based on electrophysiological studies (Sah 1996; Vergara *et al.*, 1998; Meech, 1974; Gárdos, 1958; Blatz and Magleby, 1987). Unlike IK/SK channels that have six transmembrane segments, the BK channels have a total of seven transmembrane helices (Meera *et al.*, 1997). The N-terminus of the BK channels is in the extra-cellular space as the extra TM segment precedes the S1 to S6 segments and is named

the S0 segment. The C terminus is believed to be involved in binding Ca^{2+} ions (Meera *et al.*, 1997) (Figure 4-3).

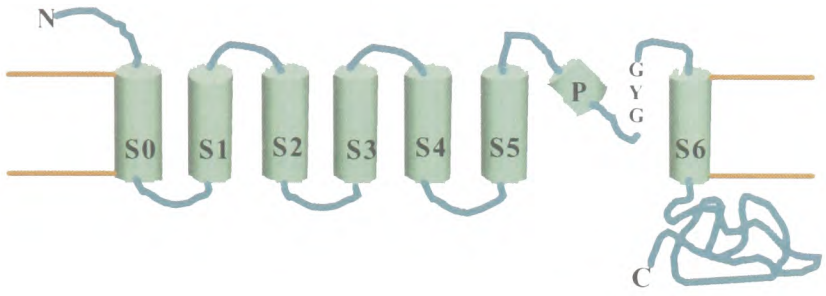


Figure 4-3. Membrane topologies and features of BK channels. Schematic representation of one subunit of the tetrameric structure is shown.

The opening of BK channels depends on a change of voltage in the presence of elevated concentrations of cytosolic Ca^{2+}. On the other hand, opening of IK/SK channels has little voltage dependence and the cytosolic free Ca^{2+} ions regulate the IK/SK channels.

4.1.3 Inwardly rectifying K^+ channels (K_{ir} channels)

Another large family of voltage-independent potassium channels is the inwardly rectifying or inward rectifier K^+ channels. These channels gain their name by conducting inward current more easily than outward current as a result of voltage-dependent blocking by intracellular Mg^{2+} ions and endogenous polyamines (Lu and MacKinnon, 1994; Wible *et al.*, 1994; Yang *et al.*, 1995; Taglialatela *et al.*, 1995; Kubo and Murata, 2001).

Inward rectifier potassium channels (Kir channels) are a distinctive subfamily of K^+ channels from prokaryotic to eukaryotic cells. In 1993 three Kir channels were cloned and expressed (Kubo *et al.*, 1993a, 1993b; Ho *et al.*, 1993). At that time they named the channels: ROMK1 (renal outer medullar K^+ channel), IRK1 (inward rectifier K^+ channel) and GIRK1 (G protein coupled inward rectifier K^+ channel), respectively. Subsequently many more K^+ channels were cloned. Doupnik *et al.* proposed a more logical nomenclature based on the sequence homology (Duopnik *et*

al., 1995). Using the new nomenclature these channels are called Kir1.1 (ROMK1), Kir2.1 (IRK1) and Kir3.1 (GIRK1) but both names are still found in the literature.

A functional Kir channel, like all K^+ channels, is a tetramer with one pore loop per subunit. Unlike K_v channels each Kir channel subunit has only two putative transmembrane segments with the N- and C- terminal domains located in the cytoplasm. The transmembrane segments correspond to the S5 and S6 segments of K_v channel (Figure 4-4).

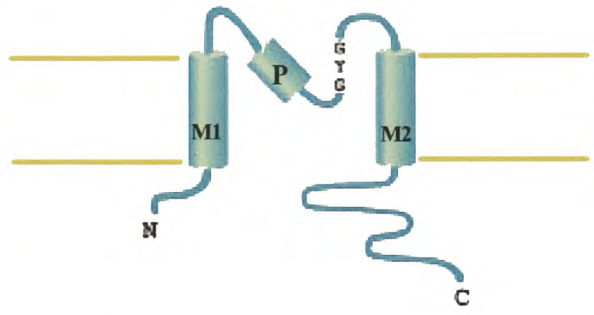


Figure 4-4. Membrane topologies and features of Kir channels.
Schematic representation of one subunit of the tetrameric structure is shown. M1 and M2 correspond to S5 and S6 segments of the K_v channels.

Within the Kir channel family there is a special type of Kir channels, the K_{ATP} channel. A functional K_{ATP} channel has four subunits associate with four sulfonylurea receptor subunits to form an octameric complex. Elevated intracellular ATP inhibits K_{ATP} channel thus forming a link between the energy metabolism and the electrical activity of the cells (Ashcroft and Ashcroft, 1990).

4.1.4 Tandem pore potassium channels (K_{2P} channels)

By searching the gene data bank researchers found another family of potassium channels. This type of potassium channel forms a dimer as a functional channel. Each monomer contains 4 transmembrane segments and two P-loops. The family is classified as tandem pore K^+ channels (Ketchum *et al.*, 1995; Lesage *et al.*, 1996) (Figure 4-5).

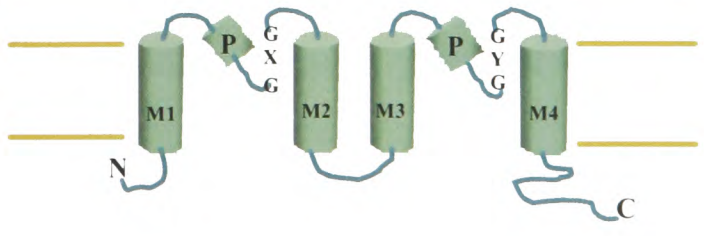


Figure 4-5. Membrane topologies and features of K_{2P} channels.
Schematic representation of one subunit of the dimeric structure is shown.

Recently this family of potassium channels has been studied in greater detail by physiologists. The 2P K^+ channels express in different tissues but some 2P K^+ channels, such as TRAAK, only expressed in the brain, spinal cord and retina (Maingnet *et al.*, 1999). TASK1 is gated by volatile anesthetics making it a clinically important channel. They belong to non-voltage dependent background channels. Some 2P K^+ channels are regulated by external pH others are activated by intracellular second messengers, for example Ca^{2+} (Kim *et al.*, 1995; Czempinski *et al.*, 1997).

4.1.5 Bacterial Kir channels

Over the last decade, many bacterial genes have been recognised by their similarity to eukaryotic K^+ channel sequences. Three years after Schrempf *et al.*, (1995) published the *Kcs.A* gene from the bacterial *Streptomyces lividans*, the first K^+ channel crystal structure emerged (Doyle *et al.*, 1998). The landmark structure proved Hodgkin and Huxley's theory that K^+ ions move across cell membranes in single file. The real picture is more complicated than this as will be explained later. Since both prokaryotic and eukaryotic K^+ channels have similar gene sequences, the architecture of the prokaryotic K^+ channels can represent the K^+ channels in higher organisms. With the breakthrough of successful over-expression of bacterial ion channels in *E.coli*, more bacterial K^+ channel structures have been solved over the previous five years. We solved one of the K^+ channels, KirBac1.1.

Many research papers reported a "genomic approach" to membrane protein structural studies. This method works by expressing many related membrane proteins from different organisms and selecting for those which express, purify and crystillise easily. This approach tends to rule out those proteins that cannot fold, express to high levels, or those that are digested by endogenous proteases during cell growth or the

following purification steps. Even so it is a good approach with recent successes of including a CLC chloride channel (Dutzler *et al.*, 2002) and a glycerol-3-phosphate transporter (Huang *et al.*, 2003).

By searching unfinished microbial genomes, Durell and Guy identified five prokaryotic Kir channels (Durell and Guy, 2001). The monomer of these prokaryotic Kir channels contains one pore-loop and two transmembrane segments with N- and C-terminal portions in the cytosolic side, identical to eukaryotic Kir channels. This result adds prokaryotic Kir channels to the large inward rectifier potassium channel family that was only previously found in eukaryotes. The function of bacterial K^+ channels is still an unknown. The identification of the prokaryotic Kir channel opened up the possibility of structural studies for this family of K^+ channels.

4.2 Materials and Methods

4.2.1 Materials

Restriction enzymes were purchased from New England Biolabs and Roche (UK), primers were synthesized from Sigma (UK), PCR purification kit and plasmid spin column purification kit both were from QIAGEN (UK). Detergents were from Anatrace (USA) and Glycon (Germany). TALON resin was from BD Bioscience Clontech (UK). Polyethylene glycol (PEG) and other chemicals were from Sigma (Fluka), analytical grade. Crystallisation trays were from Charles Supper Company (USA). Crystal screen kits MembFac and Detergent Screen 1, 2, & 3 were from Hampton Research (USA), Cryo I, Cryo II, Wizard I, and Wizard II were from Emerald BioStructures (USA), MDL I and MDL II were from Molecular Dimensions Limited (UK). Crystallisation tools were purchased from Oxford Cryol System (UK) and Hampton Research (USA).

4.2.2 Methods

The strategy employed to determine the structure of the prokaryotic Kir channel centered around the over-expression of the gene using the *E.coli* system. Purification of the channel involved two stages with the starting process being immobilized metal affinity chromatography (IMAC). Next the final contaminants were removed using either gel filtration or ion exchange chromatography. Once the purity of the protein reached the acceptable level, crystallisation trials were begun. On finding a suitable target for structural analysis phasing procedures were employed while the quality of the crystal was improved. An outline of the strategy is shown in Figure 4-6.

Outline of methods

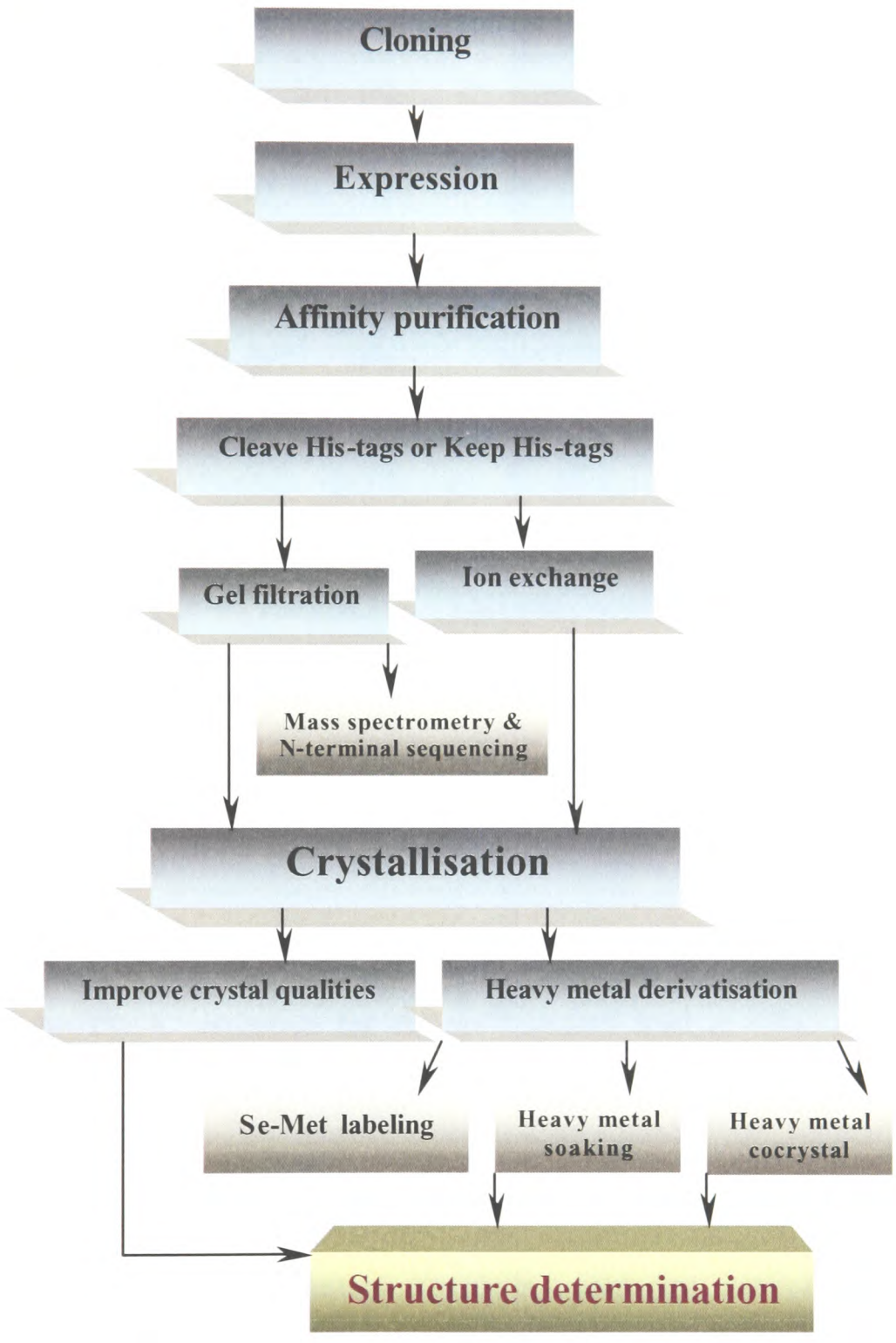


Figure 4-6.

Flowchart indicating the methods and techniques employed in the protein expression, purification, crystallisation and structure of determination KirBac1.1.

4.2.3 Cloning of *KirBac1.1*

4.2.3.1 Assigning the starting codon for *KirBac1.1*

The genomic DNA from *Burkholderia pseudomallei* was purified and provided by professor Ezaki's lab (Gifu University, Japan). As the amino acid sequence of KirBac1.1 was not in a database the DNA sequence was obtained from the Sanger Centre's unfinished genome database (http://www.sanger.ac.uk/Projects/Microbes/). Amino acid sequence alignments of KirBac1.1 with eukaryotic Kir channels suggested a potential beginning for the channel. Just before the first homologous region at the N-terminus of the alignment, the closest Met residue was chosen as the starting site of KirBac1.1. The translation of the gene from the start Met produced MNVDPF....

Applying standard PCR method the KirBac1.1 gene was cloned into a pET30a vector (Novagen) using *Nde*I and *Nco*I restriction sites. The result of the cloning produced a protein with a hexa-histidine tag (his-tags) on the C-terminus. Sequencing indicated that the DNA sequence for the 69^{th} amino acid is GTG instead of GCG converting the alanine to a valine residue.

4.2.3.2 *KirBac1.1Δ12*

Secondary structure prediction suggested that the final twelve C-terminal amino acids were not structured well. The results of the N-terminal sequencing further confirmed that this section was susceptible to proteolysis. Therefore, the KirBac1.1 gene with this twelve residues removed was re-cloned into the same vector with a thrombin cleavage site inserted upstream of the C-terminal his-tags using standard PCR methods and confirmed by DNA sequencing (Sequencing Facility of Department of Biochemistry or Department of Zoology, University of Oxford). The

construct was named *KirBac1.1Δ12* and was used in most protein expression procedures. The crystal structure was determined using this construct.

4.2.4 Bacterial growth and expression

The *E. coli* strain BL-21(DE3) Star* was chosen to be the host strain (Invitrogen) for *KirBac1.1Δ12*. Routinely 6 litres of LB media were inoculated with a starter culture from a plate with the freshly transformed *KirBac1.1Δ12*. A 20 ml of OD_{600} = 0.5 - 0.6 starter culture was added to a 4 litre flask with 1 litre of LB media containing 50μg/ml of kanamycin. The cultures were incubated at 37°C with shaking at 160 rpm to an OD_{600} = 1.0 to 1.1. The temperature was lowered to 25°C and 0.5 mM isopropyl β-D-thiogalactopyranoside (IPTG) was added to the culture to induce the protein expression overnight.

4.2.5 Affinity purification

KirBac1.1 was genetically engineered to have six histidine residues as an affinity tag on the C-terminal end of the protein. This allows protein to have a higher binding affinity for the immobilized metal resins than other cellular proteins. With this construct Co^{2+} immobilized metal affinity chromatography (IMAC) was applied as the initial protein purification step.

4.2.5.1 Cell harvesting

Overnight cells were harvested by centrifugation at 4,200 g for 20 minutes (Beckman Avanti™ J-20). The pellets were weighed (usually 5 - 6 g per litre) and resuspended in 20 ml of lysis butter (50 mM Tris-HCl pH 8.0, 150 mM KCl, 250 mM sucrose, 10 mM $MgSO_4$) per 6 g of pellet. Before disruption a Complete EDTA-free protease inhibitor tablet (Roche) plus 5 μM pepstatin A were added.

4.2.5.2 Cell disruption

The cells were lysed by running through a high pressure homogenizer (Avestin Inc. Canada) five times at 6°C. During processing PMSF was added to a final concentration of 1 mM. The lysate was centrifuged at 9,800 g for 30 minutes at 4°C to remove the unbroken cells and cell debris. The supernatant was centrifuged at 50,000 rpm (70Ti rotor) for 2 hours at 4°C to precipitate the total membrane proteins.

4.2.5.3 Membrane protein purification and solubilisation

The supernatant was carefully removed. The membrane proteins were then dissolved and extracted in lysis buffer with 30 mM n-Decyl-β-maltoside (DM). The extraction volume depended on the total volume of the culture growth, normally 30 ml volume per one litre of cells. The extraction was carried out at room temperature by rotating a sample bottle slowly for 2 hours. Solubilised total membrane proteins were centrifuged for 30 minutes at 45,000g at 19°C to precipitate the insoluble components.

4.2.5.4 IMAC purification

A low-pressure chromatography (Bio-Rad) Econo-column (2.5 cm x 13 cm) was packed with 20 ml of TALON cobalt resins (50% slurry) and washed with 10 volume of H_2O followed by 50 ml of lysis buffer. Before binding the protein Co^{2+} resins were equilibrated with 5 ml of lysis buffer containing 10 mM DM.

The washed and equilibrated resins were transferred into a sample bottle containing solubilised total membrane proteins. The batch method was carried out to let the his-tagged KirBac1.1 channel bind the Co^{2+} resin. This took 1 hour at room temperature. After binding, the resin was transferred back to the column and washed with 40 ml of lysis buffer containing 10 mM DM.

At this stage a peristaltic pump (Anachem, Ltd) and an Econo UV monitor (Bio-Rad, Ltd) were connected to the column to monitor the elution profile by following the change in OD_{280}. Another 40 ml of lysis buffer containing 10 mM DM was used to wash the protein through the peristaltic pump before 50 ml of high salt buffer was applied (50 mM Tris-HCl pH 8.0, 500 mM KCl and 10 mM DM). In order to remove non-specifically bound proteins the resin was washed with 50 ml of 20 mM imidazole in the high salt buffer with 4 mM of the desired detergent such as n-Tridecyl-β-D-maltoside (triDM) instead of DM. Finally the his-tagged protein was eluted with 30 ml of elution buffer (50 mM Tris-HCl pH 8.0, 150 mM KCl, 500 mM imidazole and 2 mM triDM).

The eluted protein was dialysed overnight in 200 ml of dialysis buffer (50 mM Tris-HCl pH 8.0, 150 mM KCl and 0.5 mM triDM) to reduce the imidazole concentration. All steps were carried on at room temperature.

4.2.6 Cleavage of the his-tag

Overnight-dialysed protein was concentrated to 10-12 mg/ml and the his-tag removed by proteolytic digestion. The protease thrombin (Roche) was used at 0.5 unit/1 mg of his-tag-fusion protein. The thrombin was freshly weighed and dissolved in 100 - 150 µl of dialysis buffer. The dissolved thrombin was added to the protein. The protein was digested at room temperature for 2 hours.

4.2.7 Gel filtration

A further purification step was carried out by gel filtration using a Superdex 200 analytical column with a FPLC system (Pharmacia). The running buffer included 50 mM Tris-HCl pH 8.0, 150 mM KCl and 0.5 mM triDM. The S-200 column was equilibrated with 50 ml of running buffer (two column volume) at 0.5 ml/min speed.

The 300-350 µl of thrombin-digested protein was injected into a 500 µl volume sample loop and the main peaks were collected and pooled.

The gel purified protein was concentrated to 10 - 14 mg/ml using a 100 kDa molecular weight cut-off Centricon YM-100 (Amicon) and dialysed overnight in a 50 kDa cut off dialysis tubing against 200 ml of buffer containing 10 mM Tris-HCl pH 8.0, 50 mM KCl and 0.05 mM triDM at room temperature.

4.2.8 Ion exchange chromatography

In the ion exchange chromatography purification the proteins still contained the his-tag. The eluted protein from the Co^{2+} resin was dialysed overnight to lower salt concentration and directly loaded to the ion exchange column.

After affinity purification the channel was dialysed against 10 mM Tris-HCl pH 8.0, 30 mM KCl and 0.5 mM triDM overnight at room temperature. A 5 ml Hi Trap Q FF column was linked to a peristaltic pump and an Econo UV monitor. The column was equilibried with 4 column volumes of binding buffer (10 mM Tris-HCl pH 8.0, 30 mM KCl and 0.5 mM triDM), 4 column volumes of elution buffer (10 mM Tris-HCl pH 8.0, 1 M KCl and 0.5 mM triDM) and 4 column volumes of binding buffer again. The samples were loaded into the column running at a flow rate of 1 ml/min. After proteins were bound to the column 5 column volumes of binding buffer (10 mM Tris-HCl pH 8.0, 30 mM KCl and 0.5 mM triDM) was applied to wash the resin. The protein was eluted using a gradient to 1.0 M KCl with all other components unchanged. The central peak was treated in the same ways as previously described for the main peak observed during gel filtration (see 4.2.7).

4.2.9 N-terminal sequencing and mass spectrometry

The KirBac1.1 was checked using N-terminal sequencing and electrospray mass spectrometry by Dr. Jeff Keen from University of Leeds. The protein sample with the his-tag was 9.7 mg/ml in 10 mM Tris-HCl pH 8.0, 50 mM KCl, 0.05 mM triDM. Identical components and a similar concentration were used for the protein sample without a his-tag.

4.2.10 Crystallisation of KirBac1.1

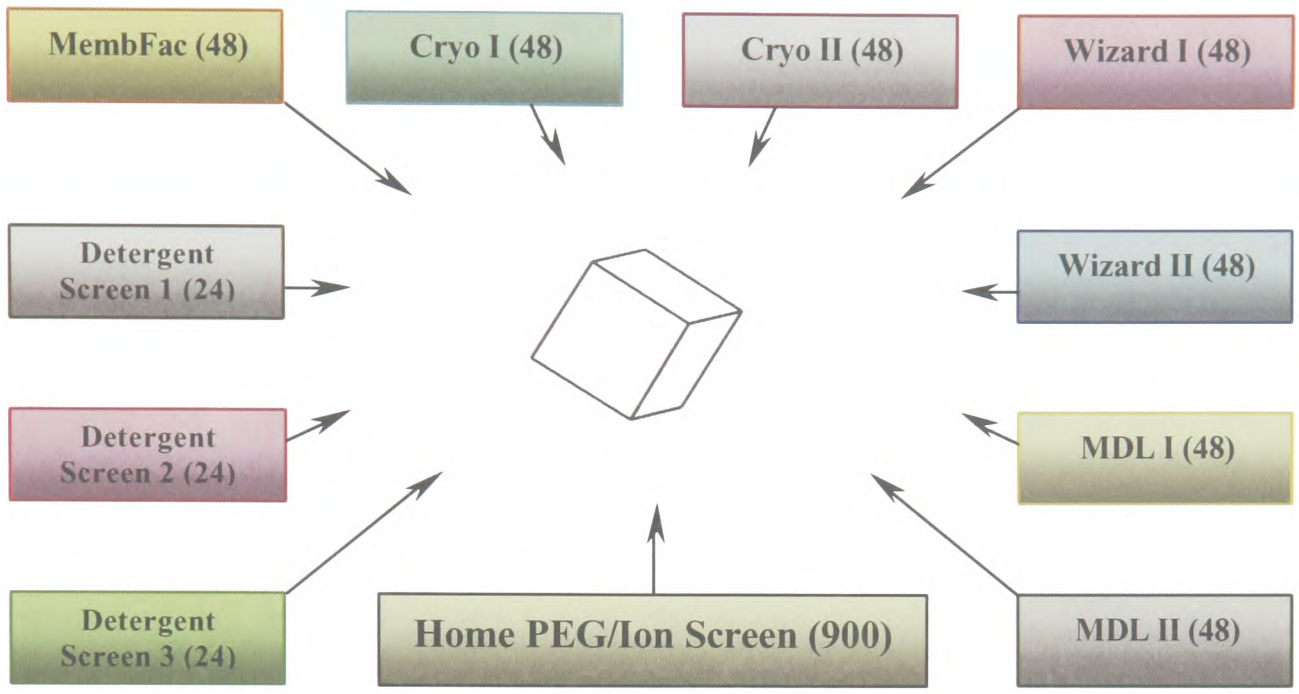
The initial crystallisation screens included all available commercial screens plus a home crystallisation screen. The commercial screens included screens from Hampton Research (U.S.A.), Emerald Biostructure Company (U.S.A.) and Molecular Dimensions Limited (U.K.). The homemade screen is based on a PEG concentration screen versus pH. Molecular weight PEG ranging from 400 to 8000 were used while the pH ranged from 4 to 9 in steps of one pH unit. The optimisation narrowed down the conditions to less than 100 broad screens and finally the conditions were adjusted to less than 50 screens.

4.2.10.1 Determine protein concentration

The protein concentration was determined from absorbance reading at 280 nm (A_{280}). The measurement was made in a micro-cell using an Ultrospec 1100 pro spectrophotometer from Amershampharmacia. Protein concentration was calculated based on the number of tyrosine, tryptophan and cysteine residues in relation to the molecular weight (Appendix C-1). The protein concentration was adjusted to 8 - 14 mg/ml using dialysis buffer (10 mM Tris-HCl, 50 mM KCl and 0.05 mM triDM).

4.2.10.2 Initial screening

All commercially available screen kits and home formulation screen kits were used at the beginning (Figure 4-7).



MembFac, Detergent Screen 1, Detergent Screen 2 and Detergent Screen 3 are commercially available from Hampton Research (U.S.A.).

Cryo I, Cryo II, Wizard I and Wizard II screen kits are purchased from Emerald Biostructure Company (U.S.A.).

MDL I and MDL II screens are equivalent to **Hampton Crystal Screen 1** and **2** but are purchased from Molecular Dimensions Limited (U.K.).

Home PEG/Ion Screen 900 is Dr. Doyle's formulation (University of Oxford, U.K.).

Figure 4-7.

Numbers and sources of the initial crystallisation screens in the KirBac1.1 project.

4.2.10.3 Sitting drop vapour diffusion crystallisation

Crystallisation conditions were screened using the sitting drop vapour diffusion method. The crystal growth trays were the standard plastic plate of 24 chambers. Each vapour diffusion chamber has a plastic post in the centre of the well to hold the protein drops. The reservoir solution is held within the narrow moat surrounding the support post to prevent splashing whenever the plates are moved.

Typically 300 µl of screen solution was pipetted into the reservoir well. The first screen of full length KirBac1.1 was carried out on protein in DDM only. 2 µl of 10 mg/ml protein in 10 mM Tris-HCl, 50 mM KCl and 0.2 mM DDM was added to the post then 2 µl of precipitant solution was pipetted onto the drop. The plastic plate was sealed with a Crystal Clear Sealing tape (Charles Supper Company). The crystals were grown in an incubator at 20°C. Drops were monitored with a dissecting microscope on a daily basis for the first week and followed by weekly thereafter. Crystals appeared in three or four days and continued growing in two weeks.

4.2.11 Improve crystal qualities

Optimised screen solutions and detergents as additives to search the better crystal forms were two major entryways to improve KirBac1.1 crystals.

4.2.11.1 Optimisation of screen solutions

After the initial hits the conditions that produced crystals were optimised. Table 4-1 listed the optimised screen formulations.

Table 4-1. Optimised screen buffers

PEG/400 (18% - 24%), 50 mM $Mg(CH_3COO)_2$, 0.1 M Glycine pH 8.2 - pH 9.2
PEG/400 (20% -26%), 50 mM $MgCl_2$, 0.1 M Glycine pH 8.2 - pH 9.2
PEG/400 (20%), 50 – 100 mM $MgCl_2$, 0.1 M Glycine pH 8.2 - pH 9.2
PEG/400 (20%), 50 – 100 mM, $Mg(CH_3COO)_2$, 0.1 M Glycine pH 8.2 - pH 9.2

4.2.11.2 Choices of detergents and optimisation of detergent exchange

Several detergents were selected and tested such as DDM, triDM, tetraDM, CYMAL-4 and HEGA-10. The properties of these detergents are listed on Table 4-2.

Table 4-2. Detergents used in KirBac1.1 protein crystallisation

Detergent Class	Type	FW	CMC (mM)	Aggregation #
n-Dodecyl-β-D-maltoside	Neutral	510.6	0.17	79-92
n-Tridecyl-β-D-maltoside	Neutral	524.6	0.033	105
n-Tetradecyl-β-D-maltoside	Neutral	538.6	0.01	n/a
HEGA-10	Neutral	379.5	7.0	n/a
CYMAL-4	Neutral	480.5	7.6	45

Each detergent was exchanged during affinity chromatography in the wash II step. The desired detergent was then used in all remaining purification steps. Several concentrations of the detergent were tested during the Wash II step. For the n-Alkyl-β-D-maltoside class, 4 mM was optimised in Wash II, 2 mM was used in Elution and 1 mM was chosen in the gel filtration step. For the HEGA-10 and CYMAL-4 detergents, 15 mM was used in Wash II, Elution and gel filtration. Final crystallisation concentration for each detergent was based on individual CMC values and two times the CMC was chosen for use in the dialysis buffer before

crystallisation. Finally triDM was chosen as the optimised detergent in the rest of the crystallisation trials.

4.2.11.3 Using detergents as additives

One approach to search for better quality of crystals was to use detergents as additives in test trials. Mixing detergents was believed to alter micelle size. Three Detergent Screening Kits, total of 72 detergents, were used (Figure 4-7). Each detergent is at 10 times its reported CMC in water.

The precipitant was 20% PEG/400, 100 mM $Mg(CH_3COO)_2$ or 100 mM $MgCl_2$, 0.1 M Glycine pH 9.0. The protein was at 10 mg/ml in 10 mM Tris pH 8.0, 50 mM KCl, 0.05 mM tri-DM. 2 µl of protein was pipetted onto the post then 0.5 µl of the designed detergent was mixed with the protein and finally 2 µl of precipitant solution was added to the drop. The other steps were as previously described.

4.2.11.4 Optimise additive detergents

The selected detergents were then tested in three different concentrations using the same precipitant and protein described above. Table 4-3 listed two selected detergents in 3 different concentrations.

Table 4-3. Final concentration in the crystallisation wells

CYMAL-4	(0.5x CMC) **3.8 mM**	(1x CMC) **7.6mM**	(2x CMC) **15.2 mM**
HEGA-10	(0.5x CMC) **3.5 mM**	(1x CMC) **7.0 mM**	(2x CMC) **14.0 mM**

4.2.11.5 Other optimisations

Other trials were carried out such as lower protein concentration to 6-8 mg/ml and incubation of the crystal trays at 14°C.

Four different Mg salts were separately screened in the optimised screen conditions. Many repeated trials included using 50 – 100 mM $MgCl_2$, or $Mg(HCOO)_2$ $MgSO_4$ or $Mg(NO_3)_2$ in 18% - 24% PEG/400 screens to substitute $Mg(CH_3COO)_2$.

A series of PEGs were tested such as monomethyl ether PEG/350 (MME), PEG/550 (MME), PEG/600 and PEG/1000 separately to substude PEG/400.

4.2.12 Heavy metal derivatisation

In order to solve the structure of KirBac1.1, three approaches were taken to search for phase information while crystal optimisation was in progress.

4.2.12.1 Generation of cysteine residues for heavy metal soaking

For **mercury derivatisation** the amino acid cysteine can be used to covalently bind mercury compounds. As KirBac1.1 does not have any cysteine residues mutagenesis was employed to convert selected residues to cysteine. Cysteine mutation positions were selected within the predicted transmembrane helical regions of KirBac1.1. The first A125C was mutated on the basis of the alignment of KirBac1.1 with the KcsA sequence. Several residues downstream of A125C were also mutated (I126C, A127C, T128C or L129C). These residues form a complete turn of a helix. The equivalent residues of A125 and T128 in KcsA produced good mercury derivatives. The reason for this was to take into account any potential changes in helix packing between KcsA and KirBac1.1. The mutations were generated by PCR using a Quick Change Site Directed Mutagenesis Kit (Stratagene, UK). All the mutations were confirmed by DNA sequencing.

The protein expression and purification used the same protocol as for wild type except that after affinity purification 2 mM dithiothreitol (DTT) was present until the end of the gel filtration step. DTT was excluded in the final dialysis and crystallisation steps.

4.2.12.2 Heavy metal soaking

After the crystals formed and settled for more than two weeks, heavy atoms were added to the crystals to soak between 4 to 24 hours. The heavy metal solutions were prepared at twice the concentration in mother liquor and twice the concentration in protein buffer. Solution was equilibrated for a few days. Crystals were transferred to fresh 2 µl drops of mother liquor and protein buffer before the addition of 2 µl heavy metal solution. The tray was sealed by a tape and crystals were observed under a microscope for a few minutes for signs of any morphological changes, such as crystal cracking or melting. The heavy metal derivatives screened are detailed in Table 4-4 below.

Table 4-4. Heavy metal reagents used in KirBac1.1Δ12 derivatisation

Heavy metal reagents	Final concentration	Soaking
Potassium mercuric iodide	1 mM	12 hrs
Thimerosal	1 mM	12 hrs
p-chloromercuribenzene (PCMB)	10 mM	24 hrs
K_2PtCl_4	2 mM	12 hrs
$Hg(CH_3COO)_2$	2 mM	6 hrs
$HgCl_2$	10 mM	4 hrs
CH_3HgCl	4 mM	10 hrs
$CH_3Hg(CH_3COO)$	10 mM	12 hrs

4.2.12.3 Heavy metal co-crystal

Three heavy metals were used in KirBac1.1Δ12 co-crystallisation trials, thimerosal, CsCl and RbCl. 0.1 M thimerosal was dissolved in dialysis buffer and added to the concentrated protein to a final 1 mM concentration then incubated at 20°C for 12 hours before setting up trays.

Replacement of K^+ by Rb^+ or Cs^+ ions used a different approach. CsCl is more toxic than RbCl therefore a dialysis method was used to prevent excess use. After gel filtration the protein was concentrated and dialysed overnight to reduce the

K^+ concentrations to 50 mM. Then K^+ was exchanged for Cs^+ using a dialysis buffer containing 10 mM Tris-HCl pH 8.0, 60 mM CsCl and 0.05 mM triDM for 24 hours. The crystallisation setups were the same as in section 4.2.10.3 and 4.2.11.3.

For Rb^+ co-crystals, two methods were used: (1) after gel filtration and protein concentration steps the protein was dialysed for 12 hours in 10 mM Tris-pH 8.0, 150 mM RbCl and 0.05 mM triDM. The RbCl concentration then was reduced to 50 mM by dialyzing the protein in 10 mM Tris-pH 8.0, 50 mM RbCl and 0.05 mM triDM for 24 hours before setting up the trays; (2) at the gel filtration step the K^+ was replaced by using a buffer containing 50 mM Tris-HCl, 150 mM RbCl and 0.5 mM triDM. The Rb^+ ions should be fully replaced in the protein after gel filtration. The remaining steps were as previously described.

4.2.12.4 Seleno-methionine labelling

Seleno-methionine labeled his_6-KirBac1.1Δ12 (^{78}Se-Met) was prepared as follows. The his_6-KirBac1.1Δ12 construct was transformed into B834(DE3), a methionine auxotrophic stain of *E. coli*. The **growth media** contained glucose, 19 amino acids, seleno-methionine, various salts, vitamins and sulphates (Appendix D). Some compounds could not be autoclaved, therefore, they were filter sterilized through a 0.22 μm filter (Table 4-5). Finally one litre of medium was mixed by adding all compounds together in to a 4 litre flask.

Table 4-5. One litre of seleno-methionine media

Chemical Class	Compound Name	Quantity
Amino Acid	Amino acid mix I Amino acid mix II	10 ml 10 ml
Amino Acid	Seleno-L-Methionine 10 mg/ml (Filter-sterilized)	3 ml
Nutrient Source	Glucose 40% $MgSO_4$ 1M $FeSO_4$ 12.5mg/ml	10 ml 2 ml 2 ml
Vitamins	Vitamin mix	1 ml
Salts	20X M9	100 ml
Antibiotic	Kanamycin 50 mg/ml	1 ml
	H_2O (Autoclaved)	861 ml

The **cell growth** was started by growing a few colonies in 100 ml of LB media at 37°C until OD_{600} nm = 0.2. The cells then were precipitated at 4,000 g for 10 minutes and the pellet washed twice using seleno-methionine media. This wash was very important to remove excess LB media. Washed preculture was inoculated in one litre of seleno-methionine media then grown at 37°C until OD_{600nm} = 0.9 before lowering the temperature to 25°C for induction overnight. A total of 4 litres of medium were cultured. After induction the remaining steps were the same as previously described in **Affinity purification** (4.2.5). Further purification was carried out on an ion exchange column. The method was the same as **Ion exchange chromatography** section (4.2.8). The his-tag was not removed from the protein.

Crystallisation trials of Se-Met derivative KirBac1.1Δ12 were carried out in the mixed triDM with HEGA-10 detergent using the screen solutions as previously described.

4.2.13 Structure determination

The most frustrating part of the KirBac1.1 project was that almost all of the crystals that formed were beautiful but diffracted X-rays poorly. Synchrotron beam sources were used for screening crystals which were suitable for a full structure

determination and the home X-ray beam was used for searching crystals for the proper cryoprotection conditions.

4.2.13.1 Cryoprotection

All KirBac1.1Δ12 crystals were frozen prior to X-ray exposure in order to minimize radiation damage. Generally this is essential in order to collect a complete data set from a single crystal. The crystals were grown in a partial cryo-protected solution, 20% – 22% polyethylene glycol PEG/400. This percentage of the PEG/400 was not high enough to prevent ice formation when a crystal was frozen in liquid nitrogen. Several cryoprotect reagents such as glycerol (10%), glucose (10%), xylose (10%) and sucrose (10%) were added to the crystals before freezing. Unfortunately none of the reagents were suitable. The only way to make the crystals cryoprotected and not alter the diffraction was to allow the crystals to dehydrate in the wells for 30 days prior to freezing. Our previous experience with the CLC chloride channel allowed us to take advantage of the dehydration process.

Two ways of crystal freezing were tested: (1) a crystal was picked up using a small (0.3 - 0.4 mm) circular nylon loop (Hampton Research) and frozen by plunging it into the liquid nitrogen before the trip to ESRF; (2) the crystal trays were carried to ESRF and a crystal was freshly frozen in a stream of gaseous nitrogen at 100 K cryostream before data collection.

4.2.13.2 Data collection

All of the X-ray diffraction data sets were collected using beamlines ID14 EH1 and ID14 EH2 at ESRF, Grenoble France, using an ADSC Q4 CCD detector and a wavelength of 0.934Å.

Prior to collecting data on the KirBac1.1 crystals, an empty loop was aligned in the beam to check that the goniometer and cryostream was appropriate positioned.

A frozen crystal was transferred and mounted on the goniometer head which was exposed to a continuous stream of nitrogen gas cooled to 100 K by an Oxford Cryosteam. The crystal was centered to ensure that it remained in the X-ray beam during rotation of the spindle.

Optical centering of the crystal was carried out as follows. First rotate the crystal through $0^o/180^o$ and used an Allen key to move the sledge to adjust the crystal in the midpoint of the $0^o/180^o$ rotation. Second repeat the same procedure but rotated the crystal through $90^o/270^o$. Finally repeat the whole process through $0^o/360^o$ to make sure the crystal is stationary and centered through a full rotation within the beam center.

The method of data collection used was the **oscillation method** which involved rotating the crystal around a single axis perpendicular to the X-ray beam (Dauter, 1999). The oscillation angle of 1^o was applied during each exposure. Many crystals were tested to see if they diffracted and if so to what resolution. If the KirBac1.1 crystal diffracted to a resolution limit about 4Å, it was chosen as a reasonable crystal to collect more images. The second image was collected 90^o away from the first one to check for a well-formed crystal. If both images gave reasonable diffraction patterns, the crystal was chosen for data collection. An extra two images, 30^o and 60^o away from the first image, were collected and used in the automated computer program MOSFLM to predict the correct space group of the crystal (Leslie, 1992).

The KirBac1.1 crystals had a space group I222. MOSFLM using the STRATEGY command predicted the 90 images at 1^o angle rotation that would give a complete data set. Most data sets of the KirBac1.1 crystals used information collected between 120 to 180 images depending on the amount of time available.

Based on these four images, the crystal to **detector distance** and exposure time for each image was refined. Generally, the distances were set to 300 mm to 350 mm since the KirBac1.1 crystals did not diffract to a higher resolution limit than 3Å.

The **estimated exposure** times are based on the intensity of the X-ray beam, the quality of the crystals and how much beam time is available. For the KirBac1.1 crystals the exposure time of each image ranged from 30 to 60 seconds.

All native or heavy atom derivative data sets were collected from a single frozen crystal and no data sets were merged.

4.2.14 Data Processing

An overview of the processes is shown in Figure 4-8.

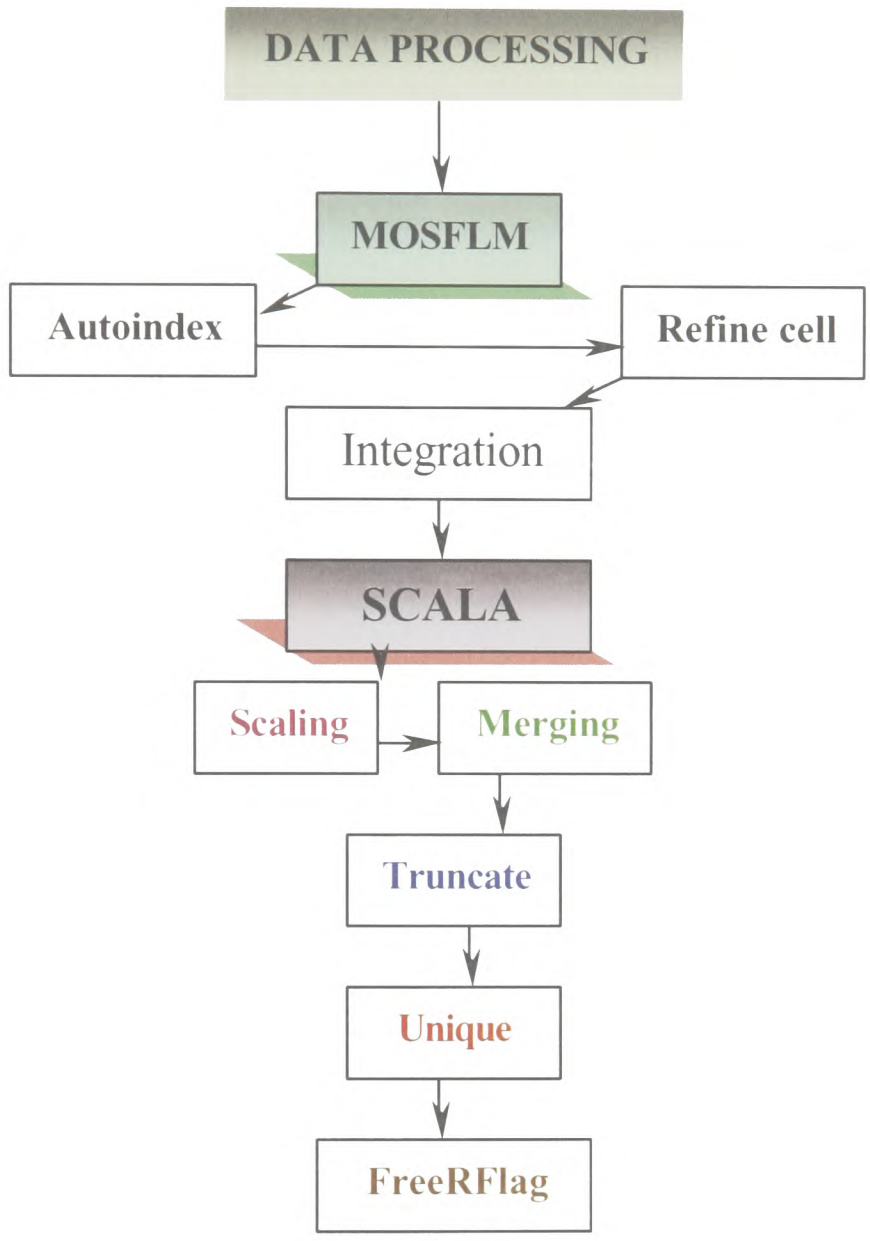


Figure 4-8.

Flowchart describes the programs used in the data processing.

4.2.14.1 Autoindexing

All KirBac1.1 data sets were autoindexed using the program MOSFLM (Leslie 1992). In the input file the parameters such as the wavelength of the X-rays, the crystal to detector distance, the detector type, the directory name and image name

were defined. Four images were chosen 0^o, 30^o, 60^o and 90^o for diffraction peak detection and unit cell determination.

The program automatically distinguished the value of a pixel to be above a certain threshold in comparison to the background measurement. The program then uses all the information from the input file and experimental data to pick out the orientation of the crystal with respect to the direct beam and to define the crystal unit cell dimensions.

MOSFLM then lists the fourteen possible Bravais Lattices with a relative score to fit the lattices of the crystal. The initial principle was to define the lattice of the crystal by selecting the highest symmetry and the lowest penalty. The program calculates the distortion of the cell parameters to fit the diffraction lattice for the fourteen Bravais Lattices, the lower the penalty the less potential distortion for the lattice. To check the potential correct lattice, the program has a prediction to pick the peak positions based on the lattice that is chosen.

Another important parameter, crystal mosaicity, needs to be set correctly for correct prediction. Like other membrane protein crystals, the KirBac1.1 crystals exhibit high mosaicity. The mosaicities of the KirBac1.1 crystals varied between 1.0^o to 2.0^o. The default setting for MAXWIDTH needs to be changed to 10 to cope with high mosaic data.

By displaying the predicted patterns overlaid on the actual observed patterns, it was judged whether or not the predicted location of the reflections matched the observed reflections. In some cases the beam centre was not properly defined in the input file. This generally leads to poor predictions. This can be adjusted by using the **Adjust** menu option to update the correct parameters. The standard deviation of spot

position is used to judge whether the autoindexing is correct, normally below 0.2 – 0.3 mm is acceptable.

4.2.14.2 Refine cell

An accurate cell determination is the next step by **post-refinement** of the unit cell. Four images were used to refine the cell, 0°, 90°, 30° and 60°. The result of the output file was checked to see if the final value for mosaic spread is still in agreement with the real diffraction data.

4.2.14.3 Integration

Integration was carried out by optimising parameters first. A block of images is integrated (10 images) to evaluate if any of the parameters need to be changed. Finally the complete dataset can be integrated.

4.2.14.4 Scaling and merging data

All integrated raw intensities from images are corrected for variations in the data collection such as changes in the beam intensity, absorption effects and radiation damages. The program SCALA was used (Evans, 2002) to scale and merge multiple reflections. The **smoothed scaling** option was used since the images of each dataset were collected from a single crystal and the beam intensity varied steadily.

The final step of the data processing was to convert merged intensities to structure factor amplitudes because all the programs used to determine the structure of the crystal, calculate electron density map and refinement used structure factor amplitudes instead of the intensities from spots. The program SCALA as part of CCP4i contains Truncate, Unique and FreeRFlag (CCP4, 1994). At this point the full unique reflections of the resolution and space group of the KirBac1.1 crystal were generated and a set of 5% of the reflections were flagged for omission for the subsequent refinement.

4.2.15 Phases

The next step involves phase determination. As part of the process, cysteine mutants were generated for heavy atom derivatisation. Data processing of the mutant derivatives is as described.

4.3 Results and Discussion

KirBac1.1 is a bacterial K^+ channel belonging to the inward-rectifier family of potassium channels. The crystallisation approach was based on the successful crystallisation of the KcsA channel (Doyle *et al.*, 1998). First, N-terminal sequencing and proteolysis were used to identify the rigid protein core. Molecular biology techniques were employed to remove the flexible poorly structured part of the protein. Crystals were screened for using all commercially available screen kits and a home screen kit. Next step involved crystal crystal quality improvement and reproducibility by identifying suitable detergents, proper pH range and PEG. Finally crystal contacts were altered by using detergent mixture. A more detailed search could be carried out for refinement of crystallisation conditions, however, we had to balance this with time constraints and external competition.

4.3.1 KirBac1.1 expression - results and discussion

Both full length KirBac1.1 and KirBac1.1Δ12 constructs were expressed in BL21(DE3) Star* cells. The BL21(DE3) Star* strain contains a mutated *rne* gene, which codes an RNaseE protein for RNA degradation. It is designed for T7 promoter–based expression systems to increase protein yield. Normal BL21(DE3) cells have a rapid transcription level due to a T7 RNA promoter in the expression vector pET 30a. T7 RNA polymerase synthesizes mRNA rapidly resulting in some mRNA transcripts being unprotected by ribosomes and therefore susceptible to endogenous RNase degradation. This mutated BL21(DE3) Star* cell line avoids degradation of transcribed RNA, therefore, increasing the target protein expression.

We found that the growth rate of these cells slowed down after induction. This phenomenon was not just found using KirBac1.1. It occurred also with the Cl

ion channels from *E.coli*. Routinely induction at OD_{600} = 1.1 or 1.2 was used for KirBac1.1. By lowering the induction temperature to 25°C for 12 hours, the KirBac1.1 proteins folded well and none was found in inclusion bodies. The KirBac1.1 is a tetramer in its native membrane environment and is likely to need time to insert, fold and form the tetramer in the membrane.

4.3.2 Protein purification - results and discussion

The KirBac1.1Δ12 produced 5 - 6 g of wet cell mass per litre of LB media. This produced 7 - 8 mg of protein from the Co^{2+} affinity purification. The purity of the protein was approximately 80 - 90%. One of the major contaminations was DNA co-purified with the protein. In an attempt to remove DNA contamination, total membranes were isolated from the crude cell extract. This step also served to reduce the internal proteases that attacked the KirBac1.1 C-terminal domain. By using 500 mM KCl in the Wash I step, most of the nucleotide contaminants were removed.

In order for 3D crystals to diffract to a reasonable resolution, highly purified protein is required. The KirBac1.1 construct has a C-terminal his-tag which binds TALON resin tighter than other native cellular proteins from the *E. coli*. In the wash step different concentrations of imidazoles were tested to maximise elution of the endogenous protein contaminations and to minimise loosing the KirBac1.1 channels. Adding 20 mM imidazole on top of 500 mM KCl in the Wash step II worked quite nicely, removing most background contaminants and retained enough KirBac1.1 protein for further purification.

The 12% SDS-PAGE gels showed that most endogenous *E. coli* proteins were washed away after application of Wash I and Wash II buffers (Figure 4-9 and Figure 4-10). The KirBac1.1 proteins were extracted in DM and exchanged to triDM. The SDS-PAGE gel shows the majority of the channel migrating as monomers with a

minor population as dimers. This is likely to be a result of tetramer disruption by the harsh SDS detergent.

The predicted molecular weight of the monomer is 37.5 kDa from the ExPASy molecular biology server (The University of Geneva; http://www.expasy.ch). But on the SDS-PAGE gel the monomer band runs below the 37 kDa marker band, a phenomenon often observed with membrane proteins.

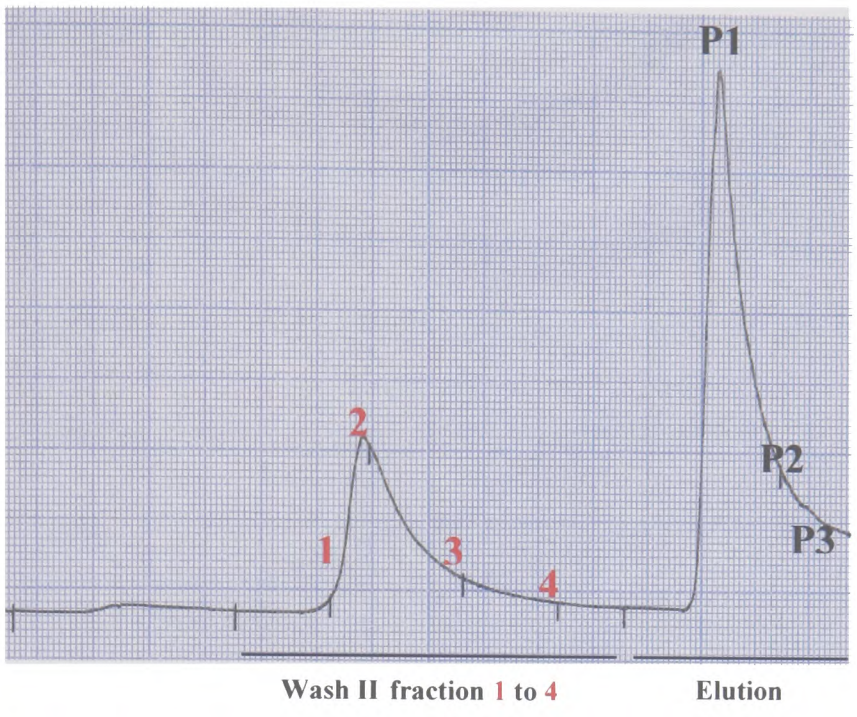


Figure 4-9. Chromatogram of KirBac1.1Δ12 proteins eluted from a Co^{2+} affinity column.
All the proteins were monitored at A_{280}. Fractions 1 to 4 were eluted with 20 mM imidazole in the wash II buffer. P1 and P2 were fractions from the main peak after adding 500 mM imidazole in the elution buffer.

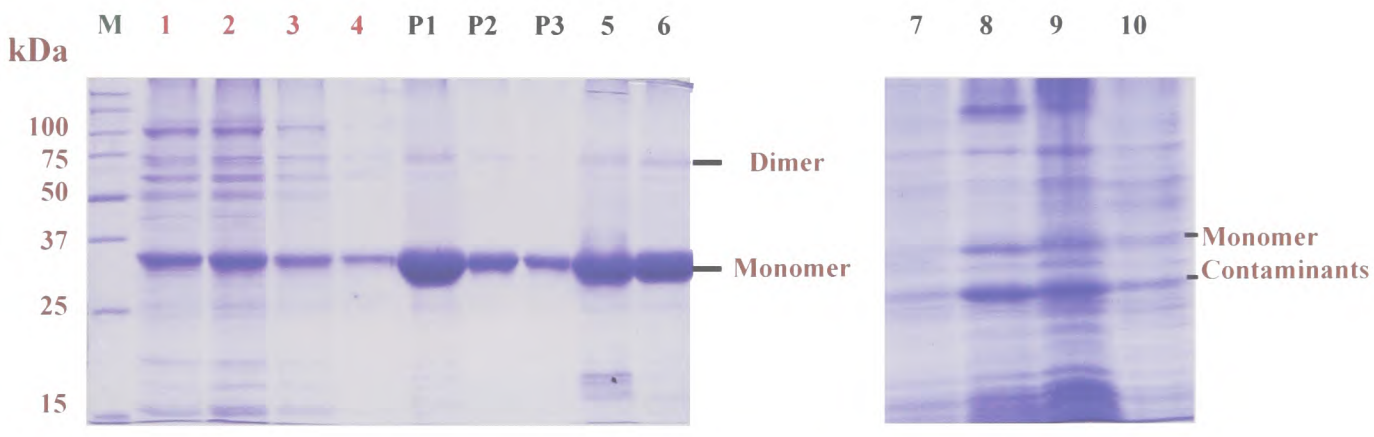


Figure 4-10. 12% SDS-PAGE gel analysis of the KirBac1.1Δ12 protein using the Co^{2+} resin affinity purification procedure.
Lane 1, 2, 3, and 4 show some contaminants being washed off by low imidazole buffer (Wash II). Lane P1, P2 and P3 show the eluted KirBac1.1 protein. Lane 5 is thrombin digested protein. Lane 6 shows the KirBac1.1 after overnight dialysis before applying the thrombin. Lane 7 is the run through after binding to the Co^{2+} resins. Lane 8 is the detergent solubilised membrane proteins, lane 9 is the protein from the high speed membrane preparation and lane 10 is the total cell extract.

4.3.2.1 Choice of detergents and optimisation of detergent exchange

All membrane proteins have hydrophobic regions which are buried in the lipid bilayer and hydrophilic regions which contact the aqueous surface. To isolate membrane proteins an excess of detergent is added. All detergents have a polar head group and a hydrophobic tail. They bind the membrane proteins with their hydrophobic tails forming a ring-like detergent micelle surrounding the protein thus replacing the lipids. Some membrane proteins are not very stable in one particular detergent. Therefore, a selection of detergents is a key aspect for solubilisation of membrane proteins.

The detergent is also important in the purification steps. During solubilisation different detergents select for different lipid types that remain associated with the proteins (Banerjee *et al.*, 1995). After solubilisation the membrane protein consists of detergent-lipid complex as well as pure detergent micelles. The co-purified lipid sometimes is required to maintain the correct membrane protein structure hence its presence is likely to influence crystallisation (Valiyaveetil *et al.*, 2002).

To solubilise KirBac1.1 protein n-Decyl-β-D-maltoside (DM) was chosen based on previous experiments with the KcsA channel (Doyle *et al.*, 1998). DM has an alkyl chain length of 10 with two sugar moities in its head group. Its critical micelle concentration (CMC) value is 1.8 mM (the CMC value is listed by Anatrace). DM is a relatively gentle non-ionic detergent. This detergent maintained KirBac1.1 in its native tetrameric state in solution and within 2 hours the proteins were completely solubilised. However, the drawback of DM is that it seldom forms crystals with protein complex. New detergents must be tried therefore DM has to be exchanged for

other detergents. As this exchange process may not be complete, a way to ensure complete exchange is to start when the protein is bound to the Co^{2+} resin.

4.3.3 His-tag - results and discussion

Most of time the his-tag at the C-terminus of the protein is considered as structurally disordered. Modification of the protein by cutting off the his-tag using the enzyme thrombin yielded a rigid protein core suitable for crystallisation. Later experiments indicated that the his-tag did not influence the crystallisation, therefore, to speed up purification time and prevent non-specific proteolysis (see results of mass spectrometry) the thrombin digestion step was removed. Speed during the purification process is essential as seen during the KirBac1.1 purification protocol. As part of the process, the protein needed to be loaded onto the gel filtration column as soon as possible after concentration otherwise the protein quickly aggregated.

4.3.4 Gel filtration - results and discussion

Further purification was carried out using size exclusion chromatography with an analytical column, S-200. This step served two purposes: (a) ensure that triDM was exchanged completely and (b) separation of the KirBac1.1 tetramer from the aggregates, his-tag and smaller contaminant proteins.

It was noticed that in all SDS-PAGE gels KirBac1.1 ran mainly in the monomeric form. To confirm the KirBac1.1 oligomeric state gel filtration was used not just for removing contaminants but also as an assessment of its native conformation. KirBac1.1Δ12 eluted as a tetrameric channel in triDM (Figure 4-11-B). The molecular marker IgG is a 158 kDa protein. The main peak on Figure 4-11-B corresponds to this weight. The overall size of the KirBac1.1Δ12 is larger than predicted because of the additional detergent around the protein.

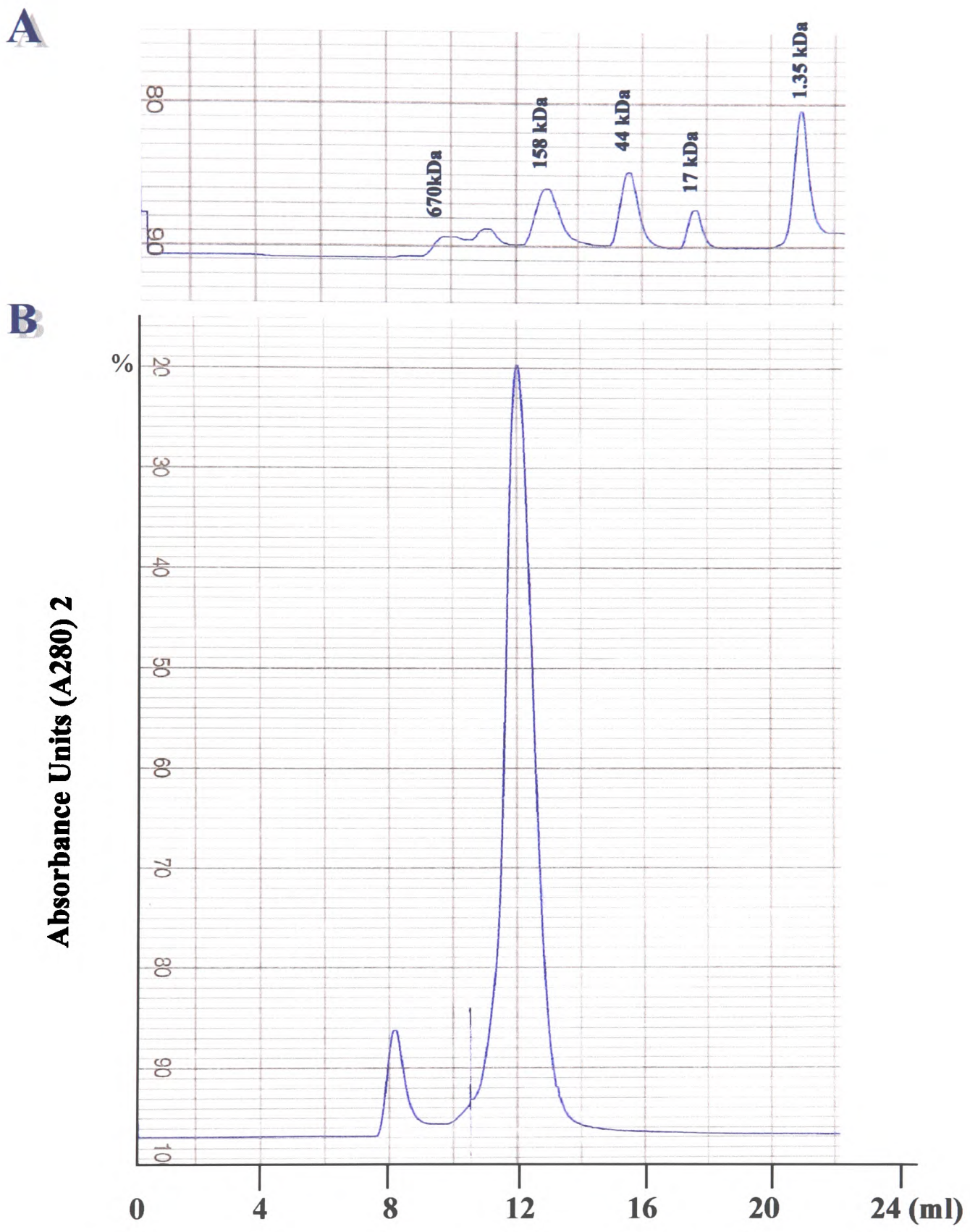


Figure 4-11-A. Elution profile of a Bio-Rad gelfiltration standard.
The markers were run in 50 mM Tris-HCl pH 8.0, 100 mM KCl and 0.5 mM triDM buffer at a flow rate of 0.5 ml per minute.

Figure 4-11-B. KirBac1.1Δ12 gel filtration profile.
The protein was run in 50 mM Tris-HCl pH 8.0, 150 mM KCl and 0.5 mM triDM buffer at a flow rate of 0.5 ml per minute.

Gel filtration yielded a >95% homogenous species. All collected peak fractions were analysed using Coomassie Blue and silver staining techniques on SDS-PAGE gels (Figure 4-12-A and B). Based on the results the fractions corresponding to A_{280} 50% and above were collected, pooled and concentrated for crystallisation trials. Silver staining is a sensitive method that is able to distinguish both acidic and basic polypeptides. Inspection of the silver stained gel revealed few minor species below the KirBac1.1Δ12 major band (Figure 4-12-B, Line 8). Line 8 was the A_{280} for 70% of the main peak and above fraction which still showed impurities.

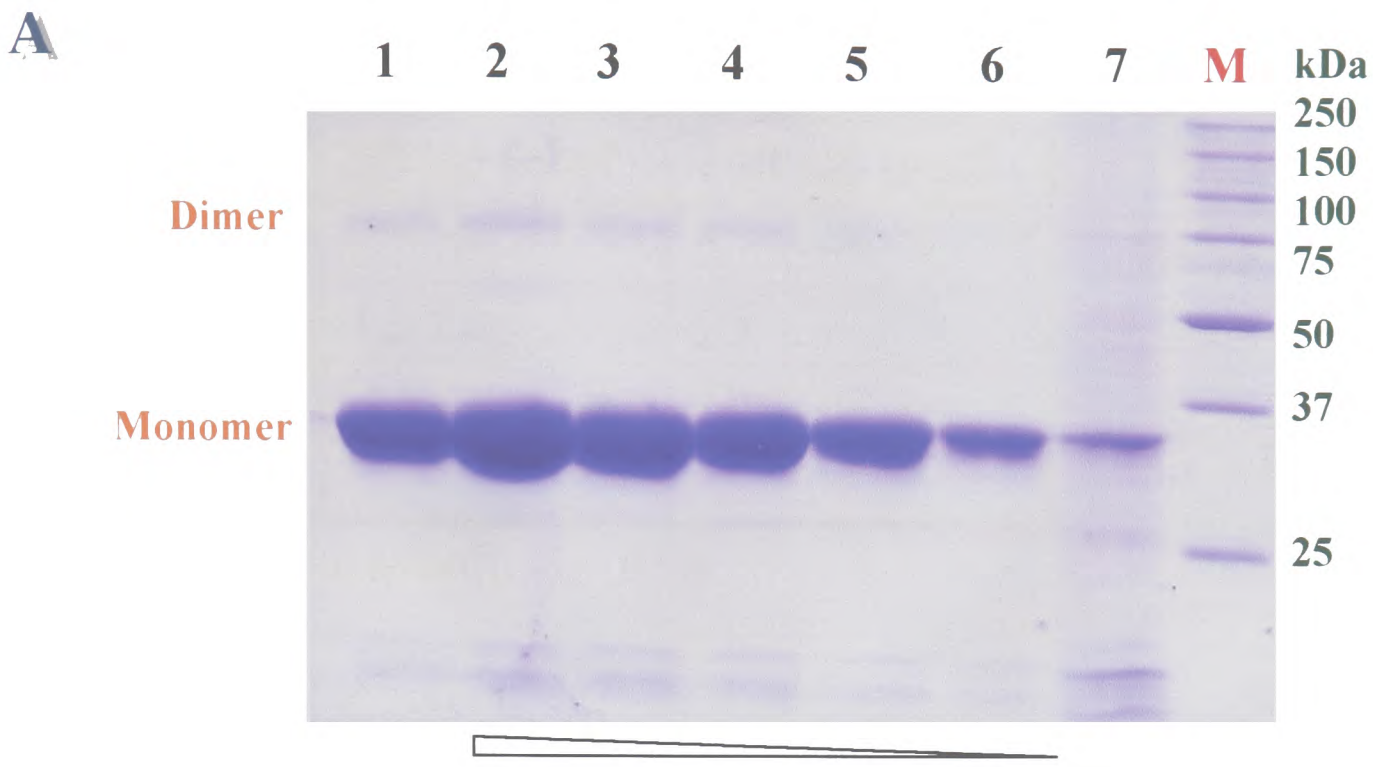


Figure 4-12-A. 12% SDS-PAGE gel stained with Coomassie Blue showing KirBac1.1Δ12 fractions eluted from a S-200 column.
Lane 1 indicated 10 μg of protein after setting up crystal trays. Lane 2, 3, 4, 5 and 6 respectively showed different percentages of the elution peak. The arrow indicated peak fractions descending from 50-10%. Lane 7 showed the aggregated KirBac1.1Δ12. Lane M is a broad range marker from BIO-RAD.

Figure 4-12-B. 12% SDS-PAGE silver stained gel showing KirBac1.1Δ12 fractions eluted from a S-200 column.
Lane 1 showed the protein before gel filtration. Lane 2, 3, 4, 5, 6, 7 and 8 indicated different percentage peak fractions ascending from 10-70%. Lane 9 indicated the aggregated KirBac1.1Δ12.
Lane M was a broad range marker from NEW ENGLAND BioLabs.

4.3.5 Ion-exchange chromatography - results and discussion

Ion-exchange chromatography provided another choice for the purification of KirBac1.1Δ12. For a long time the crystals only diffracted to 4Å resolution limit, therefore, ion exchange chromatography was used in an attempt to improve protein quality. Ion-exchange chromatography separates proteins according to their overall charge. At low ionic strength, the protein binds to the column with a pH range that depends on the isoelectric point of the protein. The KirBac1.1Δ12 has an isoelectric point of 7.0 (calculated using the server www.expasy.ch) and binds well to anion exchange resins at the basic pH of 8.0. After wash steps the protein was released using high concentration of KCl. The hope was that this method would provide a purer homogenous species and improve the crystal diffraction.

Ion-exchange chromatography proved to be successful using a Hi Trap Q FF column as seen in Figure 4-13.

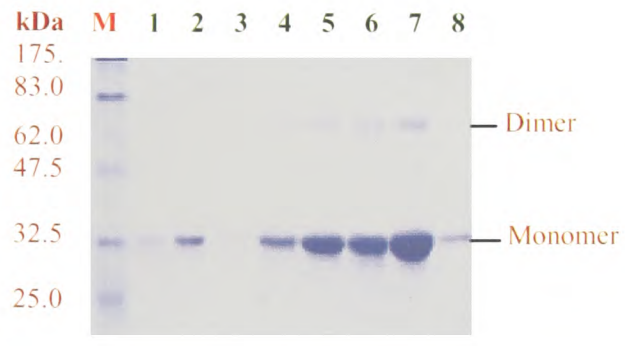


Figure 4-13. SDS-PAGE analysis of KirBac1.1Δ12 fraction eluted from a Hi Trap Q FF column.
Lanes 1 to 8 of a 12% SDS-PAGE gel showing the peak fractions eluted from a Hi Trap Q FF column in 5 mM Tris-HCl, 1 M of KCl and 0.5 mM triDM gradient buffer.

4.3.6 N-terminal sequencing and mass spectrometry - results and discussion

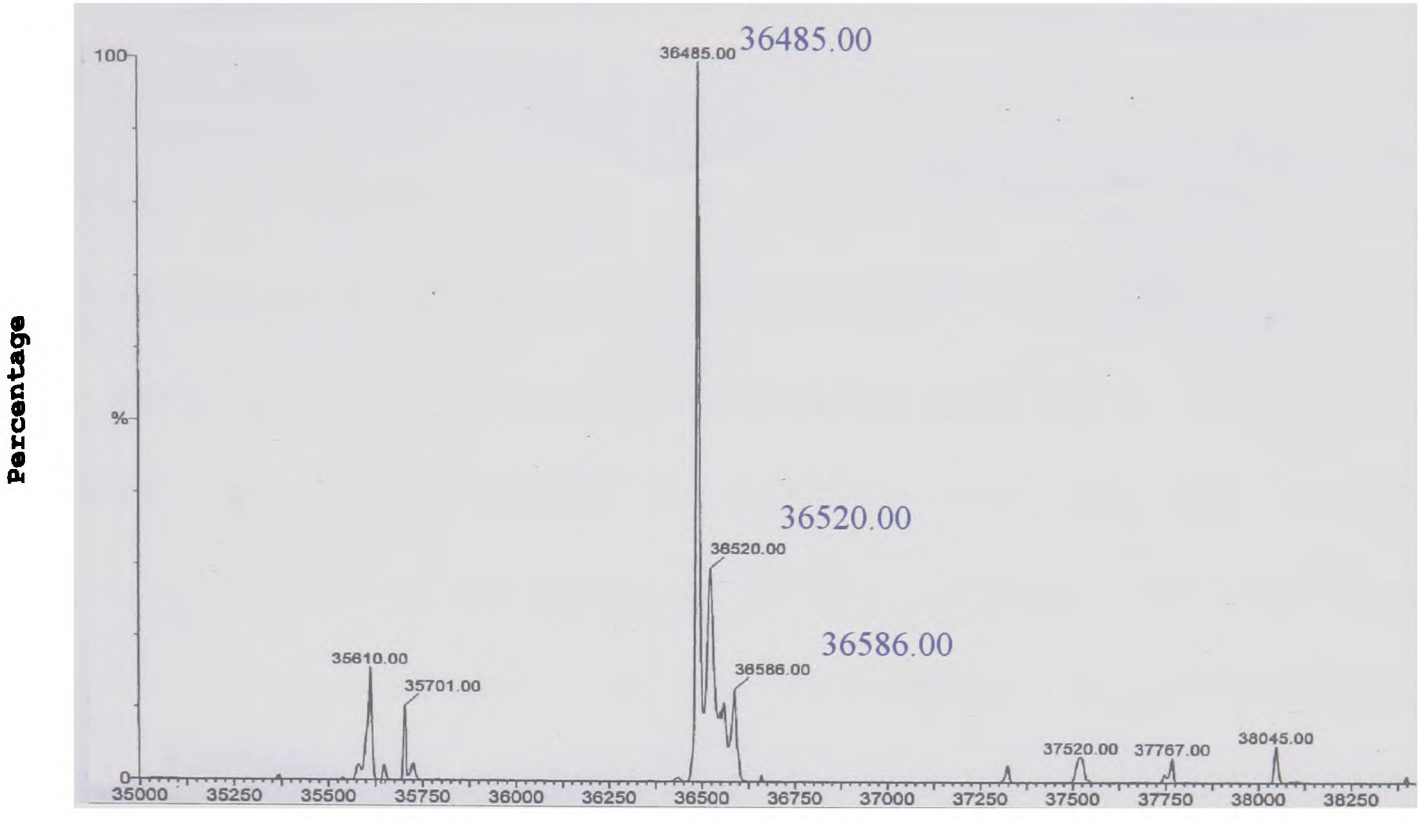
The result of N-terminal sequencing is listed in Table 4-6.

Table 4-6. N-terminal sequencing of the KirBac1.1 full length protein

KirBac1.1 full length	M-N-V-D-P-F-S-P-H-S	Major fraction
	A-A-K-P-G-E-G-D-A-R	Minor fraction

The result led us to delete these 12 amino acids from the C-terminal end of KirBac1.1 to generate a truncated construct with a thrombin site and a his-tag at the C-terminal region. This construct, KirBac1.1Δ12, was used in all remaining steps of the structure determination project. After removing the his-tag from the protein the protein's molecular weight was confirmed by mass spectrometry. Figure 4-14 shows the mass spectrum of the KirBac1.1Δ12 injected in electrospray mode showing a major peak at 36,485 Da and two minor peaks at 36,520 and 36,586 Da. The theoretical mass of the thrombin treated KirBac1.1Δ12 is 36,492.9 Da as calculated using the server www.expasy.ch (University of Geneva). The theoretical value disagrees with the observed value by -7.9 Da which is probably related to calibration errors. The minor larger size species may be a partial digest product. Considering this result we made a few purifications of KirBac1.1Δ12 with the his-tag still on. The full length protein including the his-tag was also used in crystallisation trials.

KirBac1.1Δ12



Predicted Mol. Wt. (Da)	Experimental Mol. Wt. (Da)	Discrepancy (Da) (Experimented-Predicted)
36492.90	36485.00	-7.90
36492.90	36520.00	27.1
36492.90	36586.00	93.1

Figure 4-14. Mass spectrometric analysis of thrombin treated KirBac1.1Δ12.
The sample was analysed by the electrospray ionization on a Micromass BIOQ-II-ZS spectrophotometer. The sample displayed one major peak at 36,485 Da and two minor peaks of 36,520 Da and 36,586 Da.
The determined and predicted molecular weights are shown in the table below.

4.4 Crystallisation - results and discussion

The crystal screen strategy for KirBac1.1 project was as follows: full length KirBac1.1 in LDAO or DDM detergents was screened followed by truncated KirBac1.1Δ12 in triDM or tetraDM. This added up to more than 5,000 different conditions that were tested. This took several months to complete the crystallisation stage. Based on crystal quality a second screen strategy was applied. Refined screen conditions were designed around the conditions which gave fine structured precipitates or supported the growth of KirBac1.1 crystals. The 1,300 screen conditions were narrowed down to less than 100 conditions. The third round screen focused on detergent as an additive, with more than 200 conditions being tried. Finally three detergents: CYMAL-4, MEGA-10 and HEGA-10 were chosen as additives on top of triDM which gave the initial best crystals.

4.4.1 KirBac1.1 crystallised in DDM

The full length KirBac1.1 with his-tag yielded crystals in the Home PEG/ION Screen 900 kit in the condition (20% - 30%) PEG/400, 50 mM $Mg(CH_3COO)_2$ and pH 6.0 – pH 9.0. The protein buffer was 50 mM Tris-HCl, 150 mM KCl and 0.3 mM DDM. Although the crystals were smaller with most crystals irregularly shaped, it indicated that the KirBac1.1 protein was able to crystallised (Table 4-7).

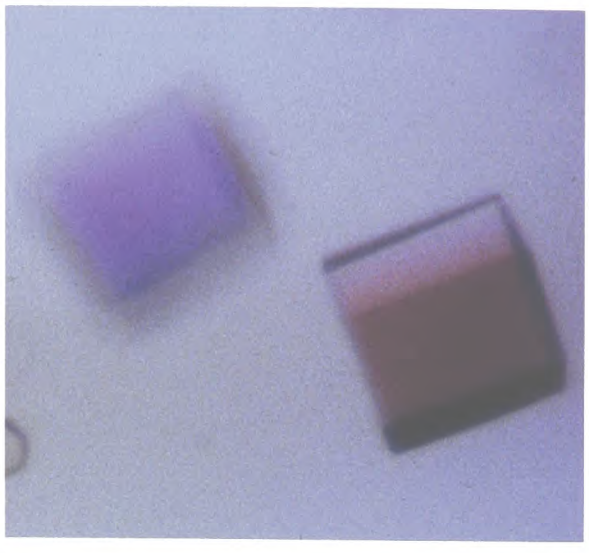
Table 4-7. Home PEG/ION screen 900 of KirBac1.1 in DDM detergent that produced crystals

IONS / PEG	$Mg(CH_3COO)_2$	$CaCl_2$	NaCl	NH_4Formate
350 MME (25%)	H, pH 9.0- 10.0			
400 (25%-30%)	H, pH 8.0 – 9.0	EB, pH 8.0	SC, pH 5.0	
1000 (20%)				H, pH 8.0
4000 (10%)				EB, pH 8.0
8000 (10%)			EB, pH 5.0	N, pH 5.0

Note: Crystal morphologies are: H, hexagonal, N, needle, EB, elongated bar and SC, small cube.

These crystals were taken to ESRF unfrozen in their crystallisation trays but most dissolved during transport. Some crystals were tested at beam ID14-EH1 but they diffracted poorly. The results indicated that KirBac1.1 in DDM did not form strong connections in the crystals resulting in poor crystals quality. Figure 4-15-A showed the morphologies of one of the DDM crystals (Figure 4-15).

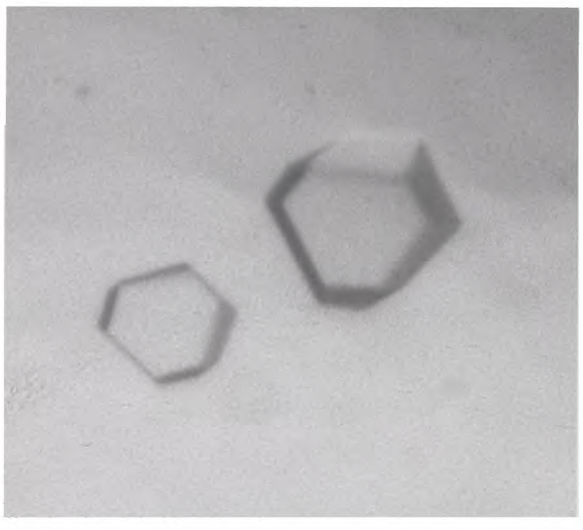
A



A. These crystals were grown in 10 mM Tris-HCl pH 8.0, 50 mM KCl and 0.3 mM DDM.
The precipitant contained 20% PEG/400, 0.1 M Glycine pH 9.0 and 50 mM $Mg(CH_3OO)_2$.

This type of crystal still diffracted to low resolution but the diffraction pattern was very mosaic.

B



B. The crystals were grown in 50 mM Tris-HCl pH 8.0, 150 mM KCl and 3 mM DM.
The precipitant contained 20% PEG/1000 and 0.1 M Tris-HCl pH 8.5.
This type of crystal diffracted to a maximum limit of 20 Å .

Figure 4-15. Initial full length KirBac1.1 crystals in DM and DDM detergents.

4.4.2 Improvement of KirBac1.1 crystal packing

A likely major problem in forming good quality crystals that diffract to high resolution is the packing since the crystals contained protein-detergent mixture, detergent alone, salts and PEG. The nature of the protein means that it has a limited contact area for formation of protein-protein crystal lattice contacts. This is why membrane proteins are difficult to crystallise. We used many ways to refine the crystal packing and each method improved the packing to some extent. The combined improvements added up to improve the quality of crystal diffraction.

4.4.2.1 Reducing KCl concentration and changing detergent

In order to solve the KirBac1.1 structure the crystals needed to diffract to a resolution close to 3.0Å. The crystal packing was considered as the main concern. The screen solutions were optimised to 20% - 26% PEG/400, 50 mM $Mg(CH_3COO)_2$ and 0.1 M Glycine pH 8.6 – pH 10.1 (Table 4-1). The original protein buffer was 50 mM Tris-HCl pH 8.0, 150 mM KCl and 0.3 mM DDM but after the ESRF trip the optimised buffer was established. It was 10 mM Tris-HCl pH 8.0, 50 mM KCl and 0.3 mM DDM. The crystals were larger and thicker but still only diffracted to 16 Å – 18 Å resolution limits. Importantly, the protein needed to be in the precipitant as soon as possible after gel-filtration, otherwise no crystals would form.

At this stage, we continued to search for a better detergent and began to test maltoside detergents with different acyl chain lengths. In the mean time the truncated KirBac1.1 construct was ready to test. The next kin to DDM is triDM but this detergent had a low CMC (0.024 mM in 0.15 mM NaCl). In order to change the detergent completely and not precipitate the protein, 4 mM triDM was used for the Co^{2+} resin step and the Wash II step then 2 mM triDM was used in the Elution step. Then triDM was reduced to 0.5 mM during gel-filtration step.

Final detergent concentration prior to crystallisation was critical and 0.05 mM triDM was found to be the best. When triDM concentration was higher than 0.05 mM, no crystals formed only phase separation occurred, therefore, after the protein was concentrated to 10 mg/ml it was always dialysed for at least 12 hours to reduce the detergent to the designed concentration.

4.4.2.2 Detergents as additives

At this point we found that our time to finish the project was limited and we needed a quicker way to improve the crystal diffraction. Based on advice from professor So Iwata (Imperial College London, UK) we began to use commercially available detergent kits as an additive in the presence of triDM. The initial trials used fixed precipitants of 20% PEG/400, 0.1 M Glycine pH 9.0 and 50 mM $Mg(CH_3COO)_2$. Some hexagonal and trigonal crystal forms grew. Other crystals were rectangular in shape. All these crystals were obtained with triDM mixed with 1 x CMC of CYMAL-4 or HEGA-10 or MEGA-10 using the KirBac1.1Δ12 construct. Two detergents CYMAL-4 and HEGA-10 were finalised after crystal testing at the ESRF. These crystals diffracted to a 4.5 Å – 5 Å resolution limit. The KirBac1.1 in solution exists as a protein-detergent-lipid complex. Specific lattice contacts in the KirBac1.1 crystals are quite complicated. If the detergent micelles are too large it can be a problem for protein crystallisation (Michel, 1983). By adding another detergent on top of the triDM this may reduce the micelle size therefore making stronger crystal contacts. After optimisation of both CYMAL-4 and HEGA-10, 2 X CMC (i.e. 15.2 mM CYMAL-4) mixed with protein containing 0.05 mM triDM yielded the best diffracting crystals (Figure 4-16).

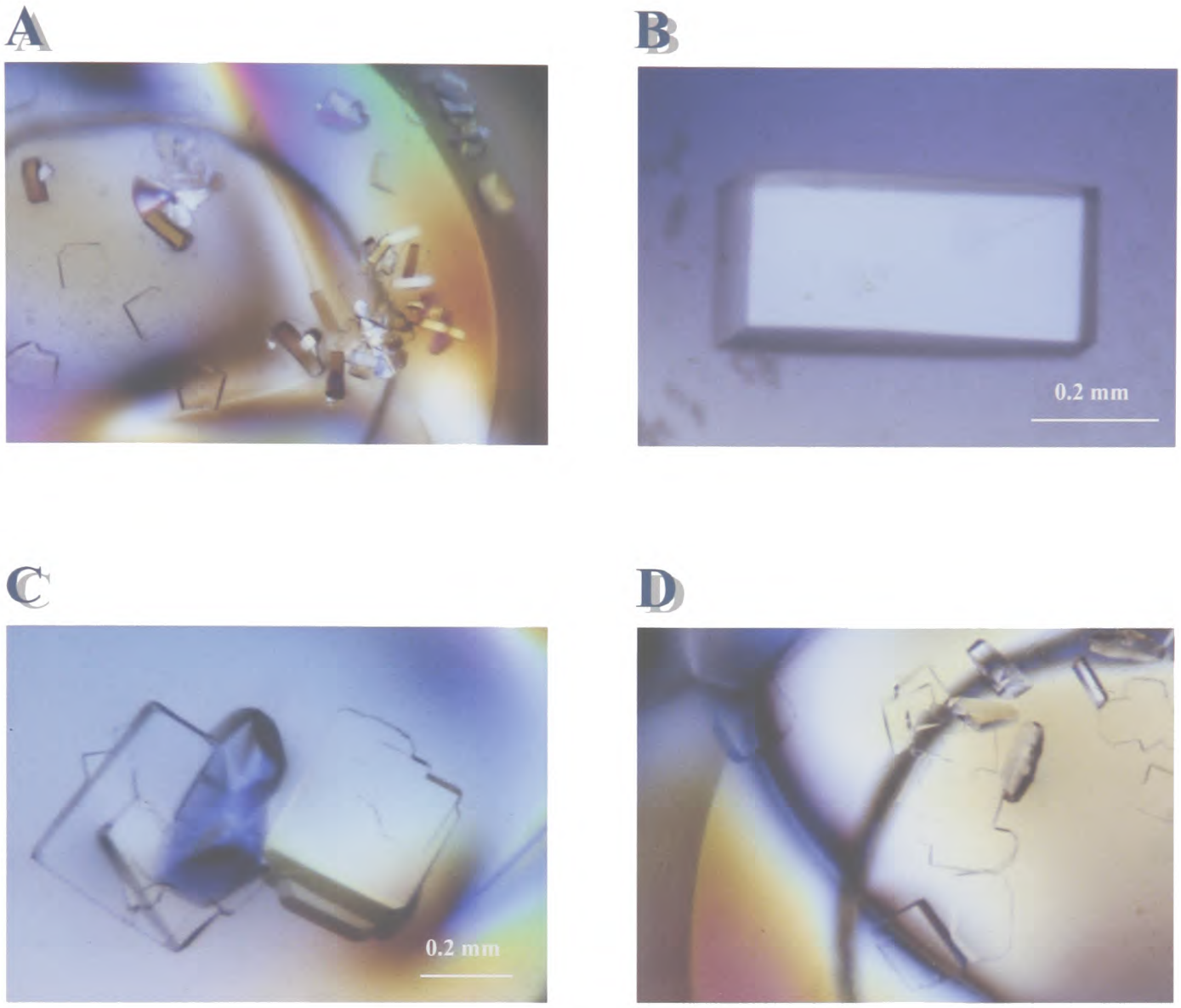


Figure 4-16. Representative KirBac1.1Δ12 crystals.
A. The crystals of KirBac1.1Δ12 grown in the presence of 20% PEG/400, 0.1 M Glycine pH 8.9 and 50 mM $Mg(CH_3OO)_2$.

B. One crystal of KirBac1.1Δ12 in the presence of 21% PEG/400, 0.1 M Glycine pH 9.0 and 100 mM $MgCl_2$.

C. The crystals of KirBac1.1Δ12 grown in the presence of 20% PEG/400, 0.1 M Glycine pH 9.2 and 50 mM $MgCl_2$.

D. The crystals of Kirbac1.1Δ12 grown in the presence of 23% PEG/400, 0.1 M Glycine pH 9.0 and 100 mM $Mg(CH_3OO)_2$.

4.4.2.3 Optimisation of precipitants

Next the precipitants were optimised. The following three screen conditions were performed: (1) 20% - 26% PEG/400, 50 mM $Mg(CH_3COO)_2$ and 0.1 M Glycine pH 8.6 – pH 10.1, (2) 20% - 25% PEG/400, 50 - 100 mM $MgCl_2$ and 0.1 M Glycine pH 9.0 and (3) 20% - 25% PEG/400, 50 - 100 mM $Mg(CH_3COO)_2$ and 0.1 M Glycine pH 9.0. Hence we searched pH, PEG concentration and $Mg(CH_3COO)_2$ or $MgCl_2$ concentration with overlapping conditions as controls.

4.4.2.4 Dehydration of the crystals

The protein concentration used was between 10-12 mg/ml. The crystals typically grew after three to four days and continued growing for another week at 20°C. The crystal quality did not deteriorate for more than one month. Dehydration occured after the crystals were in the wells for longer than a month. We found that the well solution around crystals was more viscous as compared with the previous week when the crystallisation well was opened. The comparison of diffraction images between an one week old crystal and an one month old crystal indicated that dehydration did occur (Figure 4-17 and Figure 4-18). After dehydration of KirBac1.1Δ12 crystals the mosacity reduced and there was a slight improvement in the crystal diffraction resolution limit. Normally PEG/400 at 20% concentration is not fully cryo-protective. However, after one month the crystals were cryo-protected well due to the lose of water resulting in an increased PEG and detergent concentration.

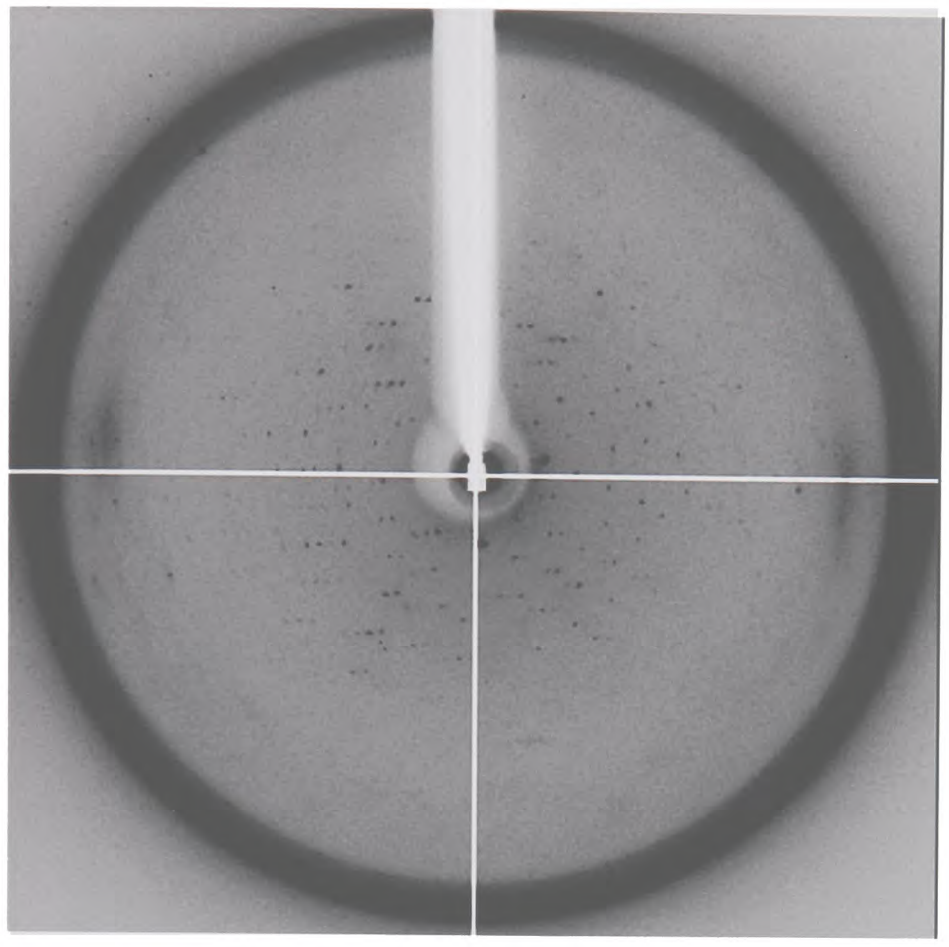


Figure 4-17. Diffraction pattern of a 10 day old KirBac1.1Δ12 crystal.
The ice ring is clearly seen from the diffraction pattern.
The test image was collected at ESRF ID-14EH2.

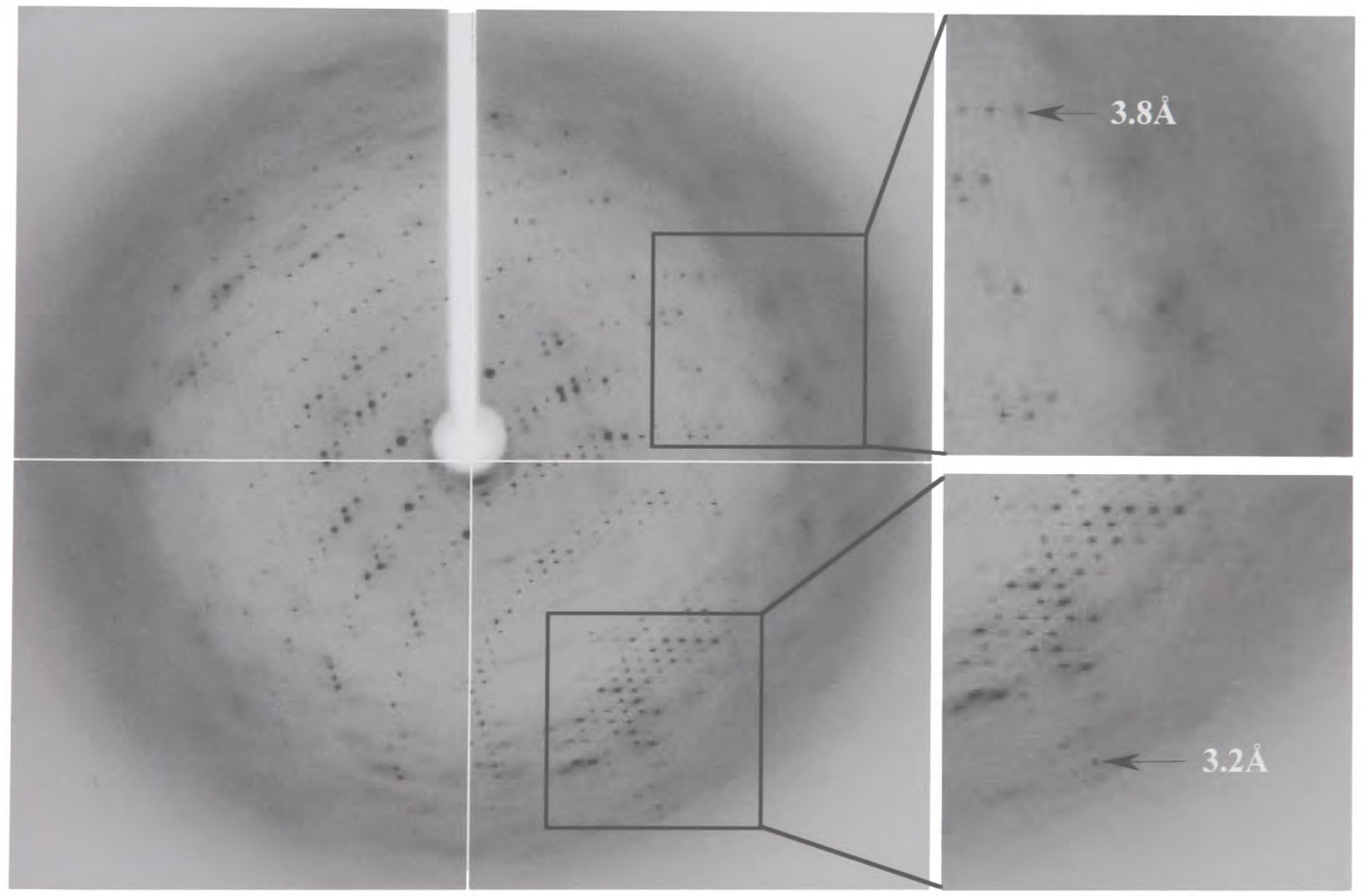
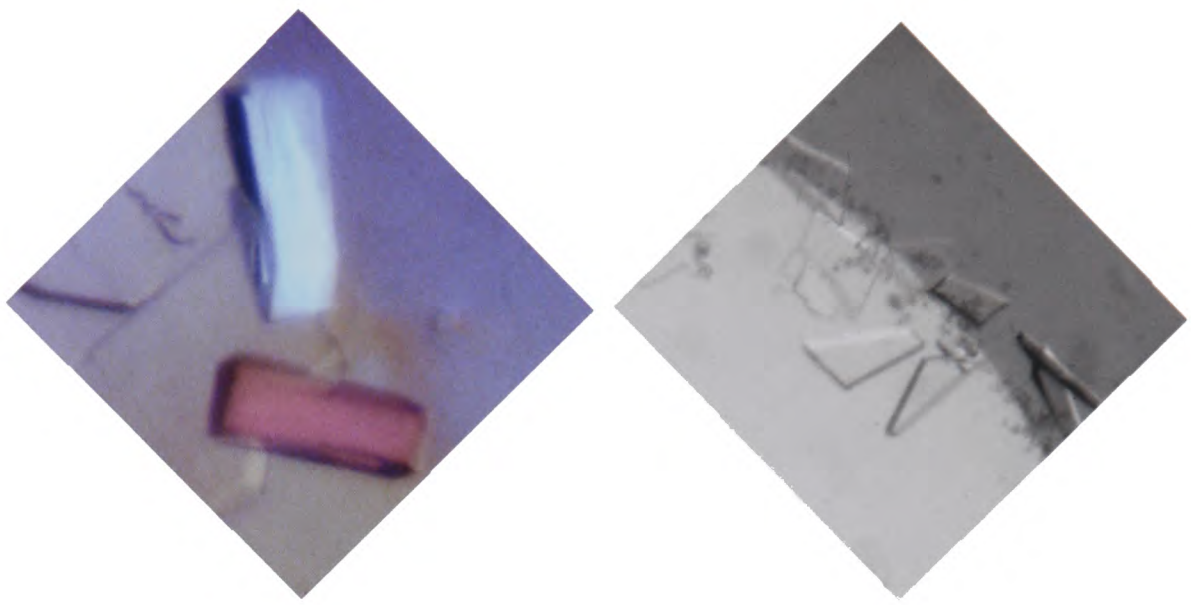


Figure 4-18. Diffraction pattern of a dehydrated KirBac1.1Δ12 crystal.
The image was collected from a crystal that was approximately 3-4 weeks.
The data was collected in ESRF ID-14EH1.
The crystal showed anisotropic diffraction pattern therefore limiting the max resolution at 3.8Å.

We were concerned about the quality of the channels after such a long period of time. Did the KirBac1.1 channels keep their intact form in the crystal or did some degradation occur? To answer this question 10 crystals were taken, washed two times and dissolved in SDS running buffer. The SDS-PAGE gel showed the protein was not just very stable but was also further purified by the crystallisation process (Figure 4-19).

A



B

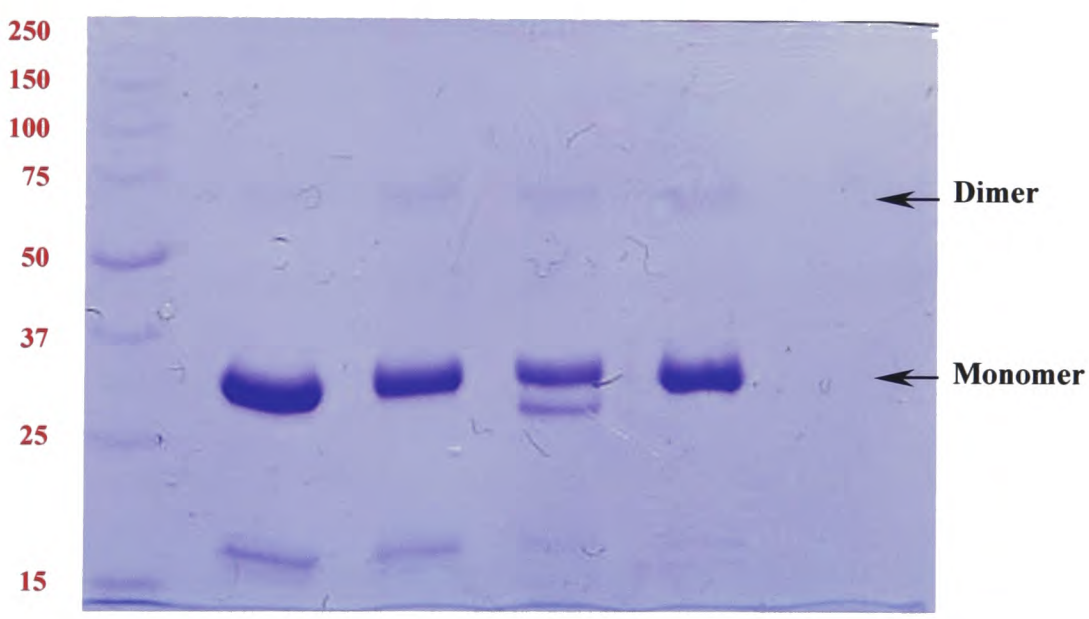


Figure 4-19-A. Pictures of the KirBac1.1Δ12 crystals.
Figure 4-19-B. 12 % SDS-PAGE gel of KirBac1.1Δ12 crystals.
The gel was stained with Coomassie Blue showing KirBac1.1Δ12 protein in its monomeric and dimeric states.
Lane 1 shows the protein before crystallisation. Lane 2 shows the growing chamber solution. Lane 3 shows the mixture of crystals and growing chamber solution. Lane 4 shows crystal protein only.
Lane 5 was the solution from the reservoir.

4.4.2.5 Other optimisation trials

After using ion-exchange chromatography to purify the protein, one of the crystals diffracted to 3.65 Å in 22% PEG/400, 100 mM $MgCl_2$, 0.1M Glycine pH 9.0 with 0.05 mM triDM/14 mM HEGA-10. Two detergents were chosen as additives: (a) truncated KirBac1.1Δ12 without his-tag using triDM/CYMAL-4 and (b) truncated KirBac1.1Δ12 with his-tag using triDM/HEGA-10. In 3D crystallisation literature there are a few examples that used mixed detergents to improve crystal packing (for examples, Kornakis *et al.*, 2000; Kuo *et al.*, 2003; Huang *et al.*, 2003).

To confirm if the mixture of detergents were necessary to yield better crystals, a single detergent 15 mM CYMAL-4 or 14 mM HEGA-10 by itself alone was exchanged in Co^{2+} wash II step and in gel filtration. The crystals grown from each single detergent diffracted badly and the sizes of the crystals grown in CYMAL-4 or HEGA-10 alone were very small and did not diffract better than 5 Å. Therefore, growing crystals in the mixed detergents did improve the quality of diffraction.

Testing four magnesium salts gave the results that $Mg(CH_3COO)_2$ and $MgCl_2$ produced the better crystals. These crystals diffracted to the resolution limit that the structure was determined. The lower temperature of 14°C did not give better crystals than those incubated at 20°C. The emphasis at this time changed to searching for phase information in order to determine the structure.

The fundamental problem in the KirBac1.1 crystal is still packing. This has been confirmed after the structure was solved. Figure 4-20 shows the packing of KirBac1.1Δ12 within the crystal. One part of crystal contact was involved in the turret regions of the channel. This region was relatively flexible in the crystal. In the packing model the red color indicates regions of high thermal motion.

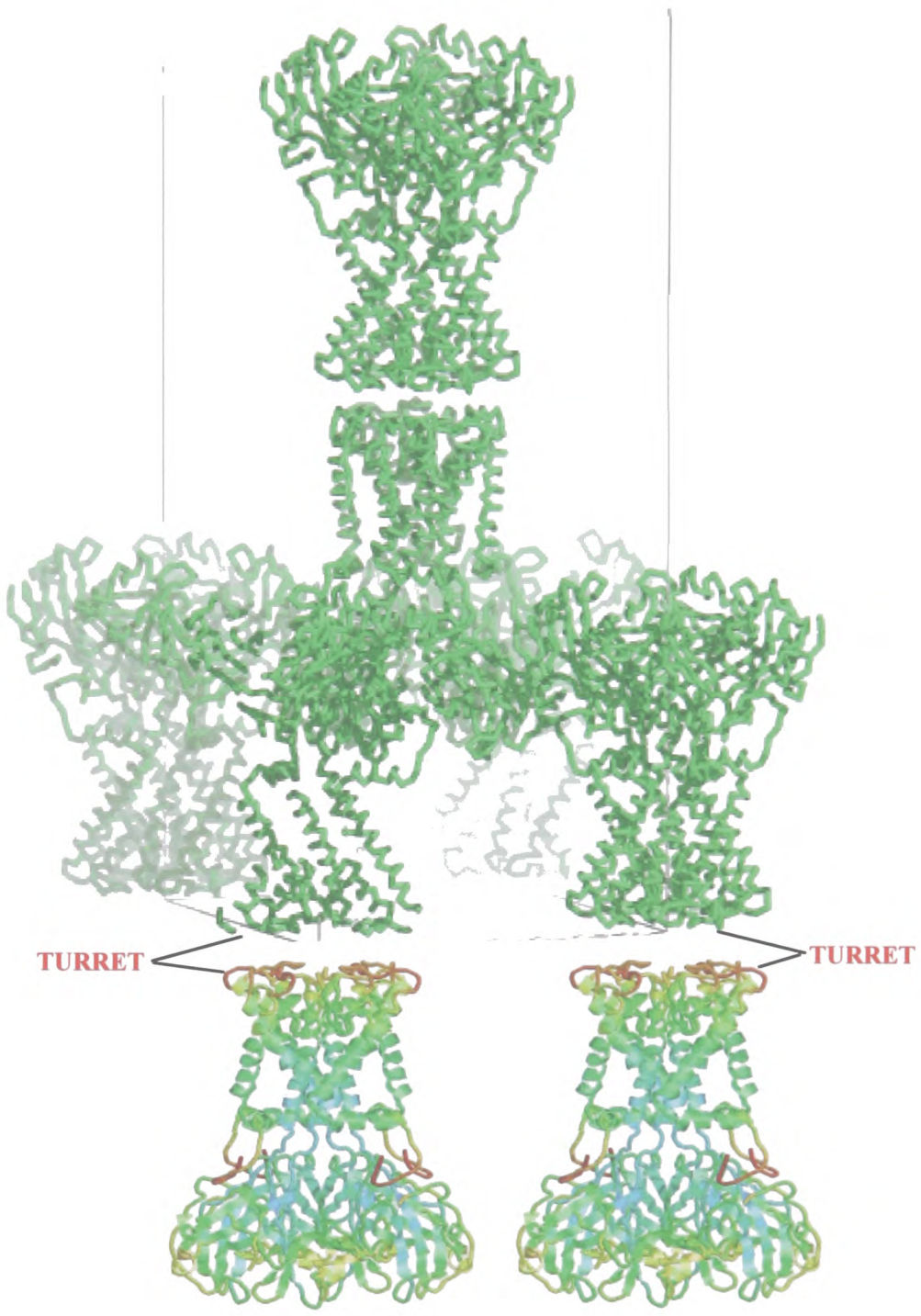


Figure 4-20. KirBac1.1Δ12 crystal packing.
The structure of KirBac1.1 was solved at 3.65 Å resolution. The low resolution was probably caused by a crystal packing problem. The space group is I222. The crystal was packed in such a way that domains contact each other through their turrets. The turrets are flexible regions that make crystal packing loose causing motion within the crystals. The two molecule models are coloured according to the temperature factors. The red colour denotes mobile regions in the structure.
The structure packing model is generated with the program PyMOL.
The structure of temperature model was generated with the program RasMOL.
KirBac1.1 PDB code is 1P7B.

4.5 Heavy metal derivatisation - results and discussion

Many different mercury compounds were tried but most of the mercury compounds destroyed the crystals. Therefore other approaches were pursued such as co-crystallisation with a mercury compound such as thimerosal.

4.5.1 Heavy metal soaking and co-crystallisation with heavy atoms

More than 15 single cysteine mutation constructs were expressed in the *E. coli* cells but only 2 constructs, A125C and T128C, gave reasonable diffracting crystals that were able to be derivatised with thimerosal. Many soaking trials failed to produce diffracting crystals due to the high reactivity of the mercury compounds toward the crystals (Table 4-8).

Table 4-8. Heavy metals tested during KirBac1.1Δ12 derivative screening

Heavy Metal Reagents	Comments
Potassium mercuric iodide	Crystals cracked.
Thimerosal	Crystals diffracted with peaks in Patterson.
p-chloromercuribenzene (PCMB)	No diffraction
K_2PtCl_4	No diffraction
$Hg(CH_3COO)_2$	Crystals cracked.
$HgCl_2$	Crystals were destroyed.
CH_3HgCl	No diffraction
$CH_3Hg(CH_3COO)$	No diffraction

The selection of cysteines was based on alignment of KirBac1.1 with KcsA. 60% of the amino acids of KcsA were mutated to find a few mutants that gave diffracting crystals. $HgCl_2$ was bound to the cysteine mutants and used to calculate phases. This accumulated knowledge helped us tremendously in the KirBac1.1 project. Within a few weeks we successfully found that A125C and T128C not only crystallised but also diffracted to around 4Å resolution. An important parameter was

that these two mutant crystals gave the same space group as the wild type crystals with the same unit cell dimensions. Unfortunately the KirBac1.1Δ12 crystals were easily damaged with $HgCl_2$ compound. This was why co-crystallisation with thimerosal was attempted. Thimerosal is a "gentle" mercury compound and gave both co-crystal and soaking crystals phase information.

4.5.2 Rb^+ and Cs^+ ions replacement of K^+ ions

Both Rb^+ and Cs^+ ions are heavier than K^+ ions. The hope was that these ions would replace the K^+ within the selectivity filter. The precise number of ions in the filter could not be discerned at the resolution of 3.7 Å, therefore, crystals grown in Rb^+ or Cs^+ were used to identify K^+ ion occupancy in the filter region. Most of the Rb^+ and Cs^+ crystals diffracted to 6 Å – 8 Å with only a few diffracting to 4 Å.

4.5.3 Seleno-methionine labelled KirBac1.1Δ12

In KirBac1.1 there are total of 16 methionines. The seleno-methionine labeled protein failed to yield any useful crystals though they did grow thin crystals. A total of 4 litres of culture yielded only 5 - 6 mg of protein after affinity purification. This indicated that the seleno-methionine incorporation effected the protein expression. Inspection of the Co^{2+} elution profile and the 12 % SDS-PAGE gel indicated that two protein components were present (Figure 4-21). The whole purification process was long involving storing the protein at room temperature for more than 12 hours. This might cause the seleno-methionine to oxidise. In the labeled protein it was possible that a fraction was not completely oxidized therefore producing two species. The Co^{2+} resin was not compatible with the use of the reducing agent DTT. Several bands appeared in the 12 % SDS-PAGE gel using silver staining technique (Figure 4-22). This might be a reason why seleno-methionine labeled protein did not form suitable crystals.

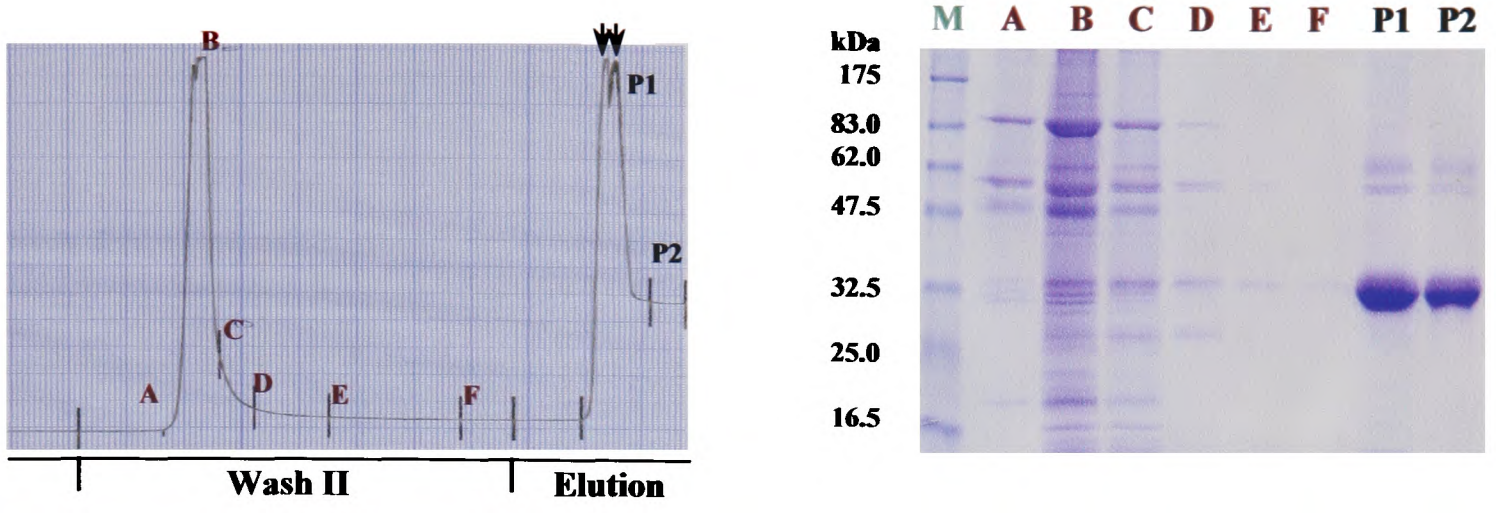


Figure 4-21. Chromatogram of KirBac1.1Δ12_Se-Met protein from Co^{2+} affinity purification and analysis of fractions by SDS-PAGE gel.
Lane A, B, C, D, E and F indicated the Wash II peak fractions.
Lane P1 and P2 were eluted peak fractions. The SDS-PAGE gel labels correspond to the chromatogram of the elution profile.

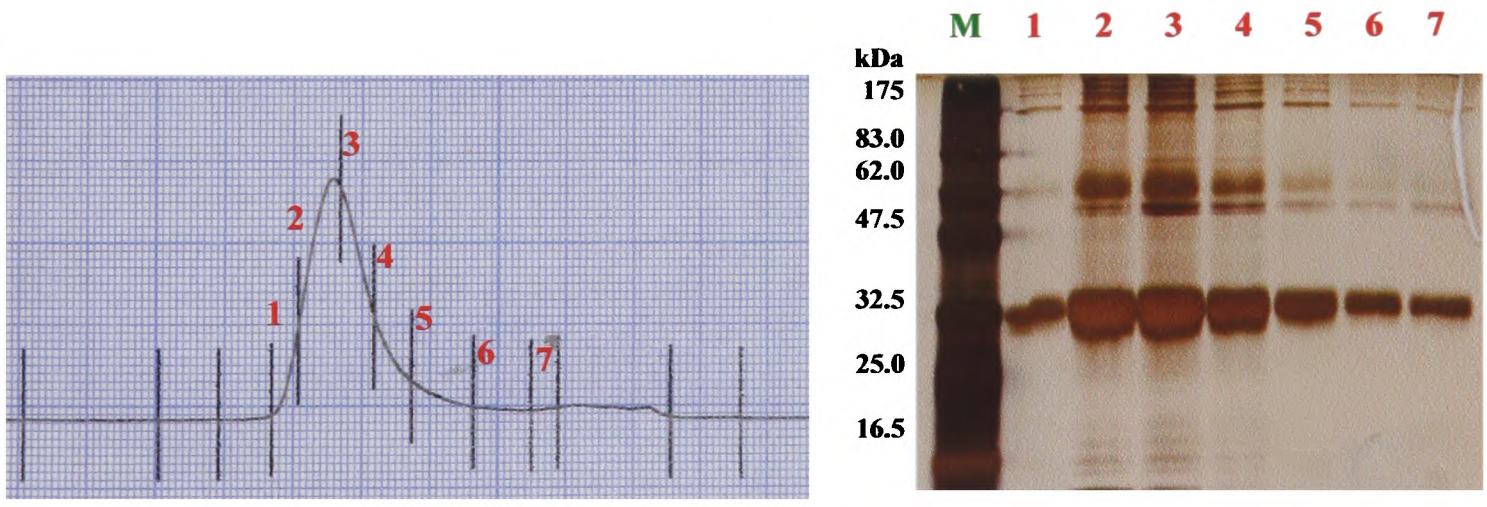


Figure 4-22. Ion exchange chromatogram of KirBac1.1Δ12_Se-Met protein and SDS-PAGE gel analysis of each fraction.
The gel was stained with silver staining solution and Lane 1, 2, 3, 4, 5, 6 and 7 were elution peak fractions from 1M KCl gradient buffer and SDS-PAGE gel numbers correspond to the elution peak fractions.

4.6 Data processing and structure determination - results

The following table lists the results of data processing of KirBac1.1Δ12.

Table 4-9. Statistics on the data sets used during the structure determination of the KirBac1.1 channel

	Native Data	T128C-Hg	A125C-Hg	CsCl
Data Collection Site	**ESRF 3-11-02**	**ESRF 13-9-02**	**ESRF 7-12-02**	**ESRF 4-10-02**
Data Collected	100°	94°	96°	95°
Temperature	100 K	100 K	100 K	100 K
Wavelength (Å)	0.934	0.934	0.934	0.934
Spacegroup	I222	I222	I222	I222
Unit Cell Dimensions (Å)	92.84 105.62 258.63	92.89 105.85 259.18	92.62 105.57 256.19	92.65 104.59 255.74
α β γ	90.00° 90.00° 90.00°	90.00° 90.00° 90.00°	90.00° 90.00° 90.00°	90.00° 90.00° 90.00°
Resolution Range (Å)	30 – 3.65	20 – 3.9	20 – 4.0	25 – 4.8
Total Number of Reflections	88035	28817	33427	15575
Number of Unique Reflections	14459	8536	10025	5644
Redundancy	6.1	3.4	3.3	2.9
Completeness	99.4 %	89.2 %	98.6 %	91.0 %
$\langle I/\sigma(I)\rangle$	5.2	7.8	5.7	6.9
R_{merge}	0.084	0.070	0.077	0.070

4.7 Structure description and functional implications

Inwards rectifier K^+ (Kir) channels belong to a large subfamily of K^+ channel which preferentially conduct K^+ ions inward at negative membrane voltages than outward at the equivalent positive membrane voltages (Katz, 1949; Hodgkin and Horowicz, 1959; Noble and Tsien, 1968; Hille and Schwarz, 1978; Hille, 2001). These K^+ channels are important in controlling the resting membrane potential of cells in many organisms. The newly solved KirBac1.1 structure is a representative of this subfamily (Figure 4-23-A). The obvious evidences come from the sequence alignment (Figure 4-24) and the comparison of the C-terminal domain of Kir3.1 with that of KirBac1.1 (Nishida and MacKinnon, 2002). Both C-terminal domains show similar fold (Figure 4-25). The structure of KirBac1.1 highlights several features unique to this subfamily of K^+ channels, whilst at the same time supporting current themes of Kir channels observed by electrophysiological and mutagenic methods. Although the structure of KirBac1.1 is not at a high resolution, it still shows the nature of the physical features for this subfamily.

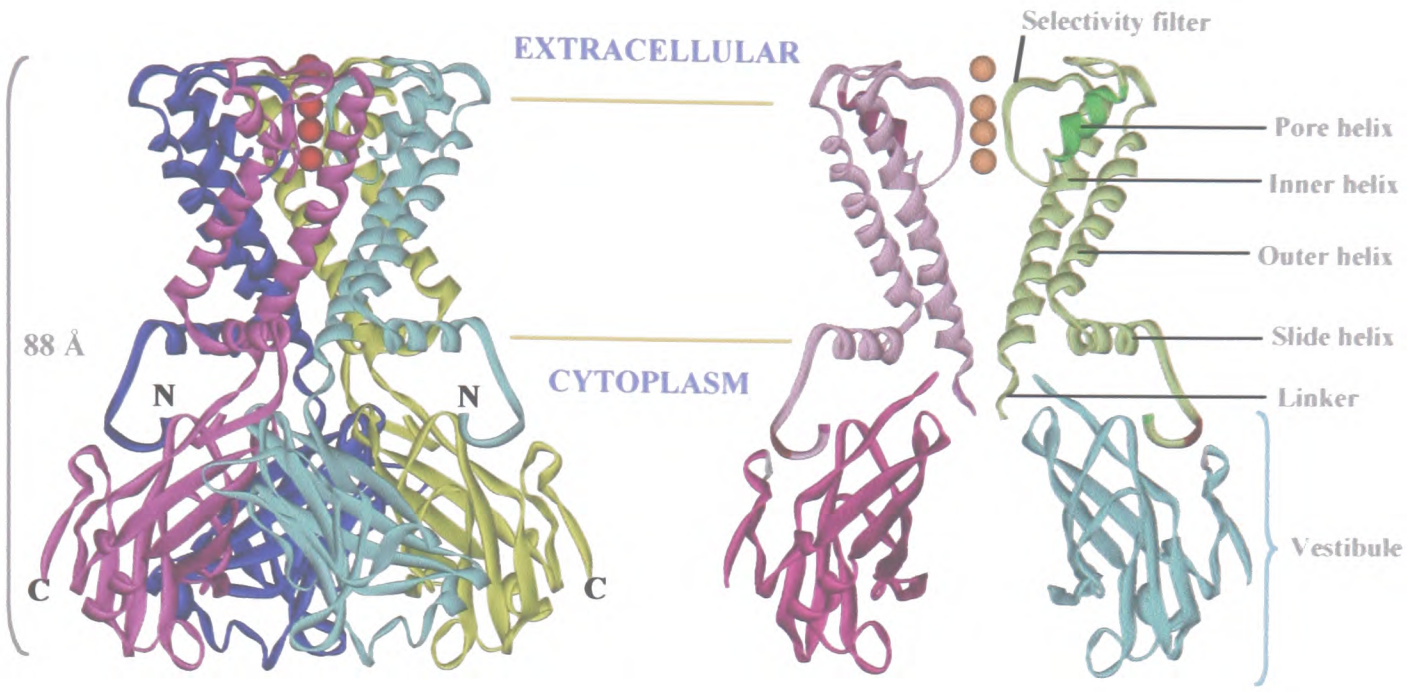


Figure 4-23-A. Overview of the KirBac1.1 structure.
Two lines represent the membranes. On the left four colored subunits highlight the secondary structural elements and domains. The total distance for an ion traveling through the channel is 88 Å. On the right the side view of the KirBac1.1 structure shows one slide helix, outer helix, inner helix (asparagus color), pore helix (green), linker (residues 151 to 155) and the vestibule. Four tangerine spheres represent K^+ ions, three in the selectivity filter and one in the extracellular entry way to the selectivity filter. Two subunits are taken away for a clear view of detailed components in the structure.
The models are generated (PDB ID: 1P7B) using WebLab ViewerPro5.0.

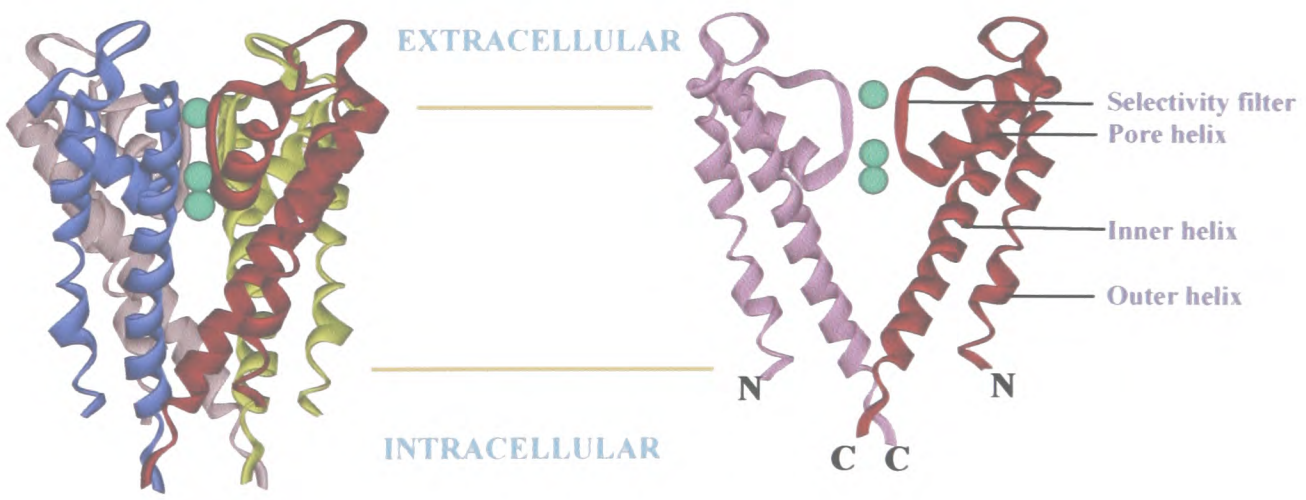


Figure 4-23-B. Overview of the KcsA structure.
Two lines separate membrane region into extracellular and intracellular domains. The left view uses four colored monomers to show secondary structural elements. On the right two monomers have been removed for clarity showing selectivity filter, pore helix, inner helix and outer helix. Green spheres represent three K^+ ions in the filter region.

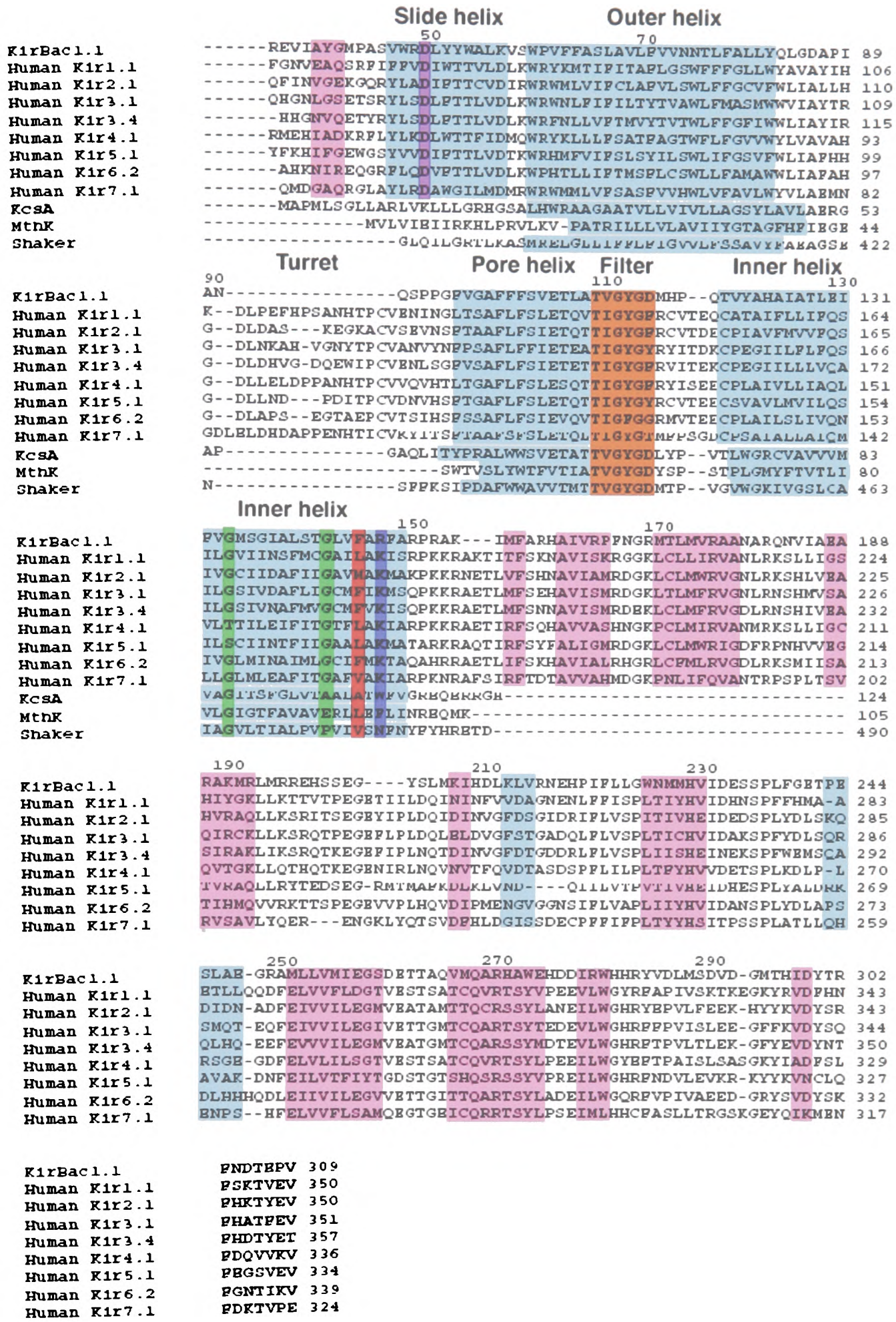


Figure 4-24. Sequence alignment of the KirBac1.1 with the eukaryotic family of Kir channels.

This sequence alignment was generated using ClustalW (http://www-igbmc.u-Strasbg.fr/BioInfo/ClustalW/).

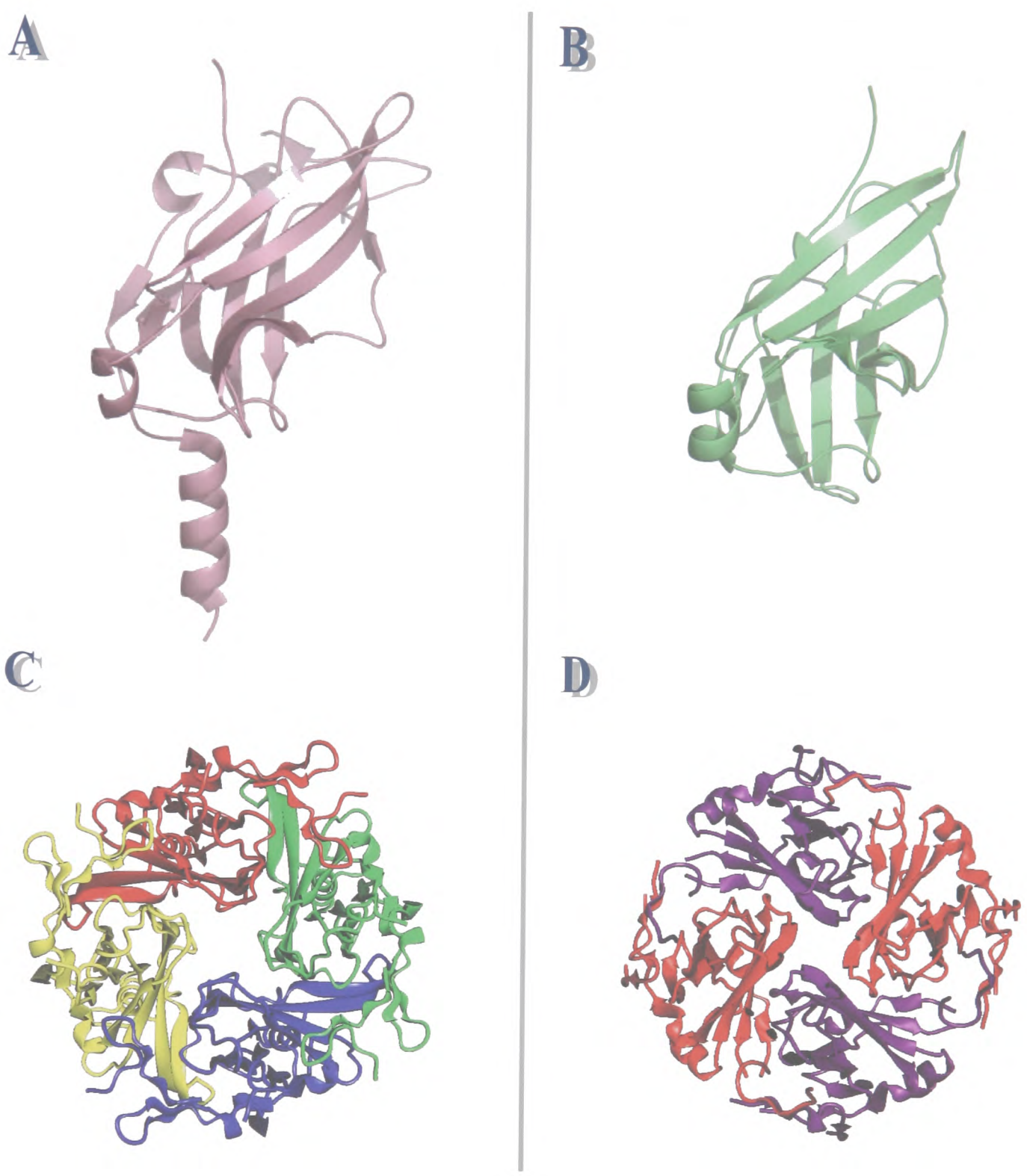


Figure 4-25. Structural comparison of the cytoplasmic domains of KirBac1.1 with Kir3.1.
A and **B** are side views of the C-terminal subunits of the Kir3.1 and KirBac1.1. The Kir3.1 domain structure is pink and the KirBac1.1 domain is lemon colour (Kir3.1 PDB:ID 1N9P). The models are generated using PyMOL.
C and **D** are the top view of the Kir3.1 and KirBac1.1 cytoplasmic domains after removed of the transmembrane sections. Both pictures are of the vestibule region viewed from the intracellular side of the membrane. Both models are prepared using Aesop (Dr. Noble, M. E. M., LMB, University of Oxford).

4.7.1 Overview of KirBac 1.1

The KirBac1.1 channel is a homo-tetramer with the ion conduction pathway in the middle of four subunits. Both N- and C- termini are found in the cytoplasm. Each subunit consists of an inner and an outer transmembrane helice, a pore helix, a slide helix and an intracellular domain of mostly β-sheets (Figure 4-23-A).

Like the KcsA K^+ channel structure, the inner helix faces the central pore while the outer helix faces the lipid membrane. Unlike the crystal structure of KcsA, KirBac1.1 has an extra helix that resides in the membrane, called the slide helix. This helix runs parallel with the membrane cytoplasmic interface (Figure 4-23-A and B). The inner helix connects to the C-terminal domain via a linker, residues 151 to 155 (Figure 4-23-A). Furthermore, three N-terminal residues 40 to 42 interact with the outer edge of an adjacent C-terminal domain 298 to 300 to form a small parallel β sheet (Figure 4-36). The total distance that an ion travels through the channel is 88Å.

The crystal structure of KirBac1.1 provides an architectural view for the Kir channel subfamily (Figure 4-23-A). Interpretation of the KirBac1.1 structure indicated that it was crystallised in the closed state.

4.7.2 Structural evidence for KirBac1.1 in the closed state

Analysis of the KirBac1.1 structure and comparison with other K^+ channel structures revealed the following evidence that the KirBac1.1 channel was captured in the closed state.

4.7.2.1 Phe146 blocks ion conduction pathway

The most obvious evidence for the closed state of KirBac1.1 was the presence of four phenylalanine (**Phe146**) side chains tightly packed in the ion conduction pathway. The Phe^{146} residue is located one turn away from the end of the inner helix.

The large four aromatic Phe residues, one from each subunit, form a plug, blocking the ion pathway (Figure 4-26). Sequence alignment of the Kir channel family indicates that residues with large hydrophobic or aromatic side chains are predominantly found in this position. The red bar in the inner helix region highlights the relative positions of other human Kir channel, blocking residues (Figure 4-24). It was also reported that hydrophobic residues block the ion conduction pathway in the structure of the acetylcholine receptor (Unwin, 1993; Unwin, 1995).

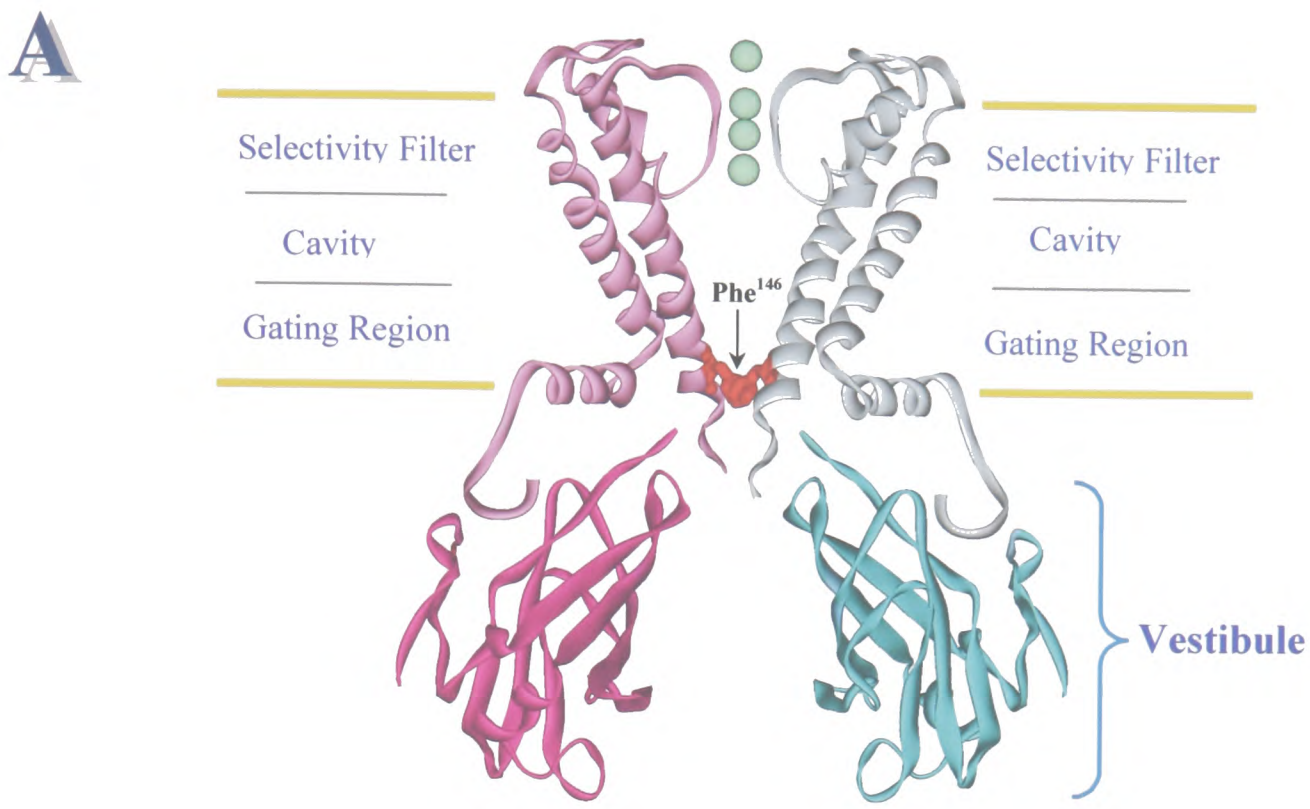


Figure 4-26. Phe^{146} blocks K^+ ions entering the conduction pathway.
Model **A** denotes the side view of the KirBac1.1 showing the residue Phe^{146} (red) blocking the pathway. The three green spheres represent K^+ ions in the selectivity filter.
Model **B** is the tetrameric KirBac1.1 channel viewed from the extracellular side. The subunits are individually colored white, light blue, eggplant and light maroon. Four Phe^{146} residues (red) block the K^+ ions (green) entering the channel cavity.
Models are prepared using WebLab ViewerPro5.0 (The PDB ID: 1P7B).

4.7.2.2 An altered selectivity filter

All potassium channels display signature sequences of TXGYG or TXGFG (X represents V or I). This is part of the selectivity filter and is also known as the pore loops (Heginbotham *et al.*, 1994). Two important features that a K^+ channel must achieve include: (1) select K^+ ions over other monovalent cations such as Na^+ and (2) approach a high speed of K^+ ion movement.

The selectivity filter in a K^+ channel is a narrow passage which links its cavity to the external area. In order for the channel to select a K^+ ion, the conserved TXGYG or TXGFG in the selectivity filter forms a special geometry. Glycine residues offer flexibility so that all of the backbone carbonyl groups point into the central ion conduction pathway (Figure 4-27).

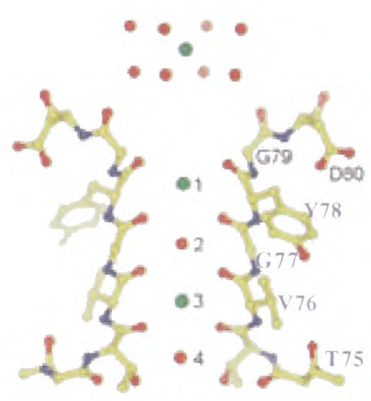


Figure 4-27. The selectivity filter of KcsA. The picture was adapted from the high resolution structure of KcsA co-crystallised with a Fab antibody (Zhou *et al.*, 2001). The green spheres represent K^+ ions and red spheres represent H_2O molecules.

When a charged ion moves across the lipid bilayer, it's charge and hydration state must be taken into account. The optimally positioned carbonyl oxygen atoms protrude along the ion conduction pathway, providing several closely spaced binding sites of the required geometry for dehydrated K^+ ions. The side chains of the pore loop residues point away from the selectivity filter and pack against the side chains from the pore helices (Figure 4-27). This packing fixes the position of the carbonyl oxygen atoms in the correct dimensions to provide binding site for K^+.

A dehydrated K^+ ion optimally fits the geometry of the selectivity filter but a dehydrated Na^+ ion is too small whereas the hydrated Na^+ ion is too large to enter the

filter region (Bezanilla and Armstrong, 1972). The channel, therefore, selects K^+ ions over Na^+ ions (Figure 4-28).

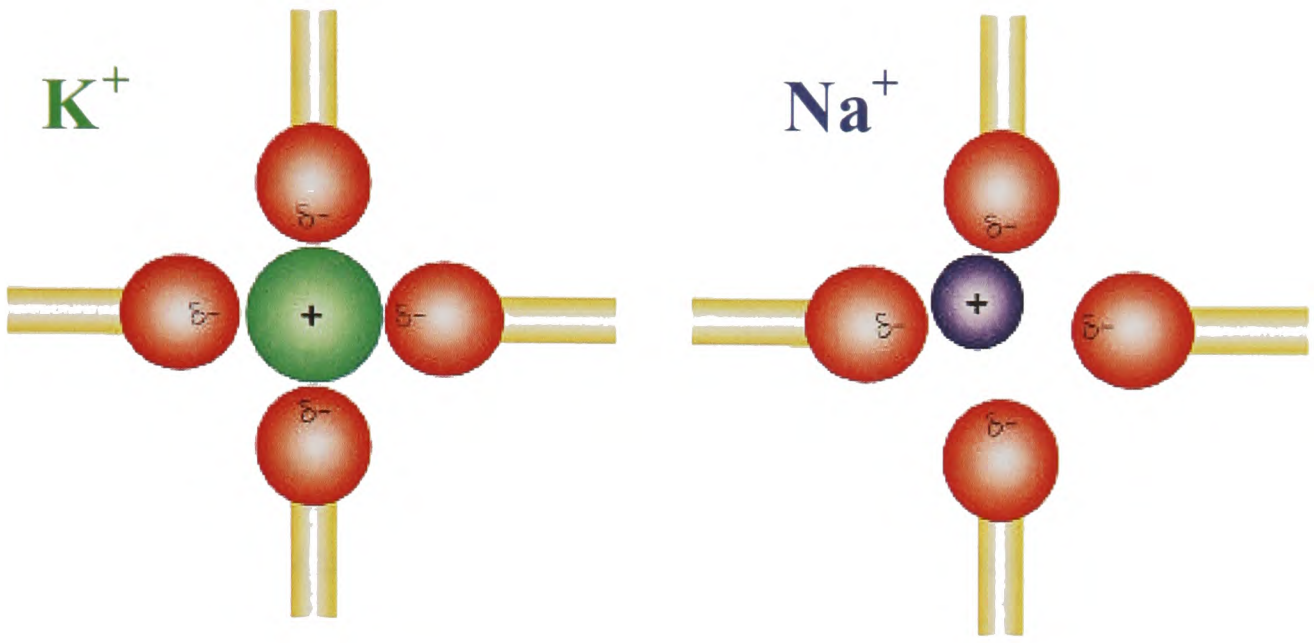


Figure 4-28. A schematic cartoon representation of the selectivity filter region of KcsA.
The four red spheres represent the carbonyl oxygen atome of KcsA. The green sphere represents a K^+ ion and a blue sphere represents a Na^+ ion.

KirBac1.1 has the same signature sequences and the same mechanism of ion selection as in all K^+ channels. However, the structure of KirBac1.1 was solved when the channel was closed. How does the channel prevent the filter from collapsing when it is closed?

The closed KirBac1.1 structure showed three K^+ ions located in S_1, S_2 and S_3 in the filter region. Generally it is believed that only two K^+ ions can simultaneously occupy the filter (either S_1 and S_3 or S_2 and S_4 sites) due to repulsion between K^+ ions (Doyle *et al.*, 1998; Morais-Cabral *et al.*, 2001; Zhou *et al.*, 2001). What we observed is an averaged view of alternate configurations of the filter within the crystal. In the crystal some channels contain two K^+ ions and others contain one K^+ ion in the filter region. As well as selecting for K^+ ions, the channel uses K^+ ions to act as a structural

component preventing the filter region from collapsing. It is known that total removal of K^+ from a K^+ channel results in total irreversible loss of function (Khodakhah *et al.*, 1997)

Analysis of the temperature (B) factors of the ions in the filter region of the KirBac1.1 structure further implies the channel was captured in the closed state. The value of the temperature factors represents the movement of an ion from a central position, reflecting its mobility. In the high-K^+ KcsA structure (Figure 4-29-A), an ion-conducting state, the temperature factors for four K^+ ions are very similar to each other. In our KirBac1.1 structure the temperature factor for K^+ ion in the S_2 binding site is significantly lower than that of the K^+ ions in the S_1 and S_3 sites. The closed conformation suggested that the selectivity filter of the KirBac1.1 is in a protected state, which, although not conductive, maintains a stable configuration in order to prevent irreversible damage. The channel, however, is prepared to move rapidly into an active conformation for ion permeation when it receives the proper signals (Figure 4-29-A). The high rate of ion movement is contributed by repulsion between K^+ ions, which destabilise one another.

The filter region of the low-K^+ structure had only two K^+ ions in positions S1 and S4. As the filter was partially collapsed it was believed to represent a non-conducting form (Figure 4-29-B). The selectivity filter of KirBac1.1 looks more similar to the high K^+ structure (Figure 4-29-A).

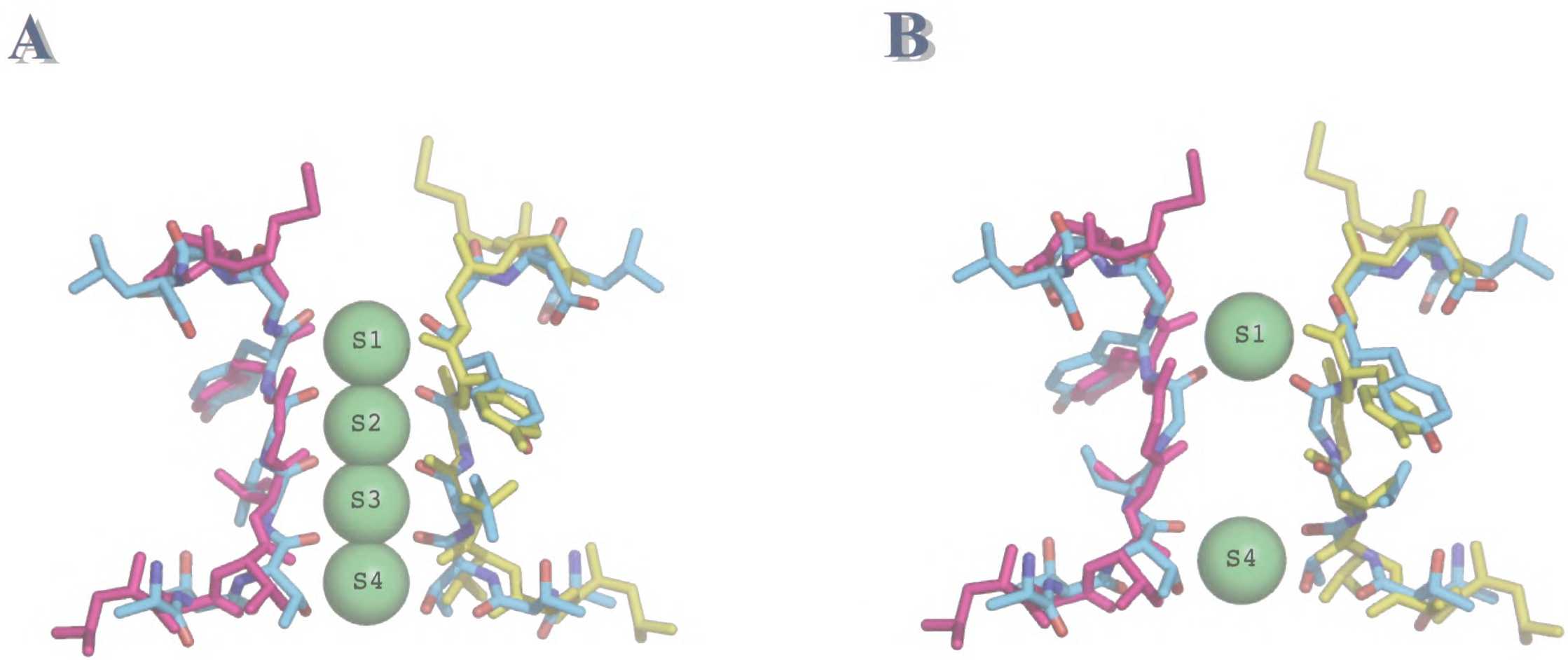


Figure 4-29. Comparison of the filter regions of KirBac1.1 to that of KcsA in high K^+ and low K^+ ions.
The structures of the filter regions were superposed using 'LSQKAB' (Kabsch, 1976) on the basis of the filter region TVGYGD (110 to 115) residues from KirBac1.1 against the TVGYGD (75 to 80) residues from KcsA in high K^+ (**A**) or in low K^+ ions (**B**). Secondary structure for both filter regions of KirBac1.1 and KcsA are drawn in stick representations. Two subunits of the filter region from both KirBac1.1 and KcsA are taken away for clarity. In KirBac1.1 structure magenta and yellow sticks represent filter region respectively while KcsA filter region is coloured according to atom type with carbon in turquoise, oxygen in red and nitrogen in blue. All spheres in green represent K^+ ions.
The models are drawn with PyMOL and PDB ID: 1K4D for KcsA in low K^+, 1K4C for KcsA in high K^+ and 1P7B for KirBac1.1.

4.7.2.3 Misaligned pore helices

All potassium channels contain four pore helices, another structural element that contributes to the stability of an ion in the central cavity. In the KcsA crystal structure the four pore helices are tilted along the edges of an imaginary inverted pyramid. The C-termini of all four pore helices point toward the centre of the cavity focusing a cation at the apex of the pyramid (Figure 4-30). Thus the negative ends of the four pore helix dipoles contribute to the stability of a K^+ ion in the cavity.

The arrangement of the pore helices in both the high and low resolution structures of KcsA implies that the channel probably represents a conducting state, at least for the selectivity filter region. The C-terminal 40 amino acids from KcsA were removed during crystallisation in both structures, hence the gating state of the KcsA crystal forms was not clear.

The KirBac1.1 structure shows that the orientation of the pore helices no longer points directly at the center of the channel cavity as seen in KcsA. The pore helices are misaligned (Figure 4-31). As the residues that form the pore helices also form part of the packing around the selectivity filter, it is believed that this misalignment is the cause of the altered ion binding in the filter.

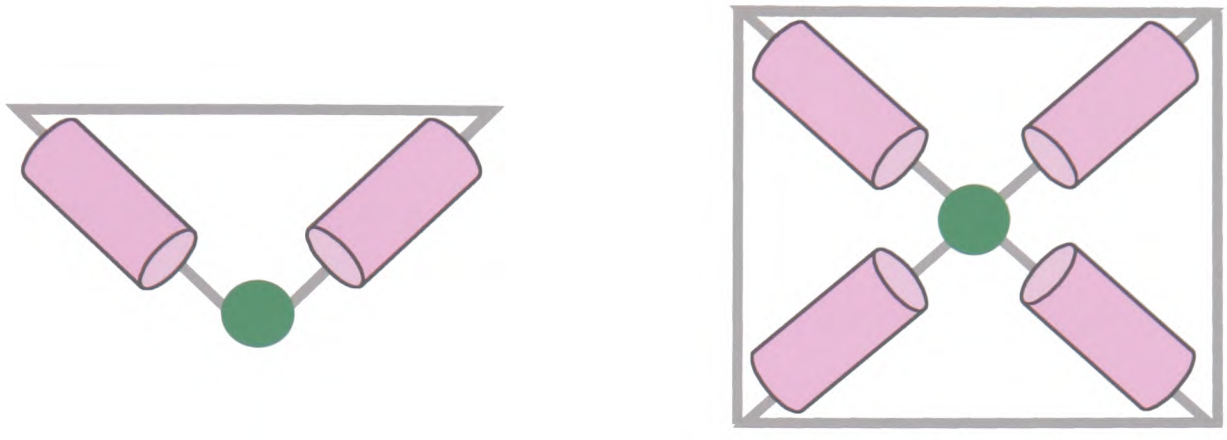


Figure 4-30. The geometry of the pore helices in the KcsA structure.
The left cartoon represents the side view of the pyramid. Each pink cylinder represents one pore helix.
The right cartoon shows four pore helices pointing toward the centre of the cavity focusing one K^+ ion (green sphere) at the apex of the pyramid.

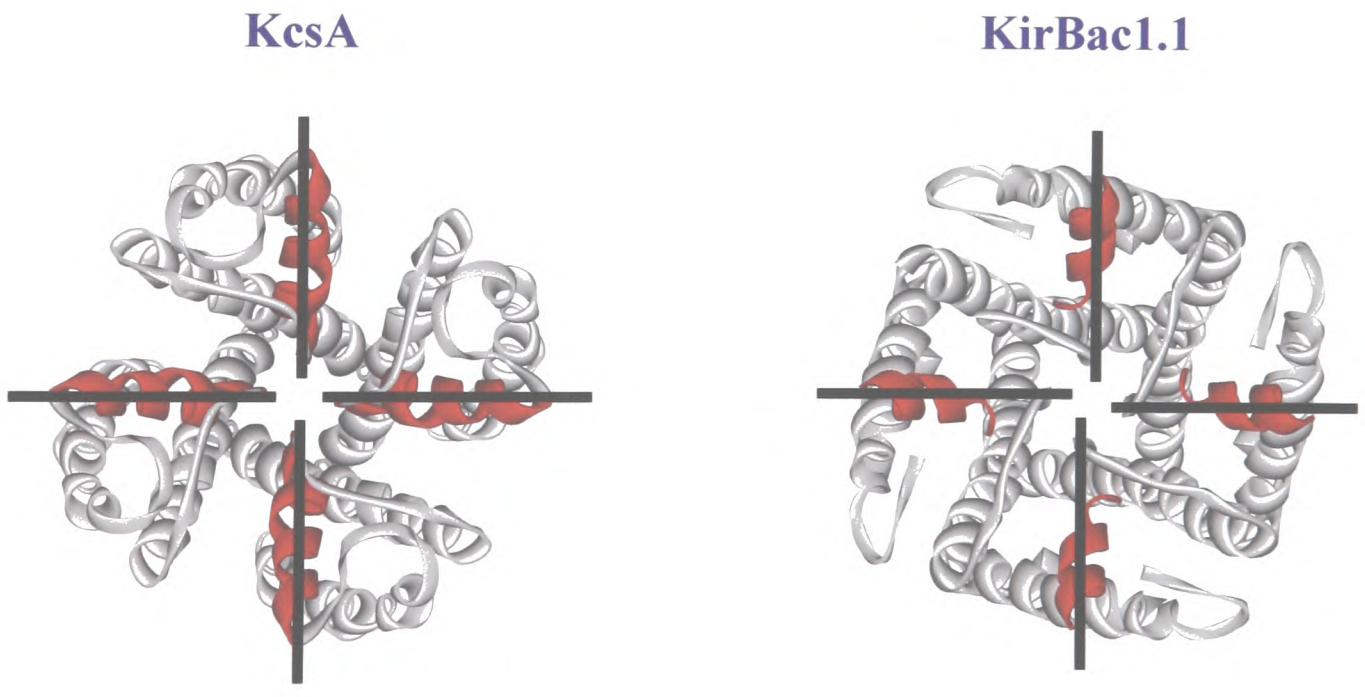


Figure 4-31. Pore helix comparisons of KcsA and KirBac1.1.
The relative positions of the pore helices are shown in red in the models of KcsA and KirBac1.1. The views are from the extracellular side of the channels looking down the central ion-conduction pathway. The black lines are artificially added on the top of the structures and indicate their relative orientation to the centers of the cavities. The drawings are generated using WebLab ViewerPro5.0.

4.7.2.4 A decrease in cavity volume

Comparing the cavity volumes of both KirBac1.1 and KcsA indicated that there is a decrease in the cavity volume of KirBac1.1. Why are the cavity geometry and volumes so important to a K^+ channel? In the centre of the biological membrane the dielectric constant is very low because of the hydrophobic lipid bilayers. A charged K^+ ion encounters an enormous energy barrier as it goes through the membrane (Parsegian, 1975). The first K^+ channel structure revealed a wide cavity in the middle of the channel (Doyle *et al.*, 1998). Thus nature designed K^+ channels in such a way that water molecules are in the centre of the membrane. Therefore the charged K^+ ions are surrounded by water molecules, hydrating the ions and thus overcoming the energy barrier (Figure 432). In KcsA about 27 water molecules can be fitted into the cavity whereas in KirBac1.1 only 20 water molecules can be accommodated (Figure 4-33). In the K^+ channel the function of the cavity is to overcome the electrostatic destabilization of the ions. Molecular dynamic simulations on a K^+ channel model indicated that water molecules significantly contribute to the stabilization of a K^+ ion in the cavity (Roux and MacKinnon, 1999). When the channel is at rest or closed, it is expected that the movement of ions and water is abolished.

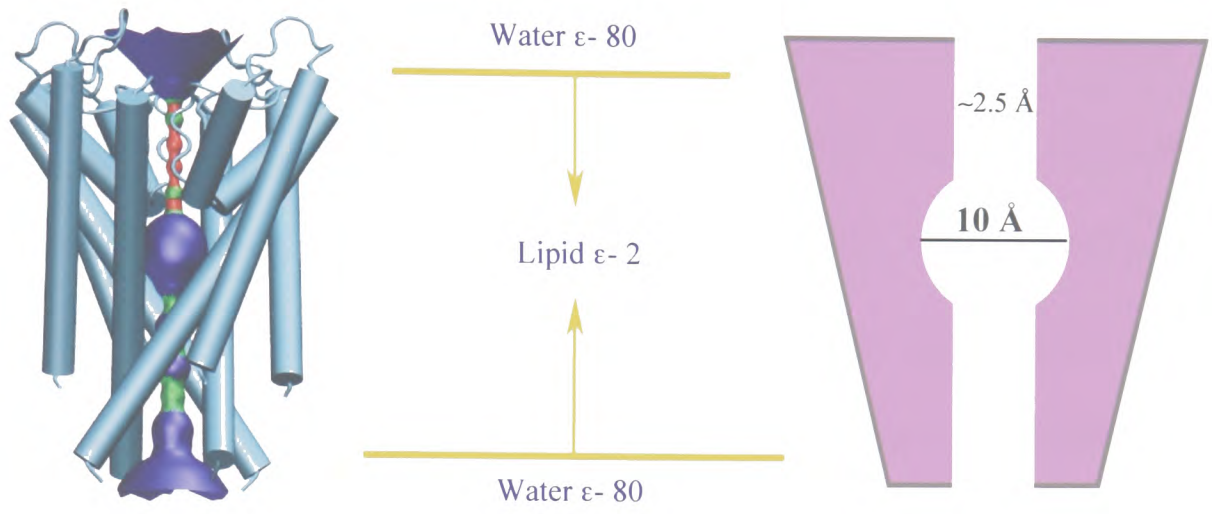


Figure 4-32. The geometry of the cavity in the KcsA structure.
The left model displays an entire internal pore from KcsA structure.
The model is generated using a program for the analysis of the pore dimension of the ion conduction pathway (Smart *et al.*, 1996).
The right cartoon represents a KcsA potassium channel in which the cavity is in the centre of the channel. The filter is about 2.5 Å in diameter whereas the cavity is 10 Å in diameter (Doyle *et al.*, 1998). The yellow lines represent lipid membranes. The electrostatic calculation is adapted from reference (Parsegian, 1975).

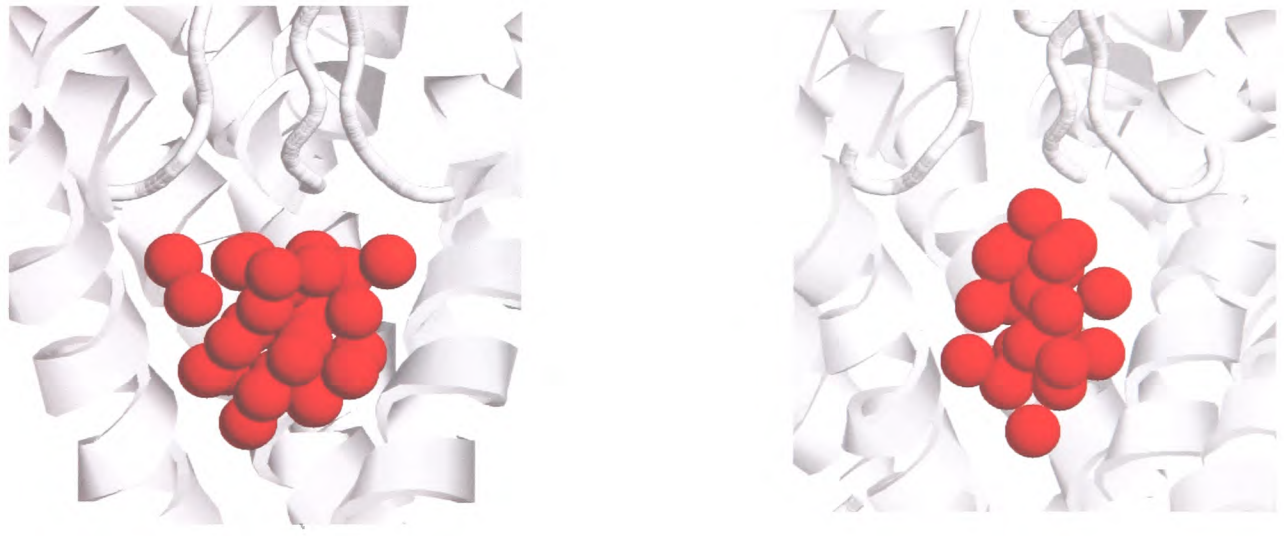


Figure 4-33. Comparing KirBac1.1 cavity volume with KcsA.
The red color spheres represent water molecules. In the cavity of KcsA there are 27 water molecules but only 20 water molecules can be accommodated in the KirBac1.1 cavity region.

4.7.3 The key residues of inward rectification

Inward rectifier potassium channels derive their name from the ability of the channels to conduct K^+ current preferentially in the inward direction under hyperpolarizing conditions and allow relatively little current to pass outward during depolarization. The phenomenon is caused mainly by intracellular Mg^{2+} and polyamines acting as blocker molecules, preventing K^+ efflux at membrane potential more positive than the resting potential (Matsuda *et al.*, 1987; Vandenberg, 1987; Lopatin *et al.*, 1994; Lopatin *et al.*, 1995).

Mutagenesis studies identified the residues that are involved in the rectification process. The critical sites for current rectification were identified first in ROMK1 (Kir1.1), residue Asn^{171}, and IRK1 (Kir2.1), residue Asp^{172} (Lopatin *et al.*, 1994; Lu and MacKinnon, 1994; Fakler *et al.*, 1994). If the residue Asn^{171} in Kir1.1 or residue Asp^{172} in Kir2.1 were reversed then the blocking affinities were also reversed (Wible *et al.*, 1994; Stanfield *et al.*, 1994). The full charge on the Asp side chains form a higher affinity binding site for Mg^{2+} and polyamines than does Asn residues. Therefore, Asp residues at position 172 (Kir2.1) results in strong rectification (outward block of K^+ flux) whereas Asn in the equivalent position produces weak rectification. Channels with an Asn residue are weakly blocked whereas those with an Asp are more strongly blocked. The residue Ile^{138} in the KirBac1.1 structure is located in the equivalent position to these residues (Figure 4-24). The Ile^{138} is at a position along the inner helix corresponding to the central cavity (Figure 4-34-A). In the future functional studies of KirBac1.1 will indicate how this residue affects the rectification process but it is likely that KirBac1.1 will be a weak rectifier.

Other residues known to affect the rectification process map to the residues Glu^{187} and Glu^{258} of KirBac1.1 (Figure 4-24). In all four subunits of KirBac1.1 the Glu^{187} and Glu^{258} side chains point to the center of the ion conduction pathway forming a double ring of negatively charged residues within the vestibule (Figure 34-B). We propose that this local concentration of glutamate side chains forms an electronegative ion cage to attract mono- or divalent cations into the vestibule.

In the eukaryotic Kir2.1 channels removing the charge of either Glu^{258} or Glu^{187} results in a decrease of the single channel conductance (Kubo and Murata, 2001). A further decrease occurs when both of the charged residues are replaced. This emphasizes that charged glutamates are also important residues in the rate of ion movement through the channel. The electrostatic sink draws ions into the conduction pathway, increasing the local ion concentration.

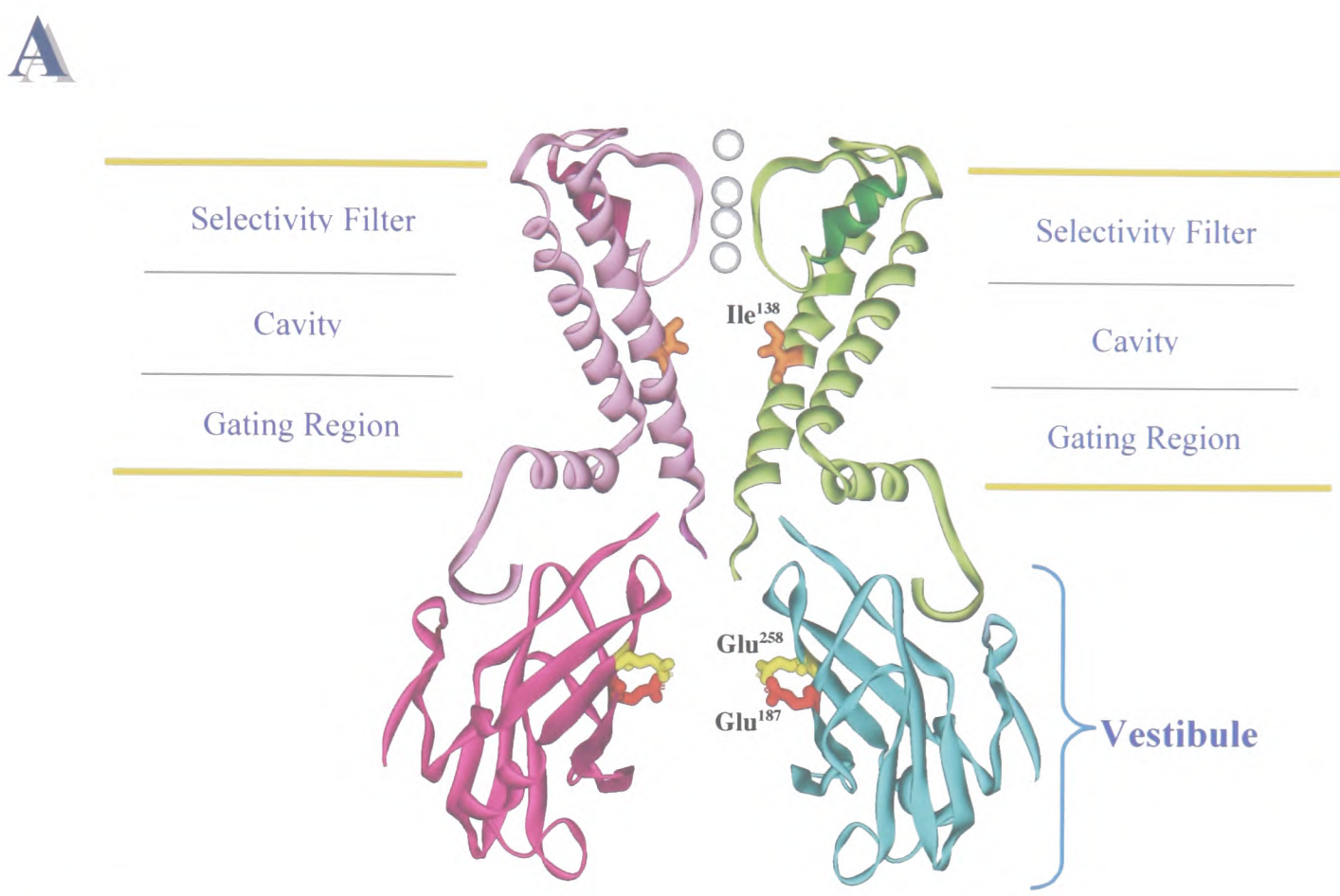


Figure 4-34. Location of important residues involved in the rectification process.

A. Side view of structure KirBac1.1 showing Ile^{138} (orange) in the cavity region, Glu^{187} (red) and Glu^{258} (yellow) in the C-terminal domain. Two subunits are removed for clarity. The yellow lines represent lipid bilayers.

B. A close up view of the KirBac1.1 cytosolic domains from the intracellular side showing eight glutamate residues in the C-terminal domains. Negatively charged Glu^{187} and Glu^{258} are highlighted in red and yellow, respectively.

4.7.4 Gating hypothesis

The mechanism of opening and closing an ion channel is called channel gating. The KirBac1.1 was crystallised in the closed conformation. A drawback of 3-D structural studies is that a single structure is generally not able to detect the dynamic movements during the gating process. However, the atomic structure of KirBac1.1 provides the foundation for understanding the structure and function relationship underlying the gating in the Kir channel subfamily.

From the structure we identified the following likely structural features important in gating: the slide helix, blocking residue Phe^{146}, the N- and C- terminal connection and the inner helix. Comparing these elements with functional studies a hypothetical gating mechanism for Kir channels was proposed.

The slide helix is positioned well at the membrane interface to form the coupling element between the gate (Phe^{146}) and the sensor domain. It is covalently attached to outer transmembrane helix and is indirectly linked to the inner helix via a negative helix dipole interaction with Arg^{148} (Figure 4-35).

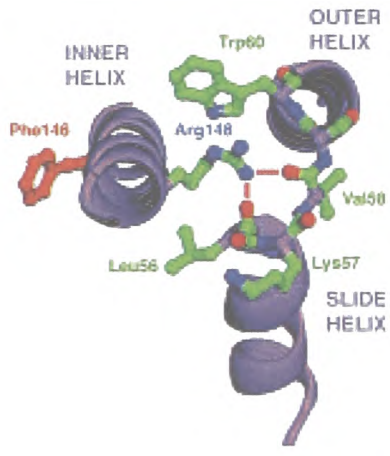


Figure 4-35. View from the intracellular side looking down onto the TM helices of the Arg^{148} slide helix connection.
Atoms are colored according to atom type with carbon in green, oxygen in red and nitrogen in blue except for Phe^{146} side chain in red.
The structure is generated using Aesop.

The N-terminal residues 40 to 42 of the slide helix from each subunit interact with a β-strand (residues 298 to 300) on the outer edge of the neighboring subunit of the C-terminal domain (Figure 4-36).

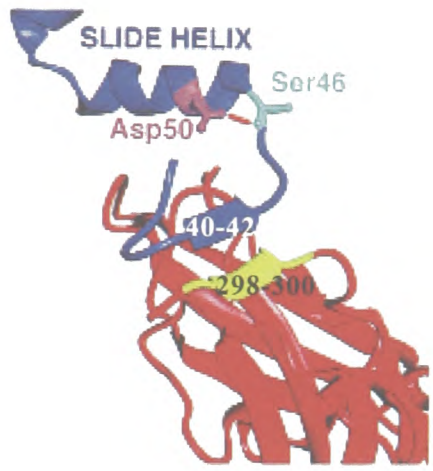
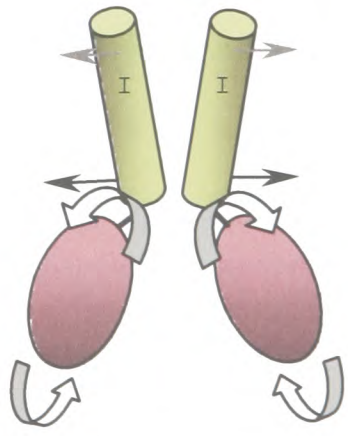


Figure 4-36. Interaction of the N-terminus with C-terminal domain.
The C-terminal domain is colored in red and the slide helix is in blue. The β-strand residues 298 to 300 are in yellow.
The model is prepared using Aesop.

This arrangement fixes the channel to an adjacent subunit so that as the domain moves it also drags the inner helices of the channel apart.

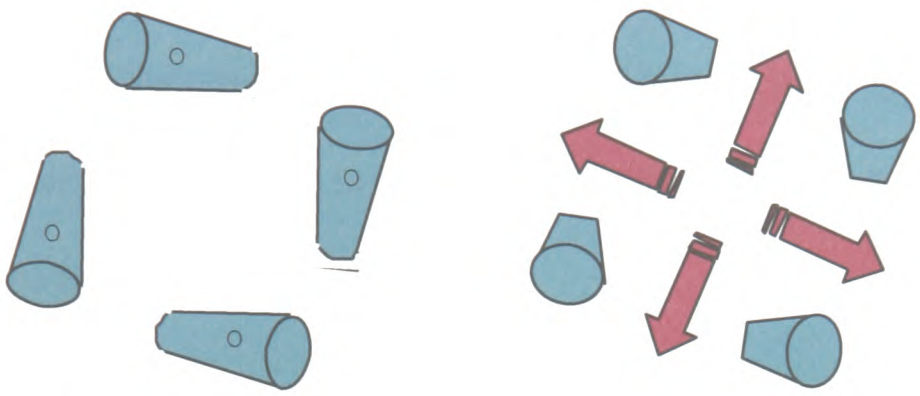
The steps involved in channel gating as the KirBac1.1 channel enters the open state are believed to be:

1. Ligand binds to C-terminal domain causing a conformational change. This change most likely involves a rigid body rotation.
2. As the inner helices are directly connected to the C-terminal domain, the rotation will drag the bottom of the inner helices away from the central axis of the channel.



3. In order to make room for the inner helices, the outer helices are also repositioned. This results in the outer helices straightening up.

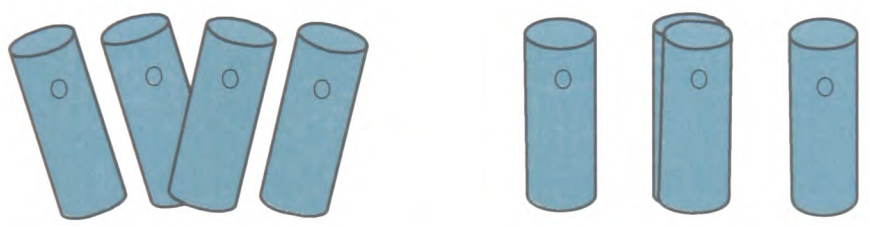
Looking down the ion pathway



CLOSED **OPEN**

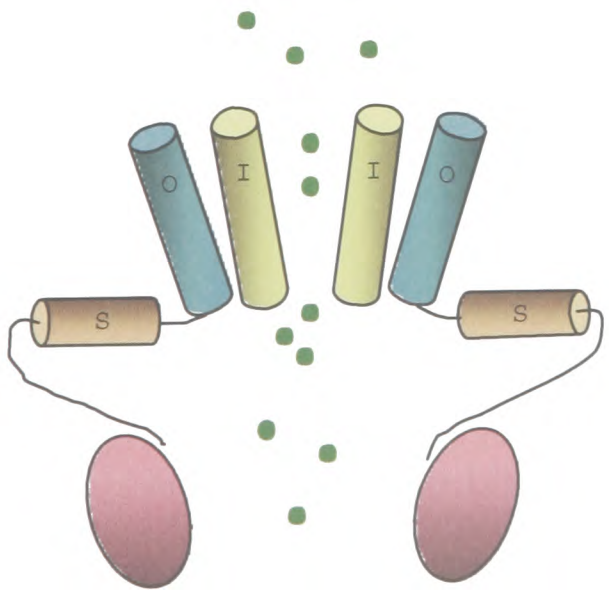
Space for inner helices to occupy in the open state. Arrows indicate the direction of movement for the inner helices

Looking along the ion pathway



CLOSED **OPEN**

4. As the N-terminus interacts with the C-terminal domain, rotation of the C-terminal domain will cause the slide helix to also move away from the central ion pathway. The outer helix is covalently linked to the slide helix, thus directing the outer helices movement.



This is a distorted representation as the N-terminus interacts with the C-terminal domain of an adjacent subunit.

The exact mechanism of KirBac channel opening is unknown, however, what must occur is the blocking residues move away from their position in the closed state. One possible way is outward rotation of the inner helix away from the center of the ion conduction pathway. In order to make room for the inner helices the outer helices must also be relocated.

Chapter 5 – A Kir channel from *Magnetospirillum magnetotacticum*

5.1 Introduction

The KirBac1.1 structure revealed the channel in a closed conformation. The gating proposal was based on the structural elements and the results of many years of functional studies. In summary, the inner helices play a very important role in controlling the flow of ions through the channel. Large conformational changes in the position of the inner helices, such as helix bending, are believed to result in the displacement of the blocking residues and proper alignment of the pore helices. The precise changes are uncertain as the 3-D crystals only captured one gating state of the channel, the closed state.

Recent electron paramagnetic resonance (EPR) spectroscopic studies indicated that the inner helices of KcsA undergo movements during channel gating (Perozo *et al.*, 1999). The crystal structure of the MthK channel, a prokaryotic Ca^{2+} gated potassium channel, also showed large changes in the positions of the inner helices (Jiang *et al.*, 2002). Hence we are interested in capturing a Kir channel in the open state. We collaborated with Dr. C. Vénien-Bryan (LMB, University of Oxford) using electron microscopy on 2-dimensional (2-D) crystals of KirBac. The 2-D crystals are formed in a lipid bilayer thus the channel is in a similar environment as in the living cell. In the closed conformation of KirBac1.1, the cavity space is small and the blocking Phe residues lie along the ion conduction pathway. This means that the inner helices are close together (~ 4.8 Å apart from one Phe^{146} in one subunit to the opposite Phe^{146} in another subunit). Opening of the channel due to the inner helices moving apart should result in less density along the central ion conduction pathway. If the hypothesis is true, an increase in the diameter of the central hole would be

detected in the projection map of the open channel in comparison with the closed state. Higher resolution of the 2-D projection map should give more detailed information on the location of the inner helices.

Two choices of target channels were available (1) KirBac1.1 or (2) using one of the other recently identified prokaryotic Kir channels.

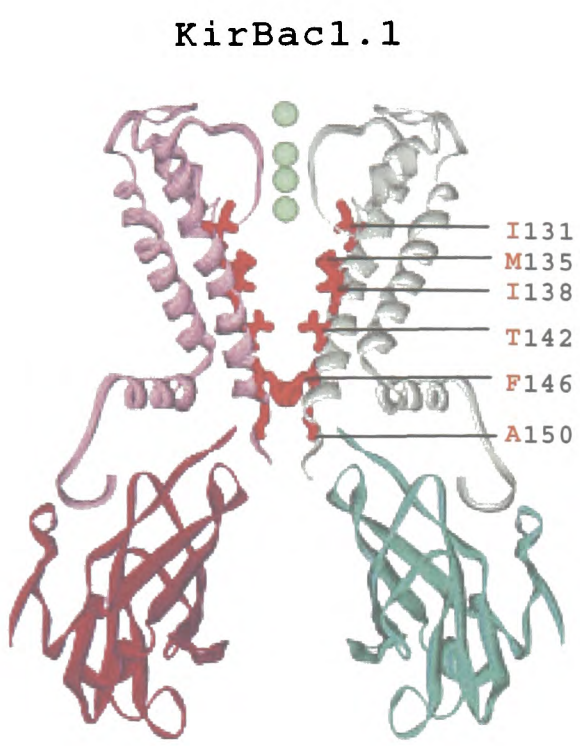
KirBac3.1 from *Magnetospirillum magnetotacticum* was chosen as a candidate based on two reasons: (1) *Magnetospirillum magnetotacticum* is not a pathogenic strain which can be grown in a class 1 laboratory thus allowing purification of its genomic DNA and (2) KirBac3.1 protein has the amino acid lysine after the GYG sequence in the selectivity filter. In other K^+ channels, such as Shaker, MthK, KcsA and KirBac1.1, all have aspartic acid instead of lysine. Since lysine has a long side chain that is positively charged it will be interesting to view the structural differences in the filter region thus gaining a greater insight into K^+ ion selectivity (Figure 5-1).

```
                          Filter Region
KirBac3.1:     -SVQTMA|TIGYGK|LI..PIGPLA--
KirBac1.1:     -SVETLA|TVGYGD|MH..PQTVYA--
KcsA      :    -SVETAT|TVGYGD|LY..PVTLWG--
MthK      :    -TFVTIA|TVGYGD|YS..PSTPLG--
HERG      :    -TFSSLT|SVGFGN|VS..PNTNSE--
Shaker    :    -AVVTMT|TVGYGD|MT..PVGFWG--
Kir1.1    :    -SLETQV|TIGYGF|RFVTEQCATA--
```

Figure 5-1. Sequences alignment of the filter region of the KirBac3.1 K^+ channel with other K^+ channels.
The red color indicates the aspartic acid, phenyalanine, asparagine and lysine residues in the filter region. All channels contain the highly conserved GYG or GFG sequence.

In the structure of KirBac1.1, the gating element of the inner-helix is believed to play an important role. The residue Phe^{146} in KirBac1.1 blocks the ion conduction pathway when the channel is closed. Comparison of the sequences from KirBac1.1

with that of KirBac3.1 also indicated a few differences in the likely residues that line the ion-conduction pathway over the inner-helix region (Figure 5-2).



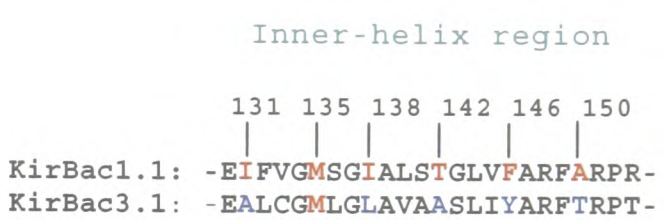


Figure 5-2. Sequence alignment of the KirBac1.1 and KirBac3.1 inner helices. Residues highlighted in red line the ion conduction pathway as shown in the ribbon diagram of KirBac1.1 on the left.

In KirBac1.1 the two important residues Phe^{146} and Ala^{150} are substituted to Tyr and Thr, respectively, in the KirBac3.1 channel. This would make the ion-conduction pathway more hydrophilic and may lead to the channel residing in the open state. How does it work and could we visualize it through 2-D crystal studies?

A significant part of this project was undertaken to form 2-D crystals of full length KirBac3.1 for electron microscopy (EM) study with help from Dr. C. Vénien-Bryan. All the EM pictures were taken and images processed by Dr. Vénien-Bryan.

The following chapter describes the development of the protocols to allow purification of the genomic DNA from the bacterium *Magnetospirillum magnetotacticum*, cloning KirBac3.1 gene into pET-30a, production of KirBac3.1 protein and making 2-D crystals in liposomes for 2-D crystallographic studies.

5.2 Outline of the methods employed in the KirBac3.1

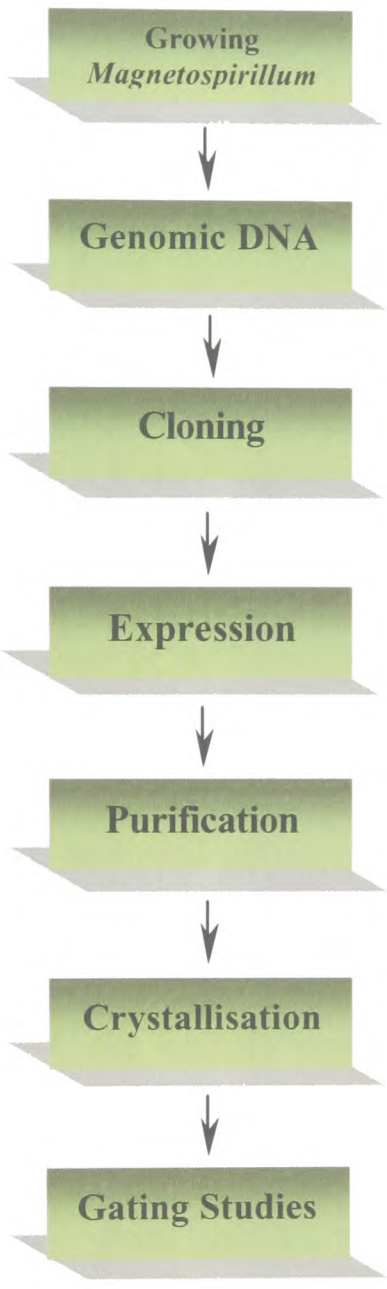


Figure 5-3.

Flowchart indicating procedures employed in the KirBac3.1 project.

5.2.1 Growing the *Magnetospirillum* strain

A liquid culture of *Magnetospirillum magnetotacticum* was purchased from DSMZ. Before the cells were cultured in a 500 ml volume bottle containing 150 ml of media, (one litre of culture media contains 1.0 g of sodium acetate, 0.5 g of K_2HPO_4, 0.5 g of sodium thioglycolate, 0.1 g of NH_4Cl, 0.1g of yeast extract and 20 μg of Ferric citrate, pH 6.8 $\pm$ 0.2 at 25°C) the medium was autoclaved and then equilibrated at room temperature for 3 days (Atlas, 1997). The cells grew in the incubator at 30°C without shaking for one week.

5.2.2 Purification of genomic DNA from *Magnetospirillum magnetotacticum*

Cells were harvested by centrifugation at 3,000 g for 10 minutes. Genomic DNA was purified using a High Pure PCR Template Preparation kit from Boehringer Mannheim except the volume of the resuspension buffer was modified as indicated below. The cell pellet was small and total pellet was re-suspended in 800 μl of PBS buffer. Next 80 μl of lysozyme (10 mg/ml in Tris-HCl, pH 8.0) was added. After incubating for 15 minutes at 37°C the sample was divided into two and transferred into two 1.5 ml microcentrifuge tubes. One hundred microlitre of proteinase K (20 mg/ml) was added to each sample. Both samples were incubated at 72°C for 10 min. The rest of the protocol was followed as per instructions for isolation of nucleic acids from whole blood or cell culture. The quality of the nucleic acids was monitored by running the DNA on a 1 % agarose gel.

5.2.3 Cloning

The pET-30a vector was chosen as the cloning vector for KirBac3.1 based on our experience with KirBac1.1 except this time no thrombin site was engineered before the his-tag at the C-terminal end of the protein. The structure of KirBac1.1

indicated that the C-terminal his-tag did not interfere with the crystallisation therefore it was left on. PCR technique was applied in the cloning of the KirBac3.1.

5.2.3.1 pET-30a vector

The restriction enzyme sites *Nde*I and *Sac*1 were chosen for insertion of the KirBac3.1 gene into the vector. The pET-30a was selected as a candidate vector because of its expression under T-7 promoter control and the high yield of KirBac1.1 expressed in BL21(DE3)Star* cells using this vector. As KirBac3.1 is similar to KirBac1.1, it was assumed the expression level would also be similar. Figure 5-4 shows a sequence alignment with KirBac1.1 and KirBac3.1.

```
                30          40          50          60
kb1.1 KPPRGGRRIWS--GTREVIAYGMPASVWRDLYYW-ALKVSWPVFFASLAA
      :::    :: .  :. ..   :.    : : .:   : :::::.. ...
kb3.1 KPPARKPRILNSDGSSNITRLGLEKRGWLDDHYHDLLTVSWPVFITLITG
          10         20         30         40         50

      70         80         90         100        110
kb1.1 LFVVNNTLFALLYQLGDAPIANQSPPGFVGAFFFSVETLATVGYGDMHPQ
      :..:.:.:::: :       : :  : .:. ::::::.:.::.::: . :
kb3.1 LYLVTNALFALAYLACGDVIENARPGSFTDAFFFSVQTMATIGYGKLIPI
          60         70         80         90         100

      120        130        140        150        160
kb1.1 TVYAHAIATLEIFVGMSGIALSTGLVFARFARPRAKIMFARHAIVRPFNG
        :....::: . :: :.:....:.::::: : ..:. . ..  :.:
kb3.1 GPLANTLVTLEALCGMLGLAVAASLIYARFTRPTAGVLFSSRMVISDFEG
          110        120        130        140        150

      170        180        190        200        210
kb1.1 RMTLMVRAANARQNVIAEARAKMRLMRREHSSEGYSLMKIHDLKLVRNEH
       .::::.: :: : . : :: . . :.: : :.::  . .::::: :.:..
kb3.1 KPTLMMRLANLRIEQIIEADVHLVLVRSEISQEGMVFRRFHDLTLTRSRS
          160        170        180        190        200

      220        230        240        250        260
kb1.1 PIFLLGWNMMHVIDESSPLFGETPESLAEGRAMLLVMIEGSDETTAQVMQ
      ::: :.:..:: ::. ::..::: :.: .... .::.. :  :. :: ..
kb3.1 PIFSLSWTVMHPIDHHSPIYGETDETLRNSHSEFLVLFTGHHEAFAQNVH
          210        220        230        240        250

      270        280        290        300
kb1.1 ARHAWEHDDIRWHHRYVDLMSDV-DGMTHIDYTRFND
      :::::.. :.: :  ..::... . ::   .:  .:..
kb3.1 ARHAYSCDEIIWGGHFVDVFTTLPDGRRALDLGKFHE
          260        270        280        290
```

Figure 5-4. Alignment of the amino acid sequences of KirBac1.1 (kb1.1) and KirBac3.1 (kb3.1).
The black colour indicates KirBac1.1 amino acid sequence while the blue colour indicates that of KirBac3.1. This sequence alignment is generated using ClustalW (http://www-igbmc.u-Strasbg.fr/BioInfo/ClustalW/).

5.2.3.2 PCR

Genomic *Magnetospirillum magnetotacticum* DNA was used as the template. All PCR reactions were run in a Bio-Rad iCycler (BioRad, UK). The primers were synthesized by Sigma-Genosys. A *Pwo (Pyrococcus woesei)* DNA polymerase was used (Thermo Hybaid, U.K.) to insure proof reading during the PCR reaction. The PCR reaction conditions are given in Table 5-1.

Table 5-1. KirBac3.1 PCR components

Components	Volume	Concentration
Pwo PCR Buffer(10x)	5.0 µl	1.0 x
dNTP (10 mM)	1.0 µl	0.2 µM
Forward primer (20 pmole/µl)	2.0 µl	0.8 pmole
Reverse primer (20 pmole/µl)	2.0 µl	0.8 pmole
Mm DNA (0.1 µg/µl)	5.0 µl	10. ng
DMSO (100%)	2.5 µl	5.0 %
Pwo DNA polymerase	0.3 µl	
Water (Autoclaved)	32.2µl	
Final	**50.0µl**	

The PCR reaction was run using the following protocol:

94°C	95°C	51°C	72°C	72°C	4°C
5 min	1 min	1 min	2 min	7 min	10min
[----Repeat 25 cycles ----]					

After the reaction was completed, the PCR product was examined by gel electrophoresis using a 1 % agarose gel. The correct size band was obtained and the PCR product was purified using a QIA-PCR kit (Qiagen).

5.2.3.3 Endonuclease digestion

Purified PCR product of KirBac3.1 and the pET-30a vector were digested with *Nde*I first for 1 hour 30 min at 37°C followed by *Sac*I for a further 1 hour 30 min at 37°C (Table 5-2).

Table 5-2. Reaction conditions for enzymatic digestions

Components	KirBac3.1 DNA	pET-30a
DNA (from PCR)	50.0 µl	4.0 µg
NEB buffer 10x	6.0 µl	6.0 µl
*Nde*I	20 units	20 units
*Sac*1	20 units	20 units
CIP	0	10 units
H_2O (Final to)	60 µl	60 µl

The pET-30a vector was further digested with Calf Intestinal Alkaline Phosphatase (CIP) for one hour at 37°C. The CIP was inactivated by adding EDTA to a final concentration of 1 mM followed by heating to 75°C for 10 minutes.

Digested products were purified by first separating on a 1 % agarose gel and further purification of the gel slots were accomplished using a QIA-quick gel purification kit. Confirmation that the correct gene product based on size was achieved by agarose gel electrophoresis.

5.2.3.4 Ligation and transformation

The quick ligation method was used to ligate the digested vector and PCR product which shortened the protocol by two days compared with the traditional method. The ligation kit was purchased from Roche Diagnostics (U.K.).

The following components were used in the quick ligation reaction.

Quick ligation mixture	**Total 21µl**
1. pET-30a	80-100 ng
2. DNA dilution buffer (5x)	2 µl
3. Water to a final volume of	10 µl
4. T7 ligase buffer (2x)	10 µl
5. T7 ligase	1 µl
6. Leave reaction for 15-20 minutes at 25°C.	

After ligation the product was incubated on ice for 10 – 15 minutes before transformation. The host strain was *E. coli* DH5α made competent using a modified Hanahan method (see Appendix B for details, Hanahan *et al.*, 1991). For transformation of the ligated product, 50 µl of competent cells were mixed with 4 µl of ice-cold ligation product and incubated on ice for 30 minutes prior to heat treatment for 45 seconds at 42°C. The heat shocked cells were quickly transferred back on ice for at least 5 minutes before adding 1 ml of LB medium pre-warmed at 42°C. The cells were incubated at 37°C for one hour and were concentrated by a slow centrifugation step (3,000 g) for 5 minute before being spread on a kanamycin agar plate. The plates were incubated overnight at 37°C.

5.2.3.5 Confirmation of the *KirBac3.1* clones

Three clones were selected from the plate and each clone was incubated in 10 ml of LB broth (50 µg/ml kanamycin) overnight at 37°C. Positive clones were screened using the procedure outlined in 3.2.1.5 except the primers were complementary to the pET-30a vecter with each primer positioned approximately 100 bps away from the KirBac3.1 gene.

The PCR components and reaction conditions were the same as the PCR set up in 5.2.3.2. After positive clones were identified the plasmids were purified using a

QIA-spin kit (QIAGEN protocol). The sequence of the KirBac3.1 gene was then confirmed by DNA sequencing (Department of Biochemistry, University of Oxford).

5.2.4 Expression

Three cells lines were tested for KirBac3.1 expression but only BL21(DE3)Star* cells were chosen for large scale expression.

5.2.4.1 Test expression

E. coli cell line, **BL21(DE3)**, was tested first for expression of KirBac3.1 protein. The cell line BL21(DE3) was tested by induction at 37°C. One plate of freshly transformed cells were resuspended in 50 ml of LB (50 μg/ml of kanamycin) medium and allowed to grow to an OD_{600} of 0.5 - 0.7. This acted as a starter culture. This starter culture was inoculated into 2 litres of LB medium containing 50 μg/ml kanamycin. Cultures were grown at 37°C in a shaker incubator until the cell density reached an OD_{600} of 1.1. The cells were induced by adding IPTG to a final concentration of 0.5 mM and expressed at 37°C for four hours.

The **BL21(DE3)AI** cell line was tested as a second choice. All the conditions were described as above except cells were induced by adding both L-arabinose to a final concentration of 0.2% and IPTG to a final concentration of 0.5 mM overnight at 25°C.

5.2.4.2 Optimisation of expression

The **BL21(DE3)Star*** was used to optimise the protein expression level. Four litres of LB cultures were grown for each preparation but the induction concentration was adjusted to 0.4 mM of IPTG, the induction temperature was chosen at 25°C and induction length was 12 hours. The remaining procedures were the same as for the test expression (see 5.2.4.1).

5.2.5 Purification

The KirBac3.1 construct contains a his-tag at the C-terminus of the protein. This tag has a high affinity binding for Co^{2+} resin unlike native *E. coli* proteins. Immobilized metal affinity chromatography (IMAC) technique was applied as part of the purification procedure.

5.2.5.1 IMAC

Cells were harvested by centrifugation at 5,000 g for 25 minutes at 4°C in a Beckman J-20 centrifuge (Beckman JLA rotor). Each cell pellet was weighed and resuspended in cell lysis buffer (20 mM Tris-HCl pH 8.0, 150 mM KCl, 250 mM sucrose and 10 mM $MgSO_4$). Cells were lysed by passing through a high-pressure homogenizer 5 times in the presence of the complete EDTA-free inhibitors (Roche Diagnostics) plus 1 mM of phenymethylsulfonyl fluoride (PMSF, Sigma). Total membrane proteins were solubilised direct from the crude cell extract or from purified total membrane proteins.

If **membrane purification** was required, the total membrane proteins were obtained by centrifugation at 9,000 g for 30 minutes at 4°C to remove insoluble debris, followed by ultra centrifugation at 50,000 rpm (Beckman 70Ti rotor) for 2 hours at 4°C to purify the membranes. Membrane pellet was solubilised in the same lysis buffer but in the presence of 30 mM DM for 3 hours. The solubilised total membrane protein was centrifuged at 30,000 rpm for 30 minutes at 19°C and the supernatant collected.

If **no membrane purification** step was required, 30 mM DM (Anatrace or Glycon) was added to the crude cell lysate and rotated slowly for 3 hours at room temperature. The solubilised total proteins were obtained by centrifugation at 18,500 rpm in a Beckman JA-20 rotor for 40 minutes at 19°C.

TALON cobalt resin (Clontech, U.K.) was added to the supernatant. Batch binding was performed at room temperature for 40 minutes. For the wash steps a high salt buffer and a high salt plus 20 mM imidazole buffer were used before protein elution with the addition of 300 mM imidazole buffer. Detergent triDM was replaced in the wash step to ensure complete detergent exchange (Table 5-3). The high imidazole concentration was reduced by dialysing the eluted protein in a dialysis buffer overnight (50 mM Tris pH 8.0, 100 mM KCl, 0.5 mM triDM and 5 mM DTT).

Table 5-3. Immobilized metal affinity chromatography buffers

Wash I	**Wash II**	**Wash III**	**Elution Buffer**
20 mM Tris pH 8.0	20 mM Tris pH 8.0	20 mM Tris pH 8.0	20 mM Tris pH 8.0
150 mM KCl	500 mM KCl	500 mM KCl	100 mM KCl
10 mM $MgCl_2$	0 $MgCl_2$	0 $MgCl_2$	0 $MgCl_2$
8 mM DM	6 mM triDM	4 mM triDM	2 mM triDM
0 imidazole	5 mM imidazole	20 mM imidazole	300 mM imidazole

5.2.5.2 Gel filtration

The sample was concentrated to about 10 mg/ml in a Centricon YM-50 (50 kDa molecular weight cut off) before filtering through a 0.22 µm spin column. A Superdex-200 column was used in a Pharmacia FPLC system for further purification (Amersham Pharmacia). All the buffers and water were filtered through a 0.22 µm filter. The column was pre-equilibrated with the buffer (50 mM Tris pH 8.0, 100 mM KCl, 0.5 mM triDM and 5 mM DTT). The injection volume was between 350 – 400 µl. The elution peak was collected into different fractions with the top fraction being used for 2-D crystallisation.

5.2.5.3 N-terminal sequencing and mass spectrometry

The gel filtration purified KirBac3.1 was sent to T. Willis for sequencing. MRC Immunochemistry Unit, University of Oxford. The N-terminal sequencing was carried out for 15 cycles using an Applied Biosystems 494A/473A Sequencer. Typically 5 – 6 μg of protein was used in the experiment.

Gel filtration purified KirBac3.1 was also submitted for mass spectrometry analysis. The analysis was carried out using MALDI-MS on a SELDI Protein Chip mass spectrometer using a laser intensity of 300 and a detector sensitivity of 10 (Dr Alison E. Ashcroft, Mass Spectrometry Facility, Astbury Centre for Structural Molecular Biology, The University of Leeds).

5.2.6 2-D Crystallisation

The successful strategy for KirBac3.1 2-D crystallisation relied on the reconstitution of the purified KirBac3.1 into lipid vesicles. The 2-D crystallisation was done under Dr. Catherine Vénien-Bryan's guidance.

5.2.6.1 Reconstitution

Two stock solutions 1,2-diheptanoyl-sn-phosphocholine (DHPC) and 1,2-dioleoyl-sn-phosphocholine (DOPC) were made by dissolving 2.0 – 4.0 mg DOPC in 1 ml of water and 10 mg of DHPC in 1 ml of water. The DHPC was from Sigma and the DOPC was from Avanti (Avanti Polar-lipids, Inc. U.S.A.). The protein (1 mg/ml) was reconstituted into DOPC (solubilised in DHPC) at a lipid to protein ratio of 0.5, 0.6, 0.7, 0.8 and 1.0 (w/w).

For the **closed conformation** of KirBac3.1, 50 μl of protein and buffer mixture were added to 50 - 75 mM $MgCl_2$ or 50 mM spermine with the added lipid solution. This was allowed to equilibrate for at least 12 hours at 4°C. For the **potential open**

conformation of KirBac3.1, 50 µl of protein and buffer were added to 5 mM EDTA or 5 – 10% phosphoinositol 4,5-bisphosphate (PIP2). Again the solution was allowed to equilibrate for more than 12 hours at 4°C. All samples were mixed in 600 µl volume micro-centrifuge tubes. After equilibration, 10 to 15 bio-beads were added to both samples then heated at 37°C for 2 hours. The Bio-Beads SM-2 (20-50 mesh) was from Bio-RAD. They were first washed once with ethanol and three times with water before storing in water with 0.01% sodium azide at 4°C. The samples were rotated slowly on a Rotator Drive STR4 rotator (Stuart Scientific, U.K.) overnight at room temperature. Next day another 10 to 15 bio-beads were added and heated at 37°C for 2 hours. For the next 4 days 10 to 15 bio-bead were added without heating the sample. When the bio-beads were 2/3^{rds} of the protein-lipid mix (v/v), no more bio-beads were added and the samples were rotated for a further 3 days. The reconstitution normally required one week to complete. Finally the samples were transferred to Eppendorf tubes and stored at 4°C. The crystals were stable for several months at 4°C.

The crystals were detected by negative staining and examined by an electron microscope in the first instance.

5.3 Results and Discussion

Structure determination of membrane proteins is still far behind that for soluble proteins. Generally, both 3-D and 2-D crystallisations of membrane proteins are more difficult to obtain than for soluble proteins. In this chapter some key points are discussed on how to obtain 2-D crystals to study the inner helices rearrangements during the gating process of the KirBac K^+ channel.

5.3.1 Purification of genomic DNA from *Magnetospirillum magnetotacticum* – results and discussion

The growth rate of *Magnetospirillum magnetotacticum* was slow but the aim of growing the cells was to obtain a small amount of genomic DNA as template for cloning the KirBac3.1 gene. A total of 5-10 µg of genomic DNA was finally obtained from 300 ml of cell culture. The principle of the DNA purification procedure is based on binding nucleic acids to glass fiber fleece (the material in the spin column). The wash buffers wash the cellular impurities and proteins away while the nucleic acids are still bound on the column. The genomic DNA then is eluted in elution buffer. The genomic DNA was shown to be of very high quality in a 1 % agarose gel (Figure 5-5).

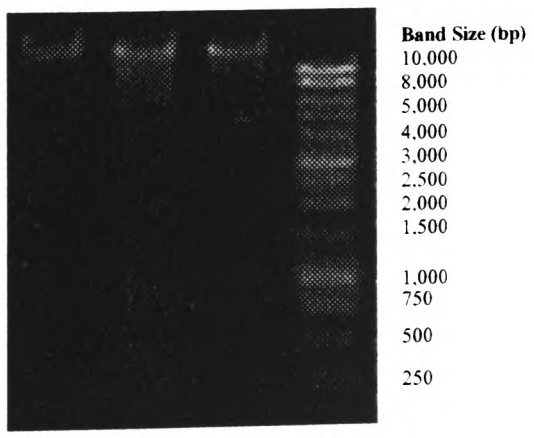


Figure 5-5. 1 % agarose gel analysis of genomic DNA from *Magnetrospirillum magnetotacticum*. Each well represented one sample and 5 µl of DNA was loaded in each well.

5.3.2 Cloning of KirBac3.1 – results and discussion

The KirBac3.1 was cloned from genomic DNA of *Magnetospirillum magnetotacticum* by PCR. After purification of the PCR product the plasmid DNA

and pET-30a vector both were digested with *Nde*I and *Sac*I endonucleases. Before ligation the quality and quantity of the plasmid were both analyzed using 1 % agarose gel electrophoresis (Figure 5-6). This step was found to be important for the successful ligation of the gene into the vector.

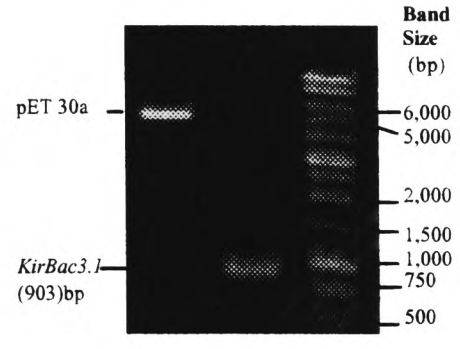


Figure 5-6. 1 % agarose gel analysis of both pET-30a and *KirBac3.1* insert after endonucleases digestion.
The left lane showed a 5.3 kb pET30a after treated with *Nde*I/*Sac*I.
The middle lane showed *KirBac3.1* digested with *Nde*I/*Sac*I.

The concentration of both vector and insert were estimated visually. The result of the ligation gave 70% success rate. The PCR results showed on a 1 % agarose gel that one clone contained empty plasmid and two clones had the correct KirBac3.1 gene size ligated into the vector (Figure 5-7).

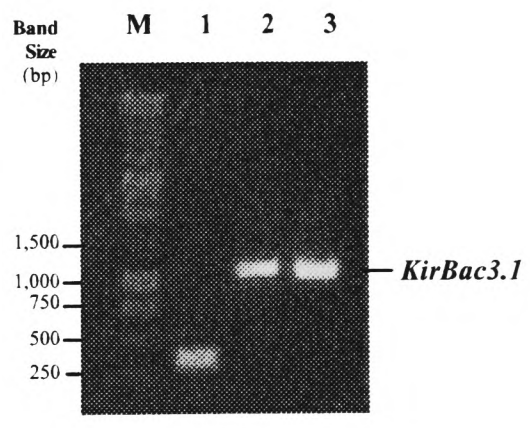


Figure 5-7. Verification of the KirBac3.1 gene in clones by PCR.
Lane 1, 2 and 3 represent PCR products from 3 individual clones

The pET-30a primers were used in the PCR reaction with each primer positioned about 100 bp away from the insert. If the clone contained the correct insert, the PCR product size would be around 1,100 bp. If the clone contained the empty plasmid, the product size would only be 380 bp. The gel showed two bands corresponding to the KirBac3.1 gene in the plasmid but clone 1 did not contain KirBac3.1 gene, therefore, the band size was below 500 bp.

The sequencing results confirmed the gene of KirBac3.1 to be essentially correct. However, five amino acid residues were different from the published paper

(Durell and Guy, 2001, Figure 5-8). Downloading the DNA sequence from the *Magentospirillum magnetotacticum* (http://www.jgi.doe.gov/) database indicated that our sequence was correct and that the published sequence was taken from an earlier unverified sequence.



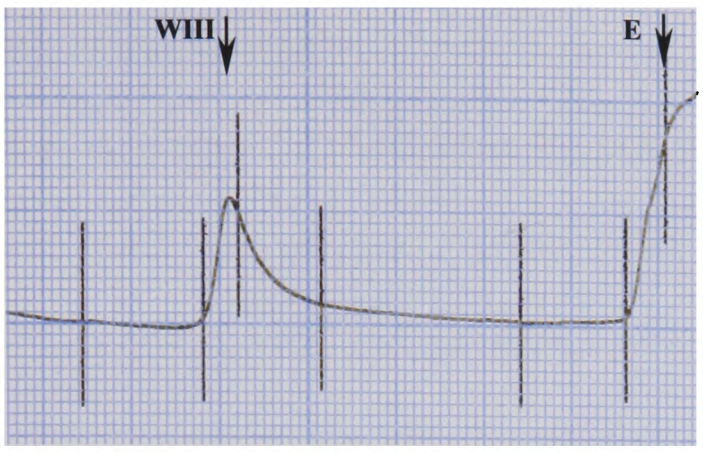
Figure 5-8. The five residues of the *KirBac3.1* sequence differ from the published sequence in Durell and Guy (2001).
The red color letters indicated the amino acid residues published from the paper.

5.3.3 Protein expression and purification – results and discussion

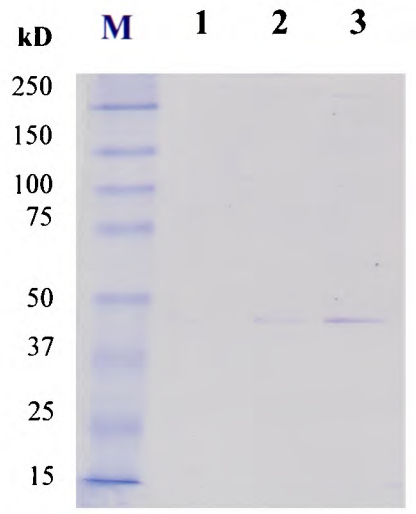
During testing it was found that the induction temperature for expression was important. The temperature was kept at 25°C overnight otherwise the protein yield was low (Figure 5-9). Normally four hours induction at 37°C would yield more protein than the result shown on the SDS-PAGE gel (Figure 5-9-A-1). This indicated that the KirBac3.1 channel was not suitable for induction at 37°C, therefore, the two other cell lines were induced at 25°C overnight. The BL21(DE3)AI *E. coli* strain is a derivative of BL21(DE3) (Studier and Moffatt, 1986; Grodberg and Dunn, 1988). It contains a chromosomal insertion of the gene encoding T7 RNA polymerase and a tetracycline transporter into the *ara*B gene (endogenous *ara*B gene is deleted in the strain). The BL21(DE3)AI is suitable for high-level recombinant protein expression from any T7-based expression vector. The protein expression is regulated under the control of the T7 RNA polymerase by adjusting the concentration of L-arabinose (Lee, 1980; Lee *at al.* 1987). Based on these advantages the KirBac3.1 channel was expected to express to a high level. Unfortunately the protein expression level was

quite low but better than BL21(DE3) induction at 37°C (Figure 5-9-B-1). Repeating the expression using BL21(DE3)Star* cells, resulted in a good expression level of the protein. After comparison of the three bacterial strains, the final result indicated that BL21(DE3)Star* gave approximately 3 mg/ml of protein after Co^{2+} purification. This is the reason that BL21(DE3)Star* was chosen for large-scale protein expression.

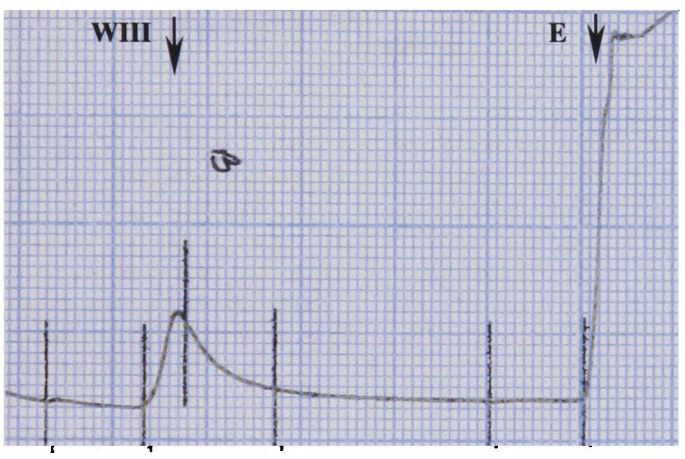
A. BL21(DE3) (37°C induction)



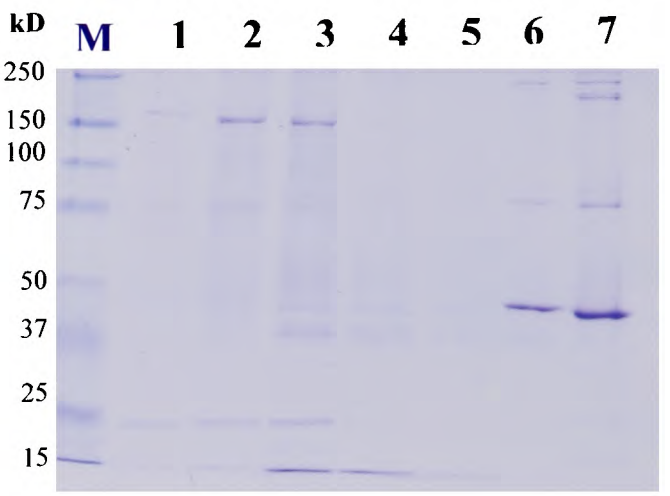
A-1.



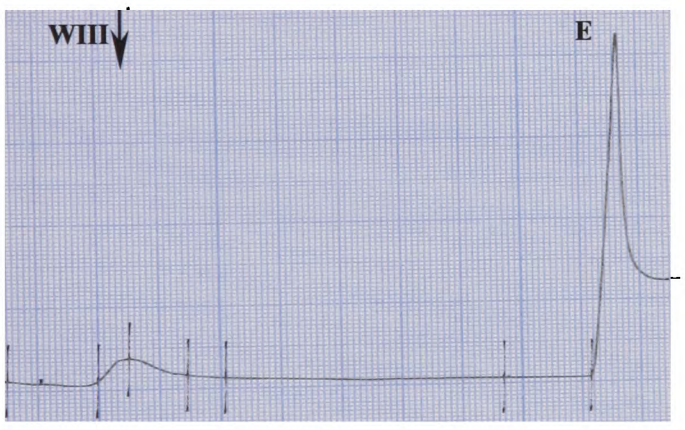
B. BL21(DE3)AI (25°C induction)



B-1.



C. BL21(DE3)Star* (25°C induction)



C-1.

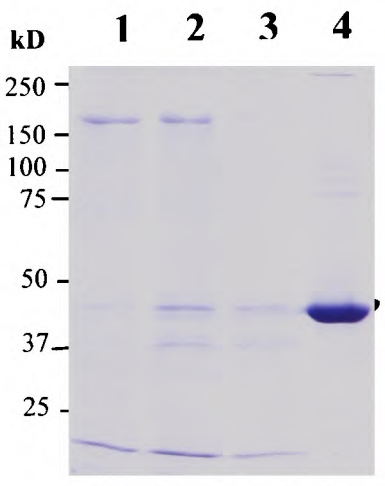


Figure 5-9. KirBac3.1 expressions in three cell lines.

A. Co^{2+} affinity purification chromatogram of KirBac3.1 in BL21(DE3) cells.

A-1 shows the eluted peak fractions run on a 12% SDS-PAGE gel.

B. Co^{2+} affinity purification chromatogram of KirBac3.1 in BL21(DE3)AI cells.

B-1 shows a 12% SDS-PAGE gel with Wash III elution fractions numbered 1-5 with lanes 6-7 from the elution peak.

C. Co^{2+} affinity purification chromatogram of KirBac3.1 in BL21(DE3)Star* cells.

C-1 shows a 12% SDS-PAGE gel. Lane 1 through 3 were non-specific binding proteins which were washed off by 20 mM imidazole in Wash III buffer. Lane 4 was the channel protein peak dialysis overnight and concentrated to be ready to inject to the S-200 column in the gel filtration step.

Further gel filtration indicated that KirBac3.1 was a homotetramer (Figure 5-10). It was noticed that the concentrated sample needed to be injected into the column as soon as possible after extraction to avoid increased aggregation of the protein. The best result was obtained by shortening the purification time scale, finishing both affinity purification and gel filtration steps in one day. The membrane preparation was not necessary for 2-D crystallisation. Both methods produced reasonable crystals as analyzed by EM.

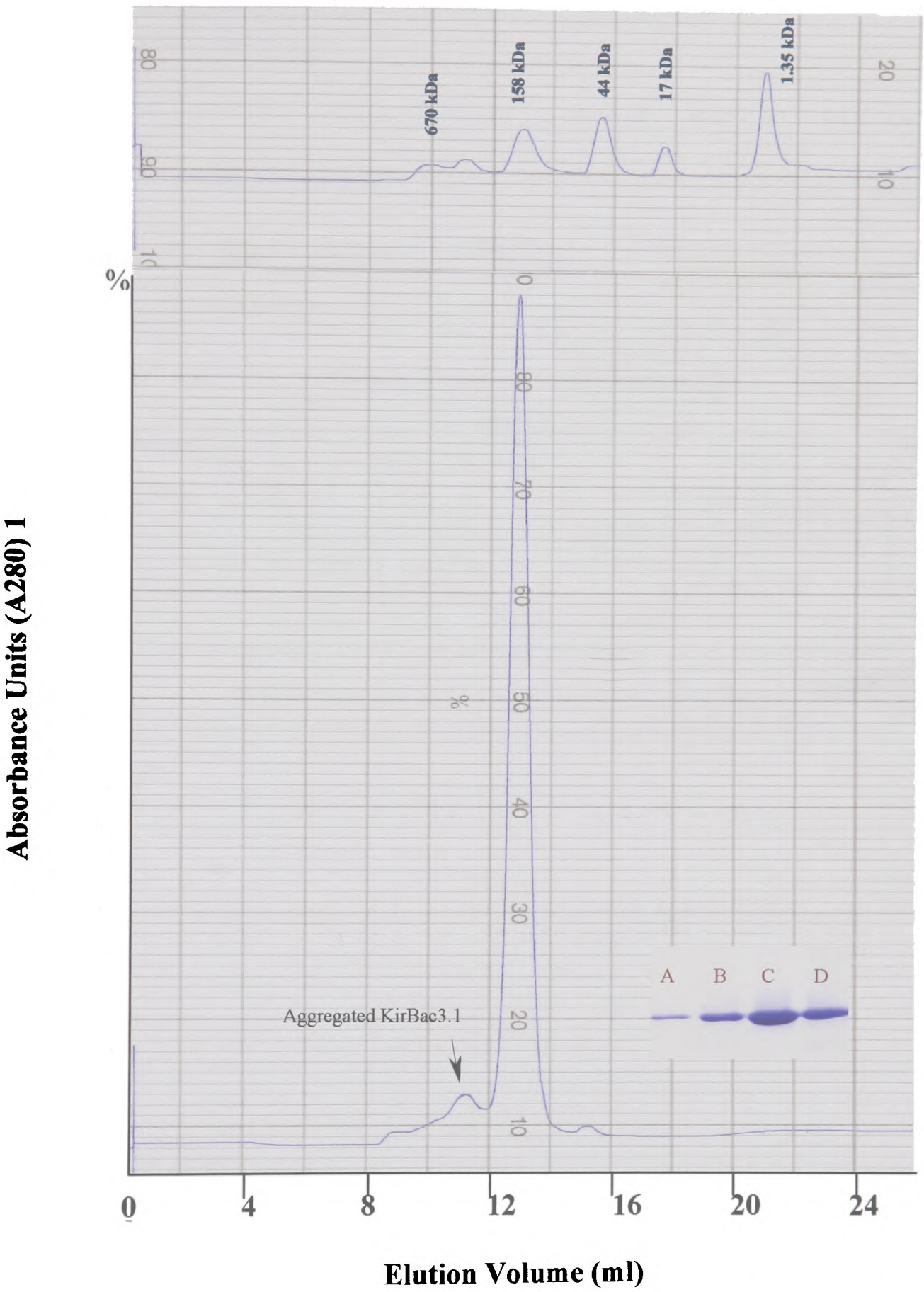


Figure 5-10. Analysis of the native state of KirBac3.1 in detergent.
Elution profile of a full length KirBac3.1 protein in 50 mM Tris-HCl pH 8.0, 100 mM KCl, 5 mM DTT and 0.5 mM triDM.
The BioRad broad range standard is in 50 mM Tris-HCl pH 8.0, 100 mM KCl, 5 mM DTT and 0.5 mM triDM.
The 12% SDS-PAGE gel shows that **A** lane is the small aggregated peak. The rest of lane **B** through lane **D** shows the peak fractions and the **C** fraction is used in 2-D crystallisation.

5.3.4 N-terminal sequencing and mass spectroscopic analysis – results and discussion

N-terminal sequencing of KirBac3.1 showed that *E. coli* strain BL21(DE3)Star* produced one major species with 72% of the recombinant protein having its first Met residue truncated (Table 5-4). No further truncations were detected from the N-terminal side of the protein.

Table 5-4. N-terminal sequencing of KirBac3.1

Cycle Number														
	1	2	3	4	5	6	7	8	9	10	11	12	13	14	15
	T[2]	G	G	M	K	P	P	A	R	K	P	R	I	L	N
Yield:	19.22(picomoles)														
	M[1]	T	G	G	M	K	P	P	A	R	K	P	R	I	L
	7.51(picomoles)														

Figure 5-11 showed the mass spectrum of KirBac3.1 channel as analyzed by MALDI-MS. A single peak was observed at 33,637.3 Da.

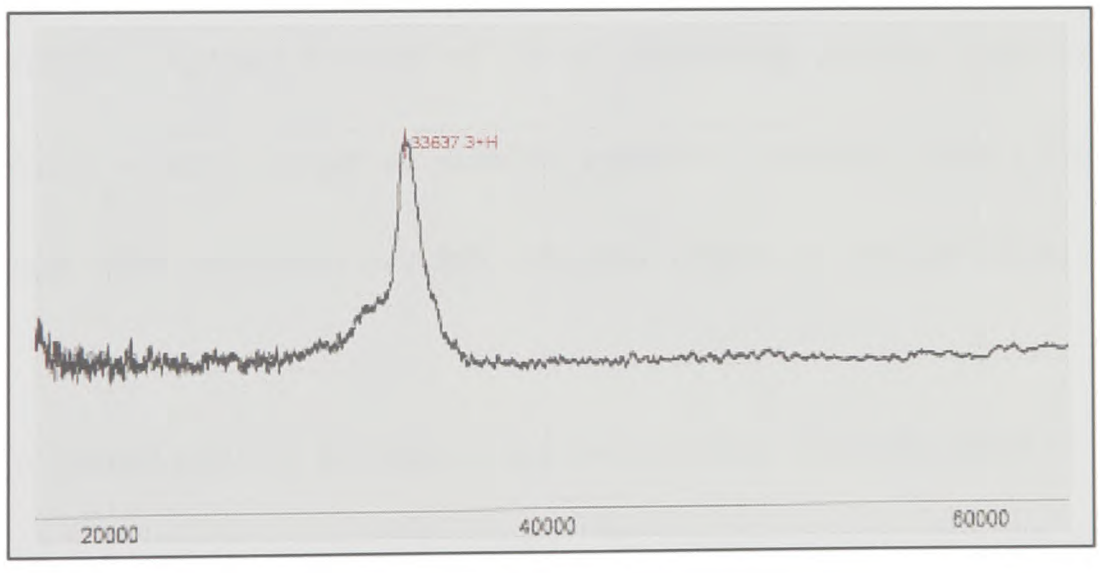


Figure 5-11. Mass spectrometry of KirBac3.1 (Dr. Ashcroft, University of Leeds). The sample was in 5 mM Tris-HCl, 50 mM KCl, 5 mM DTT and 0.05 mM triDM. Calibrants: Insulin B-chain (bovine) (3495.94+1H), Insulin (bovine) (5733.58+1H), Hirudin BKHV(7033.61+1H).

The theoretical mass of KirBac3.1 without the first Met is 33,606.6 Da as calculated using the ExPASy server (http://us.expasy.org/). The difference of 29.7 Da

may be due to poor assignment as a result of the broader peak. In general MALDI-MS normally generates a single peak for each compound in the sample. The lower molecular weight molecule gives a sharp narrow peak but higher molecular weight species gives a broader peak due to the loss of resolution between different isotope peaks

Both N-terminal sequencing and MALDI-MS indicated the KirBac3.1 was an intact protein after purification from the membrane.

5.3.5 2-D crystal formation – results and discussion

The result of reconstitution yielded 2-D sheet crystals. The initial 2-D crystals diffracted to 20 Å using negative staining (Figure 5-12). Later improvements partially came about by cryo-freezing the crystals. An important key feature was that the protein had to be of high purity. Also the protein needed to be mixed with lipid as "fresh" as possible. The word "fresh" means using the protein directly after the protein was purified from gel filtration. The volume of the reconstitution was another important variable. A total volume of 50 µl containing protein, lipid and buffer produced crystals whereas larger or smaller volumes produced none. The 600 µl micro-centrifuge tube produced crystals whereas larger or smaller tubes failed to produce any.

For the closed state of KirBac3.1 the best crystals were obtained in a lipid to protein ratio of 0.6 or 0.7 and 75 mM $MgCl_2$. For those crystals of KirBac3.1 in the potential open state, the protein to lipid ratio of 0.6 or 0.7 and 5 mM EDTA yielded nice crystals. The best crystals diffracted to 9 Å under cryo-frozen conditions (Figure 5-13). Several crystal data sets were averaged to produce the final projection map (all data processing was done by Dr. C. Vénien-Bryan).

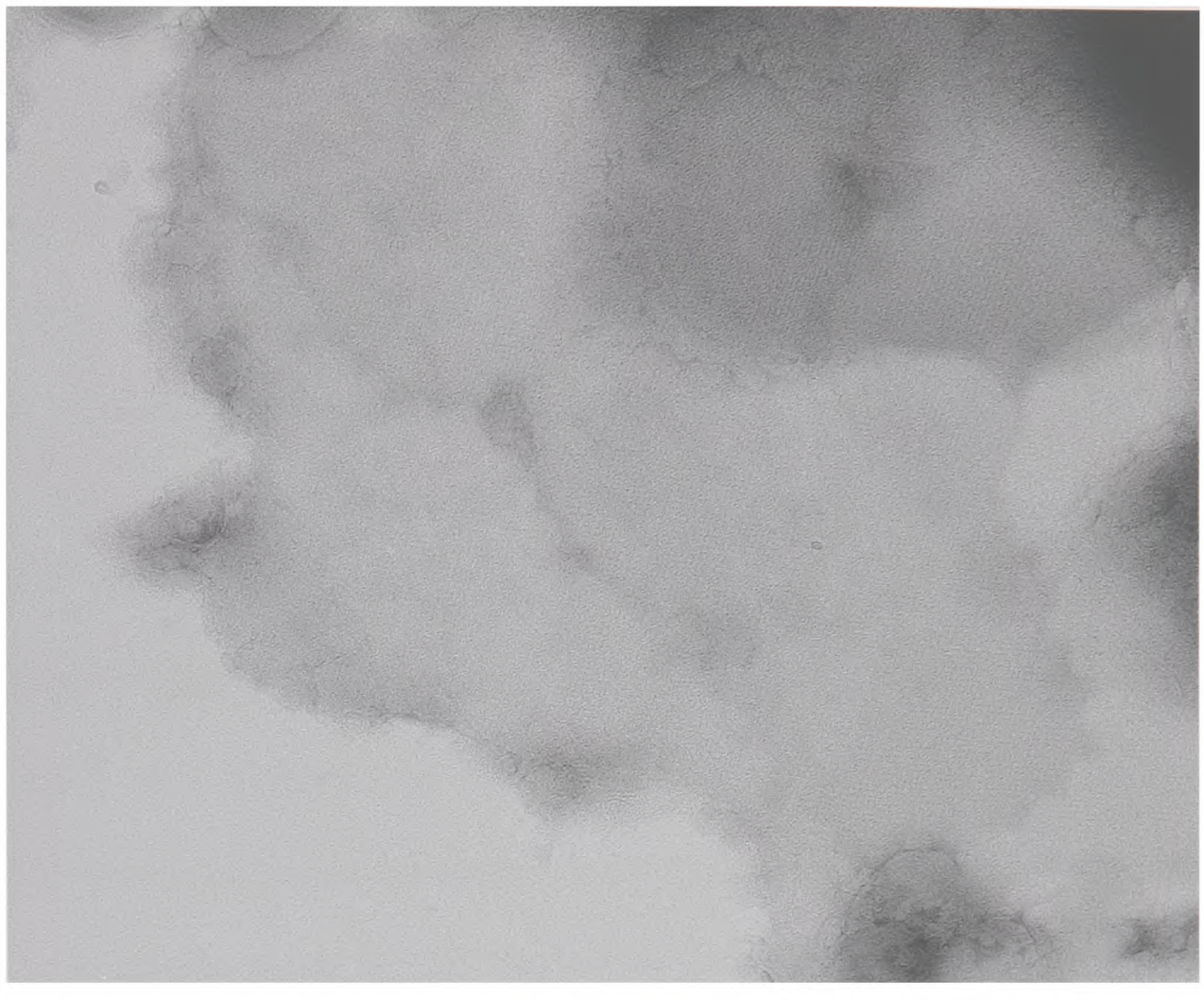


Figure 5-12. 2-D crystal of KirBac3.1 in negative stain.

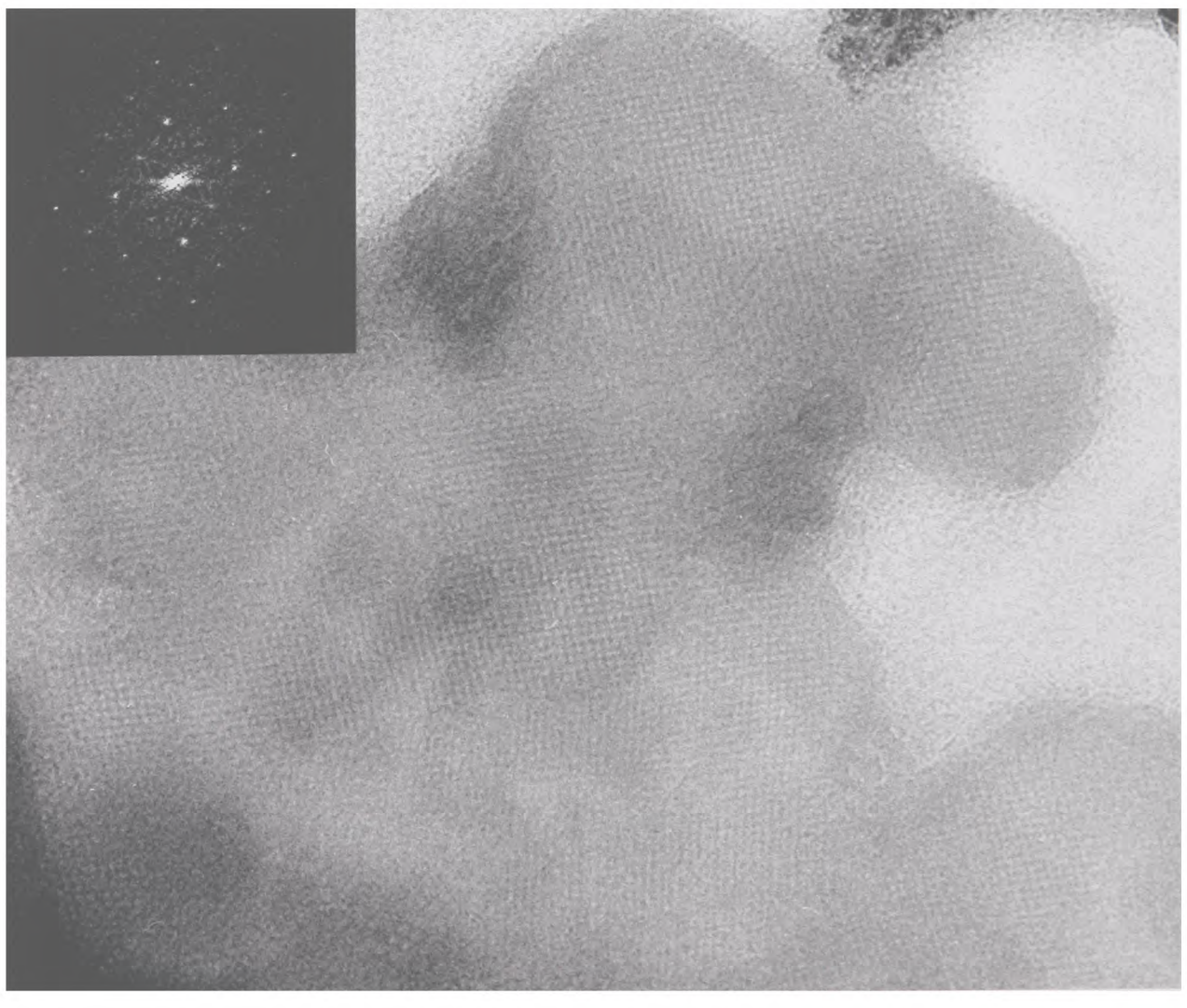


Figure 5-13. 2-D crystal of KirBac3.1 in cryo-condition.

5.3.6 Implication of EM projection map of KirBac3.1

After processing many projection maps and selecting the better crystal data to merge and average, two projection maps were generated representing two gating states: the potential open conformation and the closed conformation of KirBac3.1.

5.3.6.1 Closed conformation of KirBac3.1

The 2-D closed channel of KirBac3.1 crystals were obtained using 75 mM $MgCl_2$. It is known that internal Mg^{2+} blocks K^+ ion conductance. In 2-D projection maps the pore region in the middle is difficult to detect due to the lack of density (Figure 5-14). Inspection of the pore region for the closed state shows positive density contours close to the centre. We believe that this represents tight packing of the inner helices along the ion conduction pathway. The electron beam does not penetrate the higher density if the helices are packed tightly. This is exactly what the projection map shows.

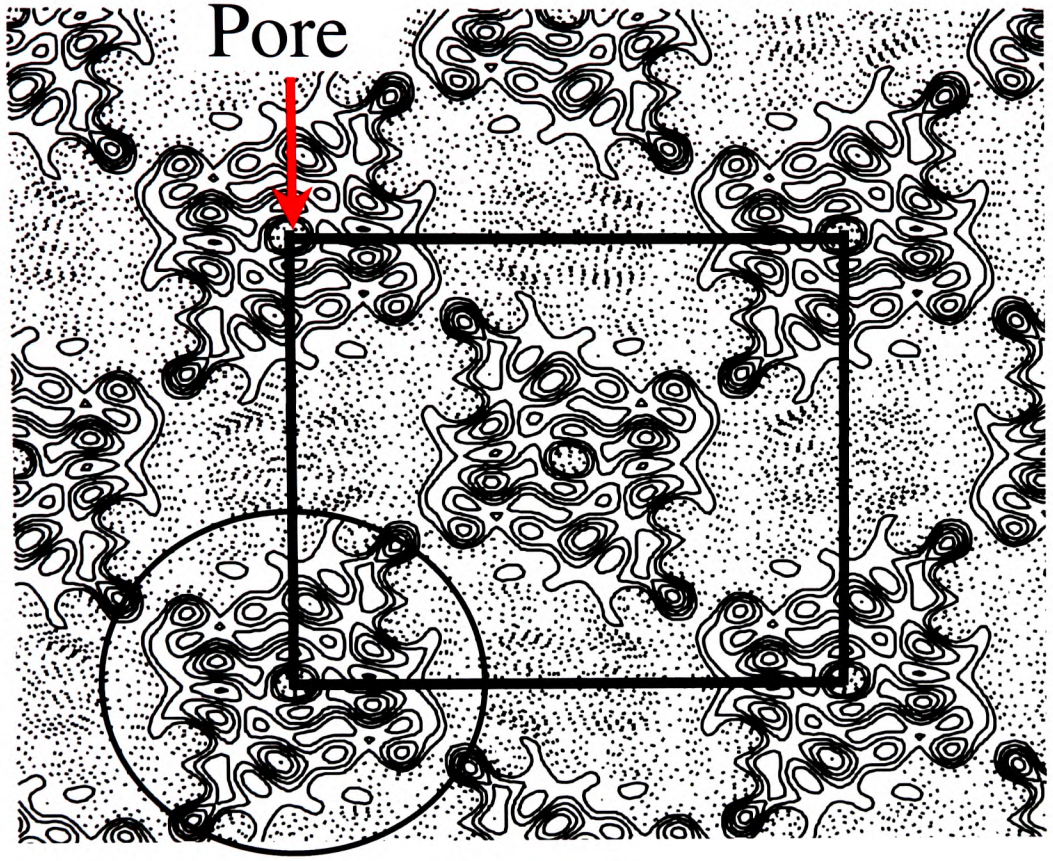


Figure 5-14. A projection map of KirBac3.1 in a closed conformation at 10Å resolution.
The unit cell of the crystal is 98 Å x 110 Å (vertical x horizontal) in space group $p22_12_1$.
Negative and positive contours are shown as dotted and solid lines, respectively.
The picture was generated by Dr. C. Vénien-Bryan.

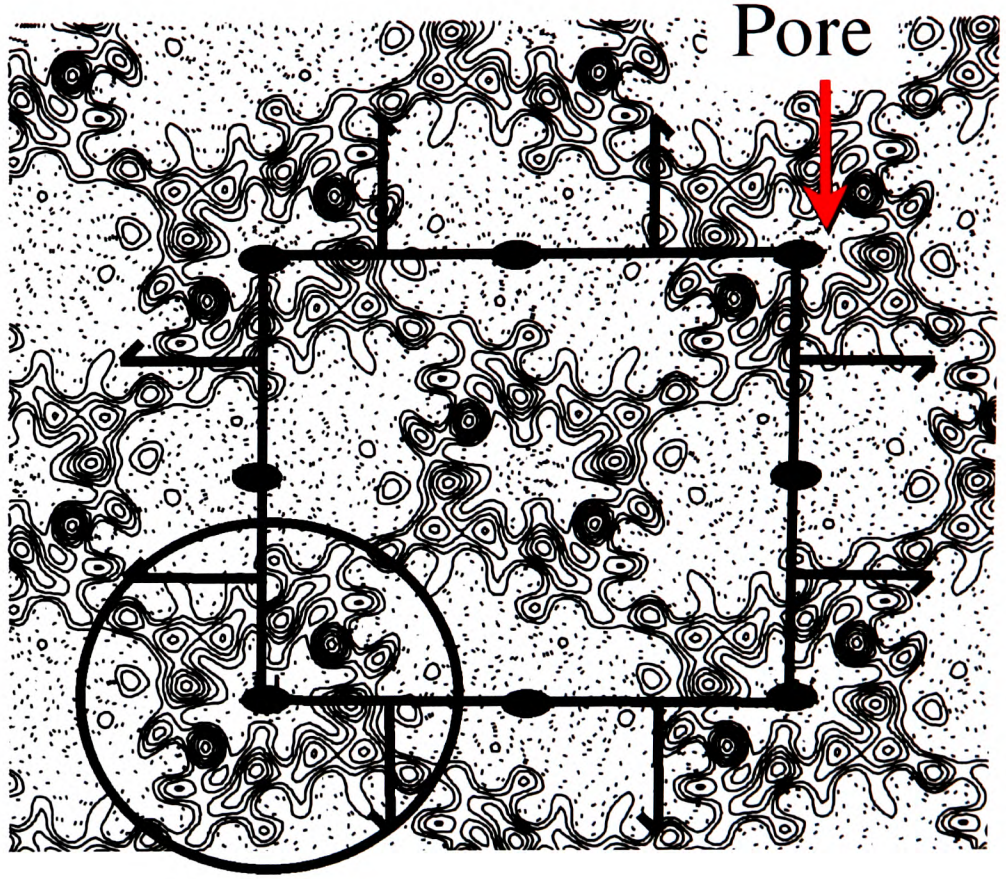


Figure 5-16. A projection map of KirBac3.1 in a potencial open conformation at 9Å resolution.
The unit cell of the crystal is 99 Å x 115 Å (vertical x horizontal) in space group $p22_12_1$.
Negative and positive contours are shown as dotted and solid lines, respectively.
The picture was generated by Dr. C. Vénien-Bryan.

The convincing evidence comes from the structure of KirBac1.1 that shows a closed state. One of the obvious pieces of evidences for the closed state of KirBac1.1 is that the Phe^{146} residues stick out forming a barrier in the center of the ion conduction pathway. These four hydrophobic side chain residues create an unfavorable environment for water, blocking a hydrated K^+ ion from going through (Figure 4-15).

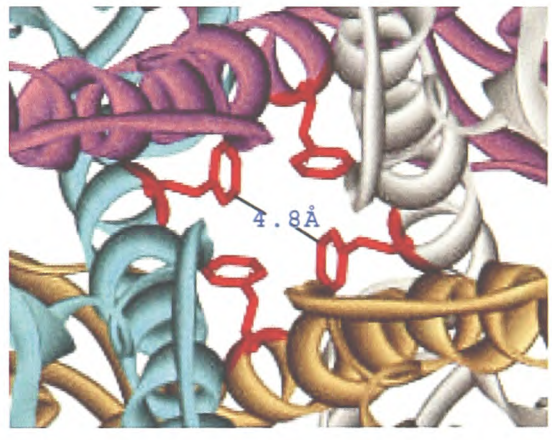


Figure 4-15. A cut-away view of the Phe^{146} blocking residues.
The distance from opposite Phe residues are measured using the program "O". The figure was prepared with the program WebLab ViewerPro5.0 (PDB ID: 1P7B).

5.3.6.2 Potential open conformation of KirBac3.1

2-D crystals of KirBac3.1 in the presence of 5 mM EDTA and crystal buffer conditions produced KirBac3.1 channel in a potential open conformation (Figure 4-16). The projection map showed one important difference from the closed state that suggests the channel is in a potential open conformation. The diameter of the central pore is significantly larger. The distance is approximately 15Å, which is 10Å wider than the closed state. The low-density region is probably the diameter of a pore produced if the selectivity filter and pore helices are removed.

The projection maps are consistent with the idea of the inner helices bending. From our data we believe that the outer helices also undergo a dramatic change in position. They straighten up in the membrane thus providing space for the bottom of the inner helices to occupy as the channel goes from the closed to the open state. Our model also suggests that there is a sequential order of helix movement during opening. First the slide helices move, followed by the outer helices and finally the inner helices.

This is the first evidence of the conformational changes required during gating from the same channel.

Chapter 6 – Conclusions

Early 3-D crystallisation of membrane proteins opened the door for structural studies on membrane proteins. Since then, numerous research labs tried different ways to grow 3-D crystals of membrane proteins but few membrane protein structures were solved comparing with the number of soluble proteins. This is frustrating since many key biological molecules are membrane proteins. Many are important drug targets and many are involved in ion and metabolic transport across the membranes, the subject area that I have been studying.

The development of recombinant DNA technology and the completion of many prokaryotic genome sequences have pushed the structures of membrane proteins to the forefront. Many eukaryotic proteins have bacterial analogues, which are functionally and structurally similar. In the ion channel area a typical example of such an analogue is KcsA from the soil bacteria *Streptomyces lividans*.

The recombinant techniques make purification of bacterial membrane proteins easier to isolate in the quantities required for crystallisation since bacterial proteins are not naturally abundant in the membrane. However, the speed of solving membrane protein structures is still far behind the speed of solving soluble proteins. The major encountered problems are (1) their amphipathic nature of the surface which makes the purification difficult, (2) poor crystal formation likely due to problems associated with the presence of detergents and (3) the cost involved in working with membrane proteins.

This thesis presents my approach to crystallising membrane proteins. Clearly obtaining well-ordered crystals is the foundation of a membrane protein structure determination. This is why my research focuses on this area since a well-diffracting

membrane protein crystal is as straightforward to determine as for a soluble protein crystal. A number of points are summarized below.

6.1 Cell culture manipulation

For crystallisation trials large amounts of protein is necessary. Our strategy involves making use of a number of *E. coli* strains for over production of the recombinant membrane proteins. For the Cl⁻ chloride channel BL21(DE3) strain was used, the Mg^{2+} transporter domain used HMS174(DE3) strain while KirBac1.1 and KirBac3.1 inward rectifier potassium channels used BL21(DE3)Star* strain. However, some proteins still expressed to low quantities when using the induction temperature of 37°C. One approach was to test different temperatures to find the optimum temperature range to produce large amounts of protein. In KirBac1.1 and KirBac3.1 the induction temperature was optimised to 25 - 27°C. Some recombinant proteins inhibited cell growth after rapid induction. All three channels studied in this thesis displayed similar phenomenon. The best way to overcome the situation was by growing cells to late-log phase (OD_{600} = 1.1-1.3) before induction. Though the induction slowed down the cell division rate there were still enough cells to produce large amounts of the target protein. We used overnight induction to ensure the ion channel inserted into the membrane and folded properly.

6.2 Important role of detergent

All membrane proteins possess a hydrophobic surface where they are in contact with lipids. They also have a polar surface that is in contact with the aqueous phases on both side of the membrane. When detergents are used to solubilize membrane proteins they cover the hydrophobic surfaces with their alkyl tails in a belt-like manner. The polar head groups of detergents face the aqueous environment. Selecting the correct detergents is one of the important steps towards membrane

protein crystallisation. Our approach is based on our experiences of crystallisation the first K^+ channel KcsA (Doyle *et al.*, 1998). In Chapter 2 the chloride ion channel was solubilized using $Zwittergent_{3-12}$. In Chapter 4 and 5 the bacterial inward rectifier potassium channels were solubilized with n-decyl-β-D-maltoside (DM). It was noticed that when KirBac3.1 was solubilized for a long time the protein yield was reduced. The effect of detergents on the stability of membrane proteins obviously varies from one protein to the other. There is no rule to follow but it is important to try several different detergents to find a suitable candidate.

Membrane proteins form three-dimensional crystals as a complex with detergents. The most critical point is to obtain a well-ordered crystal to determine the protein structure. Frequently, membrane proteins crystallise but most of the crystals do not diffract X-ray to a high-resolution limit. After searching detergents for solubilisation of the membrane proteins the second step was to find another detergent that will form well-ordered crystals. At present, this step is still trial and error. It does take a long time to find a good detergent. There are no examples to follow because each protein has its own unique characteristics.

In the chloride channel project the detergent lauryl dimethylamine N-oxide (LDAO) was used in the crystallisation set up. LDAO has a small micelle characteristic and has been used to successfully crystallise several membrane proteins. for examples a photosynthetic reaction center from the purple bacterium. a light-harvesting complex from photosynthetic bacteria and a potassium channel from soil bacterial (Michel, 1982; McDermott *et al.*, 1995; Doyle *et al.*, 1998).

For the inward rectifier potassium channel KirBac1.1. triDM was mixed with other detergents, CYMAL-4 or HEGA-10, to form well-ordered crystals. This

detergent mixture approach highlights a quicker and new way to find better-diffracting crystals. Each membrane protein has a likely detergent/protein micelle that produces the best crystals. The optimum size of the micelle can be obtained from one detergent or mixed detergents depending on the individual protein.

6.3 Anisotropically diffracting crystals

The KirBac1.1 crystals only diffracted to 3.65 Å resolutions. A major problem associated with the KirBac1.1 crystals was that all the crystals produced anisotropic diffraction with a reduction in resolution of 0.5-1.0 Å (Figure 4-18). This phenomenon was also observed for the chloride ion channel crystals as well as those of the KcsA crystals. It is believed to be due to the necessary detergent within the crystal disrupting important contacts.

To overcome this problem several methods can be tried. One method uses an antibody to bind the protein thus increasing the surface area for protein-protein contacts within the crystal (Zhou *et al.*, 2001; Dutzler *et al.* 2003). Another approach is to search different crystallisation conditions to change the crystal packing since the dynamic detergent micelle surrounding the protein might interfere with molecular arrangement within the crystal. The third way is to crystallise a new member protein from the same family e.g, KirBac 2.1 or KirBac 3.1 (Durell and Guy, 2001).

6.4 Future direction for the chloride ion channel EcCLC project

The initial purpose of this project was to solve the structure, however, during our improvement of crystal quality a group in the USA solved the structure. Although two years work did not generate the structure, the accumulated knowledge we gained was applied to the KirBac1.1 project. An interesting change in our thinking of CLC channels came about from a paper by Professor C. Miller's group. They suggested that the *E. coli* chloride ion channel was not a channel but rather a H^+-Cl^- exchange

transporter (Accardi and Miller, 2004). It seems that searching for another homologue of eukaryotic chloride channels in prokaryotic organisms with the aim of structural studies is still necessary.

6.5 CorA domain future direction

Based on our results of several constructs, it appeared that the domain did not fold properly without the membrane section. Two shortened constructs even made the aggregation process worse. From these preliminary results it may have been better to have started with the full length CorA transporter. A slow induction vector system might be used instead of a pET vector, for example the pBAD vector. A recent biochemical study of CorA transporter should be a good reference to pursue this full-length protein project (Chen *et al.*, 2003).

6.6 Future direction of inwardly rectifier potassium channel KirBac1.1

The structure of KirBac1.1 was solved in a closed conformation and several structure evidences support the closed conformation: blocking residues Phe^{146} protruding from its side chain into the ion conduction pathway, misalignment of pore helices, reduced volume of central cavity and changed conformation of the filter region. A possible gating mechanism was proposed. It will be great to visualize an open conformation of KirBac derived from 3-D crystals. Since we do not know the function of KirBac1.1 it will also be necessary to investigate the function in order to fully understand the structural information. Based on the structure a few targeted mutation studies would be feasible as a way to investigate the blocking residues and rectification process.

6.7 Future study of KirBac3.1

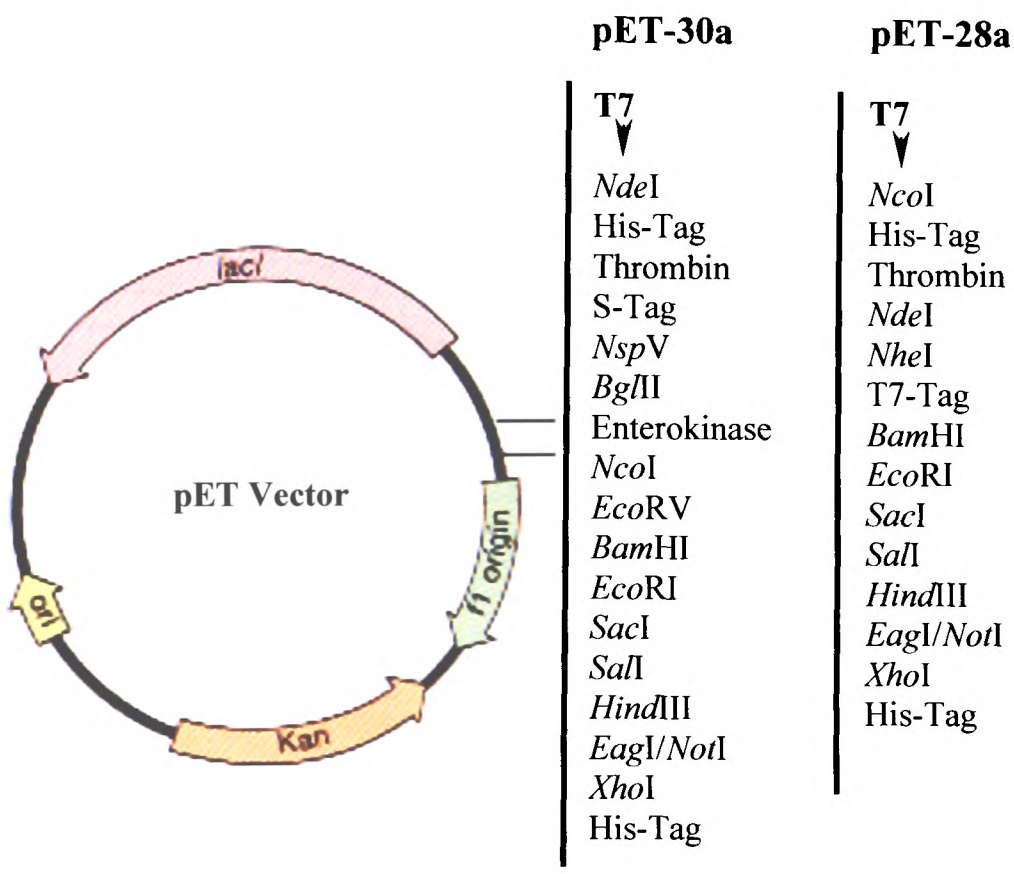
Two-dimensional crystals revealed KirBac3.1 channel in a potential open conformation. We will not know if we have detected the open state until the

functional studies show that the channel conducts current of K^+ ions. therefore we named the channel a potential open state. The resolution of 2-D crystals is still low preventing detailed description of the structure components even though the overall distinction between closed and potentially open state is clear. It would be interesting to visualize the detailed structural information of the inner, outer and slide helices in an open conformation. Based on the knowledge of these results, it will be exciting to crystallise KirBac3.1 in an open conformation.

6.8 Concluding remarks

Ion channels are central components in almost all living cells. They are essential physiological components involved in the generation and propagation of nerve impulses, pain detection, hearing, regulation of hormone secretion, control of water balance and regulation of the heart. Six years ago the first 3-D structure of the potassium ion channel KcsA opened the opportunity to combine functional and structural studies in the ion channel field. Within these years several high resolution K^+ channels structures have been available to interpret the mutagenesis studies of channel function. We learned a great deal about potassium channels behavior through structural studies. In Kir channel subfamily our structure KirBac1.1 confirmed mutagenesis studies of Kir channels, however, the crystal structure hardly shows the dynamic processes that do occur in potassium channels. The combination of different approaches such as 2-D structural studies, computational and physiological studies are required in parallel to gain a better picture of this field.

Appendix A: pET Vector Map



The vector map of pET-30a and pET-28a are adapted from the Novagen catalog. C-terminal hexahistidine tagged proteins utilised the pET-30a while N-terminal tagged proteins used pET-28a.

Appendix B: Procedure for Production of Chemical Competent Cells
--Modified Hanahan's method

1. Grow an overnight culture of the desired strain in LB medium. If the strain contains plasmid add the appropriate antibiotic to maintain plasmid selection.
2. On the next day add 1.0 ml of the saturated overnight culture to 100 ml of LB medium or LB plus antibiotics if it is relevant. Grow the cells at 30°C until the culture reaches mid-log phase (OD_{600} ~ 0.5 if the strain is *RecA* minus or if the strain is *RecA* plus the mid-log phase is OD_{600} 0.3 - 0.4).
3. Chill the cells on ice for one hour.
4. Transfer the cells to two ice-chilled tubes and spin at 4,000 g in a cold (4°C) centrifuge for 15 minutes.
5. Discard the supernatant and resuspend each cell pellet in 20 ml of cold CCMB buffer before merging the two samples into one tube.
6. Incubate on ice for 2 hours.
7. Pellet the cells as before, discard the supernatant and resuspend the cells in 6 ml cold CCMB buffer (an important point is to keep the cells cold all times).
8. Small multiple volumes of 110 µl aliquots were transferred into sterile pre-chilled Eppendorf tubes. Fresh freeze cells on dry-ice/ethanol mix then store cells at -80°C.

CCMB BUFFER

Materials	Amount /litre	Final concentration
$CaCl_2 \cdot 2H_2O$	11.8g	80 mM
$MnCl_2 \cdot 4H_2O$	4.0g	20 mM
$MgCl_2 \cdot 6H_2O$	2.0g	10 mM
Potassium acetate	10ml*	10 mM
Redistilled glycerol	100 ml	10%(v/v)

* 10 ml of a 1 M stock (pH 7.0)

Preparation. First prepare a 1 M solution of potassium acetate and adjust to pH 7.0 using KOH. Next sterilize by filtration through a sterile 0.2 µm membrane and store frozen. Now prepare a solution of 10 mM potassium acetate. 10% glycerol (v/v) using the purest water (from Sigma). Add the salts as solids and allow each salt to enter into solution before adding the next one. After all the salts are dissolved

adjust pH to 6.4 with 0.1 N HCl. Do not adjust pH upward with base. Sterilize the CCMB buffer by filtration through a 0.22 μm filter and store at 4°C (the solution is better fresh made).

Competent cells work better after the cells have been frozen at -80°C for a few weeks.

Appendix C: Protein Analysis

1. Protein Concentration Determination

All purified his-tagged protein or his-tag removed protein concentrations were determined from the optical density at 280nm using the equation:

A_{280} (1 mg/ml) = (nTrp x 5690 + nTyr x 1280 + nCys x 120)/M_r

Where nTrp = number of tryptophan residues

nTyr = number of tyrosine residues

nCys = number of cysteine residues

and M_r = calculated molecular weight

2. Silver Staining

Soak the gel in 100 ml of fix solution (40 % ethanol, 10 % acetic acid and 50 % H_2O) shaking slowly for one hour.

Soak the gel in 100 ml of DTT solution (40 µl of 1m DTT in 100 ml of H_2O) for another hour.

Briefly rinse the gel with water and add 100 ml solution containing 0.1 % (w/v) $AgNO_3$ and 40 µl of 37 % formaldehyde shaking for 30 minutes slowly.

Develop the gel by soak the gel in 100 ml of developer (2.5 % (w/v) Na_2CO_3, 40 µl 37 % formaldehyde) for a few minutes until protein bands are dark (visualize by eye).

Rinse the gel with large amounts of water several times.

Stop the reaction by adding a few drops of acetic acid.

Appendix D: Seleno-methionine Label Medium

Autoclavable M9 (20X)

Chemical Class	Compound Formula	Quantity
Salts/Buffer	NH_4Cl	10 g
	KH_2PO_4	30 g
	Na_2HPO_4	60 g
	H_2O to	500 ml

Non-autoclavable Amino Acid Mix I

Chemical Class	Compound Name	Quantity
Amino Acid	Alanine	200 mg
	Asparagine	200 mg
	Aspartic acid	200 mg
	Cystine	200 mg
	Glutamic acid	200 mg
	Glutamine	200 mg
	Glycine	200 mg
	Histidine	200 mg
	Isoleucine	200 mg
	Leucine	200 mg
	Lysine	200 mg
	Phenyalanine	200 mg
	Proline	200 mg
	Serine	200 mg
	Threonine	200 mg
	Valine	200 mg
	H_2O to	50 ml

Non-autoclavable Amino Acid Mix II

Chemical Class	Compound Name	Quantity
Amino Acid	Tyrosine	200 mg
	Tryptophan	200 mg
	Phenylalanine	200 mg
	H_2O to	50 ml

Non-autoclavable Vitamin Mix

Chemical Class	Compound Formula	Quantity
Vitamins	Riboflavin	10 mg
	Niacinamide	10 mg
	Thiamine	10 mg
	Pyridoxine monohydrochloride	10 mg
	H_2O to	10 ml

Non-autoclavable Nutrient Mix

Chemical Class	Compound Formula	Quantity
Nutient Source	Glucose 40%	20 g
	H_2O to	50 ml
	$MgSO_4.7H_2O$ (1 M)	
	$FeSO_4.7H_2O$ (12.5 mg/ml)	

Table showing chemical compounds of the non-autoclavable and autoclavable medium. All the non-autoclavable media were freshly made and filter sterilized through a 0.22 µm filter (Whatman) before use.

Appendix E: Home Salt/PEG Crystal Screen Solution

900 Home Crystal PEG/Ion Screen Fomulation

pH 4 – 9 PEG 400 (10 - 40%) PEG 1000 (10 - 40%) PEG 4000 (5 – 30%) PEG 8000 (5 – 30%)	pH 4 - 9 0.5 M KCl PEG 400 (10 - 40%) PEG 1000 (10 - 40%) PEG 4000 (5 – 30%) PEG 8000 (5 – 30%)	pH 4 - 9 0.2 M $CaCl_2$ PEG 400 (10 - 40%) PEG 1000 (10 - 40%) PEG 4000 (5 – 30%) PEG 8000 (5 – 30%)	pH 4 - 9 0.2 M Li_2SO_4 PEG 400 (10 - 40%) PEG 1000 (10 - 40%) PEG 4000 (5 – 30%) PEG 8000 (5 – 30%)	pH 4 - 9 0.2 M $(NH_4)_2 SO_4$ PEG 400 (10 - 40%) PEG 1000 (10 - 40%) PEG 4000 (5 – 30%) PEG 8000 (5 – 30%)
pH 4 - 9 1.0 M NaCl PEG 400 (10 - 40%) PEG 1000 (10 - 40%) PEG 4000 (5 – 30%) PEG 8000 (5 – 30%)	pH 4 - 9 1.0 M NH_4 Formate PEG 400 (10 - 40%) PEG 1000 (10 - 40%) PEG 4000 (5 – 30%) PEG 8000 (5 – 30%)	pH 4 - 9 0.05 M $Mg(Acetate)_2$ PEG 400 (10 - 40%) PEG 1000 (10 - 40%) PEG 4000 (5 – 30%) PEG 8000 (5 – 30%)	pH 4 – 9 0.05 M $Zn(Acetate)_2$ PEG 400 (10 – 40%) pH 7.5 (HEPES) 175 – 250 mM $CaCl_2$ PEG 400 45 – 56 %)	pH 6 – 6.75 0.1 M Cacodylate 0.05 M $Zn(Acetate)_2$ MPD (30 – 40%) pH 6.5 0.1 M Cacpdylate 20 – 150 mM ZnAcetate

pH 4.0 and pH 5.0 – 0.1 M $NaCH_3COO$

pH 6.0 and pH 6.5 – 0.1 M Cacodylate

pH 7.0 and pH 7.5 – 0.1 M Hepes

pH 8.0 – 0.1 M Tris-HCl

pH 9.0 – 0.1 M Glycine

This final pH is adjusted with 10 % HCl or 1 M NaOH at room temperature.

All chemical reagents were pre-filtered through a 0.22 µm filter.

References

Accardl, A and Miller, C (2004) Secondary active transport mediated by a prokaryotic homologue of ClC Cl- channels. ***Nature*** 427: 803-807.

Aggarwal, S. K. and MacKinnon, R. (1996) Contribution of the S4 segment to gating charge in the *Shaker* K^+ channel. ***Neuron*** 16: 1169-1177.

Alberts, B., A. Jojnson, J. Lewis, M. Raff, K. Roberts and P. Walter (2002) ***Molecular Biology of the Cell*** New York, Garland Science Publishing, Inc.

Altschul, S. F., T. L. Madden, A. A. Schaffer, J. Zhang, Z. Zhang, W. Miller and D. J. Lipman (1997) Gapped BLAST and PSI-BLAST: a new generation of protein database search programs. ***Nucleic Acids Res.*** 25(17): 3389-3402.

Atlas, R. M. (1997) ***Hand book of Microbiological Media*** 2rd ed, CRC Press, Inc.

Ashcroft, S. J. H. and Ashcroft, F. M. (1990) Properties and functions of ATP-sensitive K-channels. ***Cell Signal.*** 2: 197-214.

Ashcroft, F. M. (2000) ***Ion Channels and Disease*** London, Academic Press, Inc.

Banerjee, P., J. B. Joo, J. T. Buse, G. Dawson (1995) Differential solubilisation of lipids along with membrane proteins by different classes of detergents. ***Chemistry and Physics of Lipids*** 77: 65-78.

Bass, R. B., P. Strop, M. Barclay and D. C. Rees (2002) Crystal structure of *Escherichia coli* MscS, a voltage-modulated and mechanosensitive channel. ***Science*** 298: 1582-1587.

Bezanilla, F. and C. M. Armstrong (1972) Negative conductance caused by entry of sodium and cesium ions into the potassium channels of squid axons. ***J. Gen. Physiol.*** 60: 588-608.

Bright, J. N., I. H. Shrivastava, F. S. Cordes, M. S. P. Sansom (2002) Conformational dynamics of helix S6 from Shaker potassium channel: simulation studies. ***Biopolymers*** 64: 303-313.

Bowler, M. W. (2001) Structural studies of a membrane embedded chloride channel from *E.coli*, a prokaryotic homologue of CLC channels. ***M.Sc. Thesis***, University of Oxford.

Blatz, A. L., and Magleby, K. L. (1987) Calcium-activated potassium channels. ***Trend. Neurosci.*** 10: 463-467.

Morais-Cabral, J., Y. Zhou and R. MacKinnon (2001) Energetic optimization of ion conduction rate by the K^+ selectivity filter. ***Nature*** 414: 37-42.

Carrió, M. M. and Villaverde, A. (2001) Protein aggregation as bacterial inclusion bodies is reversible. ***FEBS*** 489 (1): 29-33.

Chen, T. Y. and Miller, C. (1996) Nonequilibrium gating and voltage dependence of the ClC-0 Cl⁻ channel. ***J. Gen. Physiol.*** 108: 237-250.

Chen, Y., J. Song, S. Sui and D. N. Wang (2003). DnaK and DnaJ facilitated the folding process and reduced inclusion body formation of magnesium transporter CorA overexpressed in *Escherichia coli*. ***Prot. Expr. & Puri.*** 12: 221-231.

Cui, J., D. H. Cox and R. W. Aldrich (1997) Intrinsic voltage dependence and Ca^{2+} regulation of *mslo* large conductance Ca-activated K^+ channels. ***J. Gen. Physiol.*** 109: 647-673.

Czempinski, K., S. Zimmermann, T. Ehrhardt, B. Muller-Rober (1997) New structure and function in plant K^+ channels: KCO1, an outward rectifier with a steep Ca^{2+} dependency. ***EMBO J.*** 16 (10): 2565-2575.

Dauter, Z. (1999) Data-collection strategies. ***Acta. Cryst.*** D55: 1703-1717.

Deber, C. M. and Therien, A. G. (2002) Putting the breaks on membrane protein misfolding. ***Nature Structural Biology*** 9: 318-319.

Dean, Michael (2002) The Human ATP-binding cassette (ABC) transporter superfamily NCBI, National Library of Medicine, Molecular Biology.

Derst, C., M. Konrad, A. Köckerling, L. Károlyi, G. Deschenes, J. Daut, A. Karschin and H. W. Seyberth (1997) Mutations in the ROMK gene in antenatal Bartter syndrome are associated with impaired K^+ channel function. ***Biochem. Biophys. Res. Commun.*** 230: 641-645.

Doupnik, C. A., N. Davidson and H. A. Lester (1995) The inward rectifier potassium channel family. ***Curr. Op. Neurobiol.*** 5: 268-277.

Doyle, D. A., M. J. Cabral, R. A. Pfuetzner, A. Kuo, J. M. Gulbis, S. L. Cohen, B. T. Chait, R. MacKinnon (1998) The structure of the potassium channel: molecular basis of K^+ conduction and selectivity. ***Science*** 280: 69-77.

Dutzler, R., E. B. Campbell, M. Cadene, B. T. Chait and R. MacKinnon (2001) X-ray structure of a ClC chloride channel at 3.0 Å reveals the molecular basis of anion selectivity. ***Nature*** 415: 287-294.

Dutzler, R., E. B. Campbell and R. MacKinnon (2003) ***Science*** 298: 1582-1587.

Durell, S. R. and Guy, H. R. (2001) A family of putative Kir of potassium channels in prokaryotes. ***BMC Evolutionary Biology*** 1: 1-14.

Estevez, R. and Jentsch, T. J. (2002) CLC chloride channels: correlating structure with function. ***Current Opinion in Structural Biology*** 12: 531-539.

Fakler, B., U. Brandle, E. Glowatzki, S. Weidemann, H. P. Zenner and J. P. Ruppersberg (1995) Strong voltage-dependent inward rectification of inward rectifier K^+ channels is caused by intracellular spermine. ***Cell*** 80: 149-154.

Fakler, B., U. Brandle, E. Glowatzki, C. Konig, C. Bond, J. P. Adelman, H. P. Zenner and J. P. Ruppersberg (1994) A structural determinant of differential sensitivity of cloned inward rectifier channels to intracellular spermine. ***FEBS*** 356: 199-203.

Ficker, E., M. Taglialatela, B. A. Wible, C. M. Henley and A. M. Brown (1994) Spermine and spermidine as gating molecules for inward rectifier K^+ channels. ***Science*** 266: 1068-1072.

Gárdos, G. (1958) The function of calcium in the potassium permeability of human erythrocytes. ***Biochem. Biophys. Acta.*** 30: 653-654.

Grodberg, J. and Dunn, J. J. (1988) OmpT encodes the *Escherichia coli* outer membrane protease that cleaves T7 RNA pollymearse during purification. ***J. Bacteriol.*** 170: 1254-1253.

Hanahan, D., J. Jessee and F. R. Bloom (1991) Plasmid transformation of *Escherichia coli* and other bacteria. ***J. Gen. Physiol.*** 82(1): 25-45.

Heginbotham, L., T. Abramson and R. MacKinnon (1992) A functional connection between the pores of distantly related ion channels as revealed by mutant K^+ channels. ***Science*** 258: 1152-1155.

Heginbotham, L., Z. Lu, T. Abramson and R. MacKinnon (1994) Mutation in the K^+ channel signature sequence. ***Biophys. J.*** 66: 1061-1067.

Heginbotham, L., M. LeMasurier, L. Kolmakova-Partensky and C. Miller. (1999) Single *Streptomyces lividans* K^+ channels: Functional asymmetries and sidedness of proton activation. ***J. Gen. Physiol.*** 114: 551-560.

Hille, B. (2001). ***Ionic channels of excitable membranes***. 3rd ed. Sinaur Associates, Inc., Sunderland, MA, U.S.A.

Hmiel, S. P., Snavely, M. D., Miller, C. G. and Maguire, M. E. (1986) Magnesium transport in *Salmonella typhimurium*: characterization of magnesium influx and cloning of a transport gene. ***J. Bacteriol.*** 168: 1444-1450.

Hmiel, S. P., M. D. Sanevely, J. B., Florer, M. E. Maguire and C. G. Miller (1989) Magnesium trasport in *Salmonella typhimurium*: genetic characterization and cloning of three magnesium transport loci. ***J. Bacteriol.*** 171: 4742-4751.

Ho, K., C. G. Nichols, W. J. Lederer, J. Lytton, P. M. Vassilev, M. V. Kanazirska and S. C. Hebert (1993) Cloning and expression of an inwardly rectifying ATP-regulated potassium channel. ***Nature*** 362: 31-38.

Hodgkin, A. L. and Horowicz, P. (1959) The influence of potassium and chloride ions on the membrane potential of single muscle fibres. ***J. Physiol.*** 148: 127-160.

Hofmann, K. and Stoffel, W. (1993) TM base – A database of membrane spanning proteins segments. ***Biol. Chem. Hoppe-Seyler*** 374, 166.

Huang, Y. F., M. J. Lemieux, J. M. Song, M. Auer and D. N. Wang (2003) Structure and mechanism of the glycerol-3-phosphate transporter from *Escherichia coli*. ***Science*** 301: 616-620.

Hunte, C., J. Koepke, C. Lange, T. Rossmanith. and H. Michel (2000) Structure at 2.3 Å resolution of the cytochrome bc(1) complex from the yeast *Saccharomyces cerevisiae* co-crystallized with an antibody Fv fragment. ***Struct. Fold. Des.*** 8: 669-684.

Jentsch, T. J., K. Steinmeyer and G. Schwarz (1990) Primary structure of *Torpedo marmorata* chloride channel isolated by expression cloning in *Xenopus* oocytes. ***Nature*** 348: 510-514.

Jentsch, T. J. and Günther, W. (1997) Chloride channels: an emerging molecular picture. ***Bioassays*** 19: 117-126.

Jentsch, T. J. (2002) Chloride channels are different. ***Nature*** 415: 276-277.

Jentsch, T. J., V. Stein, F. Weinreich and A. A. Zdebik (2002) Molecular structure and physiological function of chloride channels. ***Physiol. Rev***. 82: 503-568.

Jiang, Y., A. Lee, J. Chen, M. Cadene, B. T. Chait and R. MacKinnon (2002) Crystal structure and mechanism of a calcium gated potassium channel. ***Nature*** 417: 523-526.

Jiang, Y., A. Lee, Chen, J., Ruta, V., Cadene, M. Cadene, B. T., Chalt and R. MacKinnon (2003) X-ray structure of a voltage-dependent K^+ channel.
Nature 423: 33-41.

Kabsch, W. (1976) A solution for the best rotation to relate two sets of vectors. ***Acta. Cryst.*** A32: 922-923.

Katz, B. (1949) Les constants électriques de la membrane du muscle. ***Arch. Sci. Physiol.*** 3: 285-299.

Ketchum, K. A., W. J. Joiner, A. J. Sellers, L. K. Kaczmarek and S. A. N. Goldstein (1995) A new family of outwardly rectifying potassium channel proteins with two pore domains in tandem. ***Nature*** 376: 690-695.

Katz, A. K. and Glusker, J. P. (1998) Roles of zinc and magnesium ions in enzymes. ***Advances in Molecular Structure Research*** Vol. 4 p.227-279, London, JAI Press Inc.

Khodakhah, K., A. Melishchuk and C. M. Armstrong (1997) Killing K channels with TEA. ***Proc. Natl. Acad. Sci. USA*** 94: 13335-13338.

Koch, M. C., K. Steinmeyer, C. Lorenz, K. Ricker, F. Wolf, M. Otto, B. Zoll, F. Lehmann-Horn, K.-H. Grzeschik and T. J. Jentsch (1992) The skeletal muscle chloride channel in dominant and recessive human myotonia. ***Science*** 257: 797-800.

Kim, D., C. D. Sladek, C. Aguado-Velasco and J. R Mathiasen (1995) Arachidonic acid activation of a new family of K^+ channels in cultured rat neuronal cells. ***J. Physiol.*** 484(3): 643-660.

Koronakis, V., A. Sharff, E. Koronakis, B. Luisi and C. Hughes (2000) Crystal structure of the bacterial membrane protein ToIC central to multidrug efflux and protein export. ***Nature*** 405: 914-919.

Kubo, Y., T. J. Baldwin, Y. N. Jan and L.Y. Jan (1993a) Primary structure and functional expression of a mouse inward rectifier potassium channel. ***Nature*** 362: 127-133.

Kubo, Y., E. Reuveny, P. A. Slesinger, Y. N. Jan and L. Y. Jan (1993b) Primary structure and functional expression of a rat-G-protein-coupled muscarinic potassium channel. ***Nature*** 364: 802-806.

Kubo, Y., and Murata, Y. (2001) Control of rectification and permeation by two distinct sites after the second transmembrane region in Kir2.1 K^+ channels. ***J. Physiol.*** 531: 645-660.

Kuo, A., W. M. Bowler, J. Zimmer, J. F. Antcliff and D. A. Doyle (2003) Increasing the diffraction limits and internal order of a membrane protein crystal by dehydration. ***J. Struct. Biol***. 141: 97-102.

Kuo, A., J. M. Gulbis, J. F. Antcliff, T. Rahman, E. D. Lowe, J. Zimmer, J. Cuthbertson, F. M. Ashcroft, T. Ezaki and D. A. Doyle (2003) Crystal structure of the potassium channel KirBac1.1 in the closed state. ***Science*** 300:1922-1926.

Larrson, H. P., O. S. Baker, D. S. Dhillon and E. Y. Isacoff (1996) Transmembrane movement of the *Shaker* K^+ channel S4. ***Neuron*** 16: 387-397.

Lee, N. (1980) Molecular aspects of *ara* regulation. In ***The Operon***. J. H. Miller and W. S. Reznikoff, eds. (Cold Spring Harbor, N. Y.: Cold Spring Harbor Laboratory), pp. 389-410.

Lee, N., C. Francklyn and E. P. Hamilton (1987) Arabinose-induced binding of araC protein to $araI_2$ activates the *ara*BAD operon promoter. ***Proc. Natl. Acad. Sci. USA*** 81: 4120-4124.

Lesage, F., E. Guillemare, M. Fink, F. Duprat, M. Lazdunski, G. Romey and J. Barhanin (1996) TWIK-1, a ubiquitous human weakly inward rectifying K^+ channel with a novel structure. ***EMBO J.*** 15: 1004-1011.

Leslie, A. G. W. (1992) **MOSFLM**. in Joint CCP4 and ESF-EACMB Newsletter on Protein Crystallography., Daresbury Laboratory, Warrington.

Leslie, A. G. W. (2001) **MOSFLM** 6.2 User Guide.

Lindwall, G., M. F. Chau, S. R. Gardner and L. A. Kohlstaedt (2000) A sparse matrix approach to the solubilization of overexpressed proteins. ***Protein Engineering*** 13(1): 67-71.

Lopatin, A. N., E. N. Makhina and C. G. Nichols (1994) Patassium channel block by cytoplasmic polyamines as the mechanism of intrinsic rectification. ***Nature*** 371: 366-369.

Lopatin, A. N., E. M. Makhina and C. G. Nichols (1995) The mechanism of inward rectification of potassium channels: "long-pore plugging" by cytoplasmic polyamines. ***J. Gen. Physiol.*** 106: 923-955.

Lu, M. and MacKinnon, R. (1994) Electrostatic tunning of Mg^{2+} affinity in an inward-rectifier K^+ channel. ***Nature*** 371: 243-246.

Lucher, K. P., A. T. Lee, D. C. Rees. (2002) The *E. coli* BtuCD structure: A framework for ABC transporter architecture and mechanism. ***Science*** 296: 1091-1098.

Ludewig, U., M. Pusch and T. J. Jentsch (1996) Two physically distinct pores in the dimeric ClC-0 chloride channel. ***Nature*** 383: 340-343.

MacKinnon, R., S. L. Cohen, A. Kuo, A. Lee and B. T. Chait. (1998) Structural conservation in prokaryotic and eukaryotic potassium channels. ***Science*** 280: 106-109.

Maduke, M., C. Miller and J. A. Mindell (2000) Decade of ClC chloride channels: structure, mechanism, and many unsettled questions. ***Annu. Rev. Biophys. Biomol. Struct.*** 29: 411-438.

Maingnet, F., M. Fosset, F. Lesage, M. Lazdunski and E. Honoré (1999) TRAAK is a mammalian neuronal mechano-gated K^+ channel. ***J. Biol. Chem.*** 274: 1381-1387.

Matsuda, H., A. Saigusa, H. Irisawa (1987) Ohmic conductance through the inwardly rectifying K^+ channel and blocking by internal Mg^{2+}. ***Nature*** 325: 156-159.

McDermott, G., S. M. Prince, A. A. Freer, A. M. Hawthornthwaite-Lawless, B. A. Paiz, R. J. Cogdell and N. W. Isaacs (1995) Crystal structure of an integral membrane light-harvesting complex from photosynthetic bacteria. ***Nature*** 374: 517-521.

Meech, R. W. (1974) The sensitivity of helix aspersa neurons to injected calcium ions. ***J. Physiol.*** 237(2): 259-277.

Meera, P., M. Wallner, M. Song and L. Toro (1997) Large conductance voltage and calcium-dependent K^+ channel, a distinct member of voltage-dependent ion channels with seven N-terminal transmembrane segments (S0-S6), an extracellular N terminus, and an intracellular (S9-S10) C terminus. ***Proc. Natl. Acad. Sci. USA*** 94: 14066-14071.

Michel, H. and Oesterhelt, D. (1980) Three-dimensional crystals of membrane proteins: bacteriorhodopsin. ***Proc. Natl. Acad. Sci. USA*** 70: 2852-2857.

Michel, H. (1982) Three-dimensional crystals of a membrane protein complex. The photosynthetic reaction centre from *Rhodopseudomonas viridis*. ***J. Molec. Biol.*** 158:567-572.

Michel, H. (1983) Crystallization of membrane proteins. ***Trends Biochem. Sci.*** 8: 56-59.

Middleton, R. E., D. J. Pheasant and C. Miller (1996) Homodimeric architecture of a ClC-type chloride ion channel. ***Nature*** 383 (6598): 337-340.

Mindell, J. A., M. Maduke C. Miller and N. Grigorieff (2001) Projection structure of a ClC-type chloride channel at 6.5 Å resolution. ***Nature*** 409: 219-223.

Miller, C. and White, M. M. (1984) Dimeric structure of single chloride channels from *Torpedo* electroplax. ***Proc. Natl. Acad. Sci. USA*** 81(9): 2772-2775.

Morais-Cabral, J., Y. Zhou and R. MacKinnon (2001) Energetic optimization of ion conduction rate by the K^+ selectivity filter. ***Nature*** 414:37-42.

Nishida, M. and MacKinnon, R. (2002) Structural basis of inward rectification: cytoplasmic pore of the G protein-gated inward rectifier GIRK1 at 1.8 Å resolution. ***Cell*** 111: 957-965.

Neher E. and Sakmann B. (1976) Single channel currents recorded from membrane of denervated frog muscle fibres. ***Nature*** 260: 799-802

Nelson, D. L., and Kennedy, E. P. (1971) Magnesium transport in *Escherichia coli*. Inhibition by cobaltous ion. ***J. Mol. Chem.*** 246: 3042-3049.

Noda, M. S., S. Shimizu, T. Tanabe, T. Takai, T. Kayano, T. Ikeda, H. Takahashi, H. Nakayama, Y. Kanaoka, N. Minamino, K. Kangawa, H. Matsuo, M. A. Raftery, T. Hirose, S. Inayama, H. Hayashida, T. Miyata and S. Numa (1984) Primary structure of *Electrophorus electricus* sodium channel deduced from cDNA sequence. ***Nature*** 312: 121-127.

Nichols, C. G. and Lopatin, A. N. (1997) Inward rectifier potassium channels. ***Annu. Rev. Physiol.*** 59:171-191.

Oliver, D., T. Baukrowitz and B. Fakler (2000) Polyamines as gating molecules of inward-rectifier K^+ channels. ***Eur. J. Biochem.*** 267: 5824-5829.

Papazian, D. M., L. C. Timpe, Y. N. Jan and L. Y. Jan (1991) Alteration of voltage-dependence of Shaker potassium channel by mutations in the S4 sequence. ***Nature*** 349: 305-310.

Ponting, C. P. (1997) CBS domains in ClC chloride channels implicated in myotonia and nephrolithiasis (kidney stones). ***J. Mol. Med.*** 75: 160-163.

Perozo, E., D. M. Cortes and L. G. Cuello (1999) Structural rearrangements underlying K^+-channel activation gating. ***Science*** 285: 73-78.

Pusch, M., U. Rehfeldt and T. J. Jentsch (1995) Gating of the voltage-dependent chloride channel ClC-0 by the permeant anion. ***Nature*** 373: 527-531.

Roux, B. and R. MacKinnon (1999) The cavity and pore helices in the KcsA K^+ channel: electrostatic stabilization of monovalent cations. ***Science*** 285: 100-102.

Sah, P. (1996) Ca^{2+}-activated K^+ currents in neurons: types, physiological roles and modulartion. ***Trends Neurosci.*** 19: 150-154.

Schrempf, H., O. Schmidt, R. Kummerlen, S. Hinnah, D. Muller, M. Betzler, T. Steinkamp and R. Wagner. (1995) A prokaryotic potassium ion channel with two predicted transmembrane segments from *Streptomyces lividans*.
EMBO J. 14: 5170-5178.

Seoh, S. A., D. Sigg, D. M. Papazian and F. Bezanilla (1996) Voltage-dependent structural interactions in the *Shaker* K^+ channel. ***J. Gen. Physiol.*** 115: 123-138.

Silver, S. (1969) Active trasport of magnesium in *Escherichia coli*. ***Proc. Natl. Acad. Sci. USA*** 62: 764-771.

Bemèche, S. and Roux, B. (2001) Energetics of ion conduction through the K^+ channel. ***Nature*** 414: 73-77.

Smart, O. S., J. G. Neduvelil, X. Wang, B. A. Wallace and M. S. P. Sansom (1996) A program for the analysis of the pore dimension of ion channel structural models.
J. Mol. Graphics 14: 354-360.

Smith, R. L., J. L. Banks, M. D. Snavely and M. E. Maguire (1993) Sequence and topology of the corA magnesium transport systems of *Salmonella typhimurium* and *Escherichia coli*. ***J. Biol. Chem.*** 268: 14071-14080.

Smith, R. L. and Maguire, M. E. (1995) Distribution of the corA Mg^{2+} transport system in gram-negative bacteria. ***J. Bacteriol.*** 177: 1638-1640.

Stanfield, P. R., N. W. Davies, P. A. Shelton, M. J. Sutcliffe, I. A. Khan, W. J. Brammar, and E. C. Conley (1994) A single aspartate residue is involved in both intrinsic gating and blockade by Mg^{2+} of the inward rectifier, IRK1. ***J. Physiol.*** (*Lond*) 478: 1-6.

Studier, F. W. and Moffatt, B. A. (1986) Use of bacteriophage T7 RNA polymerase to direct selective high-level expression of cloned genes. ***J. Mol. Biol.*** 189: 113-130.

Taglialatela, M., E. Ficker, B. Wible and A. M. Brown (1995) C-terminus determinant for Mg^{2+} and polyamine block of the inward rectifier K^{+} channel IRK1. ***EMBO J.*** 14: 5532-5541.

Terstappen, G.C. and Reggiani, A. (2001) In silico research in drug discovery. ***Trends Pharmacol. Sci.*** 25: 368-374.

Unwin, N. (1993) Nicotinic acetylocholine receptor at 9 Å resolution. ***J. Mol. Biol.*** 229: 1101-1124.

Unwin, N. (1995) Acetylcholine receptor channel imaged in the open state. ***Nature*** 373: 37-43.

Vandenberg, C. A. (1987) Inward rectification of a potassium channel in cardiac ventricular cells depends on internal magnesium ions. ***Proc. Natl. Acad. Sci. USA*** 84:2560-2564.

Valiyaveetil, F. I., Y. F. Zhou and R. MacKinnon (2002) Lipids in the structure, folding, and function of the KcsA K^{+} channel. ***Biochemistry*** 41(35): 10771-10777.

Vergara, C., R. Latorre, N. V. Marrion and J. P. Adelman (1998) Calcium-activated potassium channels. ***Curr. Opin. Neurobiol.*** 8: 321-329.

Wang, D. N., M. J. Lemieux and J. M. Boulter (2003) Membrane protein protocols: Expression, purification and characterization. (Selinsky, B., Ed) Humana Press, Totowa, New Jersey, 239-256 pp.

Wang, Q., J. Shen, I. Splawski, D. Atkinson, Z. Li, J. L. Robinson, A. J. Moss, J. A. Towbin and M. T. Keating (1995) SCN5A mutations associated with an inherited cardiac arrhythmia, long QT syndrome. ***Cell*** 80: 805-811.

Wang, Q., M. E. Curran, I. Splawski, T. C. Burn, J. M. Millholland, T. J. VanRaay, J. Shen, K. W. Timothy, G. M. Vincent, T. de Jager, P. J. Schwartz, J. A. Towbin, A. J. Moss, D. L. Atkinson, G. M. Landes, T. D. Connors and M. T. Keating (1996) Positional cloning of a novel potassium channel gene: KVLQT1 mutations cause cardiac arrhythmias. ***Nature Genet.*** 12: 17-23.

Weinreich, F. and Jentsch, T. J. (2001) Pores formed by single subunits in mixed dimmers of different CLC chloride channels. ***J. Biol. Chem.*** 276: 2347-2353.

Wible, B. A., M. Taglialatela, E. Ficker and A. M. Brown (1994) Gating of inwardly rectifying K^+ channels localized to a single negatively charged residue. ***Nature*** 371: 246-249.

Yang, J., Y. N. Jan and L. Y. Jan (1995) Control of rectification and permeation by residues in two distinct domains in an inward rectifier K^+ channel. ***Neuron*** 14: 1047-1050.

Yellen, G. (2002) Voltage-gated potassium channels and their relatives. ***Nature*** 419: 35-42.

Zhou, Y., J. H. Morais-Cabral, A. Kaufman and R. MacKinnon (2001) Chemistry of ion coordination and hydration revealed by a K^+ channel-Fab complex at 2.0 Å resolution. ***Nature*** 414: 43-48.

Publication

Recent publication

Kuo, A., J. M. Gulbis, J. F. Antcliff, T. Rahman, E. D. Lowe, J. Zimmer, J. Cuthbertson, F. M. Ashcroft, T. Ezaki and D. A. Doyle (2003) Crystal structure of the potassium channel KirBac1.1 in the closed state. ***Science*** 300: 1922-1926.

Kuo, A, W. M. Bowler, J. Zimmer, J. F. Antcliff and D. A. Doyle (2003) Increasing the diffraction limits and internal order of a membrane protein crystal by dehydration. ***J. Struct. Biol.*** 141: 97-102.

Previous publication

Doyle, D. A., J. Morais-Cabral, R. A. Pfuetzner, **A. Kuo**, J. M. Gulbis, S. L. Cohen, B. T. Chait and R. MacKinnon (1998) The structure of the potassium channel: molecular basis of K^+ conduction and selectivity. ***Science*** 280: 69-77.

MacKinnon, R., S. L. Cohen, **A. Kuo**, A. Lee and B. T. Chait (1998) Structural conservation in prokaryotic and eukaryotic potassium channels. ***Science*** 280: 106-109.

Raman, C., **A. Kuo**, J. Deshane, D. W. Litchfield and R. P. Kimberly (1998) Regulation of casein kinase 2 by direct interaction with cell surface receptor CD5. ***J. Biol. Chem.*** 273(30): 19183-19189.

Kuo, A., S. Cappelluti, M. Cervantes-Cervantes, M. Rodrguez and D. S. Bush (1996) Okadaic acid, a protein phosphatase inhibitor, blocks calcium changes, gene expression and cell death induced by giberellin in wheat aleurone cells. ***Plant Cell*** 8: 259-269.

Dai, H., Y-S. Lo, **A. Kuo**, B-Y. Lin and K-S. Chiang (1991) Inheritable instability of colony morphology of *Xanthomonas campestris* pv. *citri*. ***Bot. Bull. Academia Sinica*** 32: 271-277.